The role of FcγRIIa polymorphisms in determining oligomerisation and IgG subclass binding preferences

Eleanor Grace Foy

Submitted in accordance with the requirements for the degree of
Doctor of Philosophy

The University of Leeds
Leeds Institute of Rheumatic and Musculoskeletal Medicine
School of Medicine
Faculty of Medicine and Health

July, 2019

The candidate confirms that the work submitted is his/her own, except where work which has formed part of jointly-authored publications has been included. The contribution of the candidate and the other authors to this work has been explicitly indicated below. The candidate confirms that appropriate credit has been given within the thesis where reference has been made to the work of others.

Chapter 3: Comparison of the FcγRIIa-IgG interaction using two different biophysical techniques. Some of the work in this chapter aimed at optimising a cell adherence protocol for use on the LigandTracer has been published in a jointly authored publication:

Bondza Sina, Foy Eleanor, Brooks Jonathan, Andersson Karl, Robinson James, Richalet Pascale, Buijs Jos. Real-time Characterization of Antibody Binding to Receptors on Living Immune Cells *Frontiers in Immunology*. 2017;8:455.

The candidate performed cell adhesion optimisation for HEK293 cells, and carried out ligand binding assays with IV.3 binding to FcγRIIa-expressing HEK293 cells. Statistical analyses was carried out by Sina Bondza. The candidate read, reviewed, and approved the final version of the manuscript.

Acknowledgements

It would not have been possible to complete this work without the help and support of a number of people, whom I am extremely grateful for.

Firstly, I would like to offer special thanks to my supervisors, Dr. Jim Robinson, Prof. Ann Morgan, Prof. Adrian Goldman and Dr. Euan Baxter, who have provided me with endless advice, encouragement and assistance with this project. I would also like to give massive thanks Dr. Maren Thomsen, who gave me expert guidance in the field of structural biology. Without her knowledge and kind support this work would not have been possible.

I would also like to thank several people for their training and teaching along the way, including Dr. Stephen Harborne, Amelia Lusiuk, Sina Bondza and Prof. Karl Andersson.

I would like to thank the whole of the Molecular Rheumatology group, and all of level 8 for their friendship and support both in and out of the lab, particularly Dr. Nikki Re, Dr. Mark Waterhouse and Dr. Amy Graham.

Finally I would like to thank my friends and family, who have supported me throughout my PhD, including my Mum and Dad, Rachel, Abi, Brendan & Grace, and Jacob & Flo. Special shout out to my important ones: Amy-Rose, Georgina, Carmen, Declan, Martin and Carlos.

Abstract

Fc-gamma Receptors (FcγRs) are expressed on the majority of immune cells and have a major role in the defence against infections. They bind IgG and immune complexes, triggering a signalling cascade to induce effector functions, such as antibody-dependent cell cytotoxicity, phagocytosis and cytokine release. The most widely expressed FcγR in mammals is FcγRIIa, which is polymorphic at 2 positions: 27 and 131. These non-synonymous genetic polymorphisms can be associated with greater risks of auto-immune diseases such as rheumatoid arthritis; however, it is not known how these polymorphisms contribute to disease. Previous work has suggested that these polymorphisms may affect both the quaternary structure and their binding preferences for different IgG subclasses, with the 131R allotype showing decreased IgG2 binding.

By producing and purifying recombinant FcγRIIa ectodomains, SEC- MALLS revealed that all allotypes were monomeric in solution. Polymorphisms in this receptor also affect the binding preferences for different IgG subclasses for the ectodomains in surface plasmon resonance experiments, and the full-length protein in LigandTracer experiments.

On further inspection of the previously published structure of FcγRIIa in complex with IgG1-Fc, substantial errors were found. Therefore, work was carried out to re-refine this structure. After re-refinement, it was demonstrated that the FcγRs family have a conserved binding pattern. Furthermore, analysis of the interaction revealed a structural basis for the allotype preference for IgG2, as well as the reason for FcγRI being the high affinity FcγR.

Table of Contents

List of Tables

List of Figures

Chapter 1
Introduction

1.1 FcγRs bind to the Fc region of Immunoglobulin G

Fc-gamma receptors (FcγRs) are mammalian cell surface glycoproteins, which recognise and interact with the Fc domain of immunoglobulin G (IgG; Figure 1.1) [1, 2]. FcγRs are expressed on the surface of most immune cells such as macrophages, natural killer cells, platelets and neutrophils and upon IgG binding can mediate a variety of effector functions, which are crucial for an effective immune response. These effector functions include phagocytosis, antibody-dependent cell cytotoxicity (ADCC), and pro-inflammatory mediator release. FcγRs are considered a crucial link between the humoral and cellular components of the immune system [3]. The Fc region of IgG is also capable of binding to the complement component 1q (C1q), which is the first step in the initiation of the complement cascade [4], as well as the neonatal Fc receptor (FcRn) which protects IgG from being degraded and allows IgG to be recycled hence maintaining circulating levels [5]. Additionally, it has been reported that FcγRs may also bind pentraxins, such as C-reactive protein (CRP) and serum amyloid P (SAP), which are sometimes referred to as innate antibodies [6]. Thus FcγRs also play an important role in linking the adaptive and innate arms of immunity.

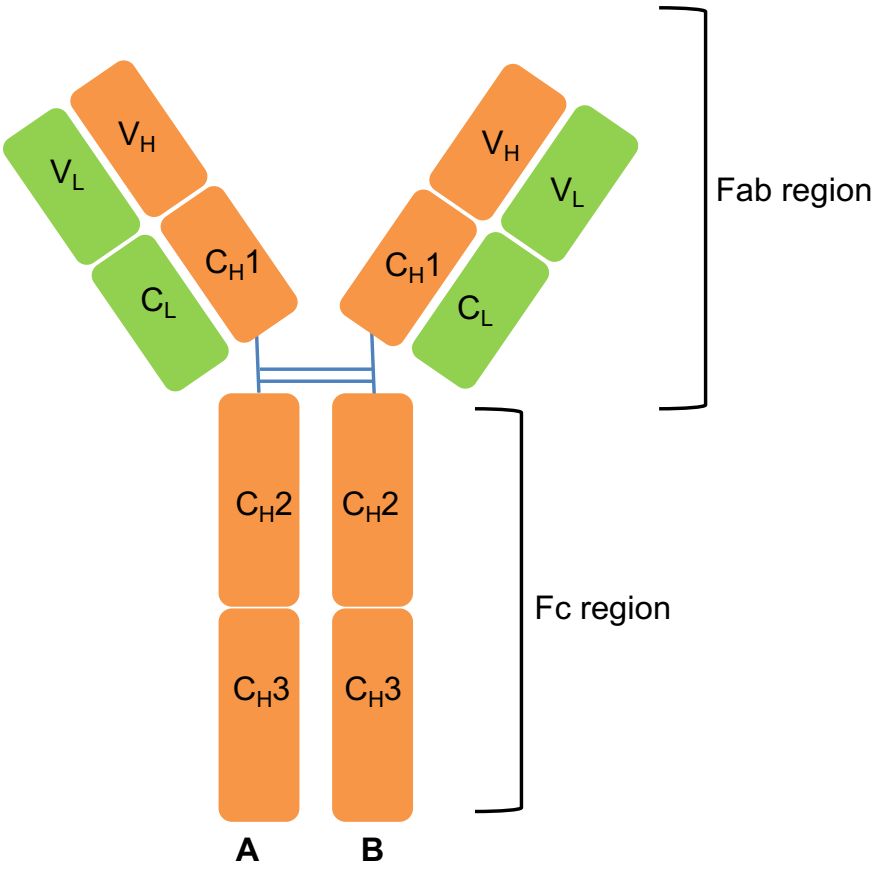

Figure 1.1 A schematic of an immunoglobulin G molecule.

Immunoglobulin G is made up of constant heavy (C_H) chains, constant light (C_L) chains, variable heavy (V_H) chains and variable light chains [7]. The variable regions make up the fragment antigen binding region (Fab region) which binds to antigens, and the Fc-region binds to FcγRs, FcRn and C1q [8].

1.1.1 Carbohydrates are essential for the FcγR-IgG interaction

IgG is a glycoprotein with one conserved N-linked glycosylation site at asparagine 297 (N297) of the C_H2 domain of Fc. This allows IgG to be glycosylated at 2 sites, one on each C_H2 domain [9]. The glycosylation state of IgG N297 plays a crucial role in maintaining IgG-Fc structure and binding to FcγRs [10, 11]. The first three-dimensional x-ray structure of IgG-Fc published in 1983 [12] suggested that glycosylation at N297 is crucial in stabilising IgG protein structure, forming a bridge between the two C_H2

domains and holding them together; however, more recent studies have challenged this. A study by Prabakaran *et al*. [13] has shown that the unglycosylated form of the C_H2 domain has the same structural integrity as the glycosylated form. It is clear that the glycans attached to IgG C_H2 can vary hugely, and that the distance between the two C_H2 domains can differ [14]. Nevertheless, studies have shown removal of the glycans at N297 causes IgG to have reduced FcγR binding and abrogates ADCC [15, 16], indicating that they are important elements mediating IgG effector functions.

It is thought that glycosylation of FcγRs is also crucial for antibody binding, and differential glycosylation patterns can modulate binding affinity [17]. Each of the FcγRs possess at least two N-linked glycosylation sites [10]. There are some structural data to show that human FcγRIIIa glycans interact with those present on N297 of afucosylated IgG1, demonstrating the importance of FcγR glycosylation in IgG binding [18]. Furthermore, a study by Patel *et* al [19] has suggested that the N-glycans present on FcγRIIIa may have a greater effect on binding affinity than IgG glycosylation. Evidence has also been found to suggest that FcγR glycosylation can differ depending on the immune cell they are expressed on [20, 21]. For example, FcγRIIIa expressed on NK cells display high mannose- and complex-type oligosaccharides, whereas FcγRIIIa on monocytes lack high mannose-type oligosaccharides completely [21]. Additionally, a study by Hayes *et al* [22] demonstrated that Chinese hamster ovary (CHO) cells, murine non-Ig secreting (NS0) cells and HEK293 cells all produced distinct glycoforms of FcγRIIIa.

1.2 FcγR subclasses

There are three classes of FcγRs: FcγRI (CD64), FcγRII (CD32) and FcγRIII (CD16). These are classified according to homology and their affinity for IgG [23] and can be further divided into subclasses shown in Table 1.1. The *FCGR* genes are located in the same region of the long arm of chromosome 1 and are very closely related, leading to a highly homologous family of proteins [1, 24].

1.3 FcγR expression on immune cells

Each FcγR can be expressed differentially on a variety of immune cell types at different stages of cell differentiation (summarised in Table 1.1), and the expression profiles can be altered in response to different pathogens. The majority of the activatory FcγRs are expressed on macrophages, highlighting their role in the immune response including phagocytosis and antigen presentation. A study by Jungi and Hafner [25] showed that after differentiation of resting monocytes to macrophages *in vitro*, mature human macrophages expressed 6 times more Fc receptors than blood monocytes. This in turn enhanced cellular phagocytic capacity [25]. Interestingly, FcγRIIa is the only FcγR which is expressed on human platelets, where it can bind and endocytose IgG complexes [26], whilst FcγRIIb is the only FcγR to be expressed on B cells [27].

Class	FcγRI	FcγRII			FcγRIII	
Subclass	FcγRI	FcγRIIa	FcγRIIb	FcγRIIc	FcγRIIIa	FcγRIIIb
Structure	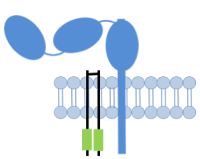	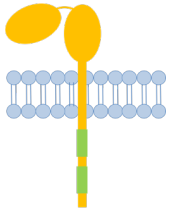	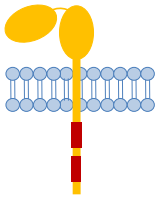	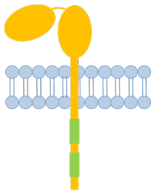	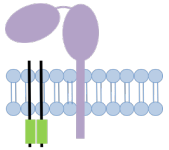	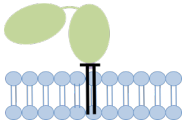
Signalling	Activatory	Activatory	Inhibitory	Activatory	Activatory	Activatory
Signalling motif	ITAM	ITAM	ITIM	ITAM	ITAM	-
Affinity for monomeric IgG	High	Low	Low	Low	Low	Low
Expression	Monocytes, macrophages, neutrophils, dendritic cells, mast cells	Monocytes, macrophages, neutrophils, basophils, dendritic cells, mast cells, eosinophils, platelets	B-cells, monocytes, macrophages, neutrophils, basophils	NK cells, monocytes, macrophages	NK cells, monocytes, macrophages	Neutrophils, basophils
Polymorphisms		131H/R 27Q/W/R	232I/T	57Q/X	158F/V 48L/H/R	NA1/NA2

Table 1.1 A summary of the different subclasses of FcγRs.

All FcγRs are classically described as activatory, with the exception of FcγRIIb. FcγRI is the only high affinity receptor for monomeric IgG. Different FcγRs are expressed on different immune cells, with FcγRIIa being the only one expressed on platelets. All FcγRs are single-pass transmembrane proteins, with the exception of FcγRIIIb which is GPI anchored. Each FcγR has polymorphic variants which can effect ligand binding and signalling. Adapted from [28-30].

1.4 Activatory FcγR signalling

The majority of FcγRs signal via an immuno-tyrosine-based activation motif (ITAM), hence initiate activatory signalling (Figure 1.2). For FcγRIIIa, this signalling occurs via a common γ or ζ chain, whereas FcγRIIa is a single chain receptor, capable of autonomous signalling; it contains an integral ITAM in the cytoplasmic domain therefore can signal without the need to associate with other adaptor proteins [31].

As receptors for the Fc region of IgG, activatory FcγRs play a crucial role in the immune response. Once a pathogen enters the body, an initial primary response is mounted against the antigen, followed by a secondary more specific immune response which includes the production of antibodies. The pathogen then becomes opsonised by these antibodies, forming immune complexes [32] which contain IgG. These IgG-containing ICs are then recognised by FcγRs, which cluster together and cross link to initiate signalling; previous studies have found that receptor clustering occurs in lipid rafts, or signalling microdomains, where local concentrations of other signalling molecules are increased [33, 34]. Upon receptor cross-linking and activation, FYN, a tyrosine-kinase, is recruited, which induces phosphorylation of the phosphatase SHP-1 at position S591. This crucial step in the signalling cascade inactivates the phosphatase, hence it cannot de-phosphorylate and inactivate other proteins in the signalling cascade. SRC family kinases are then recruited to the signalling complex, which can then phosphorylate the ITAM motif present in the cytoplasmic tail of FcγRIIa [35]. These ITAMs are crucial for receptor signalling, as phosphorylation of specific tyrosine residues creates phosphotyrosine-docking sites, enabling a

multitude of signalling proteins to bind via Src Homology 2 (SH2) domains [36]. This includes the tyrosine kinase SYK, which binds via its tandem SH2 domains and is activated through tyrosine phosphorylation, creating a docking site for yet more signalling proteins including phospholipase-C gamma (PLCγ) and VAV [37]. A key event in early FcγR signalling is the induction of cytoskeleton re-organisation, mediated by SYK. This increases FcγRs lateral mobility in the cell membrane, allowing them to associate with signalling microdomains [38-40]. In turn, this promotes receptor clustering and enhances recruitment of adaptor proteins. Due to receptor clustering, trans-phosphorylation between the receptors also occurs, which amplifies the signalling cascade further [41]. The resulting downstream effects can have many implications for the immune system; PLCγ hydrolysis of Phosphatidylinositol 4,5-bisphosphate (PIP2) into the second messenger molecules Inositol triphosphate (IP3) and diacyl-glycerol [42] causes calcium release form the endoplasmic reticulum (ER) [43], triggering inflammatory processes such as phagocytosis, ADCC, complement dependent cytotoxicity (CDC), oxidative burst and the production of chemokines and cytokines [44].

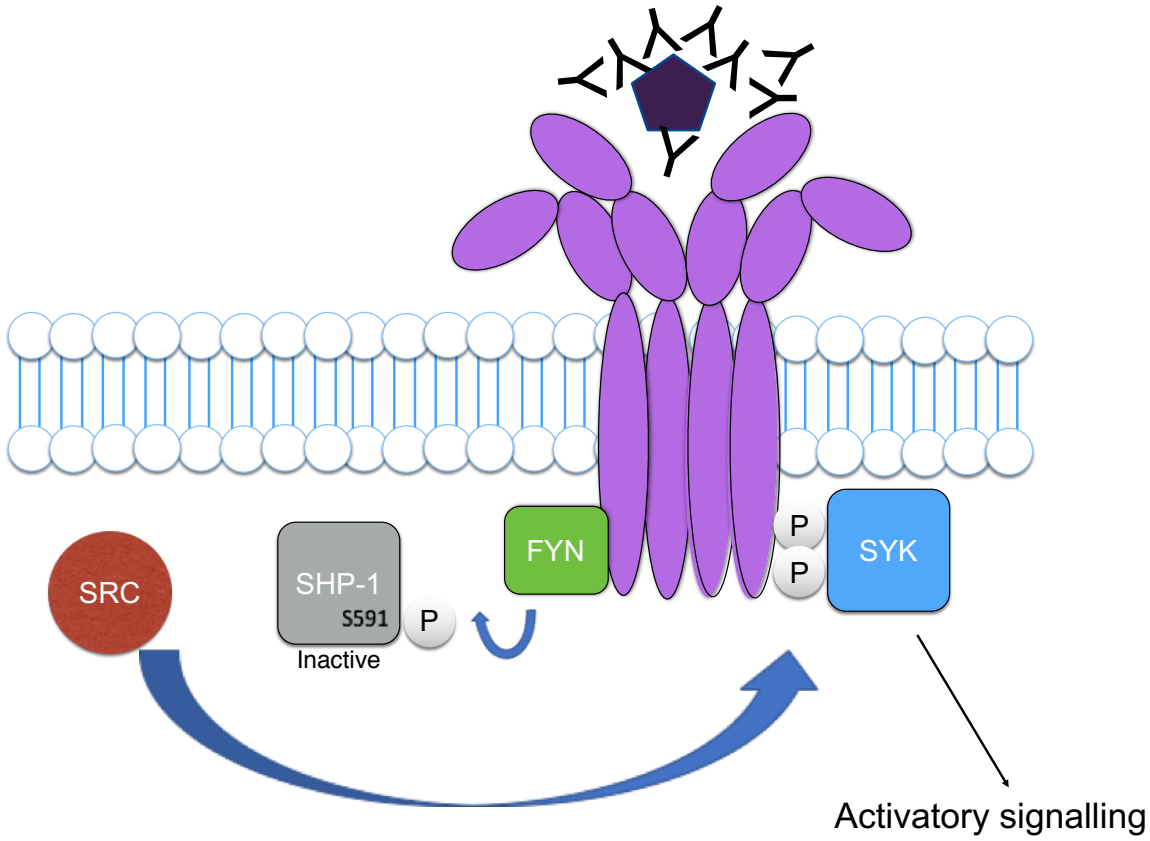

Figure 1.2 ICs bind to FcγRs.

Upon IC binding, FcγRIIa cluster together and are activated and can associate with signalling microdomains. This leads to FYN recruitment, which induces SHP-1 phosphorylation at S591 causing it to be inactive. SRC family kinases are recruited to phosphorylate FcγRIIa ITAMs, creating a docking site for other adaptor proteins such as SYK. Downstream activatory signalling is then initiated by these adaptor proteins.
IC, immune complex; ITAM, immunoreceptor tyrosine-based activation motif.

1.5 Inhibitory FcγR signalling

1.5.1 FcγRIIb

Among FcγRs, FcγRIIb is unique, as instead of signalling via an ITAM, FcγRIIb contains an Immuno-receptor tyrosine based inhibition motif (ITIM), with a conserved 13 amino acid sequence containing a YSSL motif [45]. Consequently, FcγRIIb is an inhibitory FcγR, and has a crucial role in the homeostasis of inflammatory signalling. Upon FcγR cross-linking and activation, FcγRIIb is able to associate with activatory FcγRs, and the ITIM becomes trans-phosphorylated. This then induces SHIP recruitment to the signalling complex causing hydrolysis of PIP3 to PIP2 and hence preventing the recruitment of other signalling molecules, such as PLCγ, to the plasma membrane. As a result, inflammatory signalling cascades are blocked (Figure 1.3) [31, 46]. Furthermore, FcγRIIb can recruit the active form of SHP-1, which can dephosphorylate activatory FcγR ITAMs and other crucial adaptor proteins and ITAM bearing receptors [46]. Studies have shown the importance of FcγRIIb in resolving inflammatory signalling, as the association of FcγRIIb with FcγRIIa can inhibit FcγRIIa-mediated phagocytosis and reduce tyrosine phosphorylation of FcγRIIa's ITAM [47].

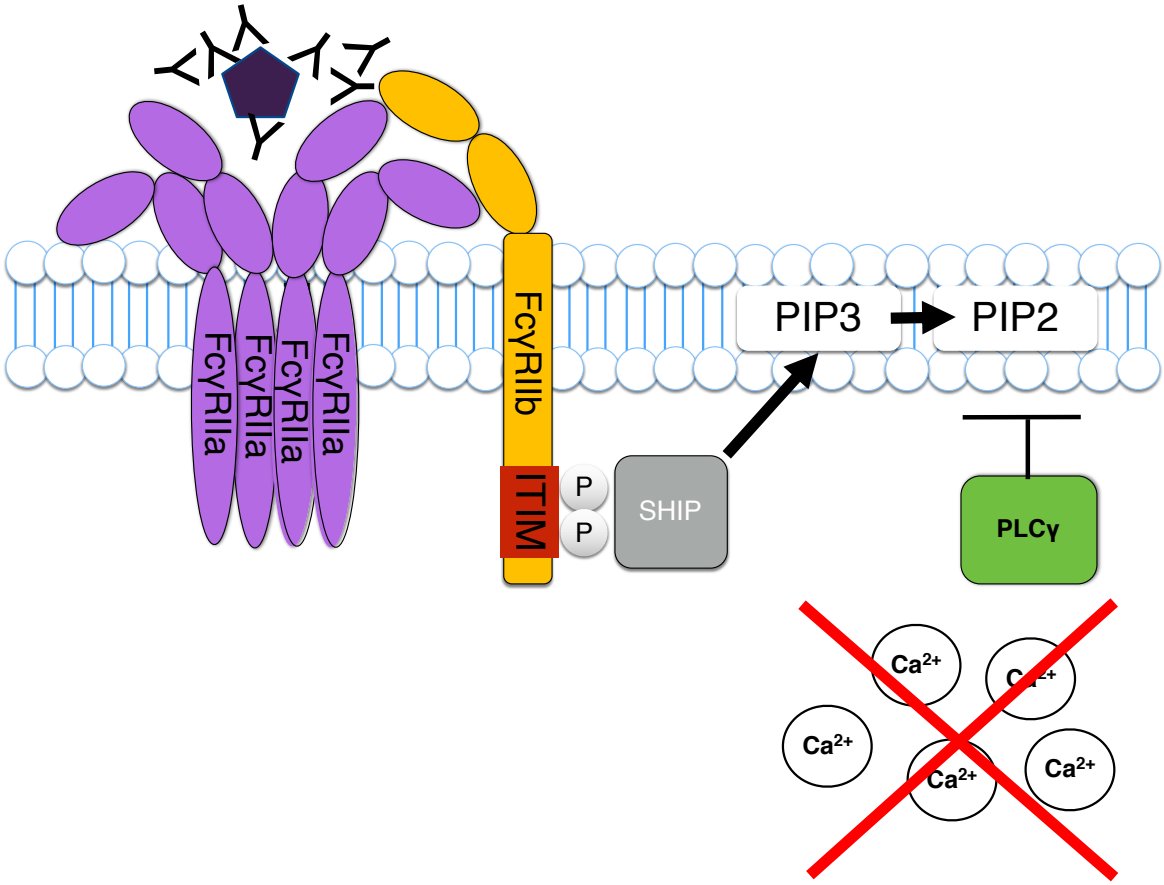

Figure 1.3 FcγRIIb inhibitory signalling.

Upon FcγRIIa clustering and activation, FcγRIIb can associate with the signalling complex due to its presence in the signalling microdomain. This leads to SHIP recruitment, which induces hydrolysis of PIP3 to PIP2 preventing PLCγ recruitment. Consequently, the resulting inflammatory signalling cascades mediated via calcium release are blocked and inflammation is resolved.

1.5.2 ITAMi

Although the majority of FcγRs are typically classified as activatory receptors, emerging evidence now suggests that these are also capable of functioning as inhibitory receptors. This signalling is mediated by the ITAM and has been termed inhibitory ITAM (ITAMi). Interestingly, both the valency of receptor clustering and the phosphorylation states of the protein tyrosine phosphatase SHP-1 govern this response and the protein kinases LYN and FYN play crucial roles; in the activatory state, multivalent receptor aggregation induced by IC binding causes FYN recruitment. FYN then phosphorylates SHP-1 at S591, causing SHP-1 to be inactive and preventing its recruitment to the active signalling complex.

In the inhibitory state, divalent receptor clustering causes recruitment of the adaptor protein LYN. This kinase causes only partial ITAM phosphorylation at position Y304, meaning SYK is only transiently recruited followed by stable recruitment of the tyrosine phosphatase SHP-1. LYN can then phosphorylate SHP-1 at position Y536, causing its activation. As SHP-1 is a phosphatase, it works by dephosphorylating and inactivating other signalling adaptor molecules on nearby receptor signalling complexes resulting in inhibitory signalling and a reduction in cytokine and reactive oxygen species (ROS) production (Figure 1.4) [48]. It is likely that ITAMi signalling may represent the resting state for FcγRIIa in healthy individuals, as monomeric circulating IgG is not sufficient for multivalent receptor aggregation; only when infection or autoimmunity is present does the active conformation of ITAM signalling occur, due to the presence of large ICs. It is also possible that ITAMi could be capable of resolving inflammatory FcγR signalling following IC clearance.

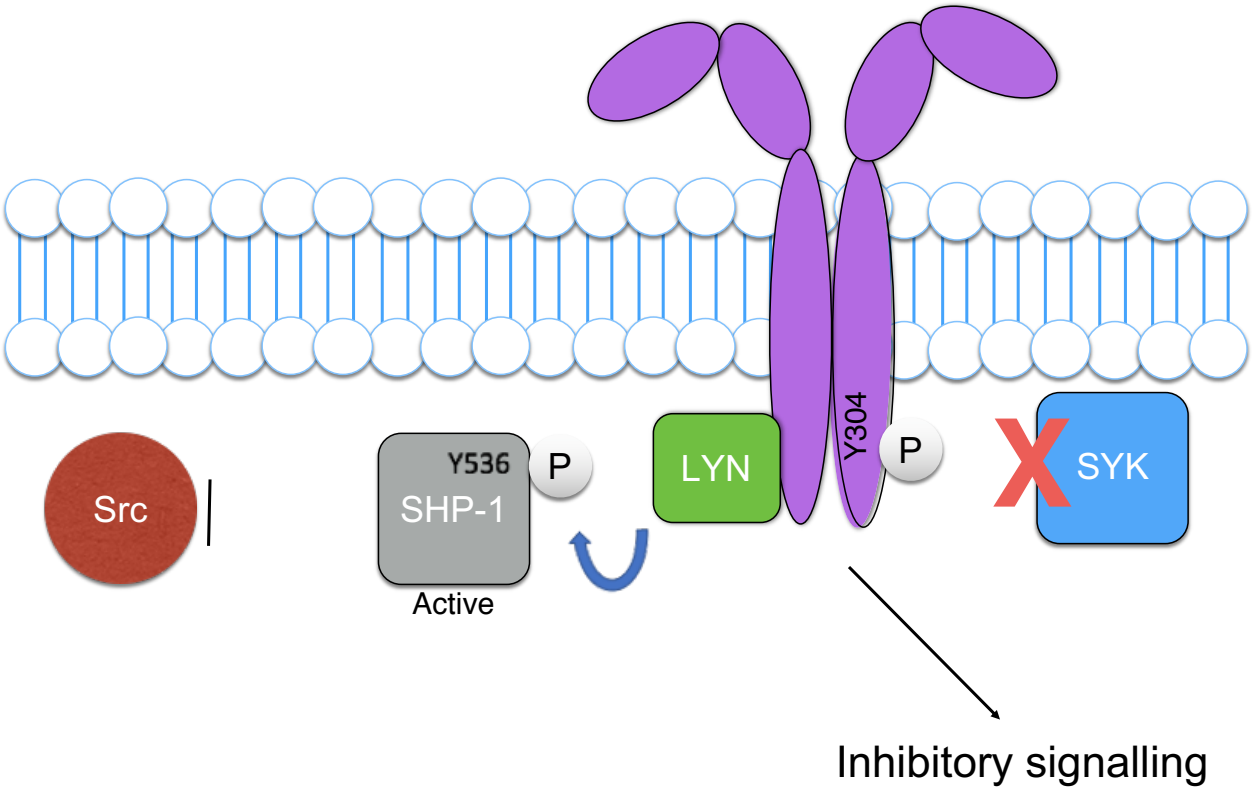

Figure 1.4 ITAMi signalling.

Divalent receptor clustering causes recruitment of the adaptor protein LYN which causes only partial ITAM phosphorylation at position Y304. SYK is only transiently recruited, followed by stable recruitment of SHP-1. LYN can then phosphorylate SHP-1 at position Y536, causing its activation. SHP-1 then goes on to dephosphorylate and inactivate other signalling adaptor molecules on nearby receptor signalling complexes resulting in inhibitory signalling.

1.6 FcγRs in health and disease

When a pathogen enters the body it becomes coated with opsonins such as IgG, complement and pentraxins [49-52]. In healthy individuals, FcγRs play a crucial role in the immune system by binding these opsonised microbes to trigger the process of phagocytosis, resulting in their elimination [53]. Immune homeostasis is then resolved through the inhibitory signalling methods mentioned previously. However, when the balance between activatory and inhibitory FcγR signalling becomes unbalanced, persistent inflammation can occur, as seen in autoantibody/IC-mediated autoimmune diseases including rheumatoid arthritis (RA, Figure 1.5).

1.6.1 Rheumatoid arthritis

RA is a progressive autoimmune disease affecting approximately 0.5 – 1% of the population [54]. It is most commonly found in females and is characterised by chronic inflammation of the synovial joints, pain and swelling. If left untreated, the chronic inflammation can cause severe joint damage and bone erosion [55].

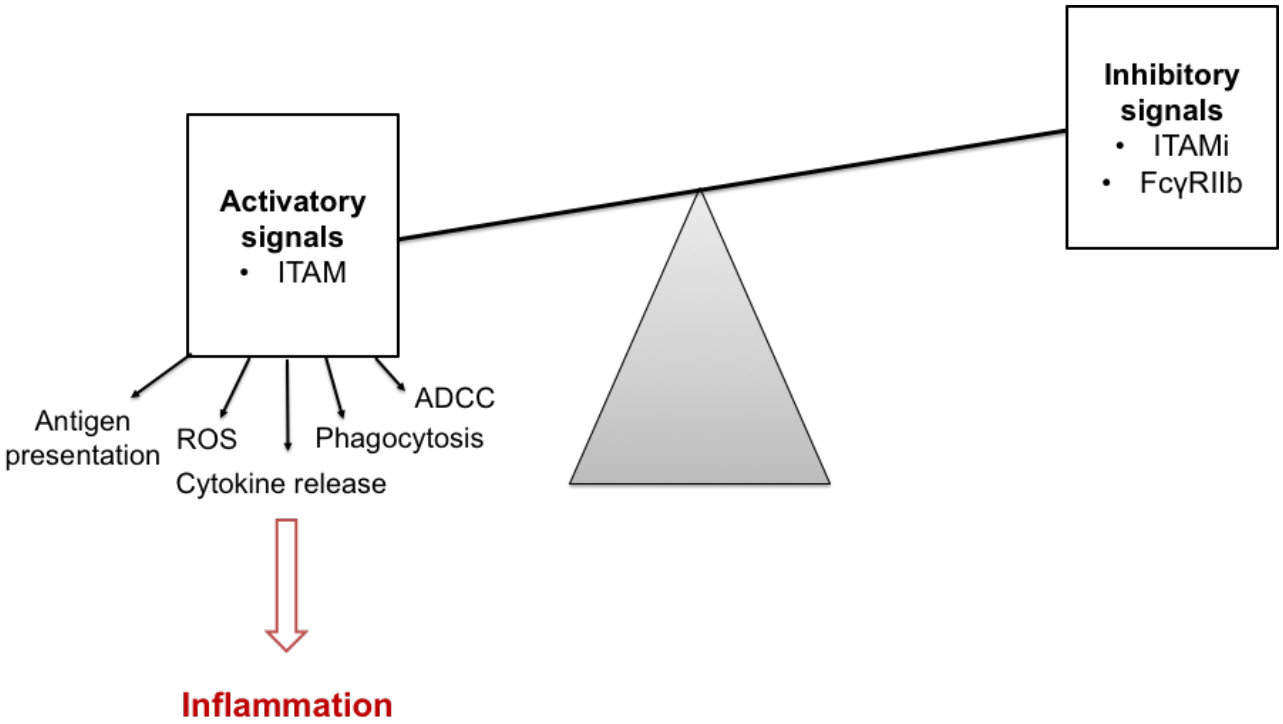

Figure 1.5 Striking the balance between activatory and inhibitory signalling.

In healthy individuals, the balance between activatory and inhibitory signalling is in equilibrium to maintain immune homeostasis. In autoimmunity, activatory signalling outweighs inhibitory signalling, leading to antigen presentation, ADCC, ROS, cytokine release, phagocytosis and consequently persistent inflammation. Conversely, if inhibitory signalling prevails, it can lead to an underactive immune system and susceptibility to infections.
ADCC, antibody-dependent cell cytotoxicity; ITAM, immunoreceptor tyrosine-based activation motif; ITAMi, inhibitory ITAM; ROS, reactive oxygen species.

1.6.1.1 Immune complexes

Both seropositive and seronegative forms of RA exist, with seropositive being the most common. Seropositive RA is characterised by the presence of circulating autoantibodies, known as anti-citrullinated peptide antibodies (ACPAs) and rheumatoid factors (RF) [56, 57]. ACPA are often of the IgG isotype, making FcγRs the primary receptor they bind to in order to initiate effector mechanisms [58], whilst RF is an anti-IgG antibody, with the most abundant being the IgM class, that forms complexes with IgG molecules, including ACPA in autoantibody positive patients. These RF-IgG molecules then aggregate to form variable sized ICs (Figure 1.6). As these autoantibodies are formed against self-antigens which are constantly present, levels of ICs are persistently high. In RA patients, high levels of ICs cause receptor clustering leading to trans-phosphorylation of both tyrosine residues favouring an autoimmune state [48]. It has been shown that the presence of both ACPA and RF can increase disease activity in RA [59]. In healthy individuals, ICs are only produced when a microbial agent is present, so levels of ICs are generally low. It is thought that in healthy individuals, mono-phosphorylated ITAMi status is maintained, as monomeric circulating IgG is not sufficient for multivalent receptor aggregation and trans-phosphorylation.

Several environmental factors have been thought to increase the risk of developing RA, such as diet, alcohol consumption and body mass index, however smoking has been shown to have a clear association with the production of ACPA [60]. This occurs through the activation of peptidyl arginine deiminases (PADs), which are the enzymes responsible for citrullinating auto-antigen proteins, hence promoting ACPA production

against these citrullinated proteins, as well as disruption of the lung mucosa equilibrium, causing immune activation and inflammation. However, these autoantibodies are not seen in all RA patients, and similarly, the presence of these autoantibodies can be present in healthy non-RA individuals [56].

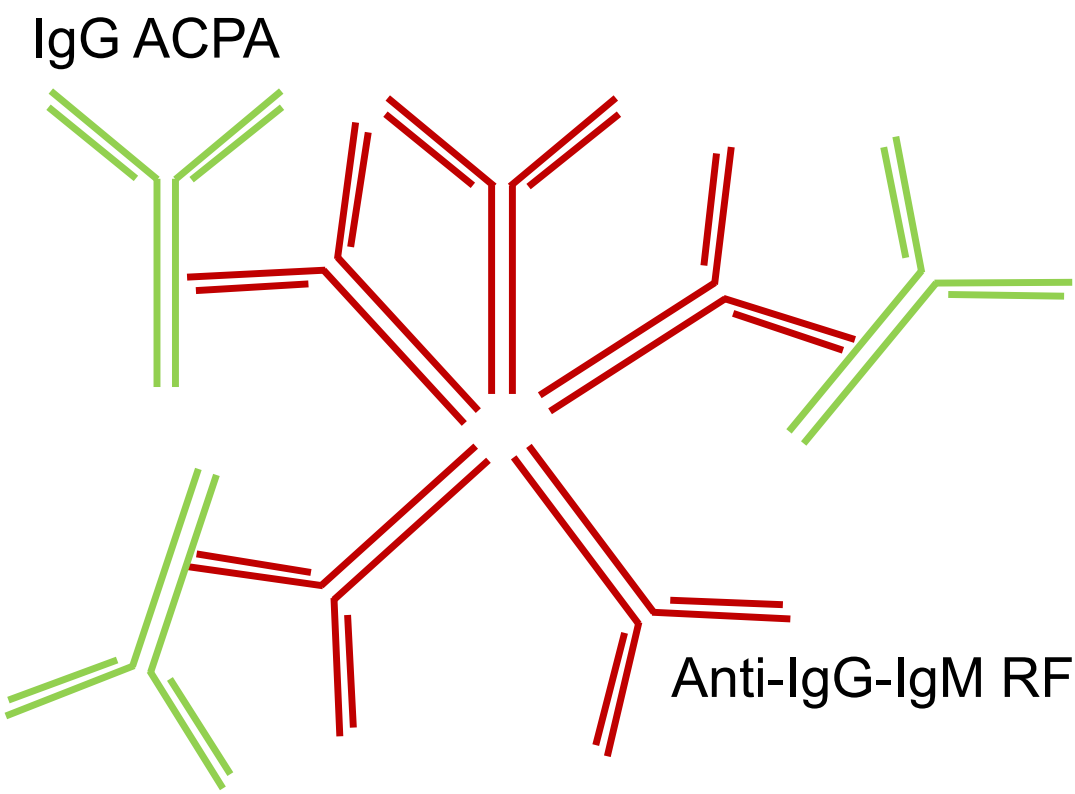

Figure 1.6 Immune complexes seen in RA.

Rheumatoid factor (shown in red) is anti-IgG-IgM, which naturally forms pentamers. The Fab region of RF binds to the Fc-region of other IgG molecules, including ACPA (green) to form large immune complexes, which bind to FcγRs driving persistent inflammation in RA.

1.6.1.2 IgG glycosylation and RA

During inflammatory disease states, the glycosylation state of serum IgG changes, and this has been studied extensively for RA. Studies previously carried out have found that the N-linked glycosylation patterns of serum IgG from RA patients show significantly lower levels of complexity, with truncated sugars and fewer galactose residues [61]. Levels of these agalactosylated forms of IgG (G0) are significantly increased in RA patients, and are thought to be pathogenic, correlating with disease activity [62]. IgG galactosylation depends on the enzyme B4-galactosyltransferase (GTase). In RA patients, this enzyme has been shown to be only partially effective [63]. Interestingly,

it was proposed that development of G0 forms of IgG may pre-dispose to the production of auto-antibodies seen in RA; the truncated sugars may in fact be an epitope against which auto-antibodies are produced [64]. It has also been shown that due to truncated sugars, sialyation levels of N-linked glycans are also altered during the course of RA, with lack of sialyation found in IgG of RA patients. Again, this may contribute to the progression of RA [65]. This is unsurprising, as it is known that sialyation of IgG is responsible for its anti-inflammatory properties, therefore lack of sialyation produces a more pro-inflammatory IgG molecule [66]. Remarkably, these sugars return back to normal once the patient has been successfully treated with anti-TNF treatment such as etanercept or disease-modifying anti-rheumatic drugs (DMARDs) such as methotrexate, with a reduction in the amount of G0 IgG observed [62, 67, 68].

The importance of glycosylation in the IgG-FcγR interaction makes it likely that these changes in glycosylation found in RA may also alter IgG binding, which may contribute to the disease pathogenesis. Notably, changes in IgG have also been seen in malignancies, infections and pregnancy, and demonstrate how the immune system uses glycosylation to fine tune immune responses [69].

1.6.1.3 Pentraxins and RA

FcγRs have been reported to recognise and bind pentraxins such as SAP and CRP [70, 71]. Pentraxins have also been shown to be associated with inflammatory diseases including RA, with elevated levels of the protein found in the serum and synovium of RA patients [72, 73]. It is not fully understood

how pentraxins contribute to the pathogenesis of RA, but it is possible that it is through activation of the complement cascade, initiation of activatory FcγR signalling and stimulation of cytokine production, all of which contribute to persistent inflammation [74].

1.6.2 One of the key FcγRs associated with RA is FcγRIIa

FcγRIIa is the most widely expressed human FcγR, and although a low affinity receptor for monomeric IgG, it can bind IgG ICs with high avidity [23]. Therefore, the ICs found in the serum of patients with RA are able to bind and activate FcγRIIa, causing persistent inflammatory signalling. The ability of ACPA-containing ICs to cause a potent inflammatory response has previously been shown to be dependent on the engagement between IgG and FcγRIIa, as blockade of this receptor can inhibit tumour necrosis factor (TNF) production significantly, thus supporting the role of this receptor in the pathogenesis of RA [75]. Interestingly, FcγRIIa is thought to be the key FcγR involved in the induction of pro-inflammatory cytokines [28]. FcγRIIa is the only FcγR to be expressed on platelets, and upon activation it can trigger a host of processes including Ca^{2+} mobilization, release of platelet factor [76], P-selectin and the generation of intraplatelet ROS [77], all of which contribute to tissue damage and inflammation. Enhanced platelet activation was observed in patients with RA [78], and high-levels of platelets and platelet-derived proteins such as P-selectin were found in the synovial fluid of RA patients [79, 80]. Furthermore, the expression levels of FcγRIIa on the macrophages of RA patients were found to be significantly higher on macrophages from RA synovium compared to controls, and this was correlated with increased TNF secretion after stimulation with heat aggregated gamma globulins (HAGGs) and a higher degree of inflammation

in the joints [81]. Although FcγRIIa is unique to humans, FcγRIIa transgenic mice have been bred allowing animal studies to be carried out. These FcγRIIa transgenic mice are highly sensitive to antibody-induced inflammation and also develop a spontaneous autoimmune syndrome with many symptoms parallel to RA. Even more remarkable is the fact that the presence of FcγRIIa allows these mice to develop collagen-induced arthritis, when they were previously genetically resistant to this [82], highlighting the importance of this receptor in RA.

Moreover, FcγRIIa has been suggested to be the main receptor for CRP, binding with micromolar affinity [71, 83, 84]. It is thought that upon binding, CRP is able to cross-link FcγRIIa, inducing ITAM phosphorylation and initiation of the inflammatory signalling cascade [85]. However, this topic is often debated, and firm conclusions are still to be made [86].

1.6.2.1 FcγRIIa polymorphisms and rheumatoid arthritis

FcγRIIa contains two non-synonymous single nucleotide polymorphisms (SNPs) in the extracellular portion, including the bi-allelic H131R polymorphism and the tri-allelic Q27W/R polymorphism, which are differentially distributed amongst worldwide populations [87]. The combination of these SNPs results in a total of 6 different possible FcγRIIa allotypes, but the 27W 131R allotype has not been observed in any population.

Several of these polymorphisms are known to be associated with both risk and severity of RA (unpublished work, Robinson, *et al*., co-authored manuscript in preparation), with the 27W-131H allotype having associations with RA [88]. This is not surprising as the H131R polymorphism is known to

effect FcγRIIa specificity and affinity for different IgG subclasses [89] and is therefore likely to effect affinity for autoantibodies. It has also previously been shown that the presence of an arginine at position 131 correlates with both higher disease activity [90] and an increased risk of developing RA [48].

1.6.2.2 Effect of FcγRIIa polymorphisms on IgG binding

To understand how these polymorphisms contribute to disease, it is important to understand how they affect ligand binding. There are 4 different subclasses of IgG (Figure 1.7; Table 1.7), each with different properties, and the polymorphisms present in the extracellular portion of FcγRIIa can affect how these subclasses bind. As various FcγR-IgG structures have shown, it is likely that the different binding specificities in the Fc-receptor family towards different IgG subclasses rely on the hinge region of IgG. IgG3 has the largest and most flexible hinge region, and IgG2 the least flexible [91]. It has previously been demonstrated that the 131H allele is capable of binding IgG2; however, the high-responder, 131R is not [7, 89]. It is not surprising that this polymorphism has significant effects on IgG binding, as residue 131 is in the IgG binding site [92]. A summary of the effect of the H131R polymorphism on IgG subclass binding is seen in Table 1.3.

As residue 27 is not in the IgG binding site, there has been little work done to study how polymorphisms at position 27 affect IgG binding. Furthermore, there are limitations to the studies which have been done, as they do not measure IgG binding to full-length FcγRIIa in a time-resolved, cellular based system. This makes the assays less biologically relevant, therefore it is clear that further work in this field is required.

Class	IgG1	IgG2	IgG3	IgG4
Molecular mass (kDa)	150	150	170	150
Amino acids in hinge region	15	12	62	12
Inter-heavy chain disulfide bonds	2	4	11	2
Relative abundance (%)	60	32	4	4

Table 1.2 Overview of the different IgG subclasses.

There are 4 different IgG subclasses with different characteristics. IgG1 is the most abundant subclass, followed by IgG2. IgG3 has the highest molecular weight with a significantly longer hinge region [93].

Subclass	Allotype preference
IgG1	H131 > R131
IgG2	H131 » R131
IgG3	H131 ≈ R131
IgG4	R131 ≥ H131

Table 1.3 Summary of H131R polymorphism on IgG binding.

It is known that 131H can bind IgG2 much more readily than 131R [94].

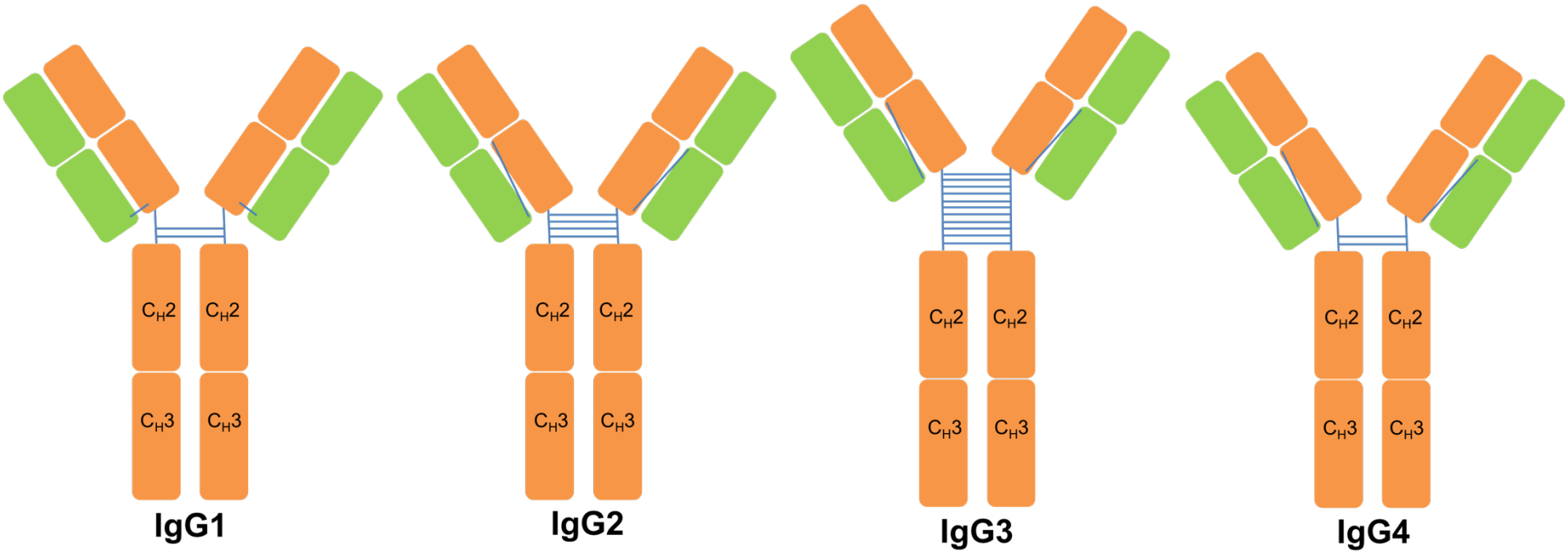

Figure 1.7 A schematic of IgG subclasses 1-4.

IgG1 and IgG4 have 2 inter-heavy chain disulfide bonds, whilst IgG2 has 4. IgG3 has 11 inter-heavy chain disulfide bonds, making this the most flexible hinge region.

1.6.3 Targeting FcγRIIa in RA

RA causes a huge economic burden to the UK each year, through several factors including loss of work and NHS costs. In a report published in 2017, the total cost of RA to the UK economy was estimated to be £3.8–4.8 billion annually [95]. Therefore, the need for new therapies is increasing. As one of the key receptors in RA, FcγRIIa is a valid therapeutic target for RA. Studies which explore FcγRIIa as a therapeutic target have previously been carried out [96].

1.6.3.1 Targeting FcγRIIa dimers

In order for activatory signalling to occur, FcγRs must be in close proximity to allow trans-phosphorylation between the ITAMs. It has previously been suggested that FcγRIIa forms homodimers at the cell surface in order for this to happen [97]. If true, then these dimers would make ideal targets for drug design, as disrupting the dimer interface could block receptor signalling.

1.6.3.1.1 Theory of 'dimeric activation complex'

Evidence for FcγRIIa forming dimers comes from the crystal structures published by Maxwell *et al*. [98] and Ramsland *et al.* [92]. Here, they suggest that FcγRIIa soluble ectodomains form homodimers (Figure 1.8) which are thought to be functional at the cell surface. Interestingly, the single amino acid polymorphism at position 131 is thought to completely alter this dimer structure, with the 131H allele forming a distinct dimer from the 131R allele (shown in Figure 1.8). Ramsland *et al.,* also described the formation of active signalling complexes, in which an inactive FcγRIIa dimer binds an IC causing the dimer to dissociate, producing an IC–FcγRIIa complex. This complex is then hypothesised to undergo rearrangement to create the 'dimeric activation complex' shown in Figure 1.9.

Targeting the dimer interface proposed by Ramsland *et al.* has previously been attempted. A study by Powell *et al.* [99] demonstrated that disruption of the FcγRIIa dimer interface by introducing the S126P mutation (S129 according to Powell *et al.* numbering) reduced both tyrosine phosphorylation and calcium mobilisation, suggesting that dimerisation is essential for efficient signal transduction. Surface plasmon resonance (SPR) studies showed that this mutation had no effect on IgG binding. Additionally, the dimer structure of the 27Q-131H allotype was used by Pietersz *et al.* [96] to design a series of small chemical entities (SCEs), intended to bind in the groove of the FcγRIIa dimer interface in order to block inflammatory signalling. The results of this study showed initial evidence that some of these SCEs could ameliorate collagen-induced arthritis, suggesting that FcγRIIa dimers may be a promising target. However, there is a fundamental flaw in this study; the SCEs used were designed based on the 27Q-131H dimer structure proposed by Ramsland *et al.*, yet, the experiments in the study tested the SCEs on the 27Q-131R allotype of FcγRIIa only, which is proposed to be distinct. Additionally, the study provided no evidence that the SCEs actually bind to FcγRIIa.

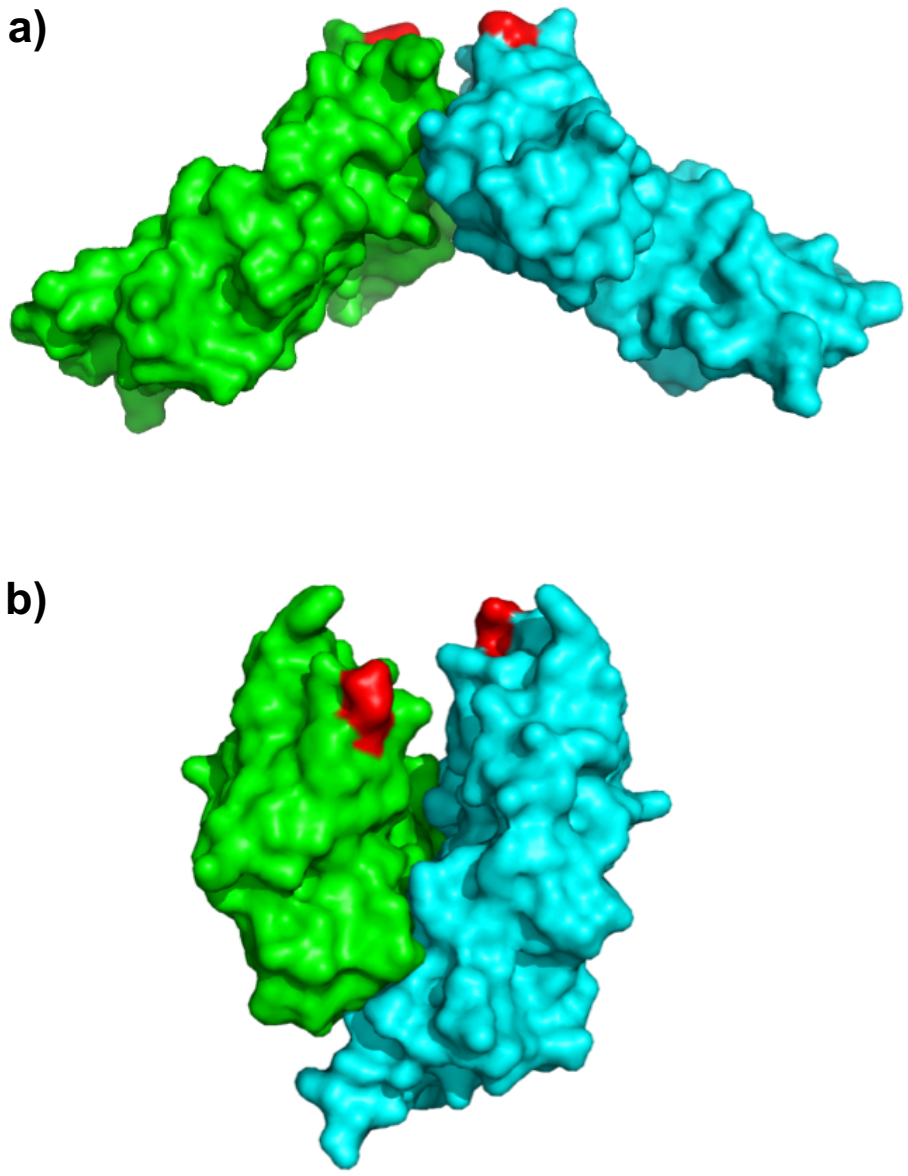

Figure 1.8 Proposed dimer structures of FcγRIIa from Ramsland *et al*.

Monomer 1 shown in green and monomer 2 in cyan. Polymorphic residue 131 highlighted in red. **a)** 131H allele **b)** 131R allele. Ramsland *et al*. proposed that the H131R polymorphism has a profound effect on dimerisation. Built in PyMol using PDB 3RY4, 3RY5.

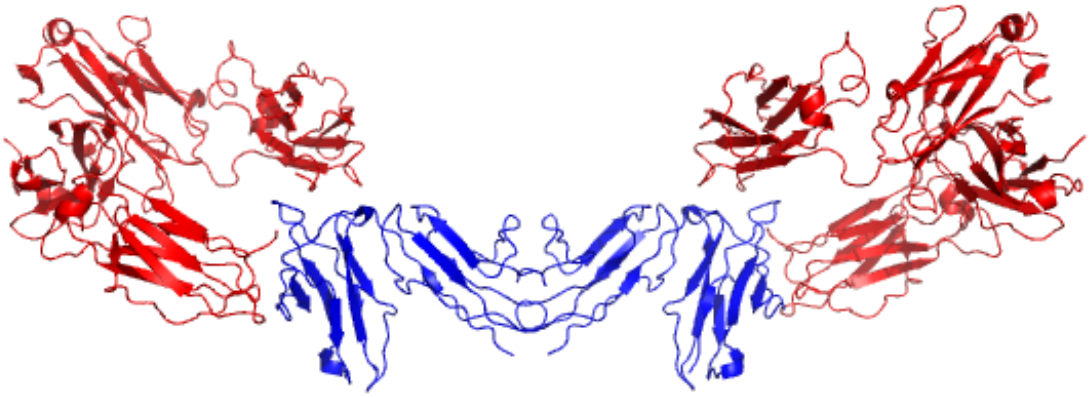

Figure 1.9 A model of the proposed 'dimeric activation complex' of 27Q-131R proposed by Ramsland *et al*.

Blue shows the FcγRIIa dimer, and red shows the IgG1-Fc molecules bound to each monomer of FcγRIIa. Built in PyMol using PDB 3RY6.

1.6.3.1.2 Theory of monomeric FcγRIIa

Even though the theory of FcγRIIa dimerisation is widely documented in the literature, there is a lot of debate around this area. Most of the evidence for FcγRIIa dimerisation derives from the ectodomain crystal structures. However, this does not reflect how full-length FcγRIIa would behave in a cell membrane, as the receptors would have restricted orientation and the transmembrane domain may mediate dimerisation. Furthermore, as the ectodomains were crystallised, there is chance that the proteins dimerised as a result of crystal packing. It has previously been shown that several monomeric proteins form non-physiological protein-protein contacts when crystallised, and that these contacts are random, rather than biologically relevant oligomers [100]. Recent work carried out by Jaumouille *et al.* [38] presents evidence to suggest that FcγRIIa may not form homodimers; in this study, macrophages were labelled with anti-FcγRIIa Fab fragments and a saturating concentration of Cy3-conjugated secondary Fab to allow the

number of labelled FcγRIIa in a complex to be quantified. The results from this revealed that FcγRIIa appeared to be monomeric in resting macrophages in the absence of ligand.

Further investigations are thus required to determine whether FcγRIIa forms homodimers, as this could have significant effects in terms of ligand binding and targeting FcγRIIa therapeutically.

1.6.3.2 Targeting the FcγRIIa-IgG interaction

Another method of targeting FcγRIIa to treat RA is to block the FcγRIIa-IgG interaction, preventing receptor activation and inflammatory signalling. This can be done by a variety of methods, such as blocking antibodies which compete for the IgG binding site, small molecule approaches to prevent the interaction, or infusion of a soluble form of FcγRIIa to act as a decoy, binding and blocking ICs [23, 101]. Furthermore, modification of therapeutic IgG glycans could also be carried out to alter the FcγRIIa-IgG interaction, which may be used to enhance or prevent binding [102]. To target the FcγRIIa-IgG interaction specifically, information about the binding interface is needed, which can be obtained from an x-ray structure.

1.6.3.2.1 Crystal structure of FcγRIIa in complex with IgG-Fc reveals a symmetric binding pattern

A crystal structure of the 27Q-131H allotype of FcγRIIa in complex with the Fc region of IgG1 was published in 2011, at 3.8 Å resolution (PDB code 3RY6) [92]. The extracellular portion of FcγRIIa is made up of two immunoglobulin-like domains, D1 and D2, which are connected by a hinge region at an interdomain angle of 52° [31, 98]. It is predominantly the D2 domain which makes major contacts with IgG, binding between IgG-Fc chain

A and chain B, with 1:1 stoichiometry [103]. Upon binding, these IgG chains come together to form a structure similar to a horseshoe with sugar moieties attached N297 of the C_H2 domain in the centre of the molecule (Figure 1.10) [104].

Interestingly, despite the high homology of FcγRs, there does not appear to be a conserved IgG-binding mechanism; the binding interface of FcγRIIa-IgG1-Fc was shown to differ from other FcγRs. Whilst FcγRIIIa [105], FcγRI [106], and FcεRIα [107] show an asymmetric binding pattern, FcγRIIa appears to bind with two-fold symmetry. Due to this, it was hypothesised that FcγRIIa would be easy to target specifically over other FcγRs.

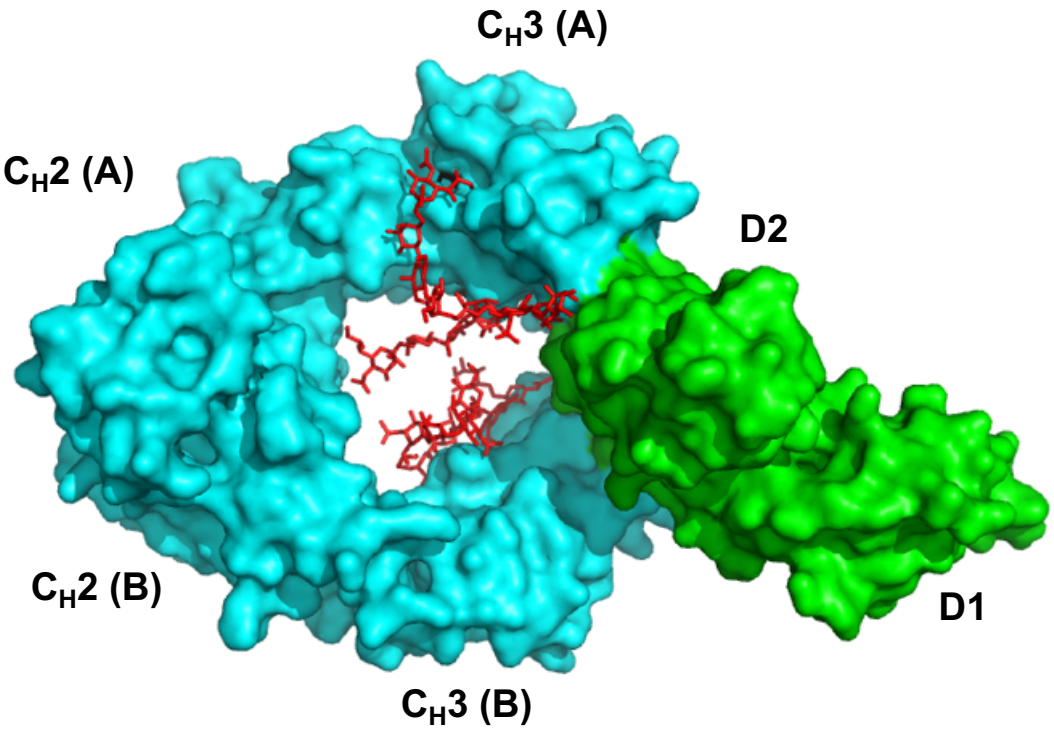

Figure 1.10 The x-ray crystal structure of the Fc-region of IgG1 in complex with the ectodomain of FcγRIIa at 3.8 Å resolution.

IgG sugar moieties are shown in red (Made in PyMol using PDB entry 3RY6). IgG1, cyan; FcγRIIa ectodomain, green.

1.6.3.2.2 Crystal structure of FcγRIIa in complex with IgG-Fc reveals the importance of carbohydrates

The published x-ray structure of FcγRIIa in complex with IgG1-Fc also reveals that the sugars attached to N297 of the IgG-Fc domain make interactions with residue S126 of FcγRIIa (Figure 1.11). This suggests that FcγRIIa glycans are critical for IgG binding.

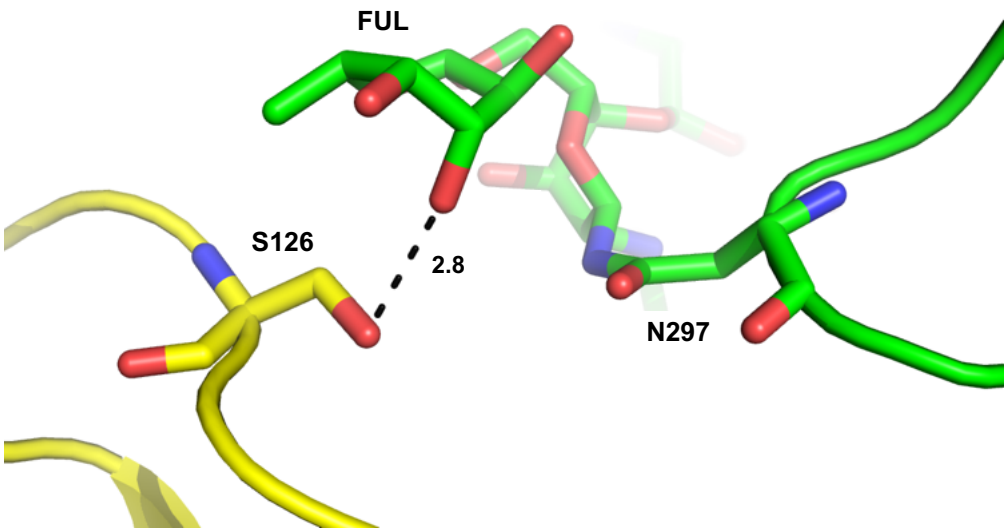

Figure 1.11 S126 of FcγRIIa makes contacts with the carbohydrates present on IgG1-Fc.

S126 of FcγRIIa (yellow) makes contacts with the fucose attached to N297 of IgG1-Fc (green).
FUL, β-L-Fucose.

1.6.3.2.1.1 Quality of the available crystal structures

Upon further inspection of the 3RY6 structure, it was found to have poor statistics, showing high numbers of rotamer and Ramachandran outliers, and above average R-free values and clash scores (Figure 1.12). This suggests that the model has not been refined optimally and may not be completely accurate. The need for accurate and good quality structures is of upmost importance when using these for future work such as therapeutic design. It is clear that further re-refinement could be carried out on this structure, as re-refinement often significantly improves x-ray structures [108].

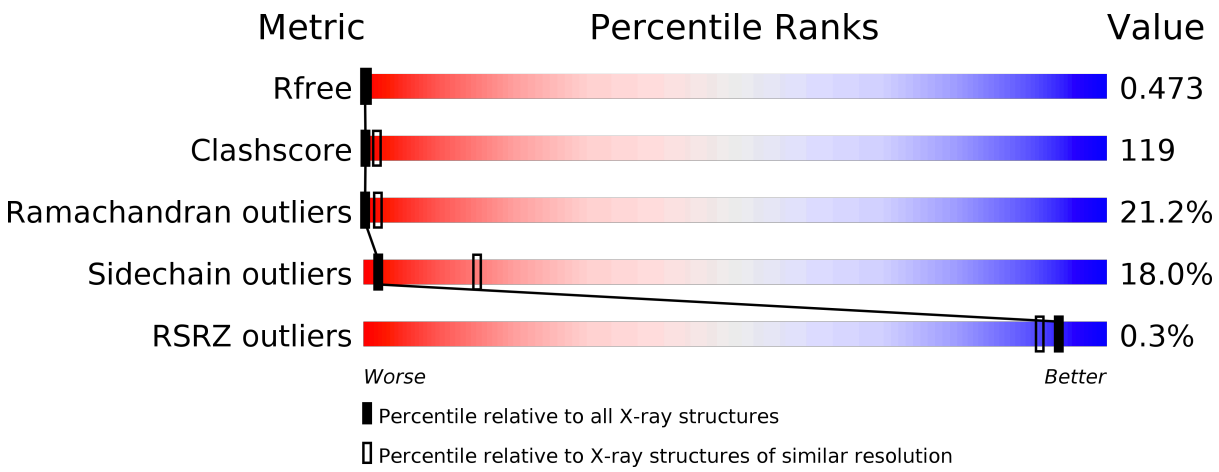

Figure 1.12 The 'percentile slider' for the 3RY6 structure of FcγRIIa in complex with IgG1-Fc (taken from the PDB validation report).

1.6.3.2.1.1.1 The problem of bad structures in the antibody/Fc-receptor field

Worryingly, after looking at several other published antibody and FcγR structures it became clear that poorly refined structures were common in this field. Of particular note is a series of structures published by Dr. Salunke's lab [109-111]. In these papers, the authors study the role of plasticity in molecular recognition by antibodies, by solving the crystal structures of a series of antibodies in complex with different antigenic peptides. However, the validity of these structures have since been challenged and subsequently re-refined by Stanfield, Pozharski *et al* [112], as the electron density maps for the peptides were not convincing. It was found that the B-factors for the peptides were significantly higher than the surrounding molecules, and that the difference omit maps provided no evidence of peptides when contoured at 3σ, hence the conclusions from Dr. Salunkes lab could not be supported.

Another example of a poor structure in this field is the structure of FcγRI in complex with IgG1-Fc (PDB 4X4M, 3.5 Å resolution) [113]. Again this structure shows poor statistics, with a high clash score of 56 and large numbers of sidechain and RSRZ outliers (Figure 1.13).

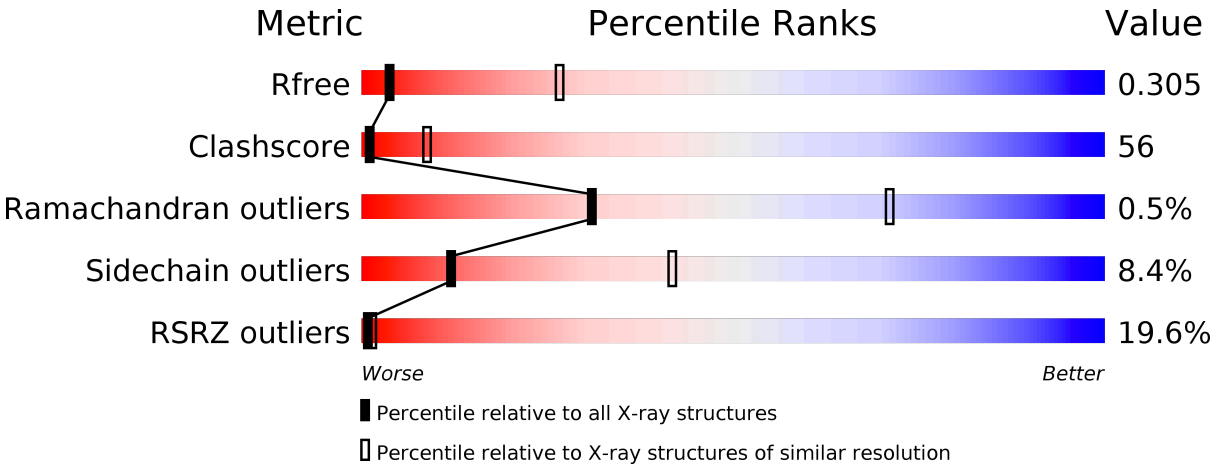

Figure 1.13 The 'percentile slider' for the 4X4M structure of FcγRI in complex with IgG1-Fc (taken from the PDB validation report).

Furthermore, the structure was found to have very poor density, with no density for any side chain conformations for the sugar contacts present. The geometry of the carbohydrates is also poor, with the fucose molecules attached to the NAG molecule with a β-link rather than the correct α-link seen in mammalian glycosylation [114].

It is clear that the structures used in this field must be used with caution.

Chapter 2
Materials and Methods

All buffer recipes can be found in Appendix A.

2.1 Cloning

2.1.1 *FCGR2A* ectodomain in pOPINGTTG-neo vector

pOPINGTTG-neo plasmids containing 4 allotypes of the *FCGR2A* ectodomains were produced prior to starting this PhD project, by the Oxford Protein Production Facility (Oxford, UK) [115]. These were the 27Q-131H, 27Q-131R, 27W-131H and 27W-131R allotypes.

2.1.2 Site Directed Mutagenesis of *FCGR2A* in pOPINTTG-neo vector

Site directed mutagenesis (SDM) was carried out to produce the remaining 2 allotypes, 27R-131H and 27R-131R using the GeneArt® Site-Directed Mutagenesis PLUS Kit (Life Technologies, Warrington, UK). This was based on the high fidelity AccuPrime™ Pfx polymerase (thermal cycling conditions in Table 2.1). This system used DNA Methylase and S-adenosine methionine (SAM) to methylate the template plasmid, which was then amplified using primers designed to incorporate the desired mutation (primers shown in Table 2.2). The sample was then transformed into DH5α™-T1R competent E.coli cells by heat shock at 37^{o}C, plated on Luria Broth (LB)-Agar plates with 100 µg/ml ampicillin (Sigma-Aldrich, Haverhill, UK) and left to incubate at 37^{o}C overnight. As the DH5α™-T1R competent E.coli cells contained a McrBC endonuclease which digested the methylated template DNA, only the cells transformed with unmethylated mutagenesis products were able to grow as colonies. Single colonies were then picked and grown in LB-broth with 100 µg/ml ampicillin, at 37^{o}C, 250 RPM overnight

in an Excella E25 shaking incubator (Eppendorf, Stevenage, UK). Minipreps were carried out and then sequenced.

Enzyme: AccuPrime **Application: Site-directed mutagenesis**	1. 37°C - 12-15 minutes for 2.8 – 5.0 Kb of template - 15-20 minutes for 5.0 – 14.0 Kb of template 2. 94°C – 2 minutes 3. 94°C – 20 seconds 4. 57°C – 30 seconds 5. 68°C – 30 seconds per Kb of template 6. Cycle to step 3 - 12-15 times for 2.8 – 5.0 Kb of template - 15-18 times for 5.0 – 14.0 Kb of template 7. 68°C – 5 minutes 8. 8°C – forever

Table 2.1 Thermal cycling conditions used for site directed mutagenesis.

Mutation	Forward Primer 5'-3'	Reverse Primer 5'-3'
Q27R	GTGACTCTGACATGC**CGG**GG GGCTCGCAGCCCTG	CAGGGCTGCGAGCCCC**CCG**GC ATGTCAGAGTCAC
H131R	TCCCAGAAATTCTCC**CGT**TT GGATCCCACCTTC	GAAGGTGGGATCCAA**ACG**GG AGAATTTCTGGGA
S126P	TTCCAGAATGGAAAA**CCC**CA GAAATTCTCCCATTTG	CAAATGGGAGAATTTCTG**GGG**TT TTCCATTCTGGAA

Table 2.2 Primers used for site-directed mutagenesis of *FCGR2A*.
The codons which cause the mutation are highlighted in bold.

2.1.3 Cloning full length *FCGR2A* into pFastBac

In order to produce the full-length FcγRIIa protein, the *Spodoptera frugiperda* (sf9) insect cell line was used, therefore the *FCGR2A* gene was cloned into a pFastBac vector. The pFastBac vector which had been modified to contain a C-terminal His-tag with a TEV cleavage site was kindly donated from Dr Maren Thompson. A schematic of the construct is shown in figure 2.1.

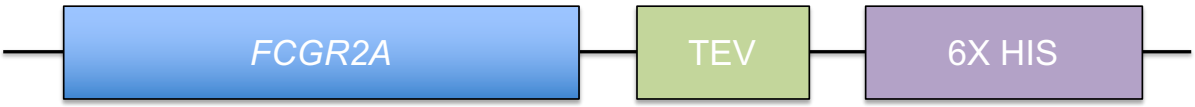

Figure 2.1 A schematic of the construct used in the pFastBac vector. Full length *FCGR2A* is followed by a TEV cleavage site and a 6X His-tag.

2.1.3.1 Restriction digest of pFastBac vector

To clone the full-length *FCGR2A* genes into this vector, standard restriction digest cloning was used. A total of 1µg of the vector was mixed with 1 µl of NotI-HF, 1 µl of PstI-HF and 2 µl CutSmart 10x buffer (NEB, Hitchin, UK). The reaction volume was made up to 20 µl with dH_2O, then incubated at 37°C for 1 hour.

2.1.3.2 Agarose gel electrophoresis

After restriction digest, the products were run on a 1% agarose/TAE (w/v) (Sigma-Aldrich, Haverhill, UK) gel for 1 hour at 80V in TAE buffer, using a Bio rad laboratories (Watford, UK) 'PowerPac Basic' electrophoresis system. The gel was stained with Midori Green Advance DNA Stain (Geneflow, Lichfield, UK) then imaged using ImageLab software and a Bio rad gel doc system (Bio rad Laboratories, Watford, UK).

2.1.3.3 Gel extraction of digest product

After running the agarose gel, the digested vector was gel extracted using a QIAquick gel extraction kit (Qiagen, Hilden, Germany) following the manufacturer's protocol which can be found in Appendix B.1.

2.1.3.4 Amplification of full-length *FCGR2A*

Full-length *FCGR2A* was polymerase chain reaction (PCR) amplified using cDNA from whole blood from healthy donors of known *FCGR2A* genotypes, using the primers used shown in Table 2.3. The gene was cloned with 5' and 3' sequences homologous to the digestion site of the pFastBac plasmid to allow homologous recombination into the plasmid. Ethical approval was granted by the NRES Committee Yorkshire and Humber – Leeds East, reference number 04/Q1206/107. Taq polymerase was used, and thermal cycling conditions can be found in Table 2.4. The PCR product was then run on a 1% agarose/TAE (w/v) and gel extracted as above.

Gene	Plasmid	Forward Primer 5'-3	Reverse Primer 3'-5'	Product size
FCGR2A	pFastBac CTH	GACGAGCTCAC TAGTCGCGGCC GCATGACTATG GAGACC	GGTTTTCCGTA CCGGGCTGCAG GTTATTACTGTT GAC	1000bp

Table 2.3 Primers used to amplify full-length *FCGR2A* for insertion into the pFastBac vector.

Enzyme: Taq Application: PCR amplification	1. 95°C – 30 seconds 2. 95°C – 15 seconds 3. 57°C – 15 seconds 4. 72°C – 1 minute 5. Cycle to step 2 for 34 times 6. 72°C – 5 minutes 7. 8°C – forever

Table 2.4 Thermal cycling conditions used for PCR amplification of *FCGR2A*.

2.1.3.5 Homologous recombination

The gel extracted PCR products were inserted into the digested plasmid by homologous recombination (Figure 2.2) using In-Fusion® (Clontech, Saint-Germain-en-Laye, France). For the homologous recombination reaction, 1 µl of the insert was mixed with 1 µl of the digested vector (NheI and PstI digested) and 1 µl of InFUSION enzyme. The reaction mixture was made up to 5 µl with dH_2O and then incubated at 50°C for 15 mins.

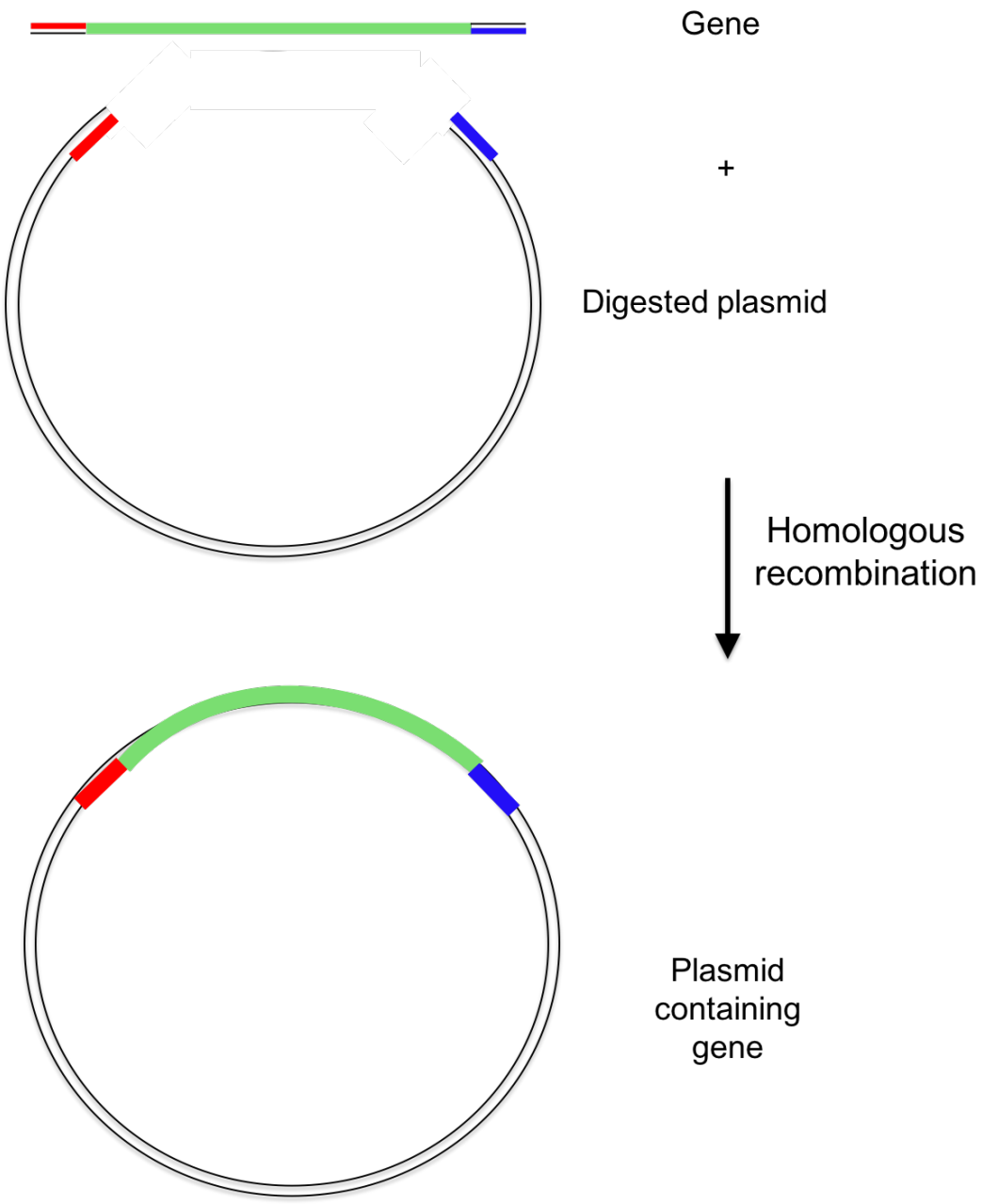

Figure 2.2 Schematic showing the process of homologous recombination.

The gene (green) is amplified with 5' and 3' sequences homologous to the digest plasmid (red and blue). These overlapping sequences combine to create a circular plasmid containing the gene.

2.1.3.6 Transformation into competent cells

After homologous recombination, the vectors were then transformed into Stellar™ Competent Cells (Clontech, Saint-Germain-en-Laye, France). Firstly, 2 µl of the homologous recombination reaction was added to 50 µl of thawed competent cells and incubated on ice for 30 mins. These were then heat shocked at 42^{o}C for 30 seconds incubated on ice for a further 3 mins, before plating onto Luria Bertani (LB)-agar plates containing 100 µg/mL ampicillin (Sigma-Aldrich, Haverhill, UK). The plates were then incubated overnight at 37^{o}C in a humidified incubator (Model no. MIR-262, Sanyo, Osaka, Japan). Single colonies were then picked and grown in LB-broth (Miller) (Sigma-Aldrich, Haverhill, UK) containing 100 µg/ml ampicillin at 37^{o}C, in an Excella E25 shaking incubator (Eppendorf, Stevenage, UK) at 250RPM overnight, and minipreps of the plasmid DNA carried out. DNA sequencing of the minipreps was carried out to confirm that the vectors contained the correct insert in the correct open reading frame (ORF).

2.1.3.6 Site-directed mutagenesis of pFastBac vectors

As only 3 ectodomain allotypes of *FCGR2A* exist in Caucasians, only these allotypes could be cloned from cDNA obtained from healthy donors. Therefore, site-directed mutagenesis (SDM) was carried out to produce the remaining 3 possible allotypes, 27W-131R, 27R-131H and 27R-131R, as above.

2.1.3.7 Plasmid Minipreps

Minipreps of plasmids containing the *FCGR2A* gene were carried out according to the manufacturer's protocol (Qiagen, Manchester, UK), which can be found in Appendix B.2. All centrifugation steps were carried out in an Eppendorf 5415D benchtop centrifuge (Eppendorf, Stevenage, UK).

2.1.3.8 DNA sequencing

Sanger sequencing of DNA was performed using a protocol based on the BigDye® Terminator v3.1 Cycle Sequencing Kit (Life Technologies, Warrington, UK).

First of all dH_2O, 5x sequencing buffer, BigDye® Terminator v3.1 Ready Reaction Mix (containing polymerase, dNTPs and ddNTPs) and the chosen primer (1.6 pMol/µl) were mixed with 100ng of the template to be sequenced. PCR amplification was then carried out (thermal cycling conditions in Table 2.5). The DNA was precipitated using 125mM ethylenediaminetetraacetic acid (EDTA) and 100% ethanol, and pelleted by centrifugation at 3900rpm. The DNA pellet was then washed with 70% ethanol to remove EDTA then air-dryed. The DNA was re-suspended in HiDi fomamide which stabilized the single stranded DNA, and then analysed by capillary electrophoresis on an Applied Biosystems 3130xl Genetic Analyser (Applied Biosystems, Warrington, UK) to create an electropherogram. Raw data were then base called to assign a nucleotide to each peak, and analysed using BioEdit Sequence Alignment Editor (Ibis Therapeutics, Carlsbad, CA, USA) [116].

Enzyme: BigDye 3.1 Application: Sequencing	1. 96°C – 1minute Ramp to 96°C at 1°C/second 2. 96°C 10 seconds Ramp to 96°C at 1°C/second 3. 50°C – 5 seconds Ramp to 50°C at 1°C/second 4. 60°C – 2 minutes Ramp to 60°C at 1°C/second 5. Cycle to step 4 for 24 times 6. 8°C – forever

Table 2.5 Thermal cycling conditions used for amplification of DNA for Sanger sequencing.

2.1.3.9 Plasmid Gigapreps

Once it was confirmed that the plasmids were the correct sequence, plasmid preps were scaled up to gigapreps to produce large amounts of DNA for transfection. EndoFree plasmid Gigapreps (Qiagen, Manchester, UK) were carried out according to the manufacturer's protocol which can be found in Appendix B.3. Centrifugation steps were carried out using an Avanti J-26 XP high-speed centrifuge (Beckman Coulter, High Wycombe, UK).

2.2 Protein production

2.2.1 HEK293T cells

To produce FcγRIIa ectodomains with mammalian glycosylation, HEK293T cells (The Leibniz Institute DSMZ, Braunschweig, Germany) were used.

2.2.1.1 Cell culture

HEK293T cells were maintained in Dulbecco's Modified Eagle's Medium (DMEM) (Sigma-Aldrich, Haverhill, UK) + 10% foetal bovine serum (FBS) (Sigma-Aldrich, Haverhill, UK) at 37°C in 5% CO_2 in a humidified tissue culture incubator (product code MCO20AIC, Sanyo, Osaka, Japan) .

2.2.1.2 Transient transfection of HEK293T cells in roller bottles

To produce the soluble FcγRIIa ectodomain proteins, transient transfection was carried out according to the Oxford Protein Production Facility protocol (OPPF, Oxford, UK) [117]. Briefly, a whole 150 cm^2 tissue culture flask (Corning, Amsterdam, The Netherlands) was seeded into a 1700 cm^2 roller bottle (Corning, Amsterdam, The Netherlands), and these were maintained in 250 ml 10% DMEM at 37°C in 5% CO_2 for 3 days in the CELLROLL roller bottle unit (product number 10543452, Integra Biosciences, Thatcham, UK) at 1.5 RPM. On the day of transfection, the spent medium was removed, 200 ml of serum-free DMEM supplemented with 1x Serum Replacement Solution (PeproTech, London, UK), 1x Lipid Mixture solution (PeproTech, London, UK) and 10 ml/L Penicillin Streptomycin (Pen Strep) (Sigma-Aldrich, Haverhill, UK) was added before returning cells to the incubator for 10 mins In one sterile container, 100 ml serum-free DMEM and 2 mg of DNA were mixed together thoroughly and in a second sterile container 100 ml serum-free DMEM and 3.5 ml 1 mg/ml 0.22 μm filter sterilised polyethyleneimine (PEI) (Sigma-Aldrich, Haverhill, UK) were mixed thoroughly. The DNA and PEI solutions were then combined and incubated at room temperature for no longer than 10 mins, before adding 50 ml of transfection cocktail to each of the four roller bottles. These were then incubated for 5 days at 37°C in 5% CO_2.

2.2.1.3 Harvesting the protein

To harvest the secreted soluble FcγRIIa ectodomains, media were collected from the roller bottles and centrifuged at 6000xg for 5 mins to remove any cells, using an Eppendorf 5810 R centrifuge (Eppendorf, Stevenage, UK). The supernatant was filtered through a sterile 0.45 μm bottle top filter

system (Corning, Amsterdam, The Netherlands) and stored at 4°C with 0.01% sodium azide (Sigma-Aldrich, Haverhill, UK) until purification.

2.2.1.4 Purification

To purify the soluble His-tagged ectodomain protein, a 2-step purification was carried out. Initially, an IgG-sepharose column was used followed by His-tag purification.

2.2.1.4.1 IgG sepharose

IgG Sepharose 6 Fast Flow (GE Healthcare, Buckinghamshire, UK) was packed into a Proteus 5 ml FliQ Column (Generon, Slough, UK) according to the manufacturer's instructions. This was attached to an ÄKTA Fast Protein Liquid Chromatography (FPLC) system (GE Healthcare, Buckinghamshire, UK). The column was first washed with 3 column volumes of 0.5 M acetic acid (Acros Organics, Geel, Belgium) pH 3.4 at 2 ml/min, followed by 3 column volumes of Tris-saline-tween (TST) pH 7.6 (2 ml/min). This was repeated until a UV and pH plateau was observed. The filtered tissue culture medium containing the secreted soluble protein was then loaded onto the column at 1 ml/min. This was then washed with TST pH 7.6 for 10 column volumes at 1 ml/min, and then 5 mM ammonium acetate (Alfa Aesar, Heysham, UK) pH 5 at 1 ml/min. A single step elution was then carried out using 0.5 M acetic acid pH 3.4, and 0.5 ml fractions were eluted into 1 ml of 1 M Tris-HCl, pH 8.0 to neutralise.

2.2.1.4.2 His-trap

To further purify the protein, HisTrap HP columns pre-packed with Nickel Sepharose were used (GE Healthcare, Buckinghamshire, UK). This was again attached to an ÄKTA FPLC system (GE Healthcare, Buckinghamshire,

UK), and flushed out with 5 column volumes of MilliQ H_2O (1 ml/min). The column was then washed with 5 column volumes of wash buffer (10 mM sodium phosphate, 500 mM NaCl pH 7.4) at 1 ml/min. The fractions from the IgG sepharose purification were combined and loaded onto the column at 1 ml/min. The column was again washed with wash buffer for 20 column volumes (1 ml/min) before eluting in elution buffer (10 mM sodium phosphate, 500 mM NaCl. 500 mM Imidazole pH 7.4). Following purification, the protein was buffer exchanged into PBS using Zeba™ Spin 0.5 ml desalting columns, 7k MWCO (ThermoFisher Scientific, Altrincham, UK) following the manufacturer's protocol (Pub. No. MAN0015751). The protein was then concentrated using Vivaspin™ 20, MWCO 10,000 protein concentrator spin columns (GE healthcare, Buckinghamshire, UK). The manufacturer's protocol was followed (Instructions 28-9331-02 AB).

2.2.2 HEK293S GnTI- cells

In order to aid crystallisation of the FcγRIIa ectodomains, protein was produced with truncated sugars. To do this, HEK293S GnTI- cells were used (The Leibniz Institute DSMZ, Braunschweig, Germany).

2.2.2.1 Cell culture

HEK293 GnTI- cells were maintained in Dulbeccos's Modified Eagle's Medium: Nutrient Mixture F-12 (DMEM/F12) (Gibco, Loughborough, UK) + 10% FBS (Sigma-Aldrich, Haverhill, UK) at 37°C in 5% CO_2. Antibiotics were not used in maintenance cultures. This ensured no low-level contaminant was present.

2.2.2.2 Transfection screen

To determine the best conditions for protein production in GnTI- cells, a transfections screen was carried out. 0.1 x 10^6 cells were seeded into each well of a 12-well plate (Corning, Amsterdam, The Netherlands) and grown for 2 days until 80-90% confluent. On the day of transfection, the medium was removed and 1 ml of 2% DMEM/F12 was added. Transfection mixtures were made with an increasing ratio of PEI to DNA, as seen in Table 2.6.

These were made up by adding DNA to serum free DMEM/F12, before adding PEI and pulse vortexing. The mixtures were incubated for 10 mins at room temperature before adding to the cells in the 12-well plates A negative control was also set up, with no DNA. Cells were incubated for 2-3 days, before collecting the tissue culture media and analysing via western blot to determine the best expression conditions.

DNA:PEI		DNA (1 mg/ml)	PEI (1 mg/ml)	Serum-free DMEM/F12
1 µg DNA	1:1	1 µl	1 µl	500 µl
	1:2	1 µl	2 µl	500 µl
	1:3	1 µl	3 µl	500 µl
	1:4	1 µl	4 µl	500 µl
	1:5	1 µl	5 µl	500 µl
2 µg DNA	1:1	2 µl	2 µl	500 µl
	1:2	2 µl	4 µl	500 µl
	1:3	2 µl	6 µl	500 µl
	1:4	2 µl	8 µl	500 µl
	1:5	2 µl	10 µl	500 µl
Negative		0 µl	3 µl	500 µl

Table 2.6 The different amounts of DNA and PEI added to the transfection mixtures.

To determine the optimal transfection conditions, Sodium dodecyl sulfate–polyacrylamide gel electrophoresis (SDS-PAGE) and western blotting was carried out.

2.2.2.3 Sodium dodecyl sulfate–polyacrylamide gel electrophoresis

A total of 20 µl of samples were mixed with 4 µl 6X SDS sample buffer. For the ectodomain proteins, 5% (v/v) β-mercaptoethanol was added and the

samples heated for 3 mins at 95°C. For full-length proteins, samples were incubated at room temperature for 10 mins. If whole cell samples were being used, cells were resuspended in 1x phosphate buffered saline (PBS) containing cOmplete™ Protease Inhibitor Cocktail tablets (Merck, Watford, UK) and sonicated for 10 seconds before adding 6X SDS buffer. 20 µl of each sample was then loaded onto a 12-well pre-cast 12% polyacrylamide gel (Bio rad Laboratories, Watford, UK) with 5 µl BLUeye Prestained Protein Ladder (Sigma-Aldrich, Haverhill, UK) and run in Tris-glycine-SDS buffer for 1 hour at 150V, using a PowerPac™ Basic power supply (Bio rad laboratories, Watford, UK) electrophoresis system.

2.2.2.4 Western blot

The gel was then transferred onto a 0.45 µm polyvinylidene fluoride (PVDF) membrane (GE Healthcare, Buckinghamshire, UK) which had been pre-wetted in 100% methanol for 20 seconds, dH_2O for 5 mins and then equilibrated in transfer buffer. A transfer sandwich was built and transfer carried out at 4°C for 60 mins at 40V using an XCell II™ Blot Module (Invitrogen, Loughborough, UK). The membrane was then blocked in 5% (w/v) bovine serum albumin (Sigma-Aldrich, Haverhill, UK) for 1 hour at room temperature, before adding the primary antibody (Anti-6X His tag® antibody [HIS.H8]; Abcam, Cambridge, UK) at a dilution of 1:1000. This was incubated overnight at 4°C on a tube roller (33rpm), and then washed in Tris-buffered saline with Tween-20 (TBS-T) 3 times for 5 mins. Fresh TBS-T was then added and the secondary antibody (horseradish peroxidase [HRP]-conjugated polyclonal rabbit anti-mouse [P0161]; Agilent, Edinburgh, UK) added in a dilution of 1:10,000. This was incubated for 1 hour at room temperature before washing in TBS-T 5 times for 5 mins. Amersham ECL

Western Blotting Detection Reagent (GE healthcare, Buckinghamshire, UK) was added and the membrane was imaged using ImageLab software and a Bio rad gel doc system (Bio rad Laboratories, Watford, UK).

2.2.2.5 Scale-up to roller bottles

Once the optimal conditions were determined by western blot, this was scaled up to 1700 cm^2 roller bottles using the following calculations:

12-well plate surface area = 4 cm^2

Roller bottle surface area = 1700 cm^2

1700/4 = 425

The best conditions were 1:2 ratio of DNA:PEI with 2 µg of DNA:

2 µg x 425 = 850 µg DNA per roller bottle

1700 µg PEI per roller bottle (1.7 mg)

The roller bottles had 425 times more surface area than a 12-well plate; therefore, everything was scaled up by a factor of 425. Consequently for 4 roller bottles, the following protocol was carried out. A confluent T150 flask of GnTI- cells, containing ~1.5 x 10^7 cells, was seeded into each of the roller bottles, and grown for 3-4 days in 10% DMEM/F12. On the day of transfection, medium was removed and 200 ml of 2% DMEM/F12 containing pen/strep was added to each roller bottle. In one sterile container, 100ml serum-free DMEM/F12 and 3.4 mg of DNA were mixed together thoroughly and in a second sterile container 100 ml serum-free DMEM/F12 and 6.8 ml of 1 mg/ml PEI were mixed thoroughly by swirling the mixture. The DNA and

PEI solutions were then combined and incubated at room temperature for 10 mins, before adding 50ml of transfection cocktail to each of the four roller bottles. These were then incubated for 5-7 days at 37^{o}C in 5% CO_2.

2.2.2.6 Harvesting the protein

To harvest the secreted soluble FcγRIIa ectodomains, the medium was collected from the roller bottles and centrifuged at 6000xg for 5 mins to remove any cells using an Eppendorf 5810 R centrifuge (Eppendorf, Stevenage, UK). The supernatant was filtered through a sterile 0.45 µm bottle top filter (Corning, Amsterdam, The Netherlands) and stored at 4°C until purification.

2.2.2.7 Purification

Proteins produced in the HEK293S GnTI- cells were purified using a 2-step purification, as previously described in section 2.2.1.4.2. However, as these proteins had truncated sugars, binding to IgG was less stable, so the protocol previously described was modified slightly.

2.2.2.7.1 IgG sepharose

Protein produced in GnTI- cells was first purified using a 5mL IgG sepharose column. The column was first washed with 3 column volumes of 0.5 M acetic acid pH 3.4 (2 ml/min), followed by 3 column volumes of TST pH 7.6 (2 ml/min). This was repeated until a UV and pH plateau was observed. The filtered tissue culture medium containing the secreted soluble protein was then loaded onto the column at 1ml/min. This was then washed with TST pH 7.6 for 10 column volumes at 1 ml/min. The protein was first eluted using 5 mM ammonium acetate (Alfa Aesar, Heysham, UK) pH 5.0, then a further

elution step was carried out with 0.5 M Acetic Acid (Acros Organics, Geel, Belgium) pH 3.4.

2.2.2.7.2 Coomassie

To confirm that both elution peaks contained protein, a denaturing coomassie gel was done. First, the protein was ran on an SDS-PAGE gel as previously described. To stain for protein using Coomassie blue, the protein gel was first incubated for 10 mins in rapid fix buffer containing 25% (v/v) isopropanol and 10% (v/v) ethanol. The gel was then left to stain for 2 hours in a coomassie staining solution containing 10% (v/v) acetic acid (Acros Organics, Geel, Belgium) and 0.006% (v/v) coomassie blue R-250 (BDH Limited, Poole, England). To de-stain, the gel was then incubated with de-stain solution overnight, containing 10% (v/v) acetic acid (Acros Organics, Geel, Belgium).

2.2.2.7.3 His-trap

Fractions were collected and then combined before further purifying using a His-trap, as previously described. The protein was then buffer exchanged into 75 mM NaCl, 5 mM Tris-HCl pH 7.4 and concentrated.

2.2.3 sf9 cells

In order to express the full-length FcγRIIa protein, *Spodoptera frugiperda* (sf9) cells were used (European Collection of Authenticated Cell Cultures, Sailsbury, UK).

2.2.3.1 Cell culture

Sf9 insect cells were maintained at $1x10^6$ cells/ ml in Insect-XPRESS™ Protein-free Insect Cell Medium with L-glutamine (Lonza, Castleford, UK) in

shake-flask cultures at 27°C, 37% CO_2 in a shaking tissue culture incubator (product code M1282-0000, New Brunswick Scientific, Stevenage, UK).

2.2.3.2 Production of Bacmid DNA

All centrifugation steps were carried out using an Eppendorf 5415 D benchtop centrifuge (Eppendorf, Stevenage, UK). pFastBac vectors containing full-length *FCGR2A* were transfected into DH10EmBacY cells by heat shock at 42°C, then incubated for a minimum of 8 hours at 220 RPM 37°C in LB-broth. This was then plated onto LB-Agar plates containing Kanamycin (50 µg/ml), Tetracyline (10 µg/ml), Gentamycin (7 µg/ml), IPTG (40 µg/ml) and X-Gal (100 µg/ml) (Sigma-Aldrich, Haverhill, UK) and incubated at 37°C for a further 24 hours. To ensure only colonies containing the plasmid were selected, blue-white selection was carried out to confirm the phenotype. Starter cultures were then grown from white colonies only, in LB containing the same antibiotics, overnight at 220 RPM, 37°C. For each allotype, 2 colonies were picked and 2 plasmid preps made.

To purify the Bacmid DNA from these cultures, a PureLink™ HiPure Plasmid Miniprep Kit (Invitrogen, Loughborough, UK) was used, but slight modifications were carried out to protect the Bacmid DNA. Briefly, cultures were centrifuged for 10 mins at 2900xg, supernatant discarded and the pellet resuspended in 300 µl resuspension buffer. 300 µl lysis buffer was then added and the tube inverted several times, very slowly to gently mix. This was incubated for no longer than 5 mins before adding 300 µl of neutralisation buffer. The tube was again inverted very slowly and gently several times to mix. This was then centrifuged 25,000xg for 10 mins at room temperature. The supernatant was then transferred to a fresh 1.5 ml

eppendorf in one clean pipette shot, before centrifuging for 25,000xg for 5 mins. Again, in one clean pipette shot the supernatant was transferred to a new 1.5ml eppendorf and 0.7 volumes of isopropanol were added to a final concentration of 40% (v/v). This was inverted very gently and slowly to mix, before centrifuging at 25,000xg for 10 mins to create a transparent DNA pellet. Isopropanol was removed without disturbing the pellet, and 70% ethanol added very gently to wash. This was centrifuged again at 25,000xg for 5 mins, then the supernatant removed and the pellet left to air dry for 10 mins before resuspending in 30 µl MilliQ.

2.2.3.3 Transfection

Sf9 cells were seeded into a 6-well plate at a concentration of $1x10^6$ cells per well, and settled to allow a monolayer culture to develop. These were then transfected with the Bacmid DNA using X-TremeGENE HP DNA (Roche, Basel, Switzerland) as a transfection reagent. The transfection reagent was diluted 1:10 with medium, and in a separate eppendorf 20 µl of each Bacmid was mixed with 200 µl of medium. These were then combined and incubated for no longer than 30 mins at room temperature, before adding 150 µl of the mix to each well. Cells were then incubated at 27°C for 60 hours before collecting the supernatant (V0) to store at 4°C. This was replaced with fresh medium, and incubated for a further 60 hours. Cells were then harvested and a western blot carried out to check for protein expression and to determine which of the 2 plasmid preps for each allotype produced the most protein.

2.2.3.4 Virus amplification

Sf9 cells in suspension at a density of $1x10^6$ cells/ml were infected with virus collected at V0. Cell growth was monitored daily, to determine when proliferation arrest (PA) occurred and to ensure density was maintained at $1x10^6$ cells/ml. On the day after proliferation arrest (DPA) V1 was harvested by spinning the cells at 250xg in an Eppendorf 5810 R centrifuge (Eppendorf, Stevenage, UK) and collecting the supernatant. Samples of cells from the DPA+24h, DPA+48h and DPA+72h were collected to run on a western blot to check expression of FcγRIIa. A timeline of the amplification process can be seen in Figure 2.3.

2.2.3.5 Titre test

To determine the optimal amount of V1 needed to cause proliferation arrest 24 hours after infection, a titre test was carried out. This was done by infecting cells with different amounts of V1 and monitoring the cell growth every 24 hours. The volume of V1 which allowed the cells to double once in 24h then stop dividing was chosen.

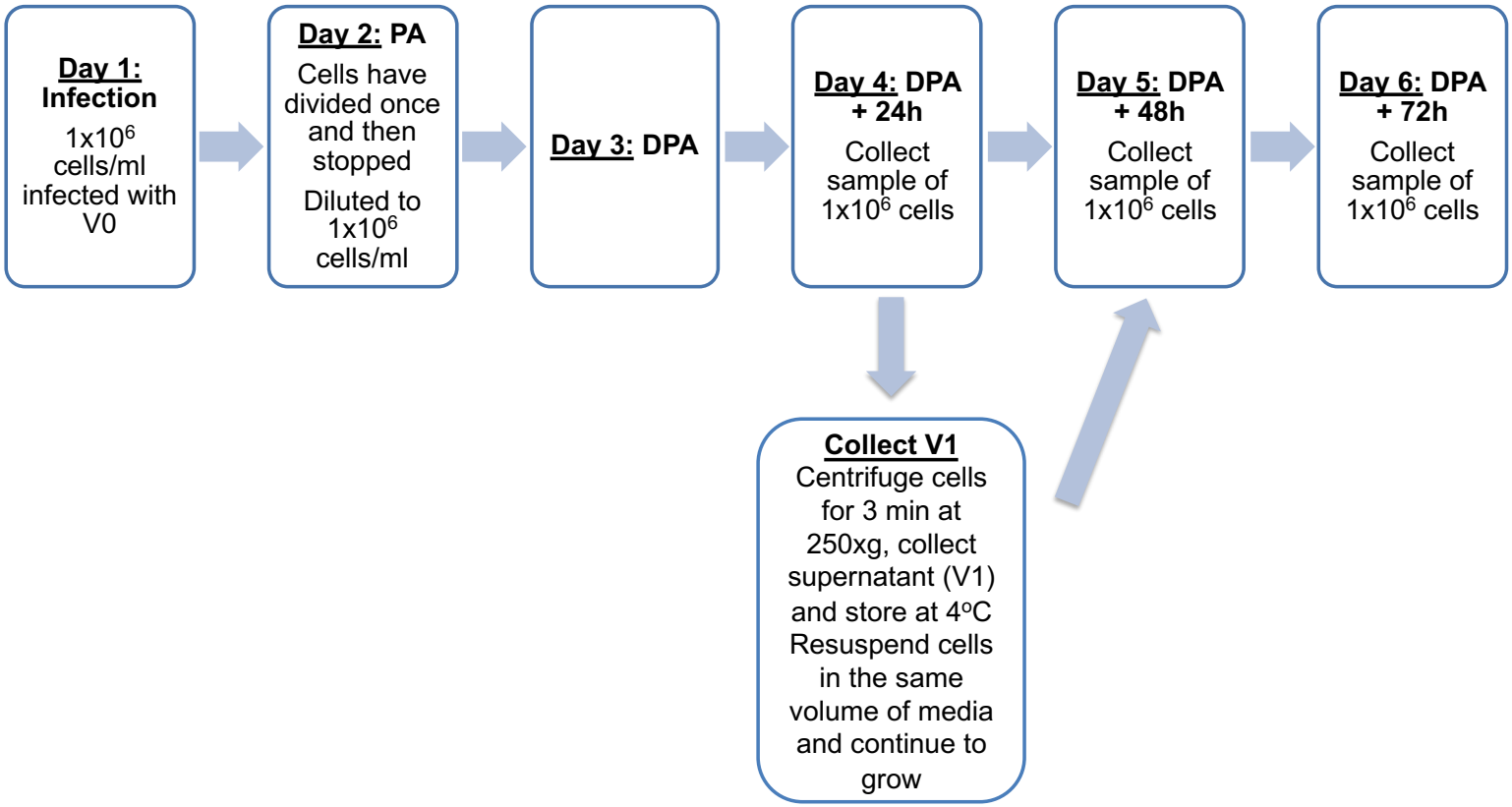

Figure 2.3 The timeline of the baculovirus amplification process.

On day 4 (DPA + 24) V1 was collected and stored for future use.
DPA, day after proliferation arrest; PA, proliferation arrest.

2.3 LigandTracer

2.3.1 Protocol development

As the LigandTracer technology (Ridgeview AB, Uppsala, Sweden) was in its infancy, substantial optimisation was needed to develop a standard protocol. This was initially done using HEK293 cells stably expressing full-length FcγRIIa, which were produced by Dr Euan Baxter (senior post-doc, Morgan Lab).

2.3.1.1 Immunofluorescence of HEK293 cells stably expressing FcγRIIa

To confirm that the stably transfected HEK293 cells were expressing FcγRIIa, immunofluorescence (IF) was carried out. Glass coverslips (22x22 mm, 0.13-0.17 mm thickness) were sterilised with 100% ethanol, before placing into each well of a 6-well plate. 1 ml of HEK293 cells stably expressing FcγRIIa were then seeded into each well at $2x10^4$/ml before incubating for 48 hours at 37°C, 5% CO_2. Un-transfected HEK293 cells were also used as a control. Once the cells were confluent on the coverslip, the coverslips were incubated in cold methanol at -20°C for 20 mins, then washed with PBS before blocking in 5% (w/v) Marvel in dH_2O for 1 hour at room temperature. Both 4',6-diamidino-2-phenylindole (DAPI) (Invitrogen, Loughborough, UK) and fluorescein isothiocyanate conjugated anti- human CD32 3D3 (FITC-3D3) (BD Biosciences, Berkshire, UK) were then added in 5% Marvel (Premier Foods, Hertfordshire, UK) and incubated for 1 hour at RT in the dark. The coverslips were then washed in PBS three times before drying, then fixing to glass slides with Mowiol 4-88 (Merck, Watford, UK). The cells were then imaged on a Nikon TiE microscope and images captured with a Nikon DS-QiMc camera (Nikon, Surrey, UK).

2.3.1.2 Labelling IV.3 with FITC

Anti-human-CD32 (clone IV.3) (BioXcell, NH, USA) was labelled with FITC.

For labelling, FITC (Sigma-Aldrich, Haverhill, UK) was dissolved in DMSO (Sigma-Aldrich, Haverhill, UK) to 1 µg/µl. The antibody, which was resuspended in PBS, was then diluted in double the volume of 50 mM borate buffer pH 9, and for every 1 µg antibody 100 ng FITC was added. The reaction was incubated at 37°C for 90 mins, and labelled antibody was purified through an NAP-5 column (GE Healthcare, Buckinghamshire, UK) by gravity flow. These are disposable columns prepacked with Sephadex™ G-25 DNA Grade, which allows buffer exchange to be carried out and hence the removal of excess dye. Labelled antibody was stored at −20°C in PBS pH 7.40 until usage.

2.3.1.3 Cell attachment optimisation

All imaging was done on an EVOS XL Core imaging system (Invitrogen, Loughborough, UK).

2.3.1.3.1 Natural HEK293 adhesion

As HEK293 cells are naturally weakly adherent cells, plates for use on the Ligand Tracer were initially set up according to the Ligand Tracer 'Seeding cells for LigandTracer®' protocol [118]. Briefly, HEK293 cells were detached with trypsin-EDTA (Sigma-Aldrich, Haverhill, UK) and resuspended in 10% DMEM. $2x10^6$ cells were then placed on a spot of a Nunc™ Cell Culture plate (ThermoFisher Scientific, Altrincham, UK), and left to adhere at 37°C, 5% CO_2 for 5 hours. The excess cell suspension was then removed and 10 ml 10% DMEM added to the plate before incubating overnight at 37°C, 5%

CO_2. Cells were then imaged on the EVOS and then run for 30 mins on the Ligand Tracer before imaging again.

2.3.1.3.2 Fibronectin

In total, 350 µl of 2 µg/ml Fibronectin in PBS was added to 2 spots of a Nunc™ Petri dish (ThermoFisher Scientific, Altrincham, UK) and incubated at room temperature for 1 hour. The excess solution was then removed, and 1ml cells at $2.5x10^6$ in 10% DMEM were then seeded into each well and incubated for 24 hours at 37°C, 5% CO_2.

2.3.1.3.3 Glass coverslips

Glass coverslips (22x22 mm, 0.13-0.17 mm thickness) were sterilised in 100% ethanol, then washed in PBS before placing in to each well of a 6-well plate (Corning, Amsterdam, The Netherlands). 1 ml cells at $2.5x10^6$ in 10% DMEM were then seeded into each well and incubated for 24 hours at 37°C, 5% CO_2. The coverslips with cells adhered to them were then glued to a Nunc™ Petri dish (ThermoFisher Scientific, Altrincham, UK) for use in the Ligand Tracer.

2.3.1.3.4 NHS-EDC

0.2 M 1-Ethyl-3-(3-dimethylaminopropyl)-carbodiimide (EDC) and 0.5 M N-hydroxysuccinimide (NHS) solution was added to a spot of a Nunc™ Petri dish (ThermoFisher Scientific, Altrincham, UK) and incubated for 20 mins. The excess solution was then removed, and washed with PBS. $2.5x10^6$ cells in PBS were then added to the spot and incubated for 30 mins at 37°C, 5% CO_2. Excess cell solution was then removed, and 5 ml PBS added to the plate before imaging on the EVOS. The plate was then run on the Ligand Tracer for 30 mins before imaging again.

2.3.1.3.5 Biocompatible Anchor for Membranes

HEK293 cells stably expressing FcγRIIa were plated for use on the Ligand Tracer as described in [119], with un-transfected HEK293 cells used as a control. Briefly, 2 mg/ml Biocompatible Anchor Molecule (BAM; Figure 2.4) (OE-040CS; NOF Corporation, Tokyo, Japan) dissolved in MilliQ H_2O was pipetted onto two defined areas of a Nunc™ Petri dish (ThermoFisher Scientific, Altrincham, UK) in a 400 µl circular drop. This was incubated at room temperature for 2 hours. Cells were trypsinised and counted using a Countess™ Automated Cell Counter (Invitrogen, Loughborough, UK). Cells were then spun down at 125xg in an Eppendorf 5810 R centrifuge (Eppendorf, Stevenage, UK) and resuspended in PBS to a concentration of $6x10^6$ cells/ml. Excess BAM was removed before adding 400 µl of the cell suspension to the defined area (approx. $2.4x10^6$ cells per spot) and incubating a further 40 mins at room temperature. The remaining suspension was the removed and 10 ml of 10% (v/v) DMEM was added to whole petri dish to block. These were incubated overnight at 5% CO_2, 37°C.

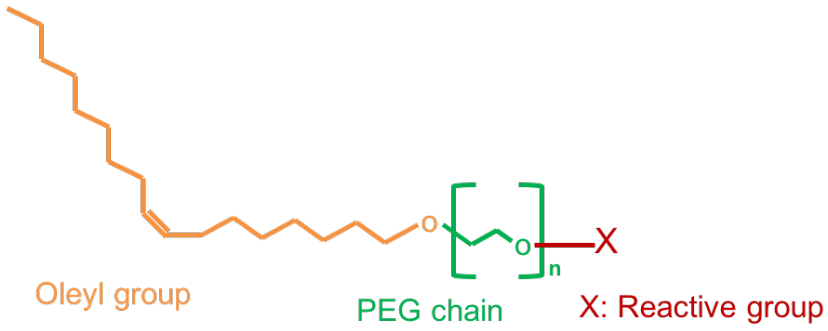

Figure 2.4 A schematic of the BAM molecule.

The oleyl group inserts into the cell membrane, the PEG chain acts as a linker, and the reactive group adsorbs to the petri dish. Redrawn from [120]
BAM, biocompatible anchor for membrane; PEG, polyethylene glycol.

2.3.1.3.5.1 Assessing cell viability with BAM

To ensure the cells were still viable after adhesion with the BAM, a viability assay was carried out by incubating the cells with 0.2% (v/v) trypan blue (Sigma-Aldrich, Haverhill, UK) for 1 min, before washing with PBS and imaging on the EVOS.

2.3.1.4 Assay run

The interaction between FITC labelled IV.3 and HEK293 cells expressing FcγRIIa was measured in real-time with LigandTracer Green (Ridgeview Instruments AB, Uppsala, Sweden) with the Blue-Green (488 nm-535 nm) detector. After overnight incubation with 10% (v/v) DMEM, the medium was removed and 3ml of fresh serum-free DMEM added. The plate was inserted into the LigandTracer instrument, and a baseline ran for 30 mins. After this, 3.75 nM of FITC labelled IV.3 was added, and the signal measured for 1 hour. A further 7.5 nM of ligand was then added (11.25nM total) and the signal measured for 45 mins. To measure the dissociation, the medium containing ligand was removed, and 3 ml fresh serum-free DMEM added before measuring the fluorescent signal for 1 hour.

2.3.2 Using sf9 cells on the LigandTracer

Once the adhesion protocol had been optimised using HEK293 cells, the protocol was then tested on sf9 cells in an attempt to produce higher signals. As the bacmid DNA contains the yellow fluorescent protein (YFP) gene, sf9 cells fluoresce YFP at 520-550 nm upon viral infection, the FITC system was not suitable. Therefore, the Red detector was used, which can measure wavelengths from 632-670 nm, and DyLight650 used as the fluorophore.

2.3.2.1 Labelling rituximab with DyLight650

To optimise the labelling of IgG with DyLight650, Rituximab, a therapeutic CD20 monoclonal antibody (mAb), was used due to large amounts being available. Surplus rituximab was kindly donated for laboratory use by Mark Stringer (Aseptic Services Manager at Leeds Teaching Hospitals NHS Trust). Rituximab was supplied at 10 mg/ml in a buffer made up of 9.0 mg/mL sodium chloride, 7.35 mg/mL sodium citrate dihydrate, 0.7 mg/mL polysorbate 80, and sterile water. As no sodium azide was present, buffer exchange into PBS was not necessary before labelling.

DyLight™ 650 NHS Ester (ThermoFisher Scientific, Altrincham, UK) was dissolved in Dimethylformamide (DMF) (Sigma-Aldrich, Haverhill, UK) to a concentration of 1µg/µl. 1mg of the antibody was diluted in double the volume of 50 mM borate buffer pH 9, and different amounts of DyLight650 added ranging from 1 µg to 50 µg. The reaction was incubated for 1 hour at room temperature in the dark, and excess dye removed using an NAP-5 column (GE Healthcare, Buckinghamshire, UK). Labelled antibody was stored at −20°C until usage. Assays were then run on the LigandTracer with the differentially labelled Rituximab using the red detector, to determine how much dye was needed to give the optimal signal with the least background signal. The optimal ratio of dye to protein was found to be 10 µg of DyLight650 per 1 mg of antibody.

2.3.2.2 Labelling monomeric IgG subclasses with DyLight650

IgG1-4 (The Binding Site, Birmingham, UK) were supplied at 1mg/ml in Tris buffered saline containing 0.099% Sodium Azide, 0.1% E-amino-n-caproic acid and 0.01% Benzamadine. As the buffer contained sodium azide, buffer exchange into PBS was first carried out using Zeba™ Spin 0.5 ml desalting

columns, 7k MWCO, then 100 µg of this was then mixed with 200 µl Borate buffer pH 9. DyLight650 NHS Ester was dissolved in DMF to a concentration of 1 µg/µl and 1 µg of this was mixed with 100 µg of the antibody, before incubating for 1 hour at room temperature. Excess dye was removed using a NAP-5 column (GE Healthcare, Buckinghamshire, UK) and the antibody eluted in PBS. Labelled antibody was then stored at −20°C until usage.

2.3.2.3 Sf9 cell attachment with Biocompatible Anchor for Membranes

To measure the interaction between FcγRIIa and different IgG subclasses, sf9 cells expressing FcγRIIa were used as the target cells, and uninfected sf9 cells used as the control cell line. Four cell patches were seeded per plate, to allow 3 different allotypes of FcγRIIa to be measured simultaneously (Figure 2.5).

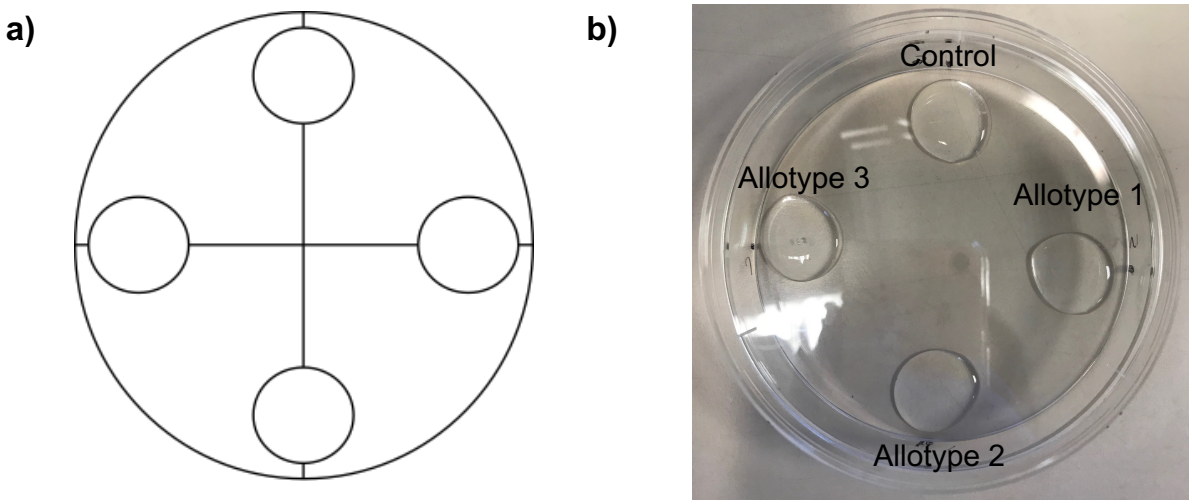

Figure 2.5 Layout of a LigandTracer plate.

a) The template used to seed sf9 cells on to the plate for Ligand Tracer experiments, to ensure cells were in the correct position. **b)** The 4 different sf9 cell patches on the plate.

Sf9 cells at $1x10^6$ cells/ml were infected with V1 to induce FcγRIIa expression. On day 2, the day of PA, they were diluted back to $1x10^6$ cells/ml and incubated for a further 24 hours, before adhering them to plates using BAM on DPA; 2 mg/ml BAM was dissolved in MilliQ H_2O and 350 µl pipetted onto four defined areas of a petri dish, using a template to ensure the cells were in the same position each time (Figure 2.5). This was incubated for 2 hours at room temperature. Cells were counted using a Countess™ Automated Cell Counter (Invitrogen, Loughborough, UK), ensuring viability was >95%. Cells were then centrifuged at 200xg (MODEL) before resuspending in Insect-XPRESS™ Protein-free Insect Cell Medium with L-glutamine (Lonza, Castleford, UK). Excess BAM was removed before adding 350 µl of the cell suspension to the defined area (approx. $2x10^6$ cells per spot) and incubating a further 1 hour at room temperature. The remaining suspension was the removed and 10ml of Insect-XPRESS medium + 5% BSA with 1x Antibiotic-Antimycotic (Penicillin, Streptomycin and Amphotericin B) (Gibco, Loughborough, UK) was added to whole petri dish to block. These were incubated overnight at 5% CO_2, 27°C. A schematic of the cell attachment process is shown in Figure 2.6 and the timeline of the cell attachment shown in Figure 2.7.

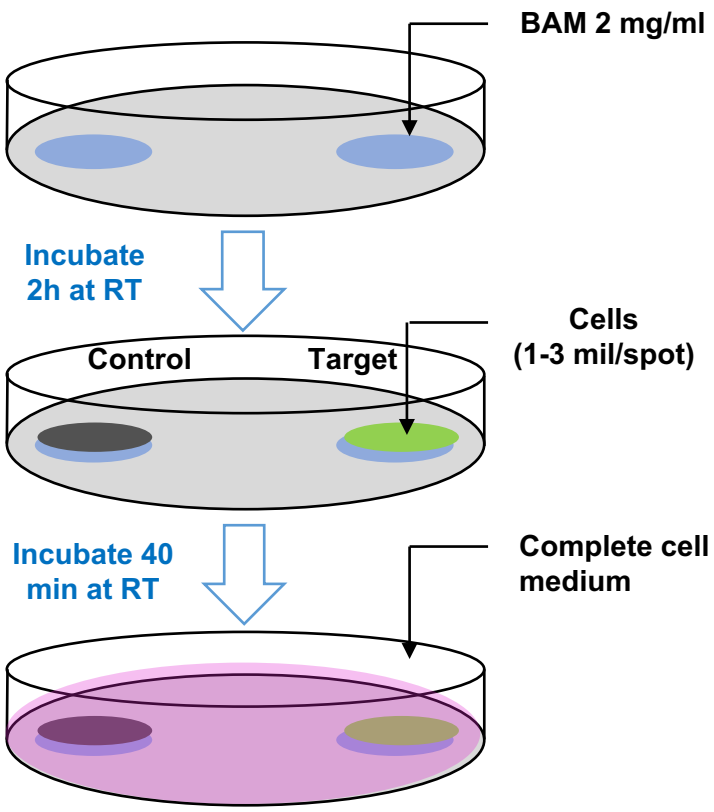

Figure 2.6 Schematic showing how to adhere cells for LigandTracer assays.

Different cells are adhered in defined areas opposite each other on a Petri dish using BAM. Redrawn from Bondza, et al. [119].
BAM, Biocompatible anchor for membranes; PBS, phosphate buffered saline; RT, room temperature.

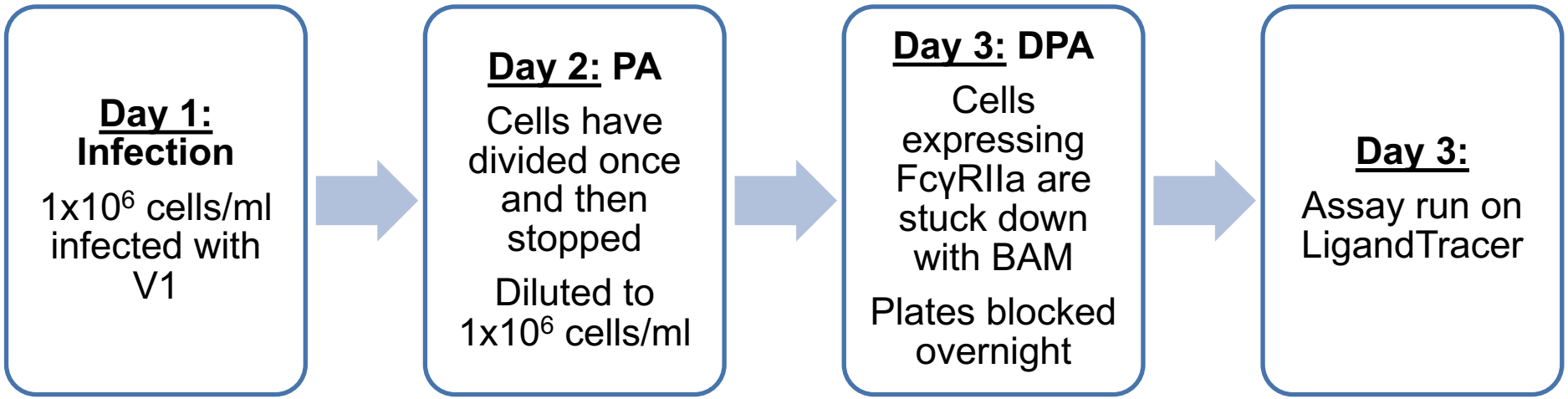

Figure 2.7 Timeline of setting up a LigandTracer assay using sf9 cells infected with baculovirus.

Cells are infected on day 1, and stuck down with BAM on day 3 before running the assay on day 4. BAM, biocompatible anchor for membranes; DPA, day after proliferation arrest; PA, proliferation arrest.

2.3.2.4 DNA extraction and sequencing

To ensure the sf9 cells infected with virus were expressing the correct allotype of FcγRIIa, DNA extraction and sequencing was carried out. DNA extraction was carried out using a Qiagen DNeasy Blood & Tissue Kit (Qiagen, Manchester, UK) according to the manufacturer's protocol which can be found in the appendix (Appendix B.4). To amplify *FCGR2A*, a PCR reaction was carried out using primers shown in Table 2.7 (previously designed by Dr Jim Robinson). Sanger sequencing was then carried out on the amplified DNA as previously described, using the same primers in separate reactions.

2A e1F primer	5' CCA GAA ACC TGT GGC TGC TTC 3'
2A e7R primer	5' GAG TCA TGT AGC CGC CGT CAG 3'

Table 2.7 Primers used to amplify and sequence the DNA extracted from sf9 cells expressing FcγRIIa.

2.3.2.5 Assay run using sf9 cells

The interaction between DyLight650-labelled IgG subclasses and sf9 cells expressing FcγRIIa was measured in real-time with LigandTracer Green (Ridgeview Instruments AB, Uppsala, Sweden) with the Red (632 nm) to near infrared (670 nm) detector.

After overnight incubation, Insect-cell Xpress + 5% BSA + AA was removed, and 3 ml of fresh Insect-XPRESS medium added to the plate. The plate was inserted into the LigandTracer instrument, and a baseline ran for 15 mins. After this, 15 nM of DyLight650-labelled IgG was added, and the signal measured for 20 mins. A further 30 nM of ligand was then added (45 nM total) and the signal measured for 1 hour. To measure the dissociation, the medium containing ligand was removed, and 3 ml fresh medium added and the signal measured for a further hour. The instrument settings used were a 10 second read time, and a 5 second delay time, allowing each point to be measured every 60 seconds.

2.3.2.6 Kinetic fitting

All kinetic analysis was carried out by Sina Bondza at Ridgeview Diagnostics, Upsala, Sweden.

2.3.2.6.1 TraceDrawer

After each assay was done in triplicate, individual kinetics were fitted and averages of the kinetic values calculated. The traces were fitted to kinetic models using the TracerDrawer software, and either a ‘one-to-one’ or a ‘one-to-two’ fit with concentration dependent bulk index (BI) was used. This accounts for any small signal jumps which occur on addition or removal of the fluorescent ligand which are attributable to technical rather than biological interactions.

2.3.2.6.2 Interaction Map

Interaction Map analysis was carried out by Sina Bondza. Interaction Map allows complex interactions to be fitted, without the need for any hypothesis of the type of interaction. Interaction Map fits each individual interaction from

a complex interaction to a one:one model, and the overall curve will be a sum of all of these one:one interactions [121].

2.3.2.7 Statistics

To determine whether the differences in kinetics between the FcγRIIa allotypes were significant, a two-sample t-test assuming unequal variance was carried out in excel, followed by Bonferroni correction. A value of $p < 0.05$ was considered to be statistically significant.

2.4 Surface plasmon resonance

All surface plasmon resonance (SPR) assays were carried out using a BIAcore T200 (Biomolecular Interaction Analysis, GE Life Sciences, Buckinghamshire, UK).

The BIAcore chip used was a CM5 chip (GE Life Sciences, Buckinghamshire, UK), a gold surface coated with carboxymethylated dextran. An anti-His antibody (GE Life Sciences, Buckinghamshire, UK) was then amine coupled to the dextran and the ectodomain proteins of the different variants of the His-tagged FcγRIIa receptors were captured onto the chip via this antibody (Figure 2.8) by flowing the protein at 1 μg/ml over the flow cell for 60 s at 5 μl/min. As the anti-his antibody was amine coupled to the chip via its Fc region, it prevented FcγRIIa from non-specifically binding to this antibody. Different analytes were then flowed over the receptors in serial dilutions ranging from 187.5 nM to 3000 nM, using single-cycle kinetics and PBS-P+ as a running buffer. These analytes included monomeric IgG1- 4 subclasses (The Binding Site, Birmingham, UK), which were injected at a rate of 30 μl/min for 60 s. A reference cell was also set up containing the receptor coupled to the anti-His antibody, with no IgG; the

response from this cell was then subtracted from the sample flow cells in order to account for the bulk refractive index change, a method known as double referencing. Raw SPR sensograms are displayed in Figure 2.9.

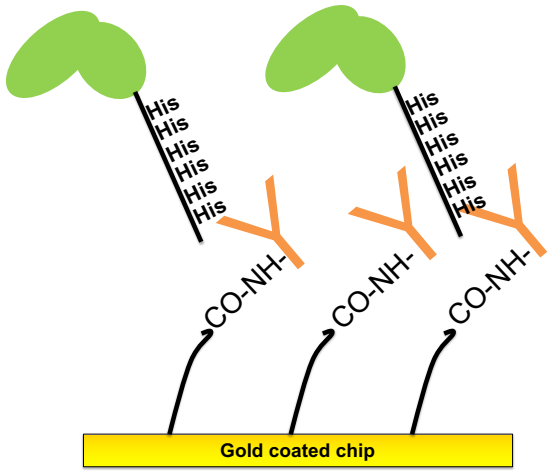

Figure 2.8 Schematic showing immobilisation of FcγRIIa receptor ectodomain onto a Gold coated chip via an anti-His antibody. The anti-His antibody was attached to the chip via amine-coupling.

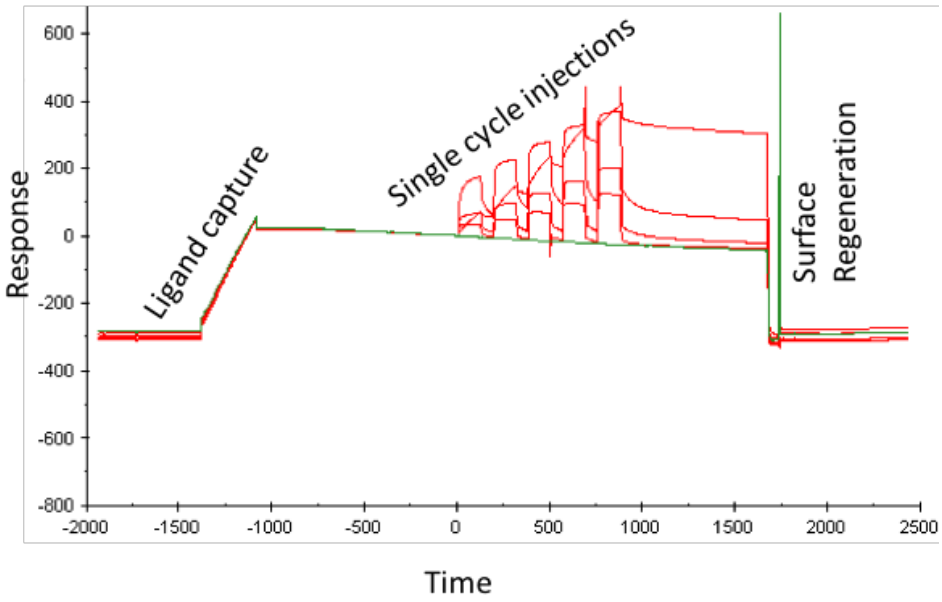

Figure 2.9 Raw surface plasmon resonance sensograms.

FcγRIIa is captured on the chip surface (ligand capture), injections of IgG at increasing concentrations (single cycle kinetic analyte injection) and finally the removal of FcγRIIa from the chip (surface regeneration). Red, sensograms for IgG subclasses 1-4 binding to FcγRIIa; Green, sensogram for the reference cell buffer only, no IgG).

2.5 Size Exclusion Chromatography with Small-angle x-ray scattering

To try and determine the oligomeric state and structure of FcγRIIa, size-exclusion chromatography with small-angle x-ray scattering (SEC-SAXS) was carried out on the 27Q-131H allotype (3.7 mg/ml) and the 27Q-131H S126P monomeric control (2.9 mg/ml). First, the proteins (in PBS pH 7.4) were separated using a Superdex75 5/150 column, at 1 ml/min flow rate using a matched buffer (PBS pH 7.4) as the running buffer. SAXS data were then collected on the B21 SAXS beamline at Diamond Light Source, at 298 K (25°C).

Following data collection, *ab initio* modelling was carried out using DAMAVER [122]. To compare the *ab initio* models between the two proteins, SUPCOMB [123] was used to overlay them. Visualisation was carried out in PyMol.

2.6 Size Exclusion Chromatography with Multi-Angle Laser Light Scattering on FcγRIIa ectodomains

Size Exclusion Chromatography with Multi-Angle Laser Light Scattering (SEC-MALLS) is a method used to determine the absolute molecular weight of a protein, regardless of the protein shape. It works by separating proteins using size-exclusion chromatography, then measuring the light scattering profile of the protein, along with the refractive index (RI) and the UV absorbance. SEC-MALLS can be used to determine the oligomeric state of a protein in solution, and the amount of protein glycosylation [124].

The gel filtration column used was a Superdex-75 5/150 with a separation range of 3,000 to 70,000 Mr (GE Healthcare, Buckinghamshire, UK). The

column was flushed overnight with PBS running buffer containing 0.02% (V/V) sodium azide (Sigma-Aldrich, Haverhill, UK). The different allotypes of the soluble receptor ectodomain proteins were filtered to remove any large aggregates and then injected onto the column at 0.3 ml/min. The proteins were separated by size, and then a series of parameters measured including UV absorbance, refractive index and light scattering using a SEC-MALS-QELS system. This is made up of a DAWN HELEOS 1184 H28 multi-angle static light scattering detector, a Wyatt QELS+ dynamic light scattering detector, and a Wyatt T-rEx 825 differential refractive index detector [125]. From this an elution profile was produced and the molecular weight could be deduced using the ASTRA light scattering software (all SEC-MALLS equipment and software from Wyatt Technology, Haverhill, UK).

2.7 Crystallography of 27W-131H ectodomain

For crystallisation of the ectodomain, protein produced in HEK293S GnTI- cells was used.

2.7.1 Protein preparation

Buffer exchange into 75 mM NaCl, 5 mM Tris-HCl pH 7.4 was carried out after purification, and the protein concentrated to 8 mg/ml.

2.7.2 Initial crystallography condition screening

Crystallisation trials were set up using the JSCG Core Suites I, II, III and IV (Qiagen, Manchester, UK). Crystallisation drops were set up as sitting drops using the NT8® crystallisation robot (Formulatrix, MA, USA) mixing 100 nl of protein at 8 mg/ml (100 ng total) in a 1:1 ratio with crystallisation solution from the JSCG Core Suites. Plates were incubated at 20°C and images

taken at different time intervals using the ROCKIMAGER® 1000 system (Formulatrix, MA, USA) to monitor crystal formation. At time 5d+ 12hours, an Ultraviolet Two-Photon Excited Fluorescence (UV-TPEF) image was taken to allow discrimination between protein and non-protein crystals.

2.7.3 Optimisation screens

Once a condition was identified that gave good crystals, an optimisation screen around these conditions was carried out. To create the optimisation screen, the FORMULATOR®, (Formulatrix, MA, USA) was used to generate 96 different conditions around the initial condition. For the *FCGR2A* 27W-131H ectodomain allotype, an optimisation plate was set up as seen in Figure 2.10. The buffer concentration was kept constant (0.1 M sodium phosphate citrate), whilst varying the concentration of polyethylene glycol 300 (PEG 300) (MolecularDimensions, Newmarket, UK) from 30% to 50% and varying the pH from pH 4 to pH 5. Plates were incubated at 20°C and imaged as above.

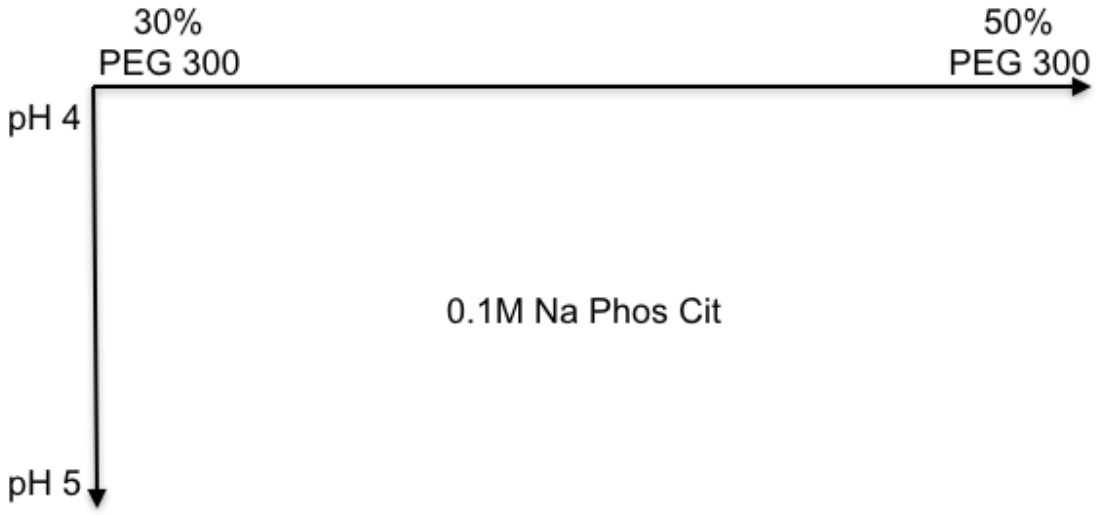

Figure 2.10 The conditions used in the optimisation plate for crystallisation of the 27W-131H ectodomain.

The concentration of PEG 300 was varied from 30%-50% (v/v) and the pH varied from pH4-pH5. The concentration of sodium phosphate citrate was kept constant at 0.1 M.

2.7.4 Crystal freezing

Crystals were mounted into cryo-loops and immediately frozen in liquid nitrogen, without any cryoprotectants. Crystals were then stored in pucks in a liquid nitrogen dewar, until being shipped to Diamond Light Source (Oxford, UK) for data collection.

2.7.5 Data collection

Data were collected remotely at Diamond Light Source, Beamline I04. 600 images were taken in total with an oscillation range of 0.30° per image, at a wavelength of 0.9795 Å and exposure time of 0.040 s. Transmission was set at 10.41% and the beam size was 32x20 µm.

2.7.6 Refining the model

All diffraction data were indexed and integrated using X-ray Detector Software (XDS; Max Planck Institute for Medical Research, Heidelberg, Germany) [126] and scaled using AIMLESS [127]. Molecular replacement was carried out using PHASER [128], using a re-refined version of PDB 3RY4 as a template. Refinement was carried out using PHENIX [129]. Ligands and sugar modifications were built manually into F_o-F_c maps using COOT [130] and the quality of the protein structure was assessed using MolProbity. MolProbity is structure validation web service for macromolecular crystallography, which assesses key parameters, including clash scores, Ramachandran outliers and rotamer outliers to indicate the quality of the model [131]. Key parameters which are assessed and a brief description of these can be found in Table 2.8.

Term	Description	Ideal value
Ramachandran outliers	Ramachandran outliers occur when a residue's Phi (φ) and Psi (ψ) angles lie outside of the 'normal' range, or plotted on the Ramachandran plot. Particular φ and ψ angles are excluded due to steric hindrance. The Ramachandran outlier score is calculated as the percentage of Ramachandran outliers with respect to the total number of residues in the structure [132, 133].	≤0.2%
Rotamer outliers	Protein sidechains have preferred torsion angle values, known as rotamers. If the angles of a residue sidechain differs from a preferred rotamer, it is considered an outlier. The sidechain outlier score is calculated as the percentage of residues with an unusual sidechain conformation with respect to the total number of residues [132].	≤1%
Clash score	The clash score is calculated as the number of atoms which are in too close proximity to each other (<2.2Å), causing a clash, per 1000 atoms [132].	N/A
R-work	A measure of how well the model fits the original X-ray diffraction data after refinement [134].	~10% of the resolution e.g. for a 2.0 Å structure the R-work should be 0.2
R-free	During refinement, a small subset of reflections are excluded. After refinement, it is determined how well the model predicts the un-refined reflections [134].	The difference between R and R-free should be <0.7 (7%)

Table 2.8 Key parameters which are assessed during refinement of X-ray models.

2.8 Re-refining FcγRIIa models

2.8.1 3RY4 and 3RY5

Experimental data and coordinates of the protein database (PDB) entries 3RY4 and 3RY5 were downloaded from the PDB and further refinement using PHENIX 1.12 [129] was performed. For both structures, stereochemistry was improved through manual model building as well as using the Ramachandran optimization tool in COOT [130]. In the case of 3RY4, additional alternative conformations were introduced due to the high resolution available, and anisotropic B factor refinement was applied during refinement. For 3RY5 isotropic B factor refinement was used.

2.8.2 3RY6

The experimental data for 3RY6 were downloaded from the PDB. As template for Molecular Replacement in PHASER [128], PDB 3RY4 (residues F88 replaced with S88 and H134 replaced with R134) and Fc-chains of PDB 1E4K [105] were used. All three chains were used as separate search templates in sequential order allowing them the freedom to move against each other. Several cycles of manual model building in COOT [130] and refinement using PHENIX 1.12 [129] were carried out, applying secondary structure and torsion angled NCS restraints. Sugar modifications were built manually into F_o-F_c density in COOT. Model validation for all structures was performed using MOLPROBITY [131].

2.9 Analysis of the structures

2.9.1 ClusPro-DC

In order to analyse the dimer structures proposed by Ramsland *et al.* [97] to help determine if they were biological, the ClusPro-Dimer Classification (ClusPro-DC) server was used (https://cluspro.bu.edu/) [135, 136].

ClusPro-DC works by estimating the stability of the interaction between two protein subunits, using a docking method. If a substantial amount of low energy docked poses centre around the predicted dimer pair, then it suggests that the interaction is stable and likely biological. Alternatively, if the docking predictions do not centre around the predicted dimer pair, then it is unlikely that the dimer is biological [136].

Firstly, following re-refinement, the dimer pair was found by generating symmetry mates within 4 Å using PyMol. Each monomer of the dimer was separated into 2 distinct chains. For the IgG1-Fc-bound dimer, the IgG1-Fc was removed. This was then input into the server, specifying the distinct chains. The server then produced the 100 possible dimer partners which had the lowest docking energy. If these all clustered around the predicted dimer pair then the result was the dimer was likely biological. If they all clustered randomly, the dimer was likely crystallographic.

2.9.2 PISA

As above, the PDB files which separated each monomer of the FcγRIIa dimer into separate chains were used for analysis using PISA, to calculate the buried surface area [137].

2.9.3 Carbohydrate analysis

To assess and validate the carbohydrates added to the re-refined structures, Glycoblock representations were produced in CCP4 Molecular Graphics (CCP4mg) [138-140]. The PDB file was entered and a schematic representation of the glycans was produced, giving information of the types of sugars and the linkages.

2.9.4 Comparisons with other FcγR structures

To compare the re-refined model with other FcγR structures, PyMol was used as a visualisation tool. The receptor complexes were superimposed using chain B of the re-refined model as reference. To align the protein sequences, the National Center for Biotechnology Information (NCBI) Basic Local Alignment Search Tool (BLAST) was used (https://blast.ncbi.nlm.nih.gov/Blast.cgi). The PDB codes of the models used are displayed in Table 2.9. All structures used were first checked for quality, to ensure there were no major errors in refinement.

Structure	PDB Code	Resolution (Å)	R-work/R-free
FcγRIa-Fc	4W4O	1.8	0.173/0.215
FcγRIIb-Fc	3WJJ	2.6	0.230/0.272
FcγRIIIb-Fc	1T83	3.0	0.226/0.282

Table 2.9 PDB codes of the different FcγR-Fc models used for comparison with the re-refined FcγRIIa-Fc model.

Chapter 3
Comparison of the FcγRIIa-IgG interaction using two different biophysical techniques

3.1 Introduction

As previously described, FcγRIIa contains 2 non synonymous coding polymorphisms in the protein ectodomain: H131R and Q27W. Unpublished data from our group has shown that the 27W-131H allotype causes an increased risk of RA. In order to assess how these FcγRIIa polymorphisms may contribute to disease, their effect on ligand binding was studied. This was done using 2 different systems: BIAcore and the LigandTracer.

3.1.1 BIAcore

The BIAcore is a surface plasmon resonance technique, and works by immobilising monomeric receptor onto a sensor chip, and flowing over the analyte (*e.g.* IgG) in a buffer. Plane-polarized light is then focused on to the back of the sensor chip and the reflected light causes excitation of surface plasmons, which induces SPR. When the ligand binds to the receptor, it causes a change in mass, which in turn alters the angle at which SPR occurs. SPR sensograms depicts these changes in the angle in real time, with responses measured in arbitrary resonance units (RU) [141, 142].

3.1.1.1 Limitations of BIAcore

Although SPR can be used to obtain K_D values, it poses many limitations. As the receptors are immobilised on a chip, their orientation is fixed and may not represent how they are orientated in a cell membrane. Furthermore, only ectodomains are used rather than full length receptors, and the receptors are unable to oligomerise, making the system less biologically relevant. This

is particularly important when measuring binding to FcγRs, as they are thought to cluster upon ligand binding, which could greatly affect the kinetics of the interaction.

3.1.2 LigandTracer

In an attempt to overcome some of the limitations of the BIAcore, IgG binding to FcγRIIa was also analysed using the LigandTracer. The LigandTracer is designed to measure ligand–receptor interactions in real-time on living cells [119]. It works by adhering cells expressing the receptor of choice to a plate, and washing over a solution containing the fluorescently-labelled ligand. The amount of labelled ligand bound to the receptors is then measured using a fluorescence detector at different time points. To account for any non-specific binding to the cells, the amount of ligand bound to control cells not expressing the target receptor is also measured, and this is subtracted from the target cells (Figure 3.1).

As LigandTracer is a relatively new technology, there was no reliable protocol for adhering cells and measuring ligand binding. Therefore, a substantial amount of work was carried out to develop a protocol for this. Attachment protocols were optimised using FcγRIIa-expressing HEK293 cells, detected using a fluorescently labelled CD32 specific antibody (IV.3) as the ligand. The rational for using IV.3 as the ligand was due to its high affinity and specificity for FcγRIIa. Furthermore, it binds to an epitope outside of the polymorphic residues (amino acids 132 - 137 [FSHLDP]), hence binds all allotypes of FcγRIIa equally [143]. Once the protocol had been established using this antibody, monomeric IgG1-IgG4 binding to FcγRIIa was measured.

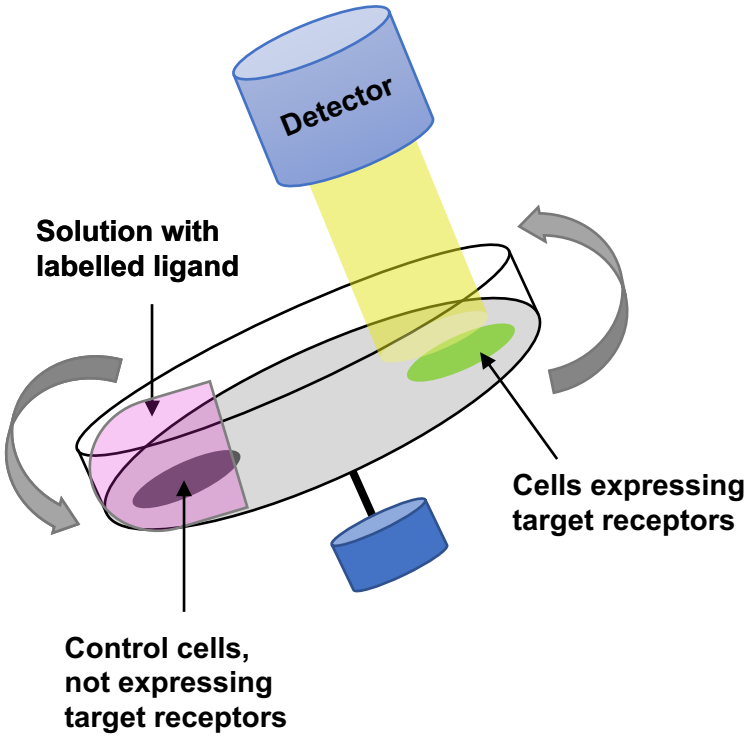

Figure 3.1 The principle of a LigandTracer assay.

Cells expressing the receptor are adhered to the plate, and the fluorescently-labelled ligand in solution in then washed over the cells, and the amount of bound ligand is measured with a detector. Redrawn from Bondza, *et al.* [119].

3.1.3 Objectives

The objectives of the work in this chapter were to derive kinetic values for monomeric IgG subclasses binding to the different allotypes of FcγRIIa, using two different techniques. IgG binding to FcγRIIa ectodomains immobilised on a chip was compared with IgG binding to full-length FcγRIIa expressed on live cells.

3.2 Results

3.2.1 Surface Plasmon Resonance measurements of monomeric IgG subclass interactions with FcγRIIa ectodomains

Sensograms from the BIAcore experiments are shown in Figure 3.2. IgG binding to these ligands confirms that the proteins were biologically active.

Results showed that the different allotypes of FcγRIIa bound IgG subclasses with different preferences. As previously stated in the literature, the 131H allotype bound IgG2 with higher affinity than the 131R allotype, regardless of the amino acid present at position 27 [7, 94]. For all of the FcγRIIa allotypes, IgG subclasses 1 to 3 appeared to have fast association and dissociation rates.

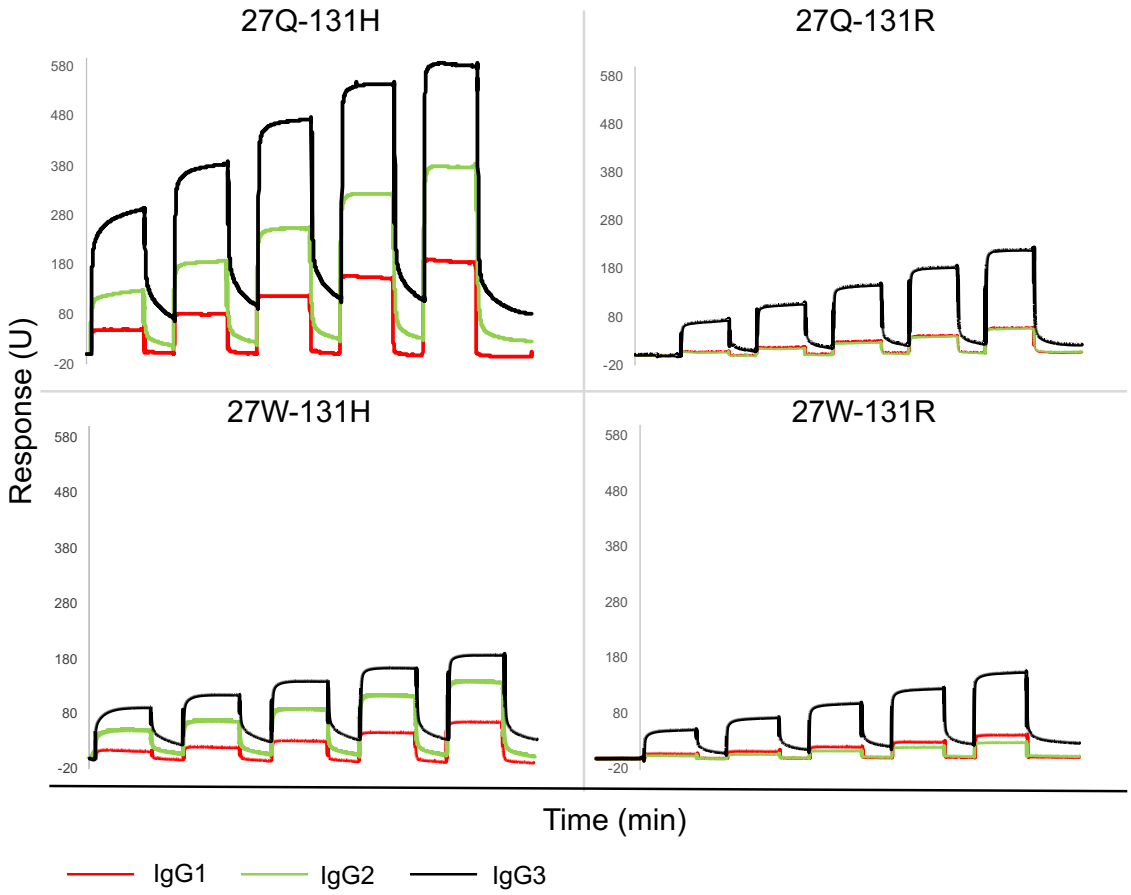

Figure 3.2 Surface plasmon resonance sensograms showing 3 monomeric IgG subclasses binding to 4 different allotypes of His-tagged captured FcγRIIa ectodomains, normalised to capture levels.

Sensograms for IgG4 are not shown, as this IgG allotype aggregated on the chip.

K_D values were calculated from the sensograms, using steady state kinetics (Figure 3.3, Figure 3.4 and Table 3.1). As the on- and off-rates were too fast for the instrument to measure, k_{on} and k_{off} values could not be derived. IgG4 accumulated on the chip super-stoichiometrically, which may have been due to aggregation. As a result, steady state was not reached for IgG4 and K_D values could not be accurately calculated for this IgG subclass.

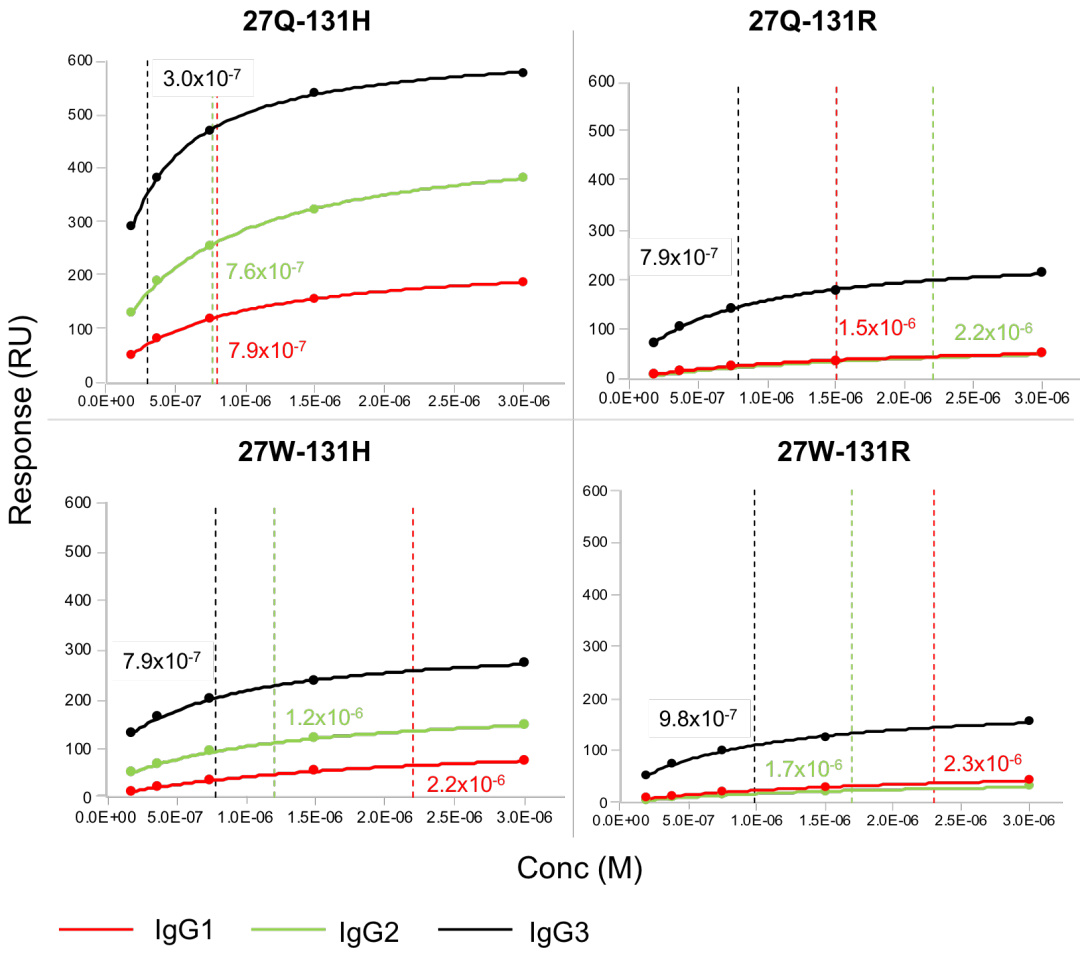

Figure 3.3 A plot of ligand concentration vs response at equilibrium (Req) to give steady state K_D values, normalised to receptor capture levels.

K_D values are indicated with a dashed line. IgG4 did not reach steady state therefore accurate K_D values could not be deduced.

FcγRIIa Allotype	IgG1 (M)	χ^2	IgG2 (M)	χ^2	IgG3 (M)	χ^2
27Q-131H	7.9×10^{-7}	0.157	7.6×10^{-7}	0.806	3.0×10^{-7}	0.617
27Q-131R	1.5×10^{-6}	0.947	2.2×10^{-6}	0.295	7.9×10^{-7}	1.420
27W-131H	2.2×10^{-6}	0.127	1.2×10^{-6}	0.395	7.9×10^{-7}	3.160
27W-131R	2.3×10^{-6}	0.695	1.7×10^{-6}	0.378	9.8×10^{-7}	6.920

Table 3.1 K_D values of different IgG subclasses binding to different allotypes of FcγRIIa, calculated using steady state kinetics. Chi^2 values show the goodness of fit, with a lower Chi^2 value indicating a better fit. K_D values are not available for IgG4, as steady state kinetics were not reached for this subclass.

The 27Q-131H allotype had a higher affinity for IgG1 and IgG2 compared to the other 3 allotypes. The R131H polymorphism on the 27Q background had an increased affinity for IgG1 and IgG2. However, when combined with 27W background, the polymorphism does not alter the receptors affinity for IgG1 or IgG2. The 27W-131H allotype which is not seen in any population, has the highest affinity for IgG3.

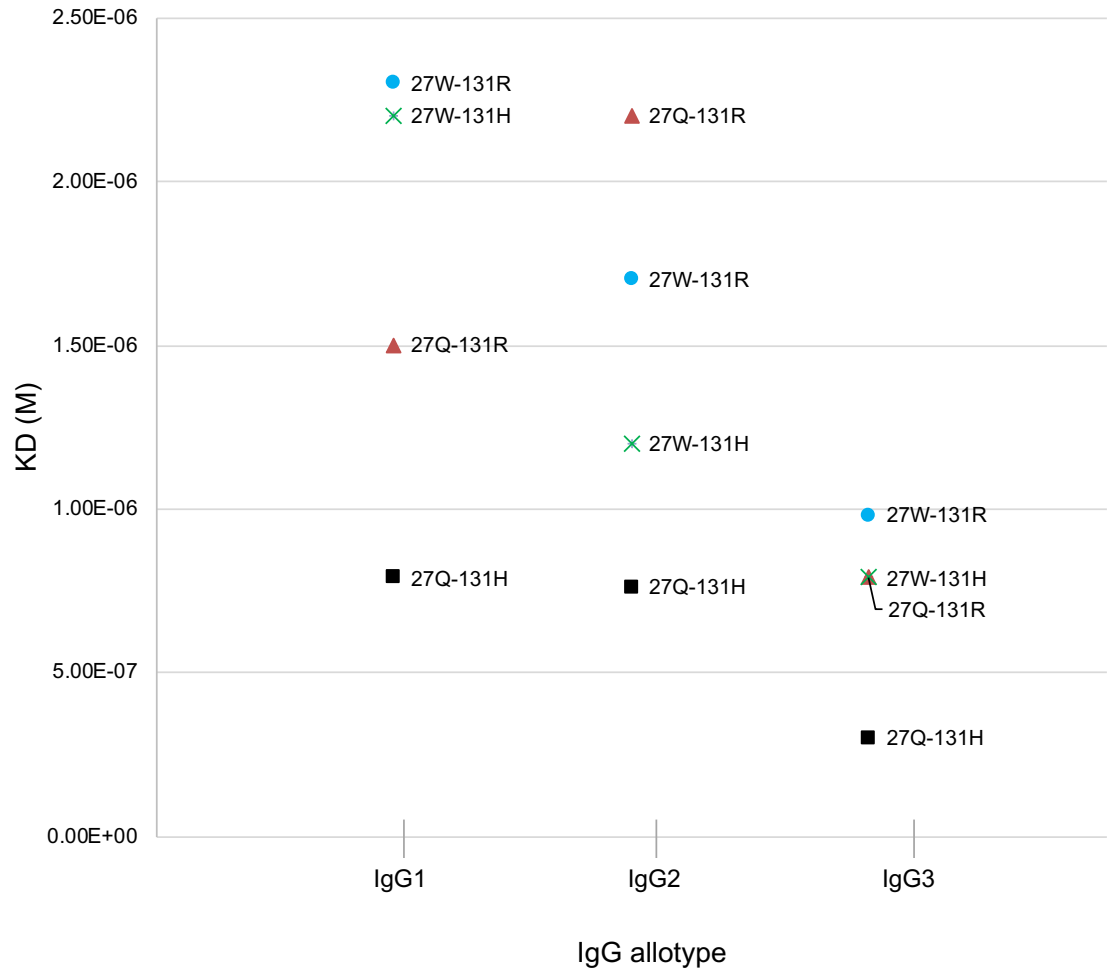

Figure 3.4 The affinity constants of different FcγRIIa allotypes plotted against IgG subclasses.

3.2.2 LigandTracer protocol optimisation

3.2.2.1 Immunofluorescence

In order to confirm that the stably transfected HEK293 cells were expressing FcγRIIa on the cell surface, IF was carried out using a high affinity anti-CD32 antibody. Results from the IF can be seen in Figure 3.5. Stably transfected HEK293 cells were stained with the FITC-3D3 antibody, confirming that FcγRIIa is expressed on the cell surface. Empty un-transfected HEK293 cells show no FITC staining, hence do not express FcγRIIa, making them a suitable negative control.

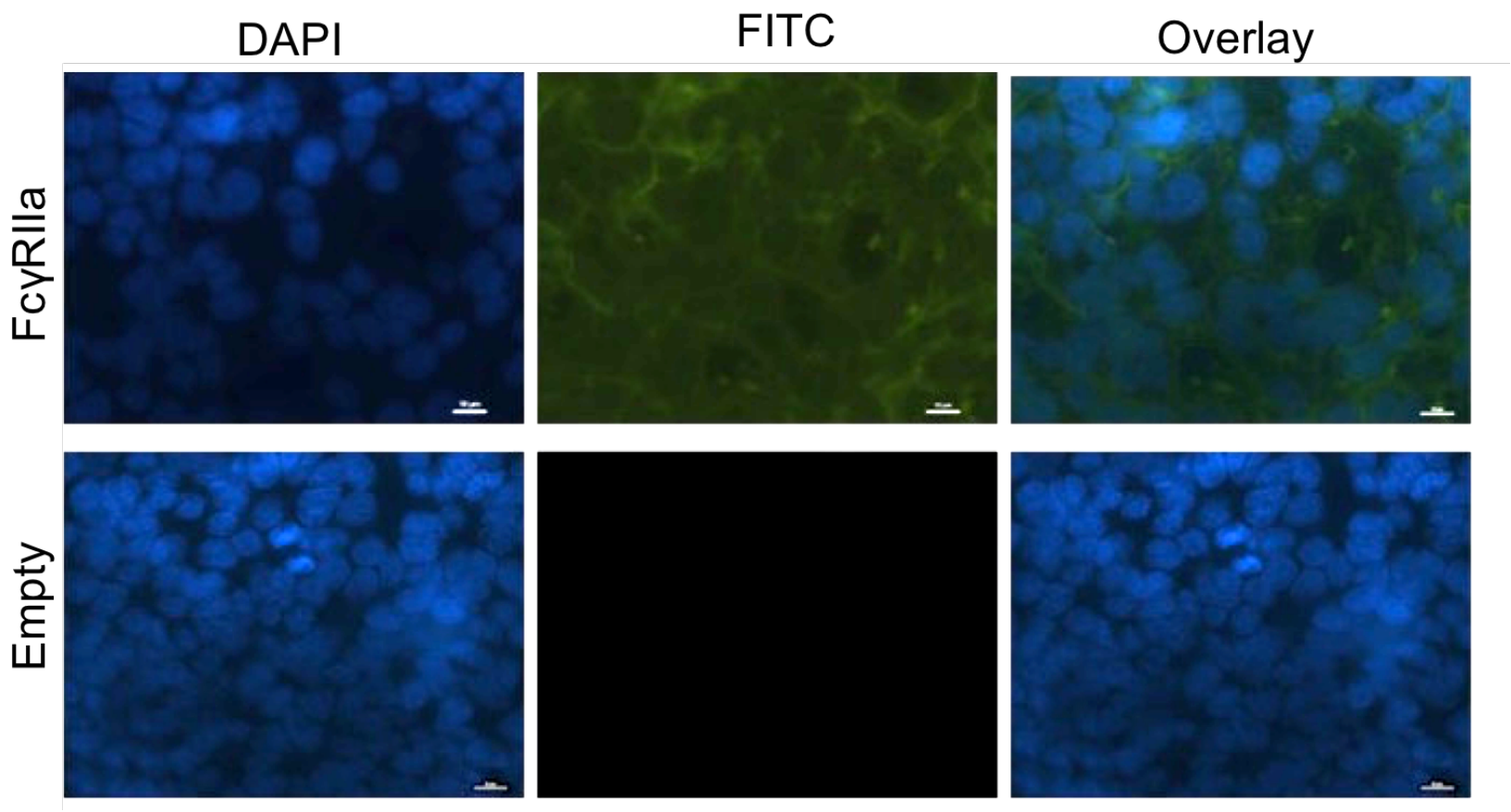

Figure 3.5 FcγRIIa expression on stably transfected HEK293 cells.

Immunofluorescence using DAPI to stain the nuclear DNA (blue), and FITC-labelled 3D3 antibody (Green) to stain FcγRIIa protein. Scale bar 10μm.

3.2.2.2 IV.3 labelling

To ensure labelling of IV.3 with FITC was successful, FACS was carried out using stable HEK293 cell lines expressing the 27Q-131R allotype of FcγRIIa. FITC-IV.3 shows a fluorescent signal similar to the commercially labelled FITC-AT10 antibody, confirming that the labelling reaction was successful (Figure 3.6). FITC-IV.3 binding was also tested against HEK293 cells transfected with an empty vector, to confirm that no non-specific binding was occurring.

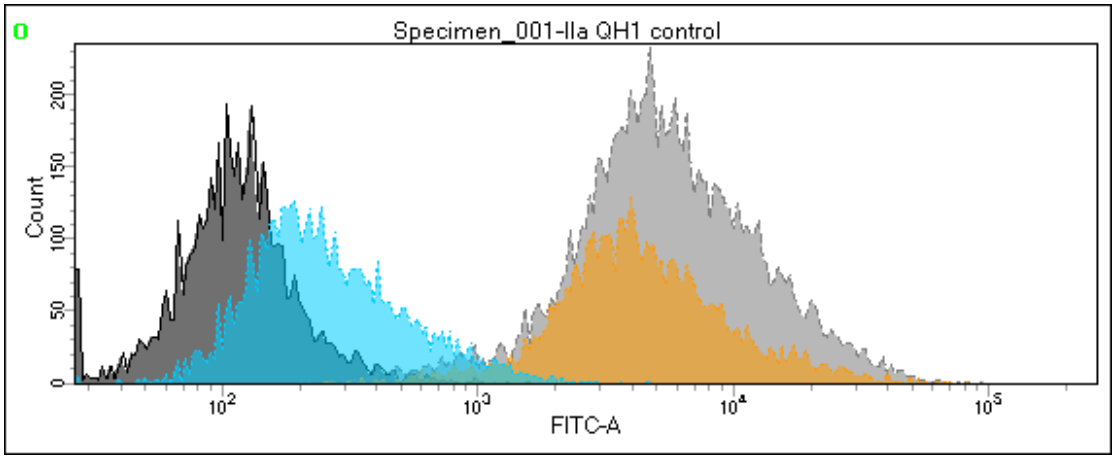

Figure 3.6 FITC-IV.3 binds to stably transfected HEK293 cells.

FACs results show that the IV.3 antibody (orange) binds to the FcγRIIa-expressing cells (27Q-131H allotype) and that the antibody labelling with FITC was successful. (Dark grey: FITC-IV.3 binding to HEK293 cells transfected with an empty vector [negative control]; Blue: FITC-3D3 binding to FcγRIIa-expressing cells [negative control]; Light Grey: FITC-AT10 binding to FcγRIIa-expressing cells (positive control); Orange: FITC-IV.3 binding FcγRIIa-expressing cells).

3.2.2.3 Natural HEK293 adhesion

As HEK293 cells are weakly adherent to untreated polystyrene, initial runs on the Ligand Tracer were carried out using cells naturally adhered to tissue culture plates. However, after only 30 mins on the Ligand Tracer all the cells had detached (Figure 3.7).

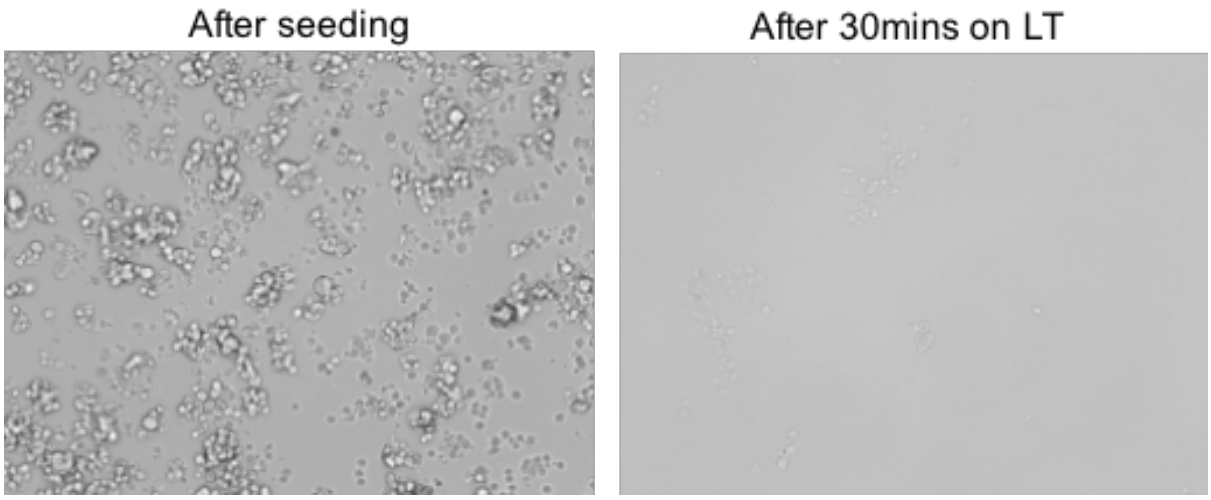

Figure 3.7 HEK293 cells naturally adhered to TC plates.

Images of HEK293 cells adhered to TC plates naturally, taken on an EVOS microscope at 20X. Although cells were initially adhered, after 30 mins on the LigandTracer all of the cells had detached.

3.2.2.4 NHS-EDC coupling

Attempts to adhere the HEK293 cells down using NHS-EDC coupling were unsuccessful. After seeding only a small amount of cells adhered, and after 30 mins on the Ligand Tracer these had all detached (Figure 3.8).

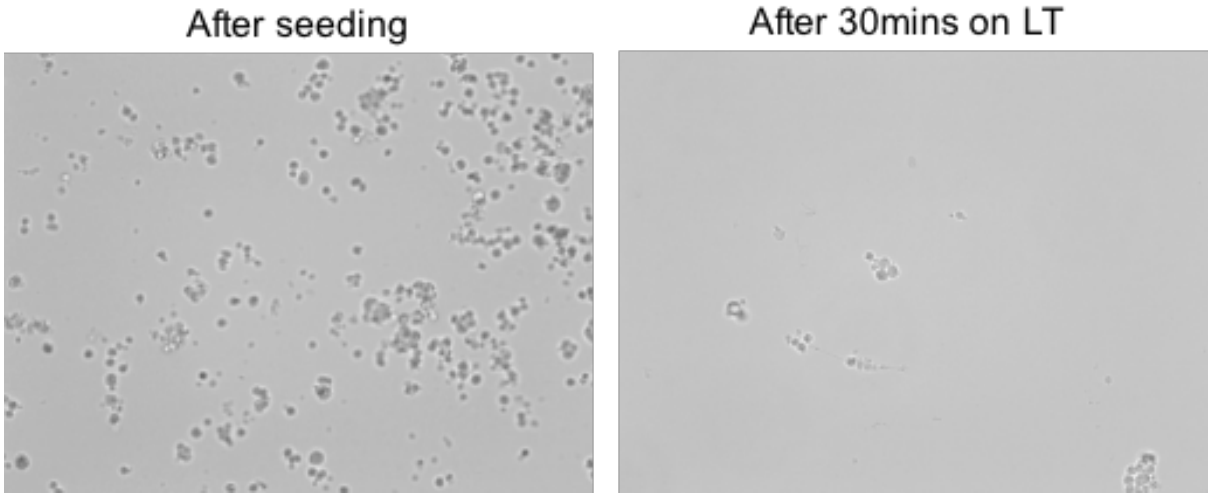

Figure 3.8 HEK293 cells adhered to Nunc plates with NHS-EDC coupling.

Taken on an EVOS microscope at 20X. Approximately 20% of cells were adhered following seeding, and after 30 mins on the Ligand Tracer virtually all the cells had detached.

3.2.2.5 Biocompatible Anchor for Membranes

Adherence to the Nunc tissue culture plates using BAM was successful (Figure 3.9). Although the cells had detached by 23 hours on the Ligand Tracer, they were still attached after 7 hours.

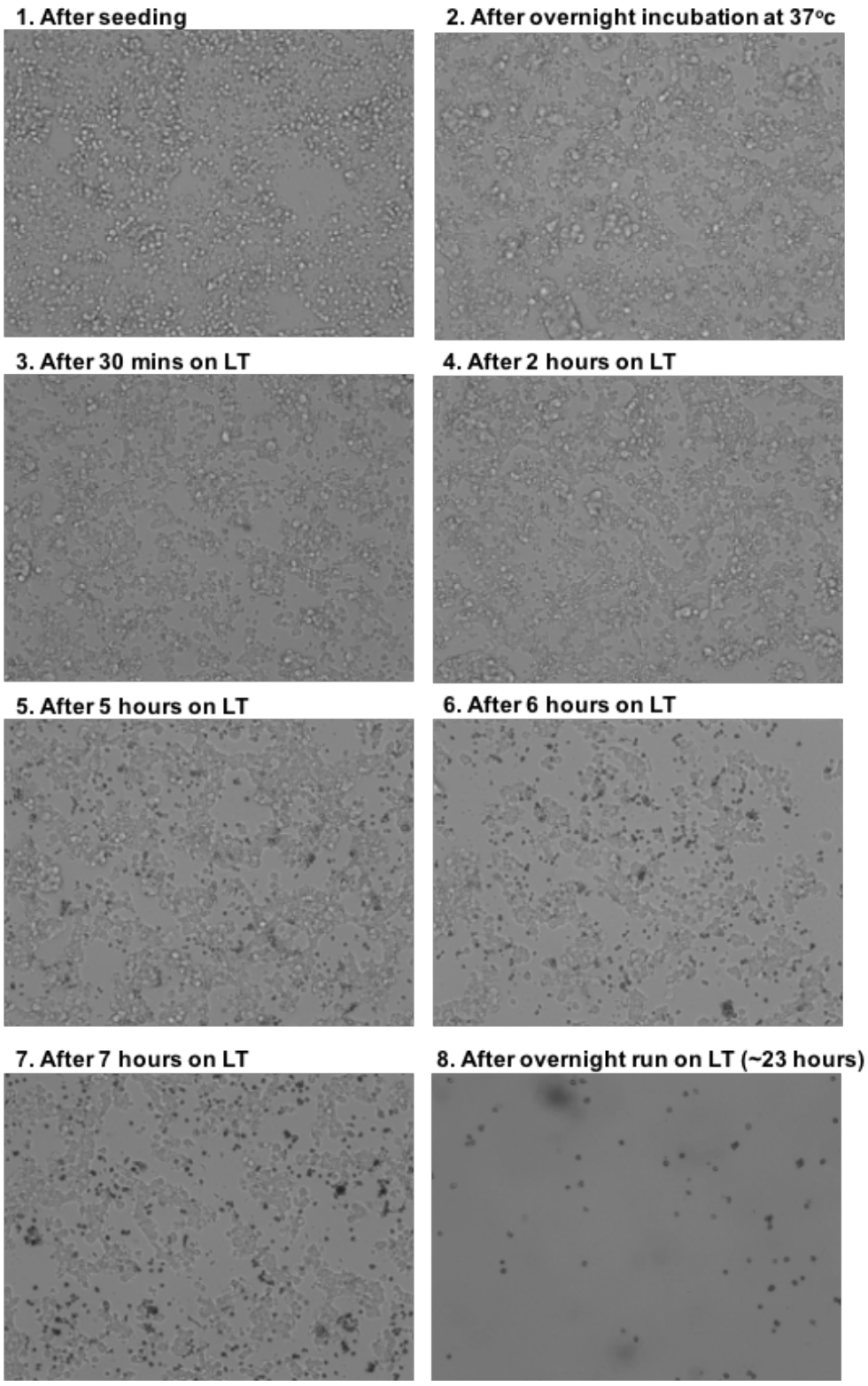

Figure 3.9 HEK293 cells adhered to Nunc plates with BAM, taken after different time points.

Taken on an EVOS microscope at 20X. Even after 7 hours on the Ligand Tracer, HEK293 cells were still adhered to the plate. After an overnight run of approx. 23 hours on the Ligand Tracer the majority of cells had detached.

3.2.2.6 Cell viability after BAM adhesion

In order to test the cell viability after adhesion *via* BAM, trypan blue was added to the cells, which were then imaged. Cells that are not viable take up the dye giving them a dark blue appearance. Results show that BAM does not notably affect cell viability, as >90% of cells are still alive (Figure 3.10).

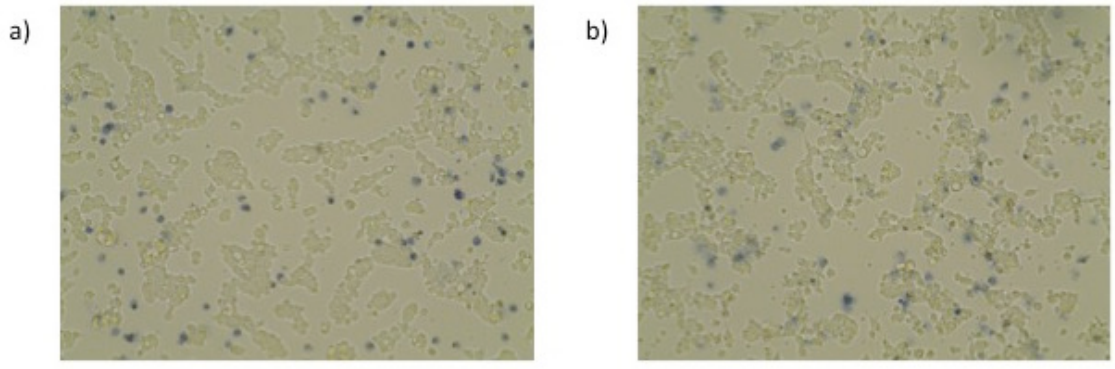

Figure 3.10 Trypan blue viability assay with **a)** stably transfected HEK293 cells after adherence with BAM **b)** un-transfected HEK293 cells after adherence with BAM.

Taken on an EVOS microscope at 20X. Non-viable cells take up the blue dye and hence appear dark blue. Both are ~90% viable after BAM adherence.

3.2.2.7 HEK293 expressing FcγRIIa and IV.3

A binding curve from FITC labelled IV.3 binding to FcγRIIa (27Q-131H) expressed on HEK293 cells is shown in Figure 3.11a. This was carried out in duplicate, and the signal normalised before fitting kinetic parameters using a 'one-to-one' model (Figure 3.11b), resulting in an affinity value of 0.04 nM (±40.8%).

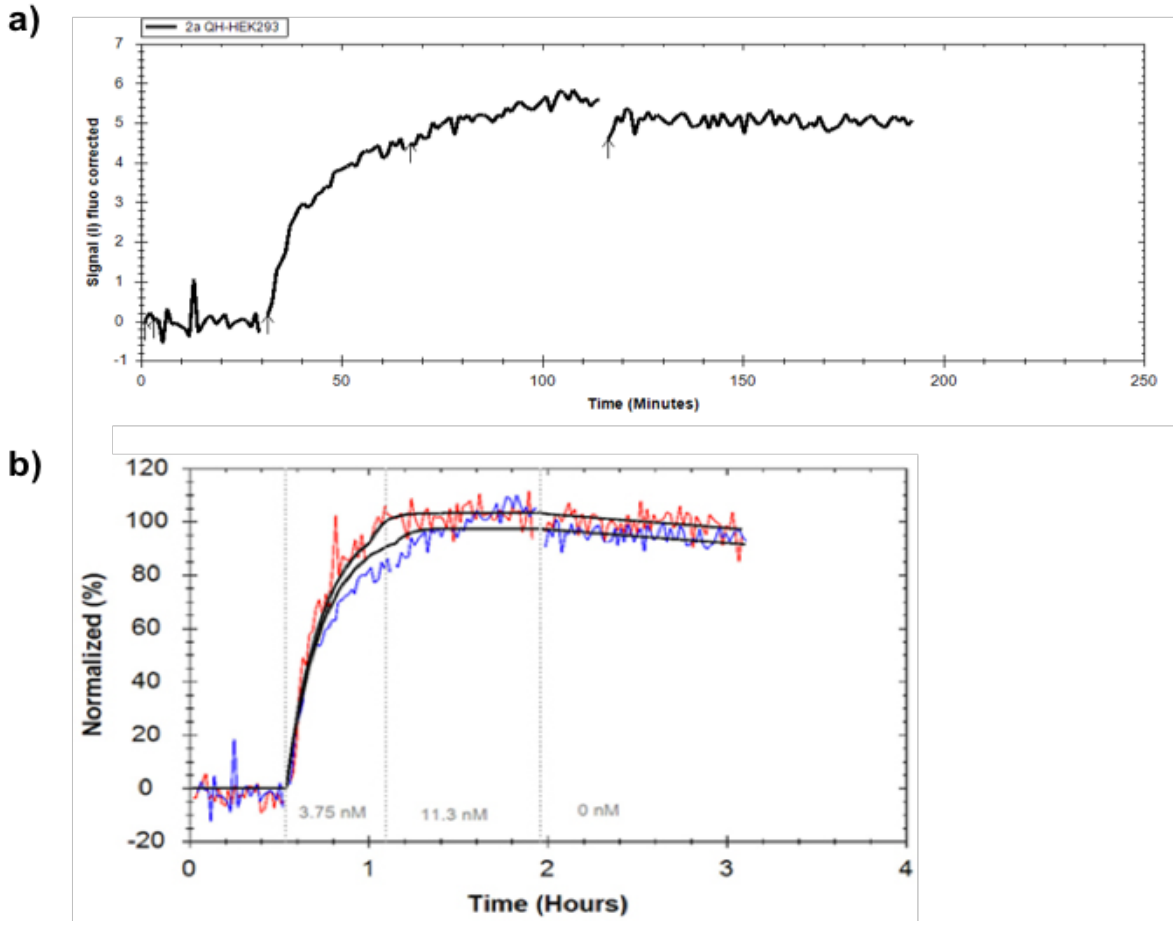

Figure 3.11 a) Binding trace for fluorescein isothiocyanate anti-CD32 mAb (IV.3) binding to HEK293 cells transfected with FcγRIIa receptor, with reference subtracted with non-transfected HEK293 cells. **b)** Results from fitting a “one-to-one” model to the individual curves (red and blue, binding traces; black, one-to-one fit).

As addition of the second concentration varies slightly in time, the results from fitting a “one-to-one” model to the individual curves are displayed (black). For all binding traces, fluorescent signals were normalized to 0% at baseline level and 100% at the end of the second ligand incubation.

3.2.2.8 BAM adhesion of sf9 cells

The optimised cell adherence protocol was tested using multiple cell lines in multiple labs [119]. However, the adherence protocol proved to be inconsistent with HEK293 cells and the results demonstrated a low signal

(~6 l), and low signal-to-noise ratio. Therefore, it was decided to test the assay using sf9 cells, which were induced to express FcγRIIa *via* baculovirus infection. The BAM protocol for cell adherence was also successful with sf9 cells, with cells remaining attached after 24h on the LigandTracer (Figure 3.12). The assay was first tested using DyLight-650 labelled IV.3, shown in Figure 3.13. It is clear that this system produced a significantly higher signal and higher signal-to-noise ratio compared to the HEK293 cells.

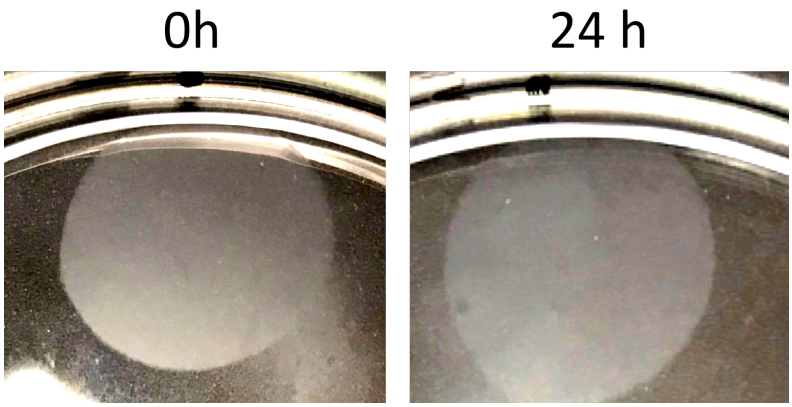

Figure 3.12 A photograph of Sf9 cells expression FcγRIIa adhered to a 10cm polystyrene Petri dish treated with BAM at 0h and 24h.

Sf9 cells successfully adhered to Nunc plates with BAM, and remained attached after 24hours on the Ligand Tracer.

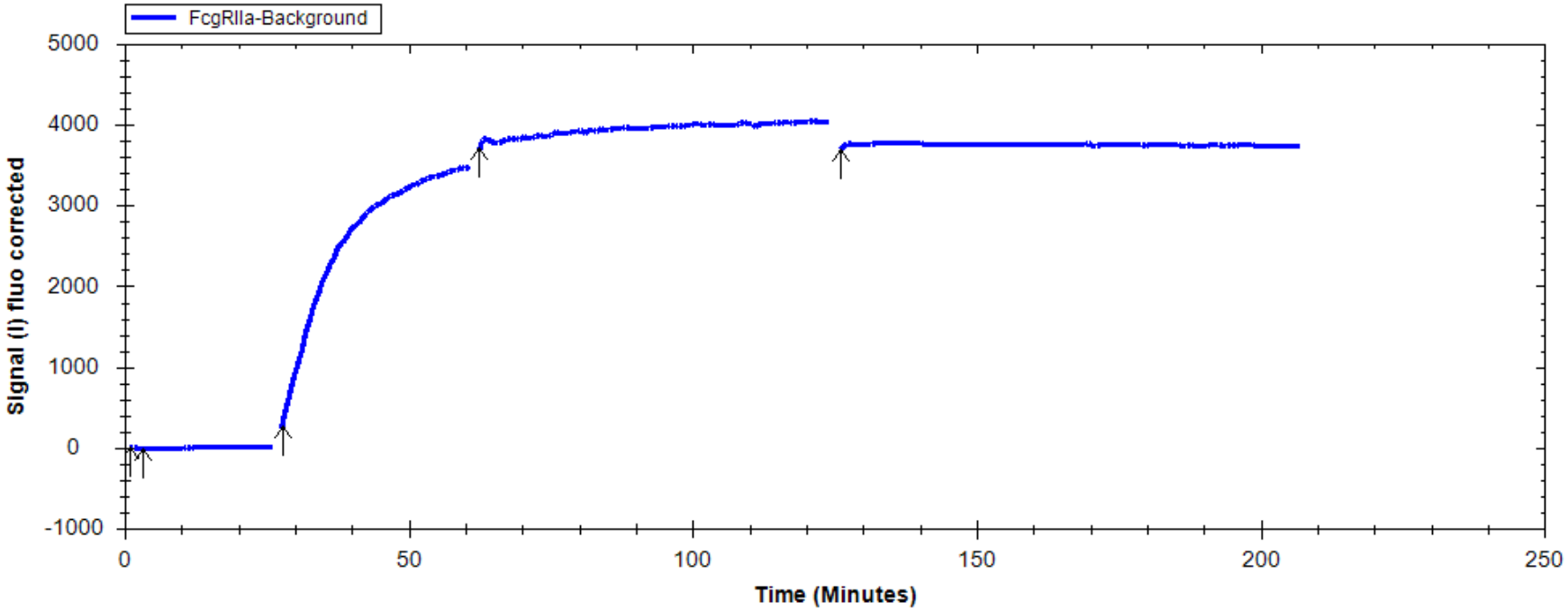

Figure 3.13 A LigandTracer curve showing IV.3 labelled with DyLight-650 binding to FcγRIIa expressed on sf9 cells.

The curve shows the signal for the FcγRIIa-expressing cells minus the reference (non-infected sf9 cells). The signal is >6 times higher than the signal for the HEK293 cells, and as the IV.3 antibody is so specific for FcγRIIa, the antibody stays tightly bound during the dissociation phase. Arrow 1, start of detector calibration; arrow 2, end of detector calibration; arrow 3, addition of first concentration of rituximab; arrow 4, addition of second concentration of rituximab; arrow 5, start of dissociation.

3.2.2.9 Optimising antibody labelling

Using IV.3 on the Ligand Tracer showed proof of principle that the assay worked with Sf9 cells. However, the IV.3 antibody is specific for FcγRIIa and binds *via* the Fab-region, the interaction was much stronger than an antibody which binds *via* the Fc-region. As the goal of this assay was to measure IgG binding *via* the Fc-region, it was necessary to also test the assay with a non-specific antibody. For this, rituximab was used due to large amounts being available. When this was labelled with DyLight650 according to the manufacturers protocol, using 50 µg of DyLight650 per 1mg of antibody, there was significant background making the signal for the FcγRIIa expressing cells negligible (Figure 3.14a). Therefore, a titration series was set up using decreasing amounts of DyLight650 to label the Rituximab, and then tested on the Ligand Tracer. It was found that the optimal labelling protocol was to use 10 µg DyLight650 per 1mg of antibody. This eliminated the problem of high background, allowing a binding curve for FcγRIIa to be produced with a high signal intensity of approximately 1500 (I) after background subtraction and before normalisation (Figure 3.14b).

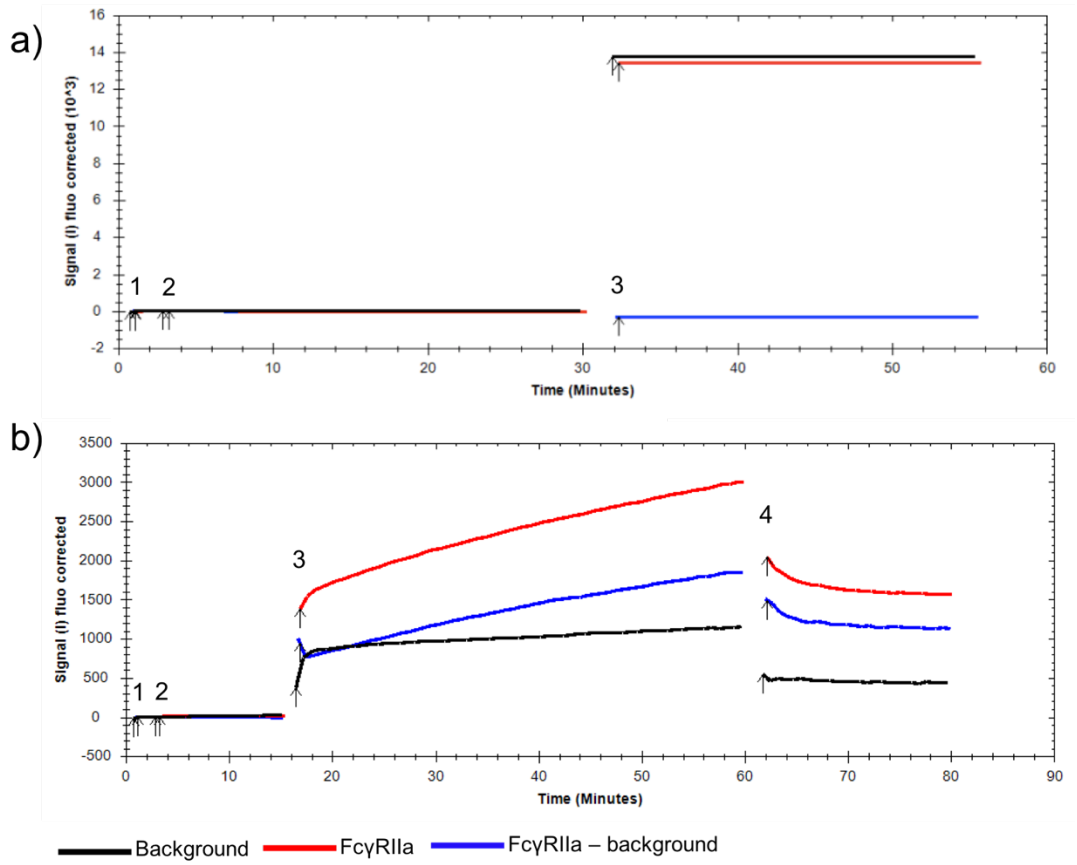

Figure 3.14 Optimisation of rituximab labelling with DyLight650.

a) Labelling rituximab with 50µg of DyLight650 per 1mg of antibody gave a high background. The signal is high, and is indistinguishable between the FcγRIIa expressing cells and the background cells. **b)** Optimal labelling of rituximab with 10µg of DyLight650 per 1mg of antibody eliminates the problem of high background. The background signal is flat and much lower than the signal for FcγRIIa expressing cells. Arrow 1, start of detector calibration; arrow 2, end of detector calibration; arrow 3, addition of 67nM rituximab; arrow 4, start of dissociation.

3.2.2.10 FcγRIIa expression levels between allotypes

Samples of the Sf9 cells expressing FcγRIIa were taken at different time points and western blots carried out to compare expression levels (Figure 3.15). The Ligand Tracer assay was carried out 48 hours after the day of proliferation arrest (DPA+48). The western blots show that at this time point, the cells are expressing relatively similar levels of FcγRIIa, with the 27W-131H allotype expressing slightly less. To account for this, the LigandTracer curves were normalised to 0% at baseline, and 100% at the maximum response (Rmax).

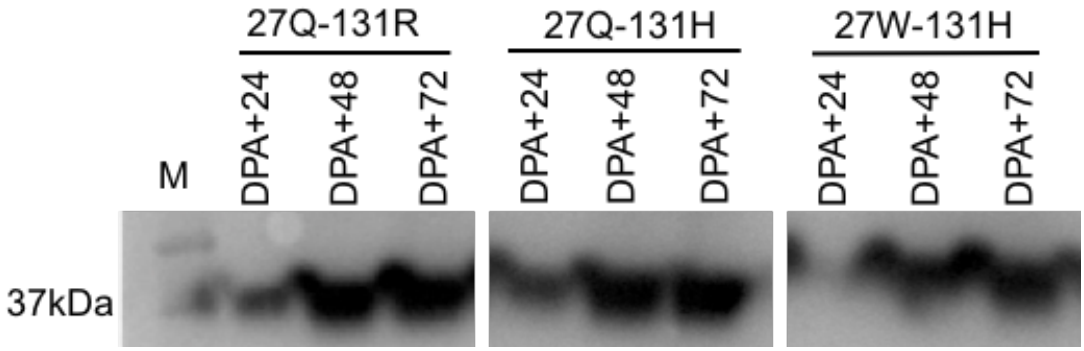

Figure 3.15 Western blot showing FcγRIIa expression levels on baculovirus infected sf9 cells, probed with an anti-CD32 primary antibody (IV.3) and a HRP-conjugated rabbit anti-mouse antibody (P0260).

3.2.3 Monomeric IgG binding to FcγRIIa allotypes: TraceDrawer™ analysis

Ligand Tracer curves can be seen for all IgG1, IgG2 and IgG3 binding to FcγRIIa allotypes found in Caucasian populations (Figure 3.16).

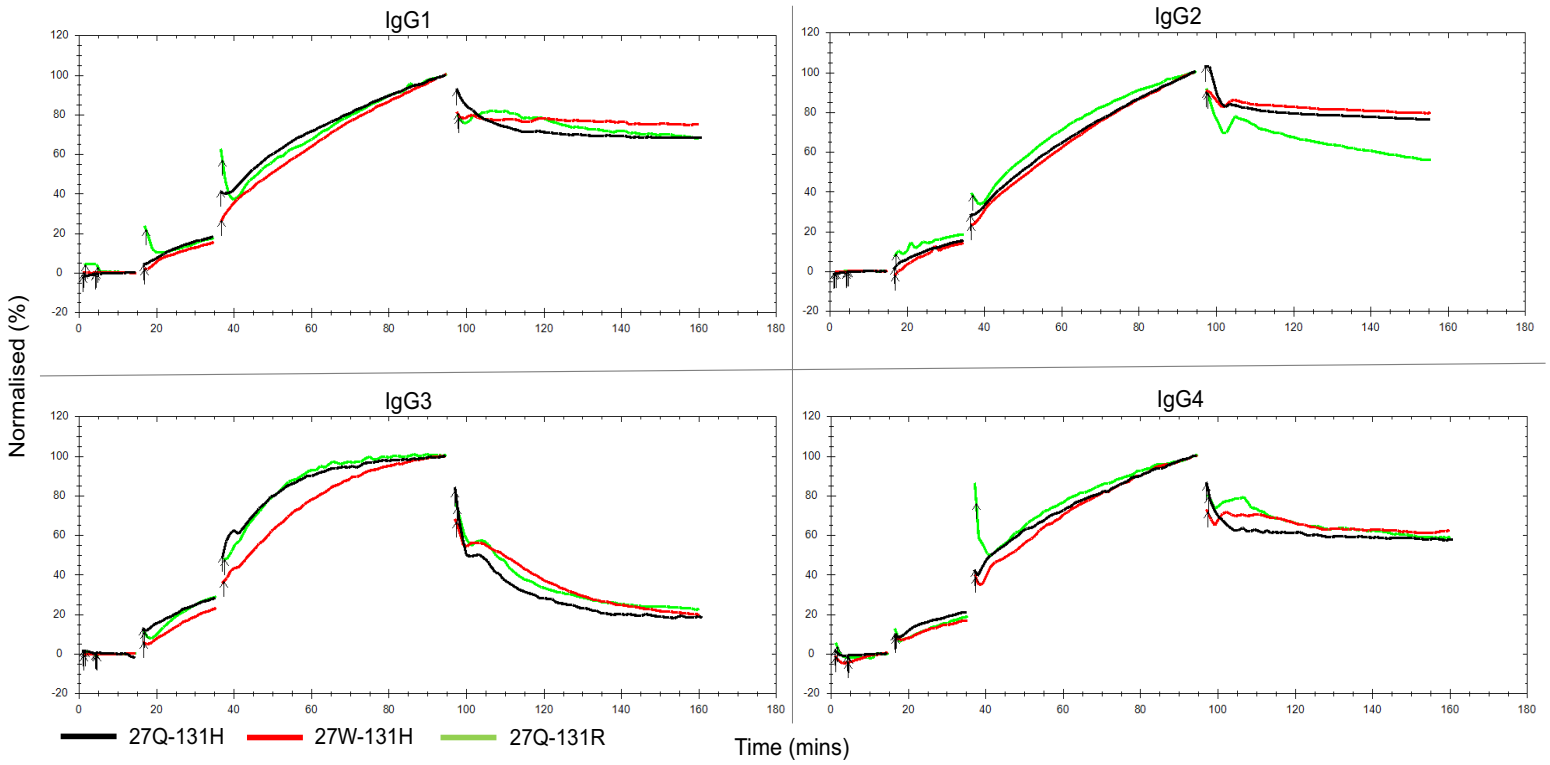

Figure 3.16 Ligand Tracer curve for DyLight650-labelled monomeric IgG1, IgG2 and IgG3 binding to 3 different allotypes of FcγRIIa, with the signal normalised to 0% at baseline and 100% following the second antibody incubation.

The first ligand concentration was 15nM which was incubated for 30 mins, followed by a second concentration of 45nM incubated for 90 mins.

3.2.3.1 IgG1

Kinetic values for IgG1 derived from LigandTracer traces are shown in Table 3.2. The fit of a 'one-to-one' kinetic model to the Ligand Tracer curve used to derive the kinetics is shown in Figure 3.17. Following a two-sample t-test assuming unequal variance, with Bonferroni correction, it was determined that the 27Q-131R had a statistically significant slower off-rate than the 27W-131H allotype (p= 0.030). None of the k_{on} or K_D rates were significantly different.

FcγRIIa Allotype	k_{on} ($M^{-1}s^{-1}$)	k_{off} (s^{-1})	K_D (M)
27Q-131H	$7.26x10^3$ (±4.7%)	$3.03x10^{-5}$ (±40.0%)	$4.24x10^{-9}$ (±45.2%)
27Q-131R	$9.84x10^3$ (±36.4%)	$4.28x10^{-5}$ (±8.8%)	$5.03x10^{-9}$ (±55.4%)
27W-131H	$5.51x10^3$ (±37.4%)	$1.89x10^{-5}$ (±31.6%)	$3.49x10^{-9}$ (±10.5%)

Table 3.2 Kinetic values for monomeric IgG1 binding to different allotypes of FcγRIIa, calculated using TracerDrawer.
Kinetic values were derived using a 'one-to-one' model.

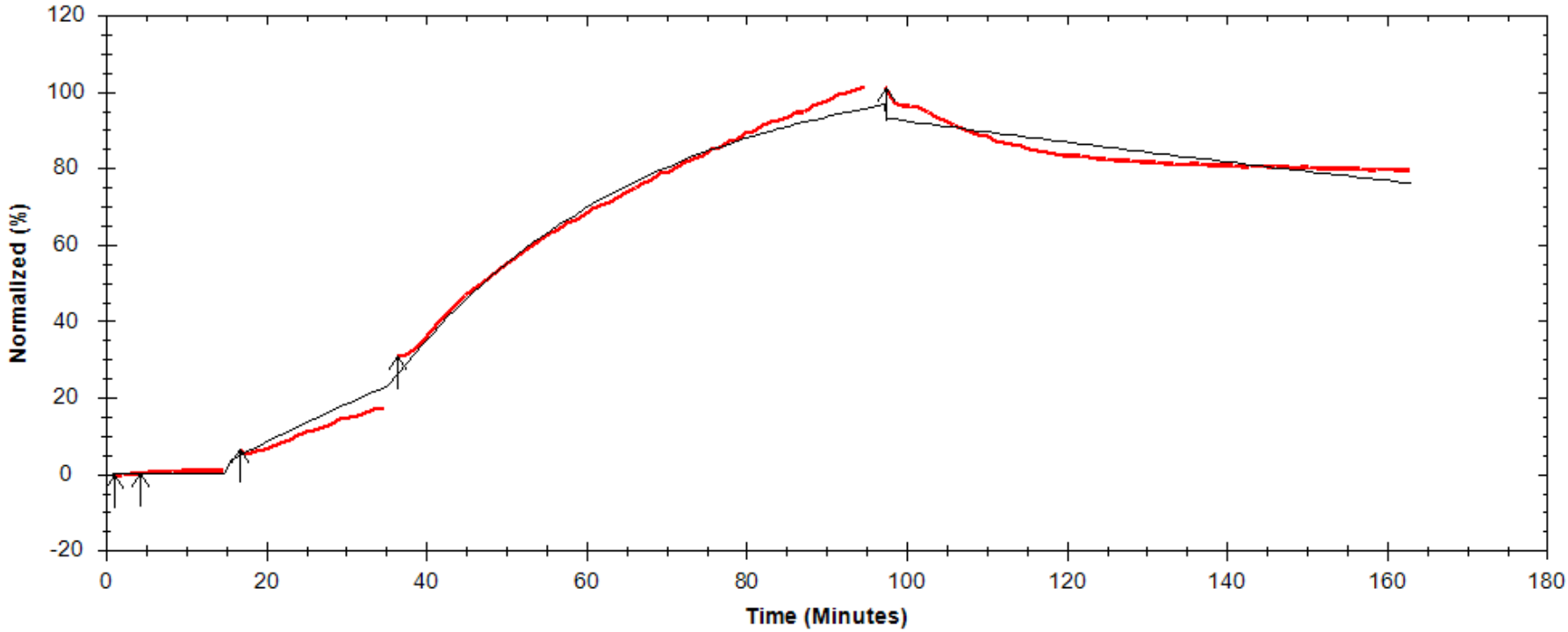

Figure 3.17 An example of a 'one-to-one' kinetic model fitted to a LigandTracer curve for IgG1 binding to FcγRIIa. The observed data is displayed in red, and the fit displayed in black.

3.2.3.2 IgG2

It can be seen from the LigandTracer curves that the 27Q-131R allotype of FcγRIIa has a much faster off-rate than the other 2 allotypes, with more of the ligand dissociating.. Kinetic values derived from these tracers are shown in Table 3.3, and the 'one-to-one' fit of a curve used to derive these kinetics shown in Figure 3.18. This was confirmed by a two-sample t-test assuming unequal variance, with Bonferroni correction, which showed that the k_{off} rate between 27Q-131H and 27Q-131R, and 27W-131H and 27Q-131R were significantly different (p= 0.010 and p= 0.005, respectively), whilst the k_{off} rate between 27Q-131H and 27W-131H was not significantly different (p= 1.000). The k_{on} rates and K_D rates were not significantly different between any of the allotypes.

FcγRIIa Allotype	k_{on} ($M^{-1}s^{-1}$)	k_{off} (s^{-1})	K_D (M)
27Q-131H	$4.54x10^3$ (±61.9%)	$4.92x10^{-5}$ (±24.9%)	$1.35x10^{-8}$ (±54.0%)
27Q-131R	$4.52x10^3$ (±23.1%)	$1.14x10^{-4}$ (±4.3%)	$2.62x10^{-8}$ (±23.7%)
27W-131H	$3.98x10^3$ (±36.4%)	$3.66x10^{-5}$ (±31.0%)	$9.55x10^{-9}$ (±23.3%)

Table 3.3 Kinetic values for monomeric IgG2 binding to different allotypes of FcγRIIa, calculated using TracerDrawer.
Kinetic values were derived using a 'one-to-one' model.

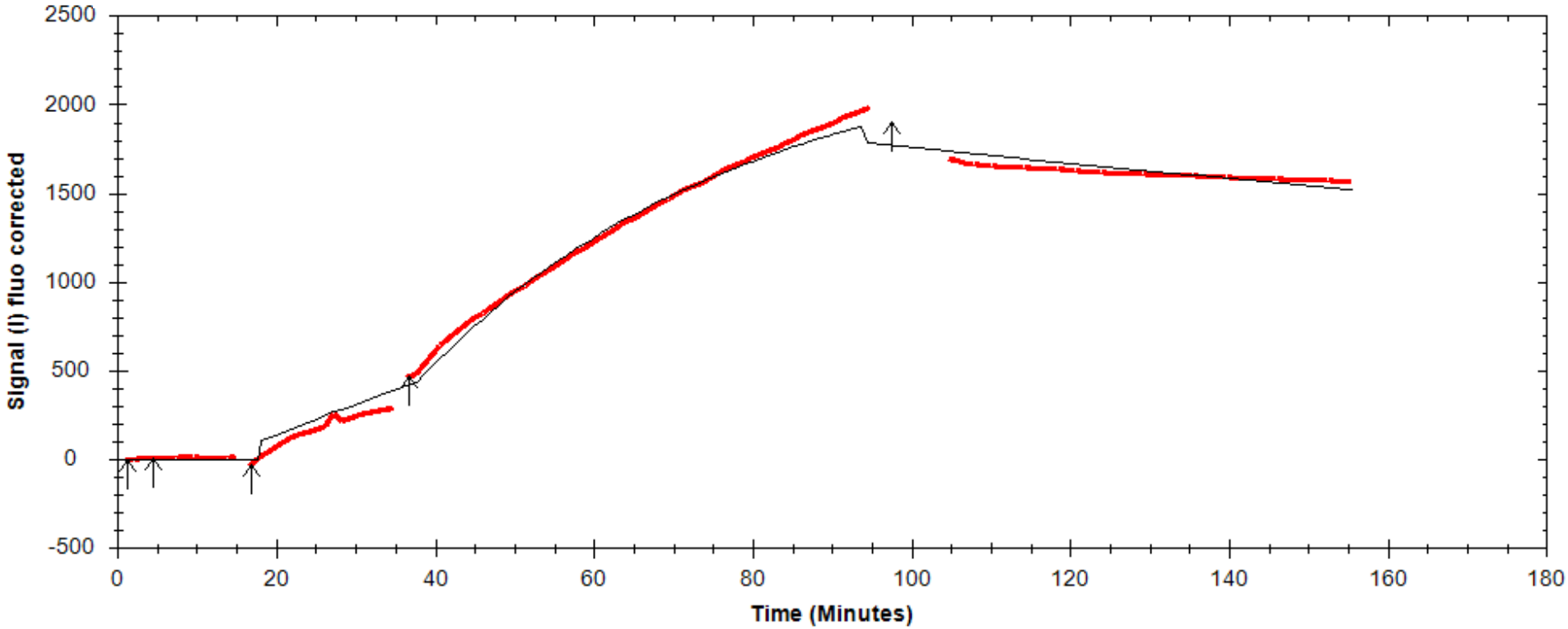

Figure 3.18 An example of a 'one-to-one' model which was fitted to the LigandTracer curve for IgG2 binding to FcγRIIa. The observed data is displayed in red, and the fit displayed in black.

3.2.3.3 IgG3

Kinetic values derived from LigandTracer traces are shown in Table 3.4. Notably, IgG3 displayed a ‘one-to-two’ binding pattern (Figure 3.19). This could be due to the more flexible hinge region of IgG3. Two-sample t-test with Bonferroni correction was carried out, and results showed that none of the kinetic values were statistically different between any of the allotypes.

FcγRIIa Allotype	$k_{on}1$	$k_{off}1$	K_D1 (M)	$k_{on}2$	$k_{off}2$	K_D2 (M)
27Q-131H	$1.39x10^4$ (±34.91%)	$1.43x10^{-3}$ (±29.04%)	$1.09x10^{-7}$ (±32.08%)	$9.01x10^3$ (±23.75%)	$1.34x10^{-5}$ (±62.49%)	$1.60x10^{-9}$ (±65.81)%
27Q-131R	$4.34x10^3$ (±44.66%)	$1.48x10^{-3}$ (±34.15%)	$3.94x10^{-7}$ (±50.51%)	$1.17x10^4$ (±80.47%)	$6.11x10^{-6}$ (±143.14%)	$84.45x10^{-10}$ (±84.45%)
27W-131H	$6.04x10^3$ (±127.07%)	$1.47x10^{-3}$ (±54.15%)	$5.54x10^{-7}$ (±96.31%)	$5.78x10^3$ (±41.39%)	$1.84x10^{-5}$ (±79.30%)	$3.55x10^{-9}$ (±70.50%)

Table 3.4 Kinetic values for monomeric IgG3 binding to different allotypes of FcγRIIa, calculated using TracerDrawer. Kinetic values were derived using a ‘one-to-two’ model.

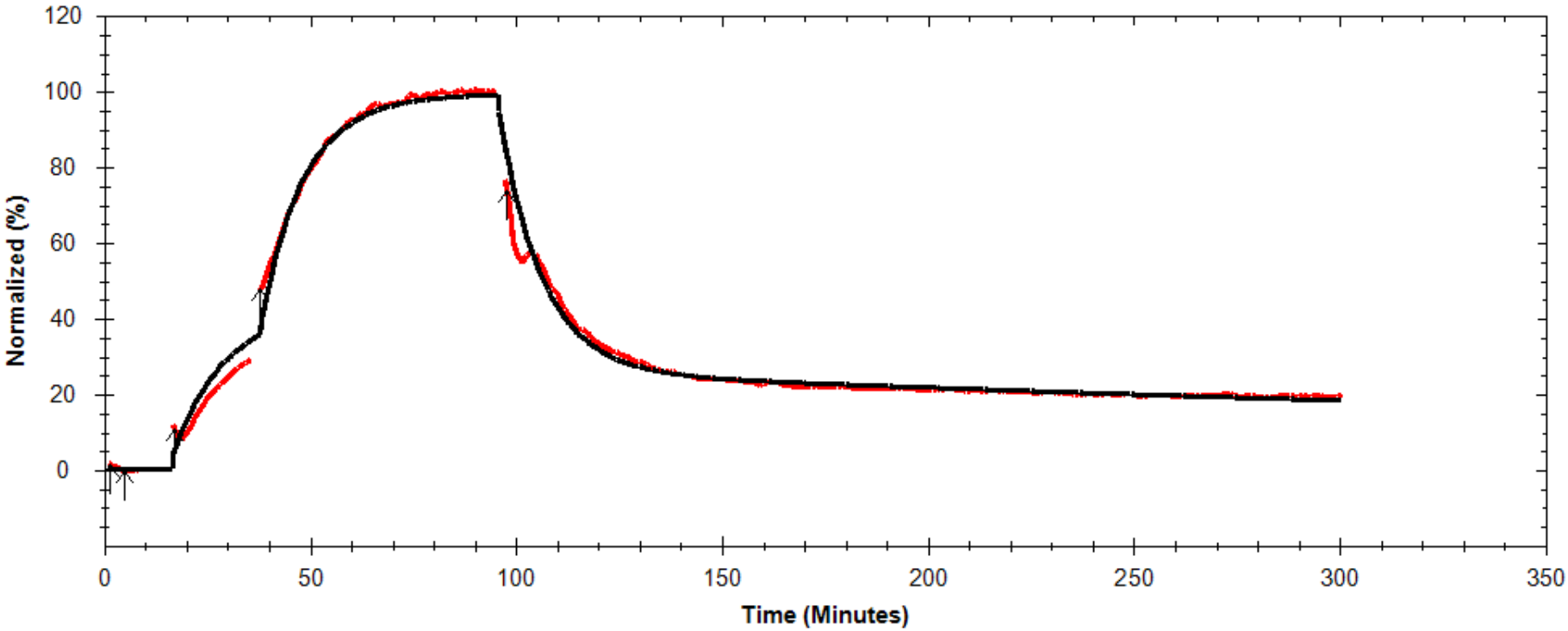

Figure 3.19 An example of a 'one-to-two' kinetic model fitted to a LigandTracer curve for IgG3 binding to FcγRIIa. The observed data is displayed in red and the fit displayed in black.

3.2.3.4 IgG4

Kinetic values derived from the LigandTracer traces are shown in Table 3.5. Notably, IgG4 also displayed a ‘one-to-two’ binding pattern (Figure 3.20). This could be due to IgG4’s ability to undergo Fc-mediated aggregation [144]. A two-sample t-test with Bonferroni correction confirmed that there were no statistical differences between any of the allotypes binding IgG4.

FcγRIIa Allotype	$k_{on}1$	$k_{off}1$	K_D1 (M)	$k_{on}2$	$k_{off}2$	K_D2 (M)
27Q-131H	$8.86x10^4$ (±68.76%)	$4.28x10^{-3}$ (±31.72%)	$5.76x10^{-8}$ (±41.44%)	$4.87x10^3$ (±17.88%)	$1.32x10^{-5}$ (±8.57%)	$2.73x10^{-9}$ (±9.32%)
27Q-131R	$9.52x10^3$ (±114.22%)	$6.06x10^{-4}$ (±27.77%)	$2.12x10^{-7}$ (±122.56%)	$5.78x10^3$ (±41.26%)	$2.22x10^{-5}$ (±34.4%)	$4.51x10^{-9}$ (±70.55%)
27W-131H	$1.27x10^5$ (±139.24%)	$1.05x10^{-2}$ (±132.05%)	$2.19x10^{-7}$ (±89.12%)	$3.80x10^3$ (±14.14%)	$8.00x10^{-6}$ (±28.74%)	$2.17x10^{-9}$ (±42.36%)

Table 3.5 Kinetic values for monomeric IgG4 binding to different allotypes of FcγRIIa, calculated using TracerDrawer. Kinetic values were derived using a ‘one-to-two’ model.

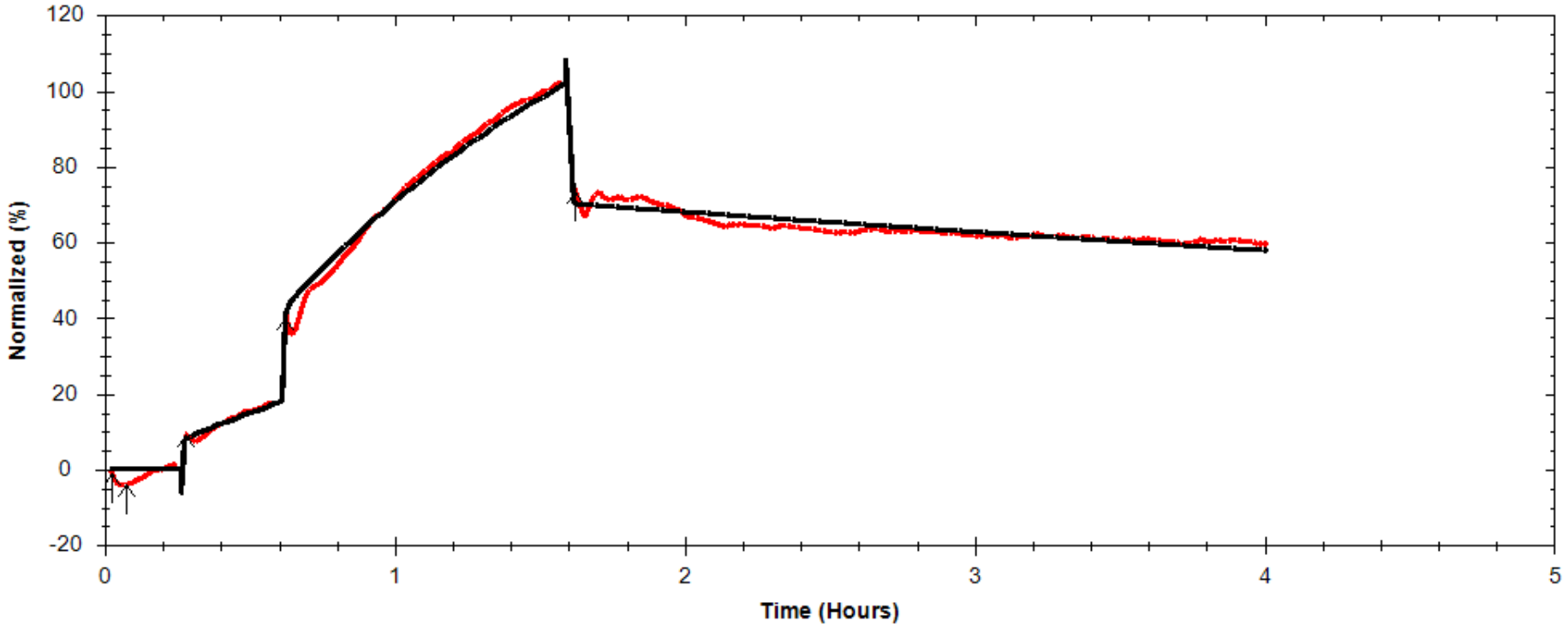

Figure 3.20 An example of a 'one-to-two' kinetic model fitted to a LigandTracer curve for IgG4 binding to FcγRIIa. The observed data is displayed in red and the fit displayed in black.

3.2.4 Monomeric IgG binding to FcγRIIa allotypes: Interaction Map analysis

To further analyse the IgG-FcγRIIa interaction, Interaction Map® software was used to decipher the different interaction processes represented by the single LigandTracer binding trace (Figure 3.21) [121]. From this analysis, kinetic parameters corresponding to the main peak in each Interaction Map were determined (Tables 3.6 to 3.9).

A shift towards the left for the main interaction peak can be observed for allotype 27W-131H compared to allotype 27Q-131R. This represents a slower off-rate and thus a more stable interaction. This holds true for all IgG allotypes and is most pronounced for IgG3, which demonstrates a statistically significant slower off-rate ($p= 0.005$).

The main interaction peak for allotype 27Q-131H also has a tendency for a slower off-rate compared to 27Q-131R, as can be seen by a shift to the left for the main peak in the Interaction Maps. However, this difference did not reach statistical significance ($p= 0.06$).

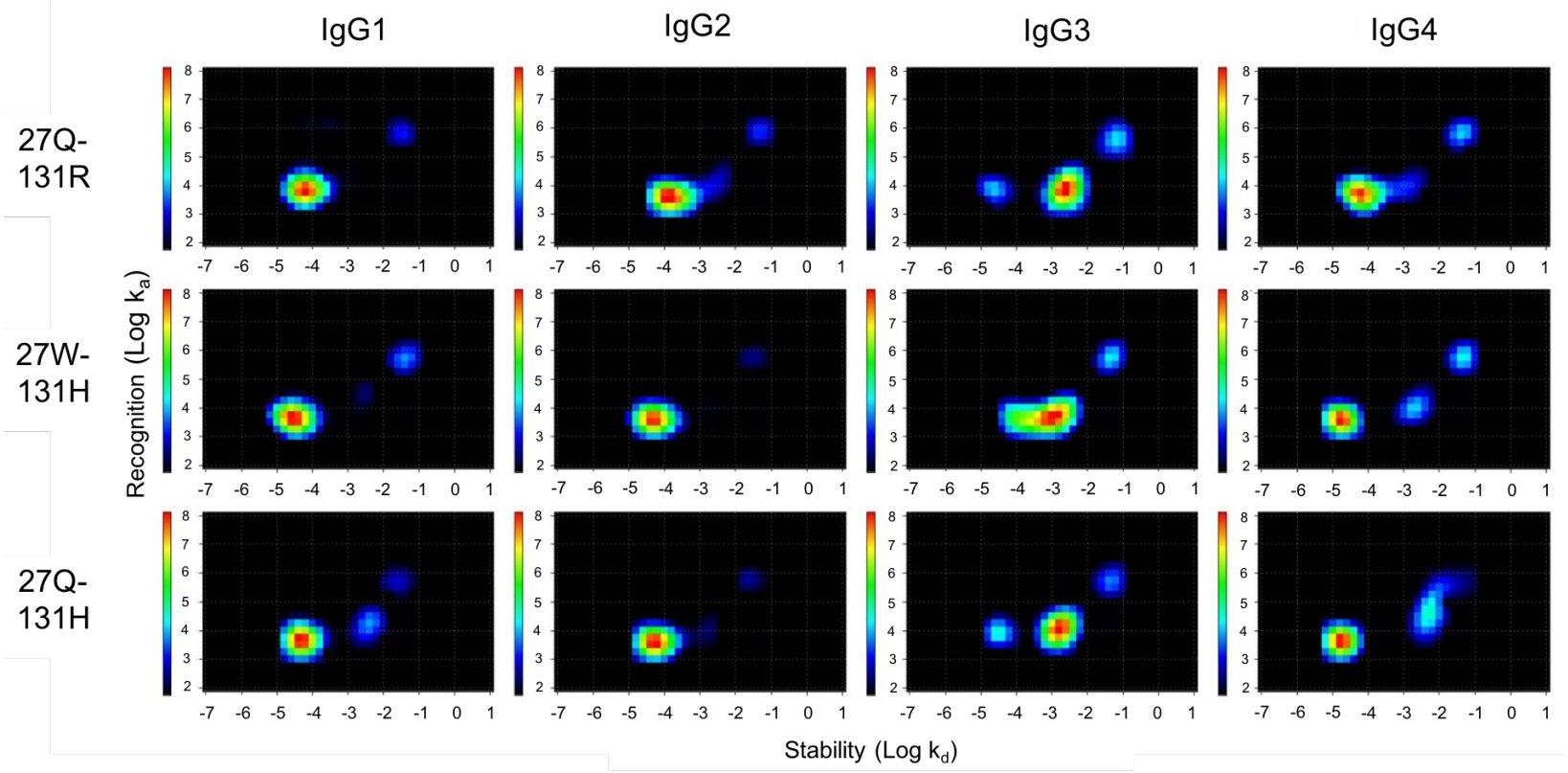

Figure 3.21 Interaction Maps for IgG1-IgG3 binding to FcγRIIa allotypes.

Global analysis was used, hence the replicates for each condition were used to create one Interaction Map. The x-axis represents k_{off} (off-rate), which reflects the stability of an interaction. The y-axis represents k_{on} (on-rate), which reflects the recognition of the molecules. The intensity indicates how much an interaction at a particular position in the map contributes to the overall binding behavior. Red=larger contribution; blue= smaller contribution.

3.2.4.1 IgG1

FcγRIIa Allotype	k_{on} ($M^{-1}s^{-1}$)	k_{off} (s^{-1})	K_D (M)	Contribution (%)
27Q-131H	$4.57x10^{3}$	$5.01x10^{-5}$	$1.07x10^{-8}$	64.95
27Q-131R	$6.61x10^{3}$	$6.61x10^{-5}$	$1.00x10^{-8}$	74.15
27W-131H	$4.37x10^{3}$	$3.16x10^{-5}$	$7.24x10^{-9}$	69.16

Table 3.6 Kinetic parameters corresponding to the main peak in each Interaction Map for IgG1 binding to FcγRIIa allotypes.

3.2.4.2 IgG2

FcγRIIa Allotype	k_{on} ($M^{-1}s^{-1}$)	k_{off} (s^{-1})	K_D (M)	Contribution (%)
27Q-131H	$3.80x10^{3}$	$5.89x10^{-5}$	$1.55x10^{-8}$	77.43
27Q-131R	$3.72x10^{3}$	$1.62x10^{-4}$	$4.37x10^{-8}$	68.50
27W-131H	$3.72x10^{3}$	$5.37x10^{-5}$	$1.45x10^{-8}$	79.11

Table 3.7 Kinetic parameters corresponding to the main peak in each Interaction Map for IgG2 binding to FcγRIIa allotypes.

3.2.4.3 IgG3

FcγRIIa Allotype	k_{on} ($M^{-1}s^{-1}$)	k_{off} (s^{-1})	K_D (M)	Contribution (%)
27Q-131H	$1.07x10^{4}$	$1.62x10^{-3}$	$1.51x10^{-7}$	56.06
27Q-131R	$6.92x10^{3}$	$2.51x10^{-3}$	$3.63x10^{-7}$	55.23
27W-131H	$4.57x10^{3}$	$6.03x10^{-4}$	$1.32x10^{-7}$	75.22

Table 3.8 Kinetic parameters corresponding to the main peak in each Interaction Map for IgG3 binding to FcγRIIa allotypes.

3.2.4.4 IgG4

FcγRIIa Allotype	k_{on} ($M^{-1}s^{-1}$)	k_{off} (s^{-1})	K_D (M)	Contribution (%)
27Q-131H	$4.17x10^{3}$	$1.74x10^{-5}$	$4.27x10^{-9}$	48.53
27Q-131R	$5.13x10^{3}$	$6.92x10^{-5}$	$1.35x10^{-8}$	61.72
27W-131H	$3.72x10^{3}$	$1.74x10^{-5}$	$4.79x10^{-9}$	50.66

Table 3.9 Kinetic parameters corresponding to the main peak in each Interaction Map for IgG4 binding to FcγRIIa allotypes.

3.3 Discussion

3.3.1 BIAcore kinetics

It is already known that different alleles of FcγRIIa bind IgG subclasses with different affinities [94]. As previously described in the literature, the H131R polymorphism modulates FcγRIIa affinity for monomeric IgG2, with 131R showing lower affinity for this IgG subclass [7], and this is also seen in the SPR results presented in this chapter. This is expected as residue 131 is in the IgG binding site. However, the Q27W polymorphism reduces this effect; 27W-131R binds IgG2 with higher affinity than 27Q-131R. This suggests that although residue 27 is not directly involved in IgG binding, it can play a modulatory role.

All allotypes show interesting kinetics with the IgG4 allotype; this IgG subclass has slow association and dissociation rates, and binds very tightly to the receptors, with much of the IgG4 remaining bound after regeneration. Due to this, steady state kinetics were not reached hence an accurate K_D value could not be calculated.

Another observation with IgG4 is that the signal continues to accumulate after injections have stopped. This subclass of IgG is known to undergo Fc-mediated aggregation [144], so it is possible that IgG4 aggregation was occurring on the BIAcore chip. To test this, IgG4 could be immobilised onto a chip as a ligand, and additional IgG4 used as an analyte.

3.3.2 LigandTracer kinetics

LigandTracer is a relatively novel, time-resolved cell-based assay, which allows the interaction between full-length FcγRs and IgG to be measured on live cells in real-time. LigandTracer has many advantages over other biophysical techniques, as the cells are not fixed, and the full-length receptor can be expressed in its native environment of the fluid cell membrane. Additionally, there is no need for complex purification methods.

Results from the LigandTracer confirmed the result that the 131H allotype can bind IgG2 with higher affinity than 131R. As k_{on} and k_{off} results can be derived, more information on the interaction could be deduced; although all 3 allotypes shown have very similar k_{on} rates, the k_{off} rate for 27Q-131R derived from TracerDrawer is significantly faster than 27Q-131H ($p= 0.01$) and 27W-131H ($p= 0.005$).

The K_D or k_{on} values for IgG1 did not differ significantly between FcγRIIa allotypes, whereas the k_{off} rates did; the k_{off} rate was statistically slower for 131R-27Q vs 131H-27W ($p= 0.030$). Interestingly, this is the opposite result to that seen for IgG2, where the k_{off} rate was significantly faster for 131R-27Q vs 131H-27W. As SPR did not provide information on the k_{on} and k_{off} rates, this was not revealed in standard SPR experiments. Furthermore,

there were no statistically significant differences in allotype binding for IgG3 or IgG4.

Notably, whilst IgG1 and IgG2 bound to FcγRIIa in a ‘one-to-one’ model, IgG3 and IgG4 bound in a ‘one-to-two’ model. Results from the InteractionMap analysis also revealed that the binding behaviour for IgG3 and IgG4 is more heterogenous than for IgG1 and IgG2, which provides assurance of the validity of model selection (one-to-two) in the TraceDrawer analysis. The main IgG3 interaction is less stable compared to all the other subtypes. This may be due to the uniqueness of this IgG subclass in terms of the flexible hinge region; IgG3 is the largest of the IgG subclasses, due to its extended hinge region, and hence is the most flexible. This flexibility may allow the receptor to bind to FcγRIIa in a different confirmation than other IgG subclasses, leading to a ‘one-to-two’ interaction. Interestingly, this is also the IgG subclass which is able to elicit effector functions such as ADCC and CDC most effectively and has the highest affinity for C1q [91, 93]. In addition to the less stable main interaction, IgG3 displays a secondary, more stable interaction for allotypes 27Q-131R and 27Q-131H.This secondary interaction resembles the main interaction for the other isotypes in terms of kinetics. For allotype 27W-131H, the secondary interaction does not separate from the main interaction, likely because the main interaction is stabilized for this allotype, moving the two components closer to each other and merging them into one wide peak. As Interaction Map allows hypothesis-free model fitting, it will fit as many models as the data will allow, preventing the problem of ‘under- or over-fitting. Therefore, no prior knowledge of the type of interaction is necessary [121]. Interaction Map analysis demonstrated that IgG4 has a tendency to display a secondary,

less stable interaction in addition to the main interaction. This secondary interaction resembles the main interaction of IgG3 in its kinetic parameters. This may be due to the ability of IgG4 to undergo Fc-mediated aggregation [144].

On the 131H background, no statistically significant differences were observed for any of the IgG subclasses between the 27W and 27Q allotypes. Therefore, the association of the 27W-131H polymorphism with an increased risk of RA cannot be attributed to this. However, it is important to note that monomeric IgG subclasses were used in these experiments, whereas it is ICs found in RA that are thought to drive inflammation and are known to bind to FcγRIIa with higher affinity than monomeric IgG.

It is not known how the different FcγRIIa allotypes affect IC binding. To determine this, IC binding to different FcγRIIa allotypes could be measured on the LigandTracer. This could be done by developing, standardised ICs which are the same size and composition.

3.3.3. Comparison of the systems

Interestingly, the results from the LigandTracer showed much stronger affinity interactions for monomeric IgG binding to FcγRIIa. This is likely to be due to many reasons. Firstly, the fact that the receptors can move around in the cell membrane, and cluster upon ligand binding to prevent fast dissociation and increasing the ability to detect avidity effects. Furthermore, the use of the full-length protein along with the orientation of the receptor in the cell membrane is much more biologically relevant; it is thought that the mechanism of membrane anchoring may affect ligand binding, as demonstrated by FcγRIII [145]. This is reflected in the different curves, as

the SPR curves show a sudden dissociation over a few minutes, with no IgG bound after the dissociation phase. On the other hand, LigandTracer curves display a slow and more steady dissociation, with much of the ligand still bound after 1 hour. It has previously been shown that association of FcγRIIa with lipid rafts can regulate IgG binding, and when constitutively associated with lipid rafts, FcγRIIa has increased capacity for IgG binding [33]. In a study by Avisar *et al.* [146], the presence of lipid rafts in Sf9 cells was confirmed by western blot analysis probed with anti-human Cav-1 Ab. Therefore, the higher affinity interactions seen in the LigandTracer results may reflect this. Additionally, the use of Interaction Map to analyse the interactions allows the more complex models to be deciphered. Using all replicates and calculating them into one, Interaction Map removes technical artefacts more efficiently and thus facilitates to pin-point the main interactions, without the risk of over-fitting.

3.3.4 FcγRIIa expression levels

LigandTracer signals were normalised to allow kinetic parameters to be derived from the curve shape irrespective of signal intensity. Nevertheless, it was important to look at expression levels of the receptors between the different allotypes. Western blots show that each allotype shows similar expression levels at DPA+48, with slightly lower levels of the 27W-131H FcγRIIa being expressed. The receptor expression level is important, as significantly higher concentrations of receptors on a cell surface may promote receptor clustering and effect the avidity of the interaction. It is important to note that FcγR expression levels vary according to cell type, and regulating FcγR expression levels is in an important mechanism of

immune regulation [147]. Therefore, there are hurdles to developing an assay which mimics *in vivo* IgG-FcγRIIa binding perfectly.

3.3.5 Glycosylation states

FcγRIIa has two N-linked ectodomain glycosylation sites, at N64 and N145, and it is thought that glycosylation of FcγRs is crucial for antibody binding with differential glycosylation patterns modulating binding affinity [17]. The ectodomains used for SPR were produced in HEK293T cells, which are known to produce proteins with mammalian N-glycosylation, with high amounts of core-fucosylated and sialylated N-glycans [148]. However, the full-length FcγRs for use on the LigandTracer were expressed in Sf9 cells. Although Sf9 cells are unable to produce complex, terminally sialylated N-glycans seen in mammalian systems, the insect N-glycosylation pathway begins like the mammalian pathway, hence proteins produced in this system still possess core mammalian glycans [149]. It is clear that further work is required to study how FcγRIIa glycosylation affects ligand binding, as the majority of work in this field is based on FcγRIIIa, and little is known about the effects of FcγRIIa-specific glycosylation on ligand binding or signalling [10].

3.3.6 Probing the interaction structurally

In order to assess how these polymorphisms convey their effect on IgG binding, crystal molecular structures can be used. Crystal structures of unbound 27Q-131H and 27Q-131R allotypes of FcγRIIa exist, as well as the 27Q-131R allotype in complex with IgG1-Fc, which may be used to study this. It would be beneficial to also have a structure of the 27W-131H allotype in complex with IgG1-Fc, to assess how these allotypes differ in their k_{off} rates, as well as the unbound 27W-131 allotype t =o evaluate if this allotype

differs structurally. Furthermore, structures of the FcγRIIa allotypes in complex with IgG2-Fc could be advantageous, as this would allow direct comparisons between the models, to assess how the H131R polymorphism affects IgG2 binding from a structural perspective.

Chapter 4
Does FcγRIIa dimerise?

4.1 Introduction

To study the interaction between FcγRIIa and IgG on a molecular scale, and to assess the effects of the known FcγRIIa polymorphisms on the structure of FcγRIIa as well as ligand binding, accurate protein structures are essential. Furthermore, as FcγRIIa has significant implications in diseases such as RA and systemic lupus erythematosus (SLE) [82, 150], it is a valid target for structure-based drug design, emphasising the need for reliable structures. Crystal structures of both the 131H and 131R variants of FcγRIIa ectodomains have previously been published (PDB 3RY4 and 3RY5), along with the structure of IgG1-Fc in complex with the ectodomain of the 131R variant of FcγRIIa (PDB 3RY6) [97]. Due to crystallographic contacts in these structures, the authors proposed that FcγRIIa forms homodimers at the cell surface, and that these dimers could be targeted to treat RA [96]. Further work by Powell *et al.* [99] demonstrated that these dimers could be disrupted, by mutation of a crucial interface residue S126P (S129 according to Powell *et al.* numbering), and that disruption of the dimer interface had a negative effect on FcγRIIa signalling. Therefore, the S126P mutant was used in this chapter as a monomeric control.

4.1.1 Indicators of the quality of crystal structures

To assess the quality of crystal structures following refinement, a series of parameters were measured, which are included in the PDB validation report. R-work values are used in crystallography to measure how well the crystallographic model agrees with the experimental X-ray diffraction data. For well refined models, this is expected to be around 0.2 [151], but can be slightly smaller for high resolution structures and larger for lower resolution structures. As well as R-work, R-free values are also measured. This is done by using a subset of reflections which are excluded from refinement, and assessing how well they fit with the refined model. A gap between R-work and R-free of larger than 10% indicates that the experimental data have been over-interpreted and may be inaccurate [134, 151, 152]. Finally, parameters such as clash-score, Ramachandran outliers and rotamer outliers are given. The lower the values are for these, the better.

4.1.2 Quality of the existing FcγRIIa crystal structures

Examination of the deposited structures made it clear that they were poorly refined with major errors. As this project relies heavily on these structures, both to analyse the proposed dimer structures and as templates for molecular replacement in further x-ray crystallography experiments, it was deemed necessary to re-refine these models completely in order to improve them, as it is known that such re-refinement often improves x-ray structures [108].

4.1.3 Objectives

The aims of this chapter were to: (i) improve the quality of the existing FcγRIIa crystal structures; (ii) to determine whether re-refined models contained any evidence for dimerisation; (iii) determine whether known

polymorphisms can affect the oligomeric state of the receptor using biophysical assays with FcγRIIa ectodomains.

4.2 Results

4.2.1 Re-refinement of 3RY4 (27Q-131H allotype ectodomain)

Values before and after refinement for 3RY4 can be seen in Table 4.1. R-work was improved by 7% and R-free by 6.3%. Moreover, the clash score was reduced, and all rotamer and Ramachandran outliers were eliminated from the model. The overall backbone trace for this model did not change following re-refinement.

Table 4.1 Comparison of the key statistics for 3RY4, before and after refinement

	Before re-refinement	**After re-refinement**
R-work	0.203	0.133
R-free	0.233	0.170
Clash score	6	1.99
Ramachandran outliers	0.6%	0%
Rotamer outliers	0.6%	0%
RSRZ outliers	4.1%	3.5%

As the resolution for 3RY4 was high (1.5 Å), electron density could be seen for alternative conformations for many of the residues, for example, the disulphide bridge between C110 and C154 (Figure 4.1). Before re-refinement, there was a large patch of negative density (red) in the F_o-F_c

map in the middle of the disulphide bridge, showing that the modelled structure applied too much model at this position than was calculated through the experimental data. There were also two patches of positive density (green) at either side of the disulphide bridge, which suggested that structure was missing at this position. After adding the alternative conformation of an open disulphide bridge, the positive and negative density in the F_o-F_c map disappeared (Figure 4.1b), indicating that the refined model agreed with the experimental data. Several alternative conformations were added to the model (Table 4.2). These eliminated many differences in map peaks and helped to reduce the R-work and R-free values in the model.

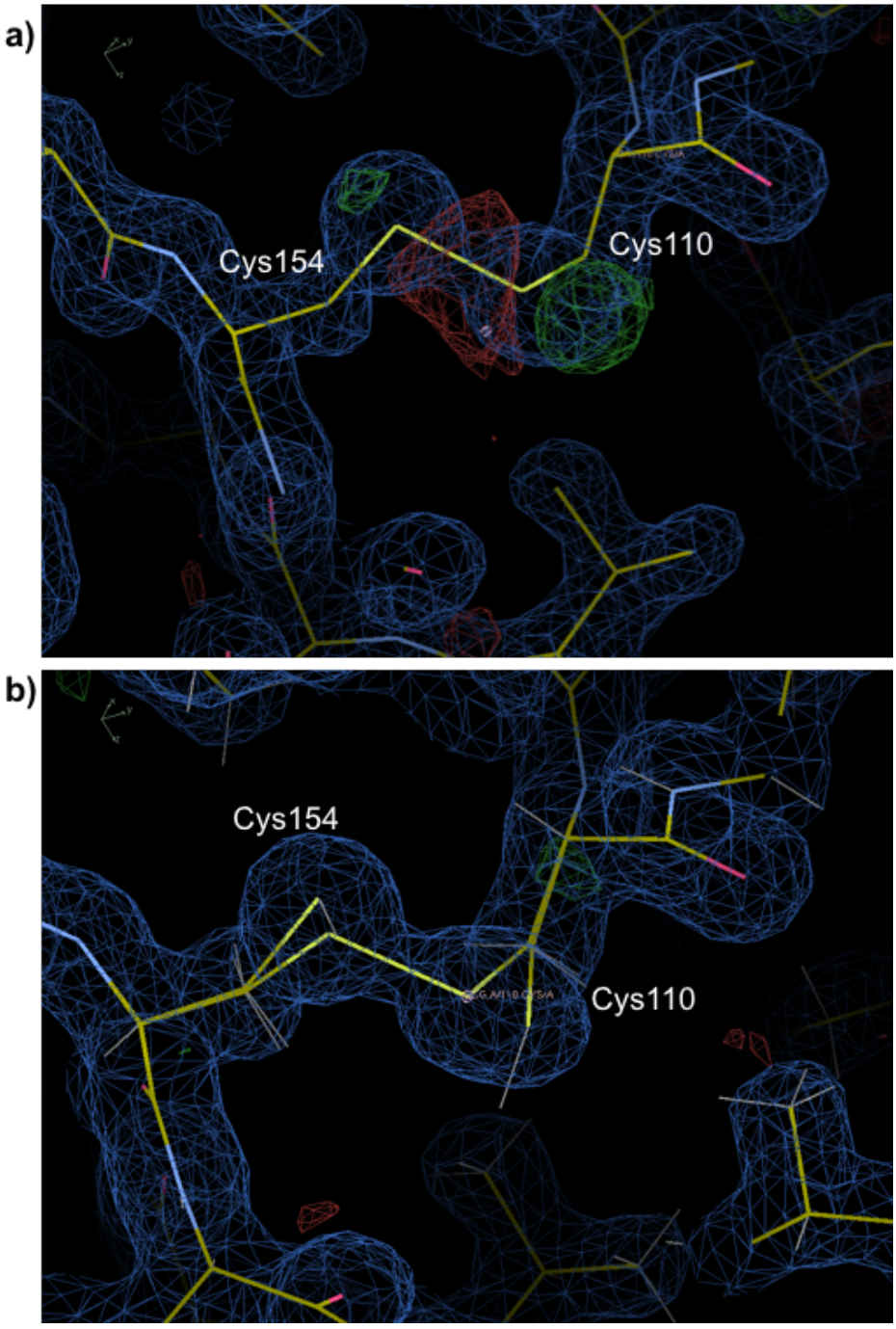

Figure 4.1 Example of improved local density fit after re-refinement shown for disulphide bridge C154.

a) C154 and C110 before adding the alternative conformation of the open disulphide bridge. Negative density (red) was seen in the F_o-F_c map in middle of the disulphide bridge, and two patches of positive density (green) at either side of the disulphide bridge. **b)** C154 and C110 after adding the alternative conformation of the open disulphide bridge. Positive and negative density in the F_o-F_c map were eliminated. $2F_o$-F_c map contoured at 1.5σ and F_o-F_c map contoured at 3.0σ.

Table 4.2 Residues with alternative side chain conformations

Residue number	Residue
21	Q
29	C
36	E
39	S
56	S
60	K
62	N
63	N
64	N
71	C
77	S
107	M
109	R
110	C
114	K
129	S
140	S
142	P
143	Q
151	D
154	C
164	S
168	V
171	T

Moreover, molecules from the crystallisation conditions were added where density was present for these (Figure 4.2). Before re-refinement, 2 water molecules had been fitted incorrectly into the density map resulting in positive patches of density between the water molecules in the F_o-F_c map. During re-refinement, these water molecules were removed, and a glycerol molecule fitted to the density, eliminating the positive density patches. Before re-refinement, there was only one glycerol molecule present in the model, compared to after re-refinement where 3 glycerol molecules and 1 Chloride ion were present.

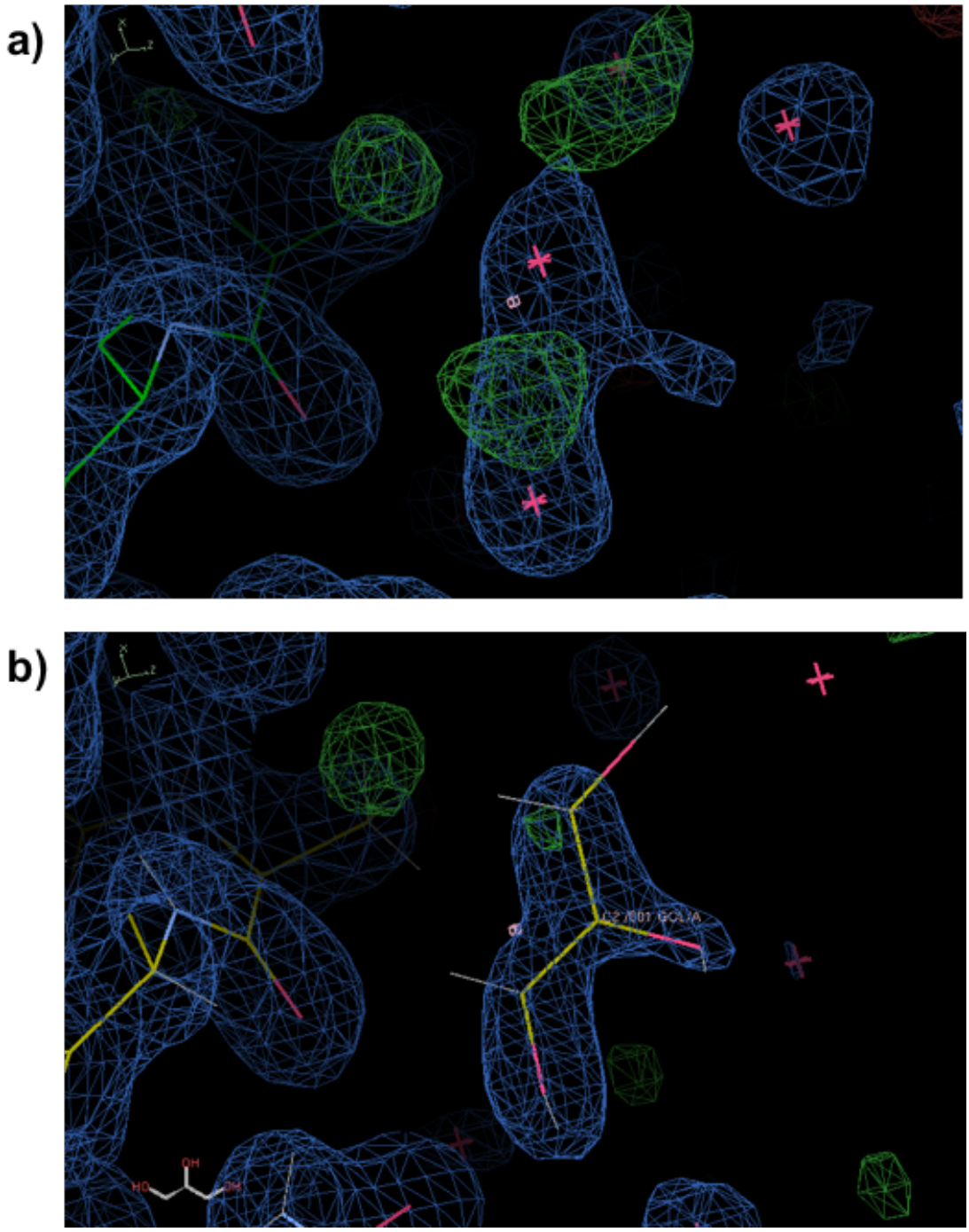

Figure 4.2 Example of improved local electron density fit after modelling molecule from crystallisation solution shown for GOL310.

a) Before re-refinement**.** Two water molecules were poorly fitted in the $2F_o$-F_c electron density map, and positive patches were present in the F_o-F_c difference map (green). **b)** After re-refinement. A glycerol molecule was fitted in to the electron density map and the large positive patches in the F_o-F_c were eliminated. $2F_o$-F_c and F_o-F_c maps before and after re-refinement, contoured at 1.5σ and 3.0σ respectively.

4.2.1.1 Analysis of 3RY4 dimer

In order to assess whether the FcγRIIa-131H dimer structure proposed by Ramsland *et al.* was likely to be a biologically relevant conformation, the re-refined model was submitted to the ClusPro-DC server. The analysis revealed that the 100 lowest-energy dimer partner predictions did not appear to centre around the dimer partner as seen in the published crystal structure (Figure 4.3a). Hence, this predicted that the dimer is likely not biological and therefore is unlikely to exist at the cell surface, but instead is a misinterpretation of crystallographic contacts. (Figure 4.3b). The dimer structure was also uploaded to PISA to analyse parameters such as the buried surface area and the contacts between protein chains [137, 153]. Again, this concluded that there were no specific interactions between the monomers and that the dimer structure was likely the result of crystallographic contacts. Additionally, the buried surface area of each monomer was found to be 236 $Å^2$. Given that the solvent accessible surface area of the monomer is 9324 $Å^2$, the buried surface area represents only 2.5% of this. Further analysis of the proposed dimer revealed that the C-terminals of the monomers were not optimally oriented for insertion into the cell membrane (Figure 4.4).

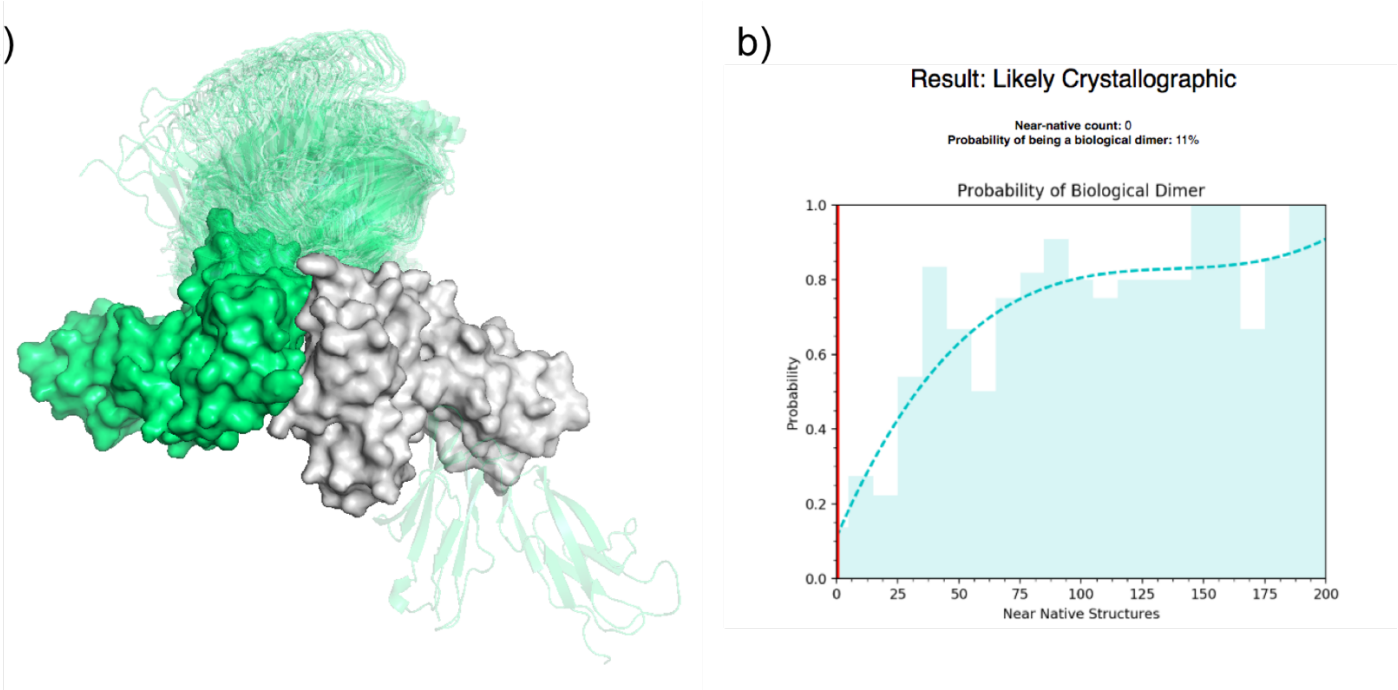

Figure 4.3 Results from the ClusPro-DC server [135].

a) Monomer 1 of the proposed FcγRIIa-131H dimer is shown in white, and monomer 2 in green (surface). The 100 dimer pairs which have the lowest docking energy to monomer 1 are displayed in transparent green (cartoon). **b)** The bar chart shows, for different near-native counts, what percentage of cases in the training set were biological dimers. The dashed green line is a fitting curve, which can be used to predict the probability of a dimer being biological [136, 154]. The vertical red line shows the number of native structures for submitted dimer, which is 0 for the proposed FcγRIIa-131H dimer. Therefore, the server predicted that the dimer structure proposed by Ramsland et al. was likely a crystallographic artefact.

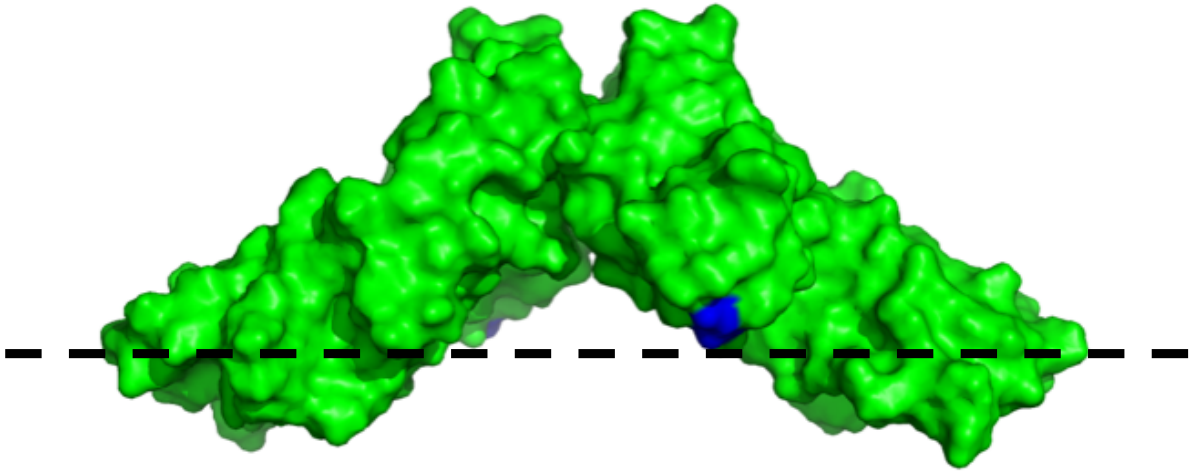

Figure 4.4 The proposed dimer of the 27Q-131H allotype.

The C-terminal residues are shown in blue. A representation of the cell membrane is shown as a dashed line.

4.2.2 Re-refinement of 3RY5 (27Q-131R allotype ectodomain)

After re-refining this model, R-work improved by 1.6% and R-free by 2.7% (Table 4.3). The clash score for this model was also reduced significantly, and there were no rotamer or Ramachandran outliers present in the model after re-refinement. The overall backbone trace did not change.

Table 4.3 Comparison of the key statistics for 3RY5, before and after re-refinement.

	Before re-refinement	**After re-refinement**
R-work	0.206	0.190
R-free	0.275	0.248
Clash score	10	0.74
Ramachandran outliers	0.6%	0%
Rotamer outliers	1.9%	0%
RSRZ outliers	3.5%	2.3%

4.2.2.1 Analysis of 3RY5 dimer

After re-refinement, the FcγRIIa-131R dimer structure was submitted to the ClusPro-DC server. Again, the analysis (Figure 4.5a) suggests that the dimer model proposed in Ramsland *et al.* was not biologically relevant, and likely the result of crystallographic contacts (Figure 4.5b).

The proposed 3RY5 dimer structure was also uploaded to PISA. Again, this concluded that the dimer structure was likely the result of crystallographic contacts. The buried surface area of each monomer of the 27Q-131R allotype was found to be 649 $Å^2$. Further analysis of the proposed dimer revealed that the C-terminals were not orientated for insertion into the cell membrane (Figure 4.6). The new PDB code after re-refinement is 6F8M).

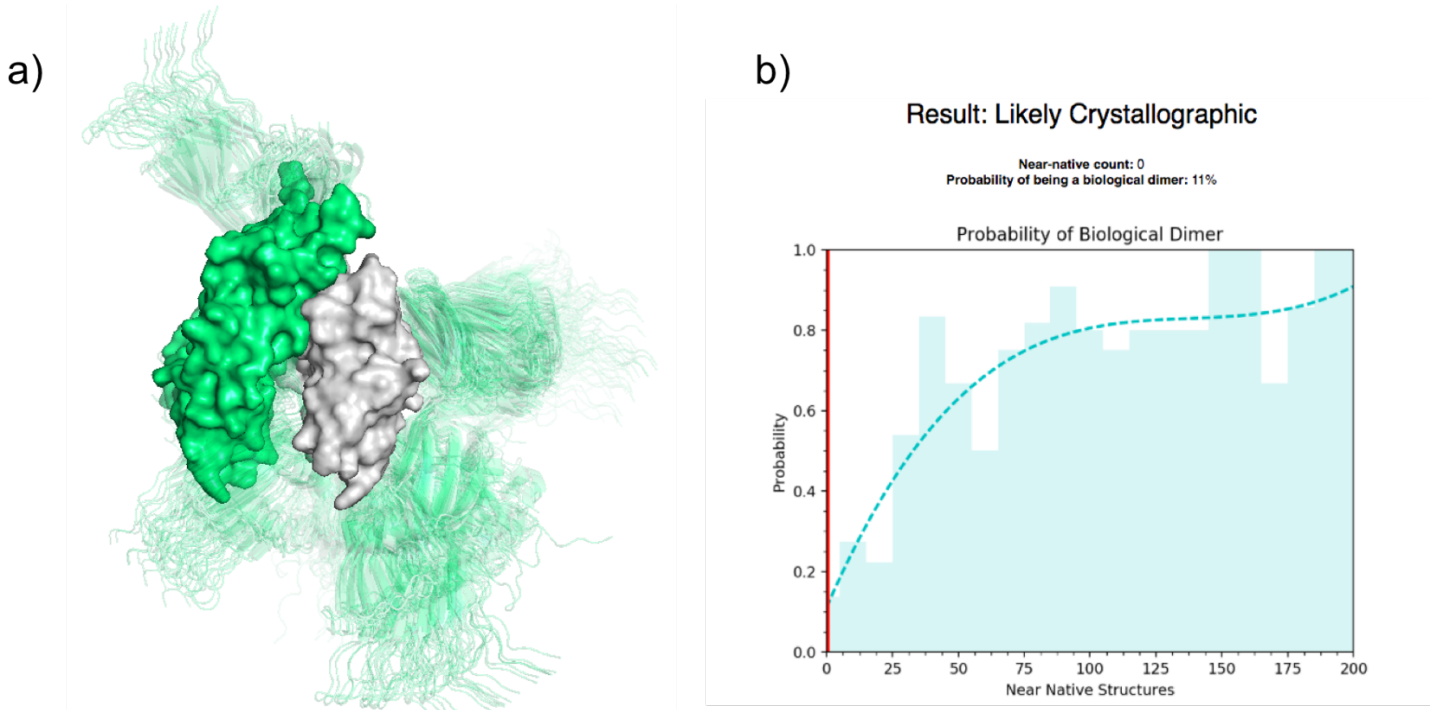

Figure 4.5 Results from the ClusPro-DC server for the unbound 27Q-131R allotype.

a) Monomer 1 of the proposed FcγRIIa-131R dimer is shown in white, and monomer 2 in green (surface). The 100 dimer pairs which have the lowest docking energy to monomer 1 are displayed in transparent green (cartoon). **b)** The bar chart shows, for different near-native counts, what percentage of cases in the training set were biological dimers. The dashed green line is a fitting curve, which can be used to predict the probability of a dimer being biological [136, 154]. The vertical red line shows the number of native structures for submitted dimer, which is 0 for the proposed FcγRIIa-131R dimer. Therefore, the server predicted that the dimer structure proposed by Ramsland *et al.* was likely a crystallographic dimer.

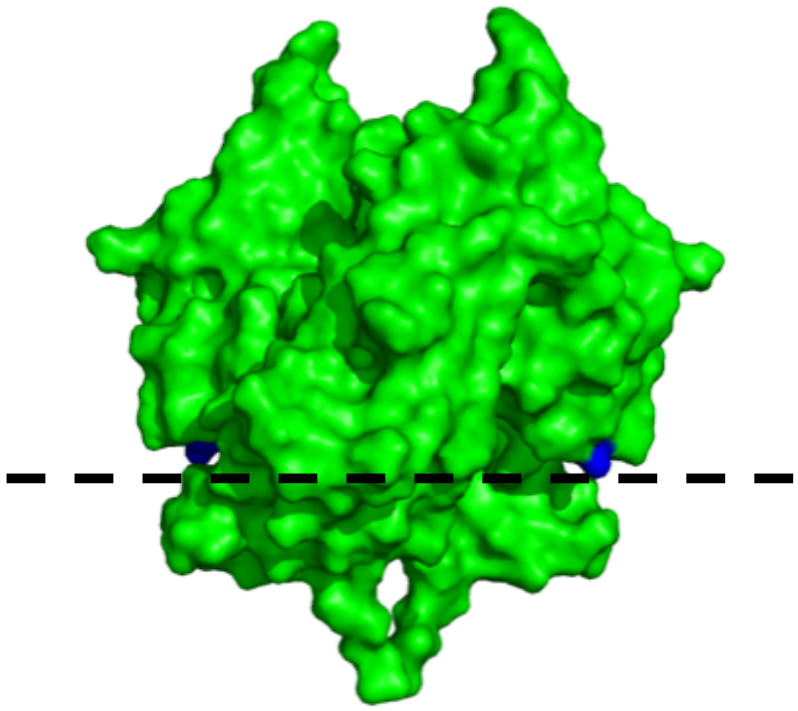

Figure 4.6 The proposed dimer of the 27Q-131R allotype.

The C-terminal residues are shown in blue. A representation of the cell membrane is shown as a dashed line.

4.2.3 Re-refinement of 3RY6 (27Q-131R allotype in complex with IgG1-Fc)

After molecular replacement using a higher resolution template, only one solution was found with a log-likelihood gain (LLG) of 1564 and Translation Function Z-score (TFZ) of 28.6, giving a strong indication that the correct solution had been found. As the 3 chains were separated for molecular replacement, they had freedom to move independently relative to each other, which improved the model statistics directly (Table 4.4). Although R-work only improved by 0.8%, R-free improved by 16%. This reduced the gap between R-work and R-free to 7% which is an improvement on the previous 22% gap. The clash score was also reduced, and both rotamer and Ramachandran outliers were completely removed from the model. Although the percentage of RSRZ outliers increased, the value was still in the acceptable range. The full PDB validation report can be found in Appendix C.1.

Table 4.4 Comparison of the key statistics for 3RY6, before and after refinement.

	Before re-refinement	After re-refinement
R-work	0.252	0.244
R-free	0.473	0.313
Clash score	119	1.44
Ramachandran outliers	21.2%	0%
Rotamer outliers	18%	0%
RSRZ outliers	0.3%	2.1%

The comparison of the overall models before and after re-refinement (Figure 4.7a) shows a considerable increase in the amount of secondary structure elements such as α-helices and β-sheets assigned by PyMol, displaying the improvement in stereochemistry upon re-refinement. Comparison of the electron density of the old model and new re-refined model with one of the β-sheets of the CH2 domain in chain B (Figure 4.7), shows that the new model has a superior fit to the electron density with a more defined secondary structure. It is clear from the Ramachandran plots (Figure 4.8) that the new model shows a large reduction in the number of Ramachandran outliers.

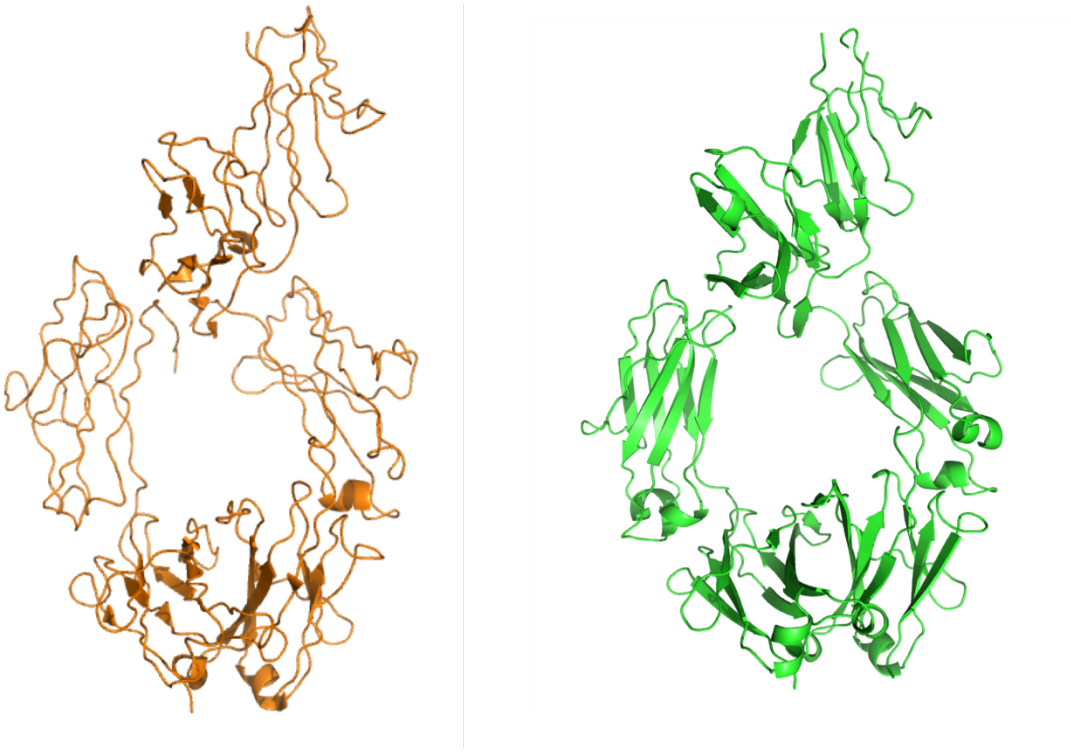

Figure 4.7 Model of 3RY6 before (orange) and after (green) re-refinement.

Overview of the whole structure shows that in the new model there is a significant increase in secondary structure elements particularly beta sheets. The $2F_o$-F_c map is shown contoured to 1.5σ.

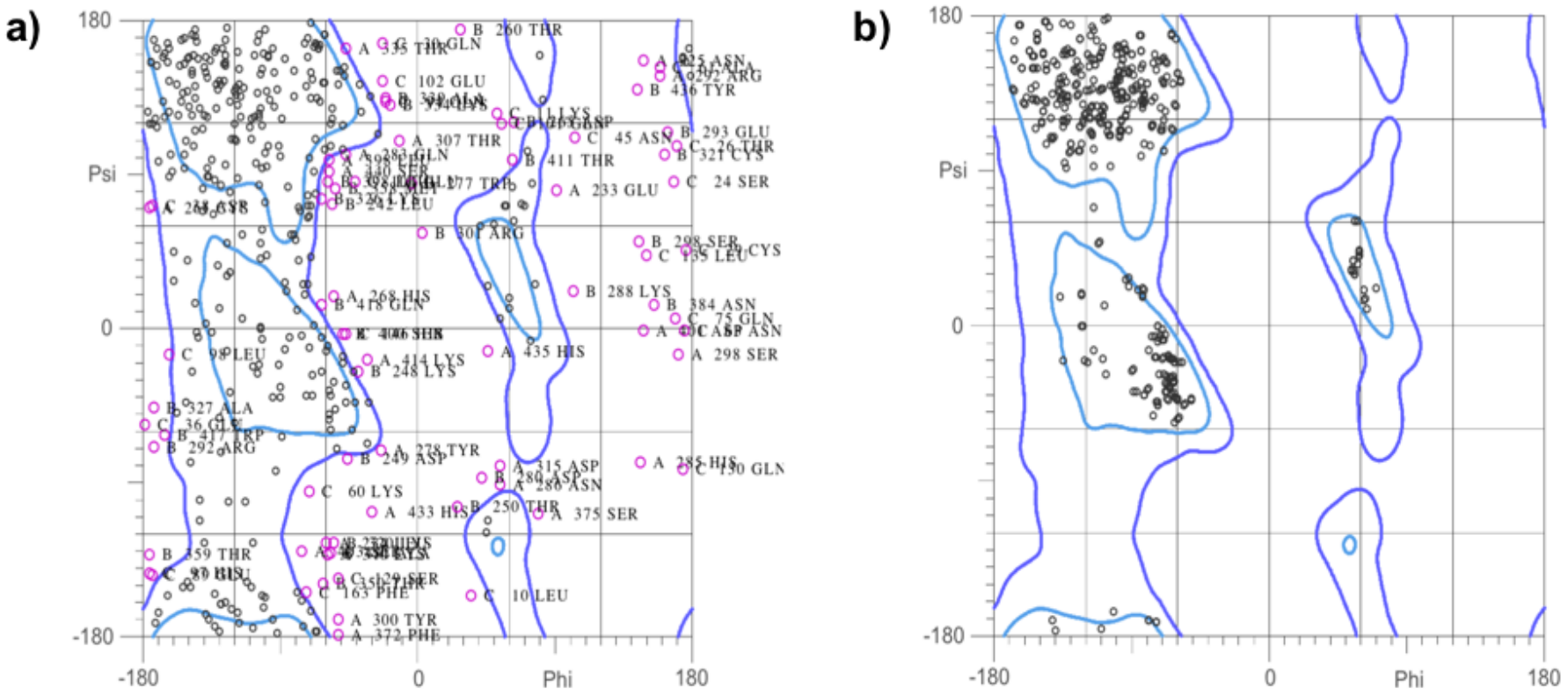

Figure 4.8 Ramachandran plots for 3RY6 before and after re-refinement.

Created using the MOLPROBITY server [131]. The area inside the dark blue line represents allowed and the light blue line represents preferred**.** Residues outside of these areas are highlighted with a pink marker. **a)** Before refinement a large number of residues could be seen in the disallowed regions (21.2%). **b)** After re-refinement all residues are in the allowed regions, with the majority in the preferred regions. No Ramachandran outliers were present after re-refinement.

Before re-refinement, the 3RY6 structure deposited in the PDB had large regions of model with no convincing electron density fit for the FcγRIIa chain, raising doubts about accuracy of the backbone trace. After re-refinement, the electron density improved significantly allowing the model to be fitted more accurately and hence reducing the R-free value. Additionally, a few residues were removed as no electron density was available (Table 4.5).

Table 4.5 List of residues missing in the model for the FcγRIIa chain after re-refinement.

Residue number	Residue
1	Ala
2	Pro
30	Arg
31	Ser
32	Pro
33	Glu
34	Ser

Many of the deleted residues were in the proposed dimer interface of IgG1-Fc-bound FcγRIIa. Before re-refinement (Figure 4.9a) the model in this region was poorly fitted to the electron density map and many residues had no electron density. This was improved following re-refinement (Figure 4.9b).

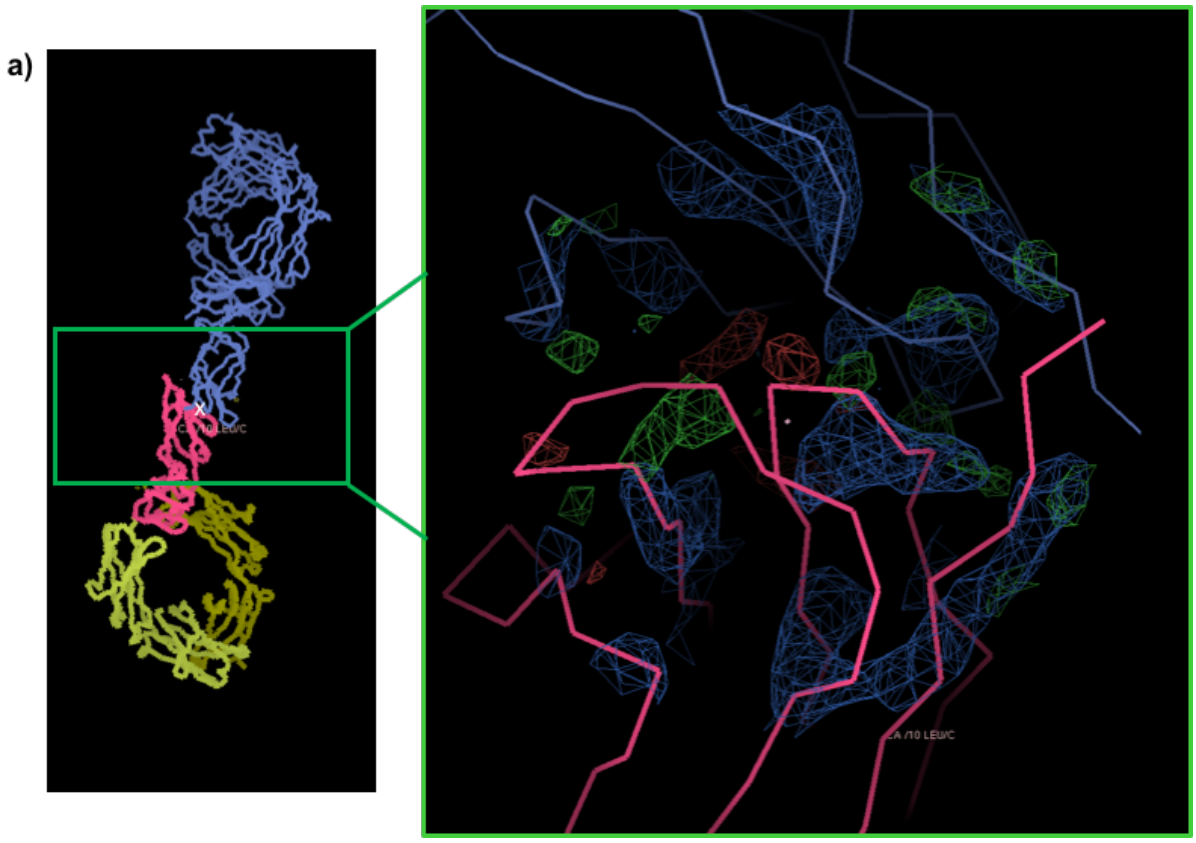
a)

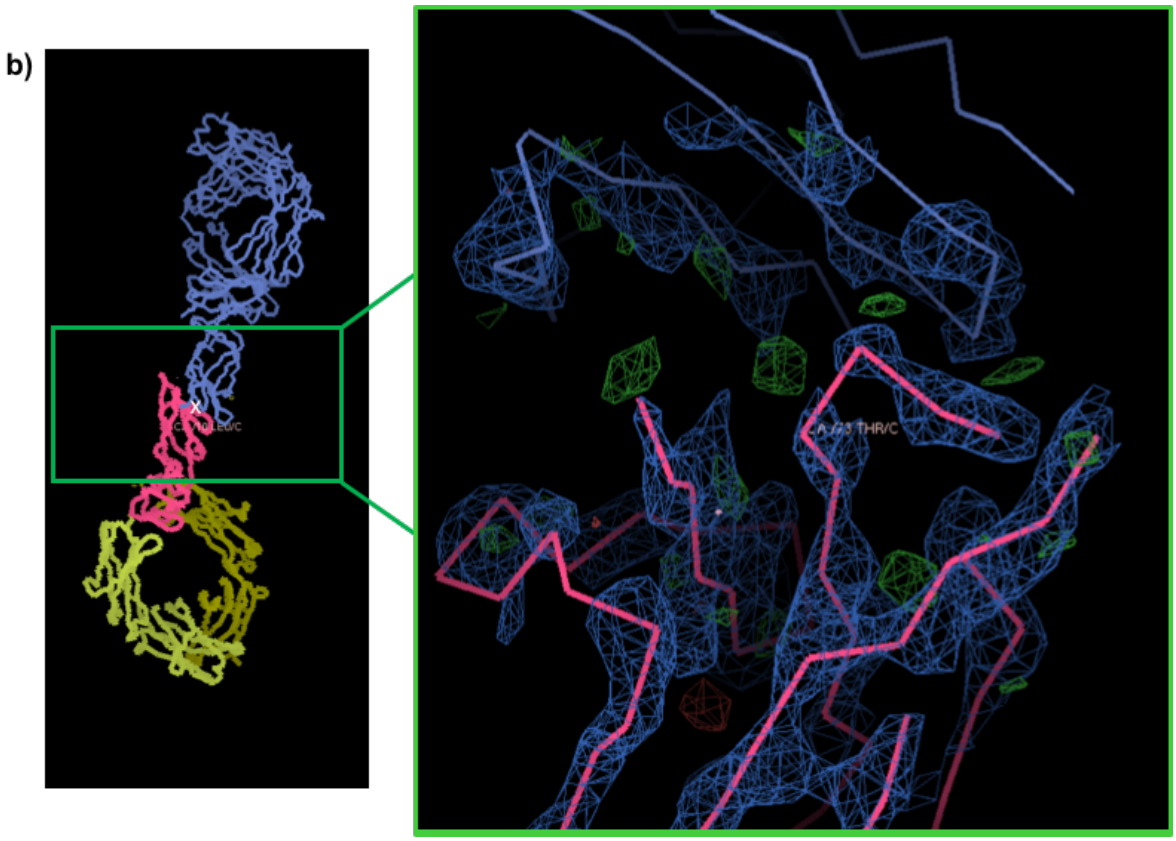

Figure 4.9 The C-alpha trace of FcγRIIa at the dimer interface of the receptor fitted into the electron density map.

$2F_o$-F_c map contoured at 1.4σ. Purple: symmetry mate of the whole complex; Pink: FcγRIIa monomer 1; IgG1-Fc bound to FcγRIIa. **a)** Before re-refinement. **b)** After re-refinement.

Alignment of the old and new model revealed that this chain was considerably different following re-refinement (Figure 4.10).

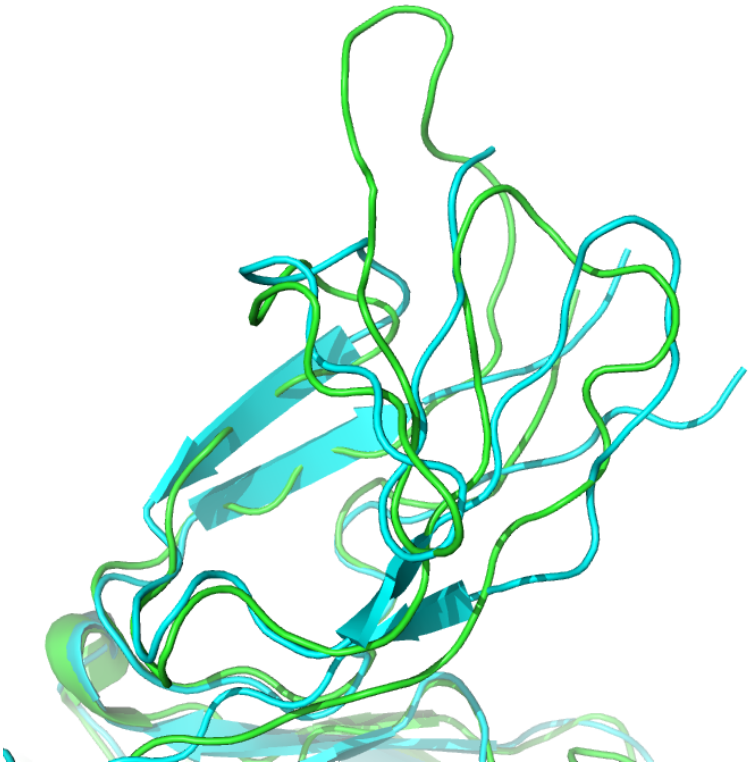

Figure 4.10 The section of FcγRIIa which is in the proposed dimer interface, following alignment the old model of FcγRIIa bound to IgG1-Fc (3RY6) and the improved, re-refined model.

Old model, green; re-refined model, cyan. All-atom rmsd = 0.959 Å.

4.2.3.1 Analysis of the IgG1-Fc-bound dimer interface

Following re-refinement, the proposed FcγRIIa dimer was again uploaded to ClusPro-DC. The results showed that the dimer was likely crystallographic (Figure 4.11). Analysis using PISA showed that the dimer had a low buried surface area, of only 336 $Å^2$ per monomer. This makes up only 3.5% of the

total surface area to be buried, and out of a total of 157 residues per monomer, only 12 residues were involved in the dimer interface. The distance between the 2 C-terminal residues was measured to be 57 Å (distance between C-α measured in PyMol).

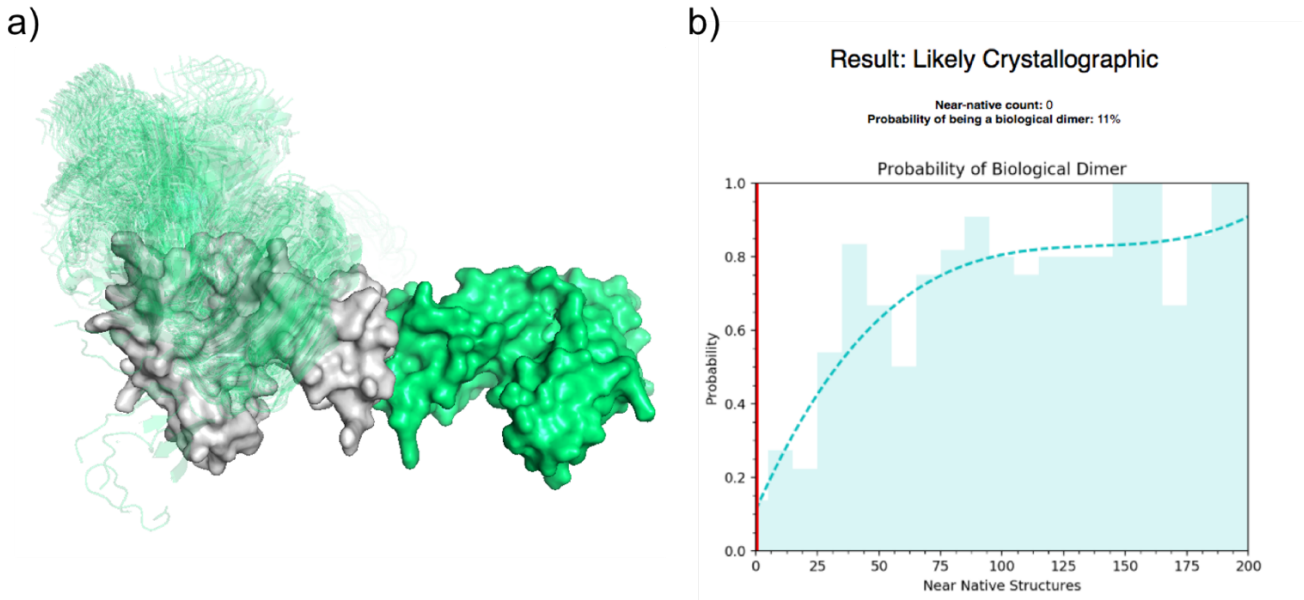

Figure 4.11 Results from the ClusPro-DC server for the IgG1-Fc bound 27Q-131R allotype.

a) Monomer 1 of the proposed Fc-bound FcγRIIa-131R dimer (Fc removed) is shown in white, and monomer 2 in green (surface). The 100 dimer pairs which have the lowest docking energy to monomer are displayed in transparent green (cartoon). **b)** The bar chart shows, for different near-native counts, what percentage of cases in the training set were biological dimers. The dashed green line is a fitting curve, which can be used to predict the probability of a dimer being biological [136, 154]. The vertical red line shows the number of native structures for the submitted dimer, which is 0 for the proposed Fc-bound FcγRIIa-131R dimer. Therefore, the server predicted that the dimer structure proposed by Ramsland *et al.* was likely a crystallographic artefact.

4.2.4 Experimental evidence to oppose the theory of dimerisation

As the dimer structures proposed by Ramsland *et al.* were predicted to be crystallographic artefacts rather than biological dimers, further experimental work was carried out to support this, using the protein ectodomains.

4.2.4.1 High-Performance Liquid Chromatography-Small-Angle X-ray Scattering

High-Performance Liquid Chromatography-Small-Angle X-ray Scattering (HPLC-SAXS) was carried out on the 27Q-131H allotype of the FcγRIIa ectodomain. As a monomeric control, the S126P mutant was used.

Unfortunately, the protein samples suffered from radiation damage, so accurate structures could not be deduced. However, some conclusions could still be drawn from this data. The HPLC elution profiles (Figure 4.12) show that FcγRIIa (27Q-131H) eluted at the same time as the FcγRIIa (27Q-131H) S126P monomeric control, suggesting that they were both the same size. The *ab initio* envelopes calculated from the x-ray scattering (Figure 4.13) again show that FcγRIIa (131H-27Q) and the S126P monomeric control had a similar size and shape, which suggests that the FcγRIIa ectodomains were not forming dimers in solution.

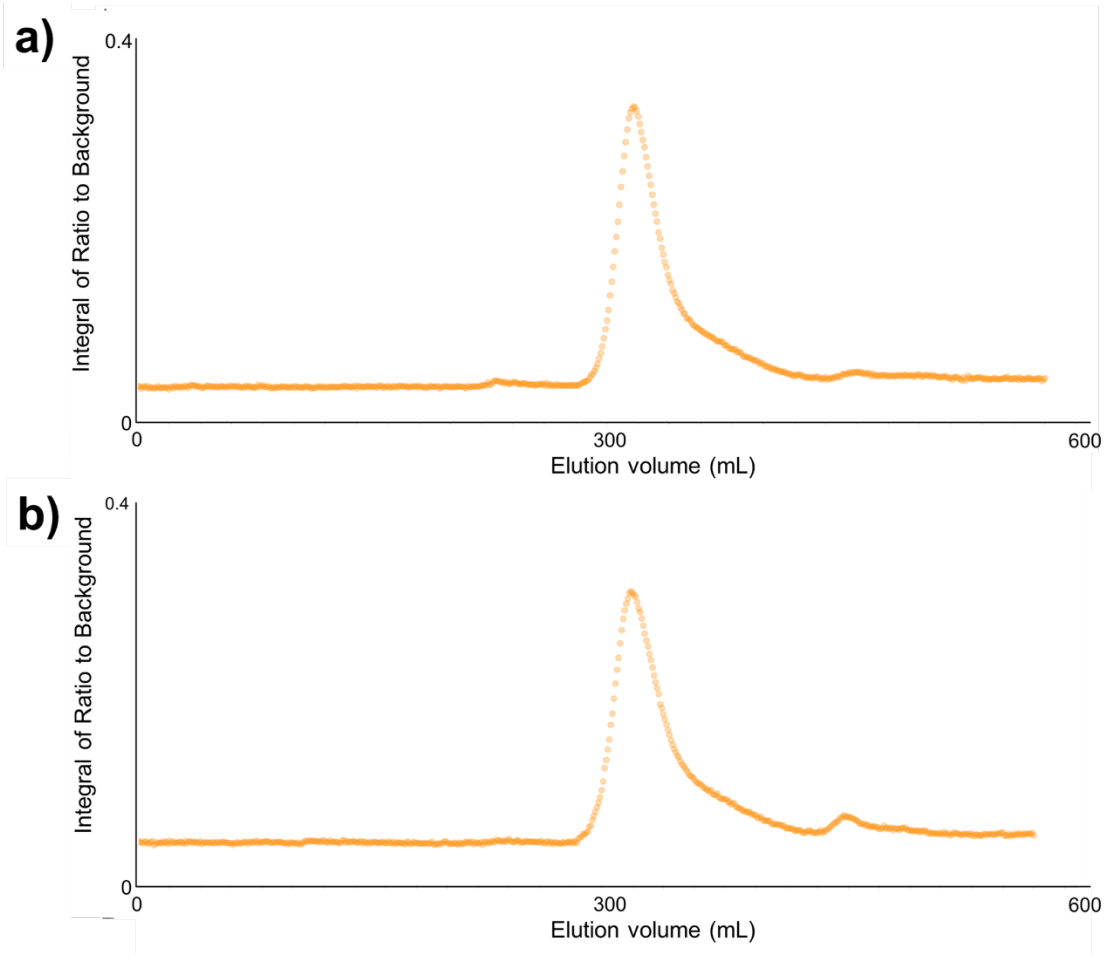

Figure 4.12 HPLC elution profiles of FcγRIIa ectodomains.

a) 131H-27Q allotype. **b)** 131H-27Q allotype with S126P mutation as a monomeric control. Both proteins eluted at the same volume (300ml) indicating that both proteins have the same size.

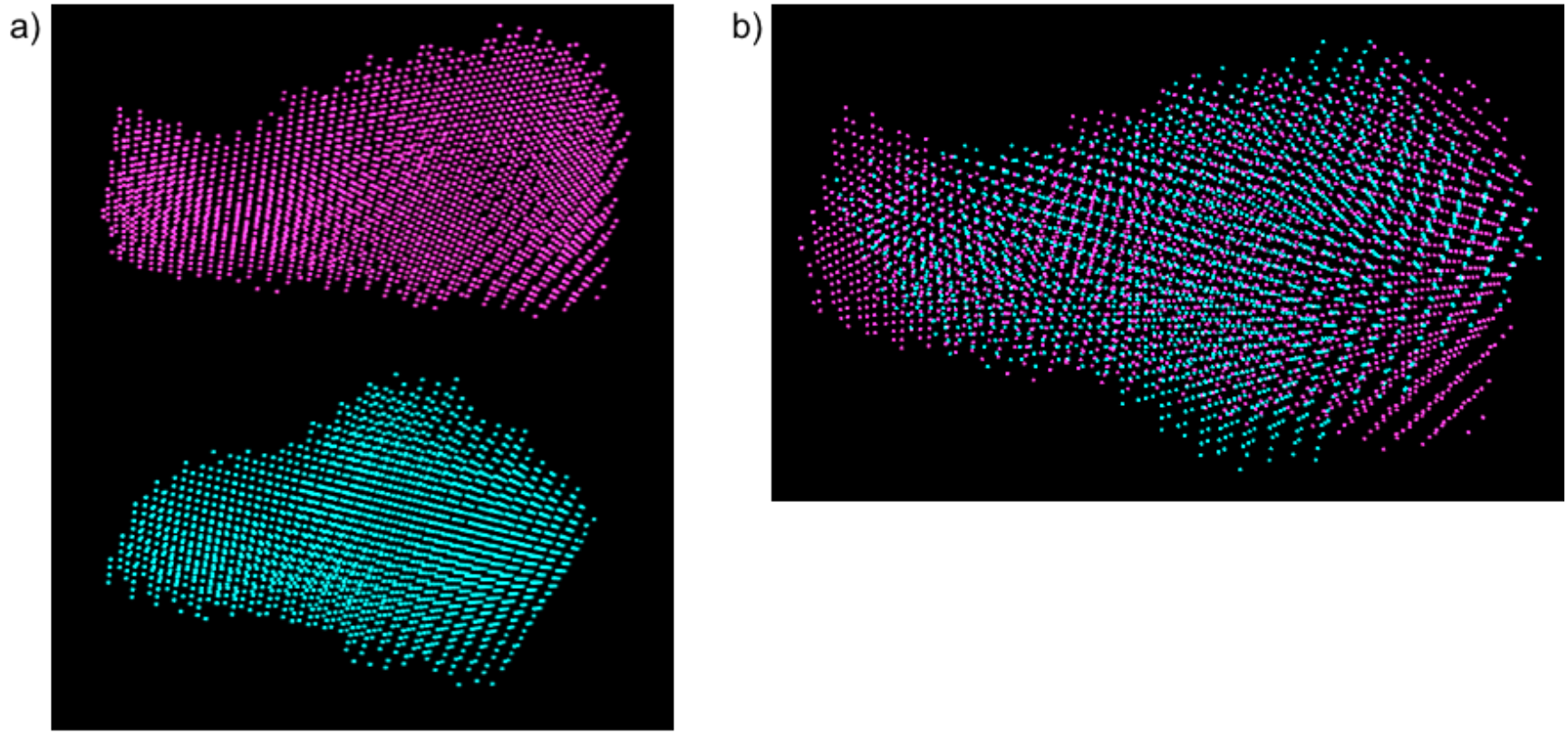

Figure 4.13 *Ab initio* envelopes of FcγRIIa ectodomain proteins from SAXS calculated using DAMMIN [155].

Pink: 131H-27Q; Cyan: 131H-27Q S126P (monomeric control). **a)** *Ab initio* envelopes side by side. **b)** *Ab initio* envelopes overlaid using SUPCOMB [123]. It can be seen that they are almost identical, indicating that the wild allotype has the same size and shape as the S126P monomeric control.

4.2.4.2 SEC-MALLS on ectodomains

Although the data from HPLC-SAXS showed that FcγRIIa (27Q-131H) and the S126P monomeric control were the same size and shape, there was no further information on the molecular weight or the oligomeric states of the protein. Therefore SEC-MALLS was carried out on all 6 allotypes of FcγRIIa.

Results from the SEC-MALLS (Figure 4.14) revealed that all 4 ectodomain allotypes of FcγRIIa were monomeric, with a molecular weight of ~30 kDa. These results confirm that the soluble ectodomain dimer structures of the 27Q-131H and 27Q-131R allotypes previously published in the literature are likely to be artefacts of crystallization. Furthermore, residue 131 is involved in IgG binding, so it is unlikely to modulate the formation of dimers.

4.2.4.2.1 Glycosylation analysis

By applying the conjugate method, analysis of the glycosylation modification of the ectodomains was carried out using SEC-MALLS. This showed that sugar modification contributed around 20% of the total MW, and the MW of the protein alone was around 25 kDa (Table 4.6). Interestingly, the 27W allotypes appear to have larger sugar modifications than the 27Q allotypes, with an extra ~1kDa of glycosylation.

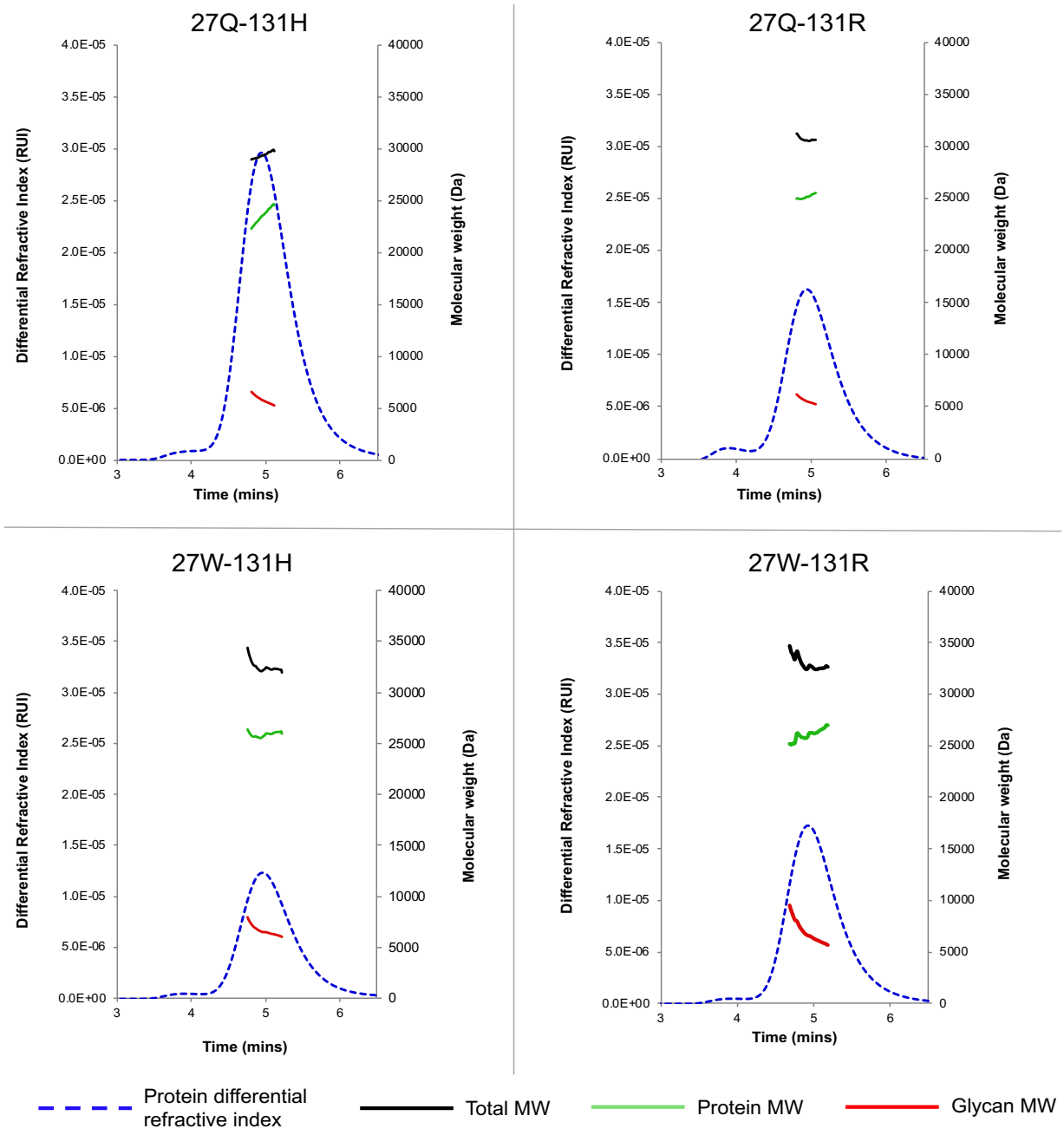

Figure 4.14 SEC-MALLS chromatograms with fit of the molecular weight.

The results show that all allotypes of the FcγRIIa ectodomains are monomeric in solution, with a MW of around 30 kDa. Sugars contribute approx. 20% of the MW (~5 kDa).

Table 4.6 Glycosylation analysis from SEC-MALLS.

Results revealed that glycans contributed around 20% of the total molecular weight of FcγRIIa ectodomains (5-7 kDa). The 27W allotypes appear to have larger sugar modifications than the 27Q allotypes.

Allotype	**Total MW (kDa)**	**Protein MW (kDa)**	**Glycan MW (kDa)**
27Q-131H	29.3 (±0.5%)	23.5 (±0.5%)	5.8 (±2.5%)
27Q-131R	30.7 (±0.3%)	25.1 (±0.3%)	5.6 (±1.8%)
27W-131H	32.5 (±0.6%)	25.9 (±0.6%)	6.6 (±3.0%)
27W-131R	33.0 (±0.4%)	26.1 (±0.4%)	6.9 (±2.0%)

4.2.4.3 Crystal structure of the RA-associated 27W-131H ectodomain protein

4.2.4.3.1 Initial crystallisation screens

From the initial JSCG core screens, crystals of the 27W-131H ectodomain grew in 0.1 M sodium phosphate citrate, pH 4.2 with 40% (v/v) PEG300 after 5 days.

4.2.4.3.2 Optimisation

Following optimisation, crystals of the 27W-131H ectodomain protein were produced in 0.1 M sodium phosphate citrate, pH 4.2 with 41% (v/v) PEG300. UV-TPEF images at 5 days, 12 hours confirmed that these were protein crystals (Figure 4.15).

4.2.4.3.3 A 1.8 Å structure of 27W-131H FcγRIIa ectodomain

Following refinement of the structure obtained from the crystals, a 1.8 Å structure of FcγRIIa was produced (Figure 4.16; Table 4.7). The structure had clear density for the sidechains, allowing the polymorphic residues 27 and 131 to be fitted.

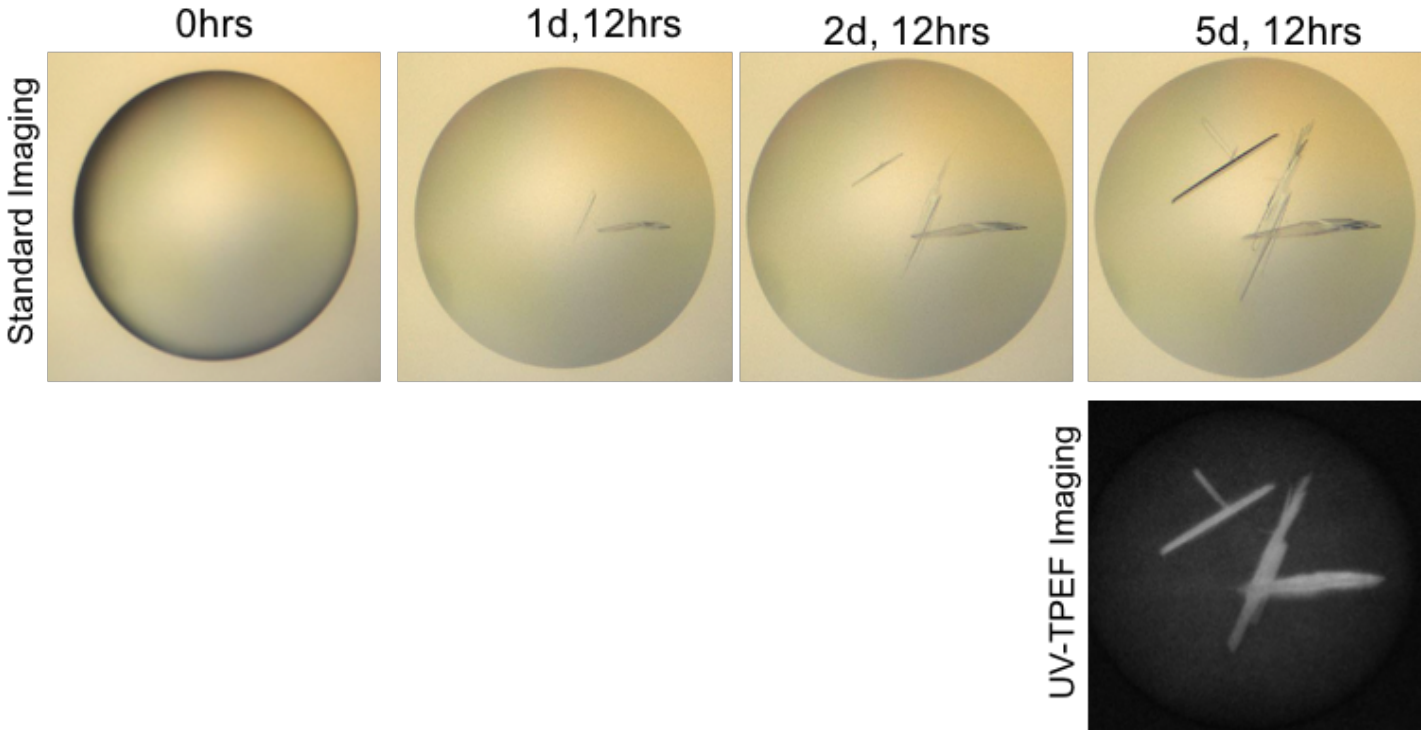

Figure 4.15 Growth of 27W-131H ectodomain crystals in 0.1 M sodium phosphate citrate, pH 4.2 with 41% (v/v) PEG300 at different time points.

After 5 days and 12 hours, large protein crystals had been produced. UV-TPEF imaging confirmed that they were protein crystals

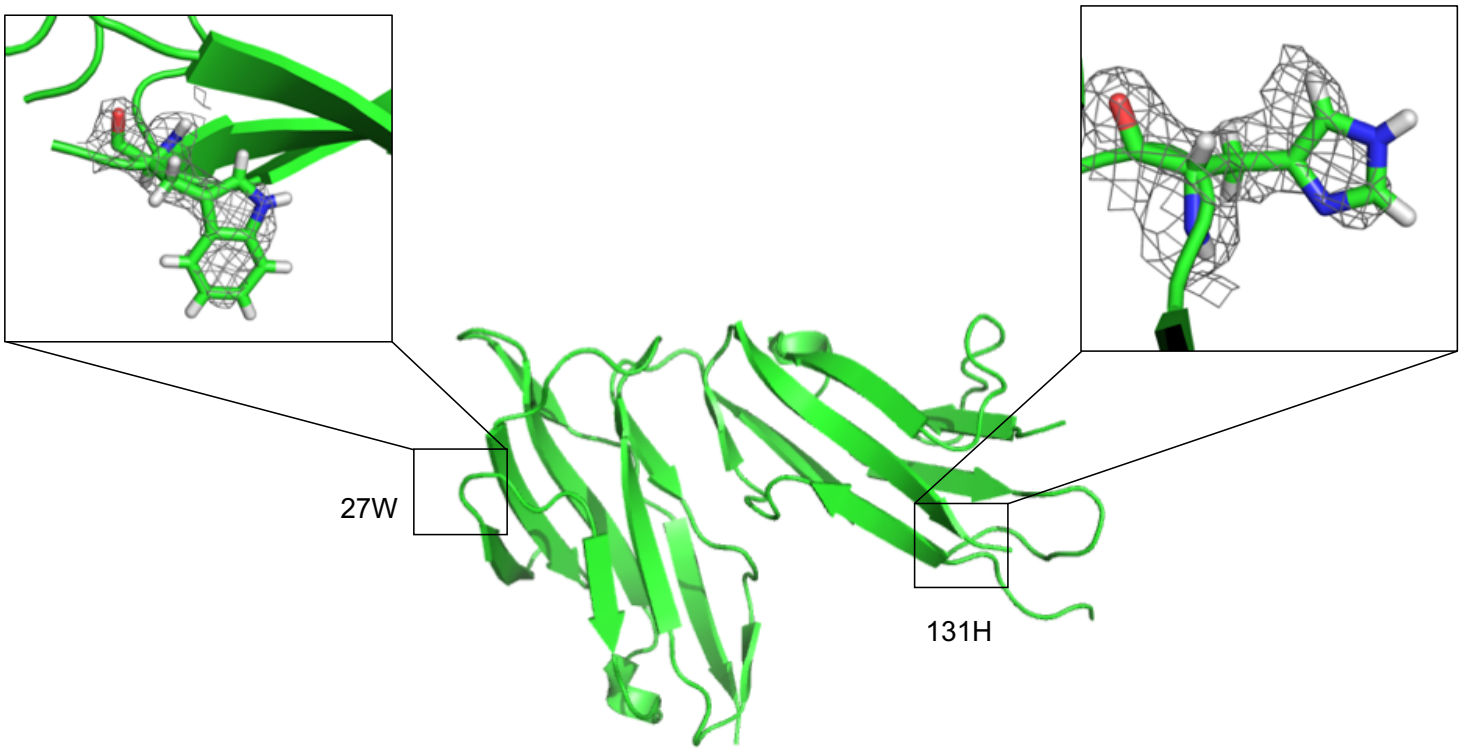

Figure 4.16 Crystal structure of the 27W-131H allotype of FcγRIIa ectodomain at 1.8 Å resolution.

Polymorphic residues 27 and 131 are highlighted, showing that there was clear density for these sidechains allowing them to be modelled. 2*Fo-Fc* map contoured to 1.5σ.

Wavelength (Å)	0.9795
Resolution range (Å)	41.82 - 1.81 (1.875 - 1.81)
Space group	C 2 2 2_1
Unit cell	49.9 76.5 108.3 90 90 90
Unique reflections	19293 (1867)
Multiplicity	6.1 (4.0)
Completeness (%)	99.0 (96.8)
Mean I/σ (I)	6.3 (1.4)
Wilson B-factor ($Å^2$)	21.7
R-merge	0.15 (0.73)
R-meas	0.16 (0.83)
R-pim	0.06 (0.39)
$CC_{1/2}$	0.99 (0.45)
Reflections used in refinement	19122 (1828)
Reflections used for R-free	907 (94)
R-work	0.193 (0.361)
R-free	0.225 (0.344)
Number of non-hydrogen atoms	1587

macromolecules	1349
ligands	127
solvent	111
Protein residues	168
RMS(bonds)	0.004
RMS(angles)	0.74
Ramachandran favoured (%)	98.8
Ramachandran allowed (%)	1.2
Ramachandran outliers (%)	0.00
Rotamer outliers (%)	0.00
Clashscore	1.4
Average B-factor	32.2
macromolecules	29.5
ligands	55.6
solvent	38.1
Number of TLS groups	6

Table 4.7 Data collection and refinement statistics for 27W-131H.
Statistics for the highest-resolution shell are shown in parentheses.

Xtriage analysis was carried out on the 1.8 Å structure. This calculated that there was only 1 copy of the protein in the asymmetric unit (ASU).

4.2.4.3.4 Does the crystal structure of 27W-131H ectodomain show dimers?

Once the structure of the 27W-131H ectodomain had been solved, it was analysed to see if a dimer pair was present. Crystallographic symmetry mates were found, an example of which is shown in Figure 4.17, with a distinct dimer interface than the other allotypes. These were also uploaded to the ClusPro-DC server, and it was found that they were also likely to be a crystallographic dimers rather than a biological dimer.

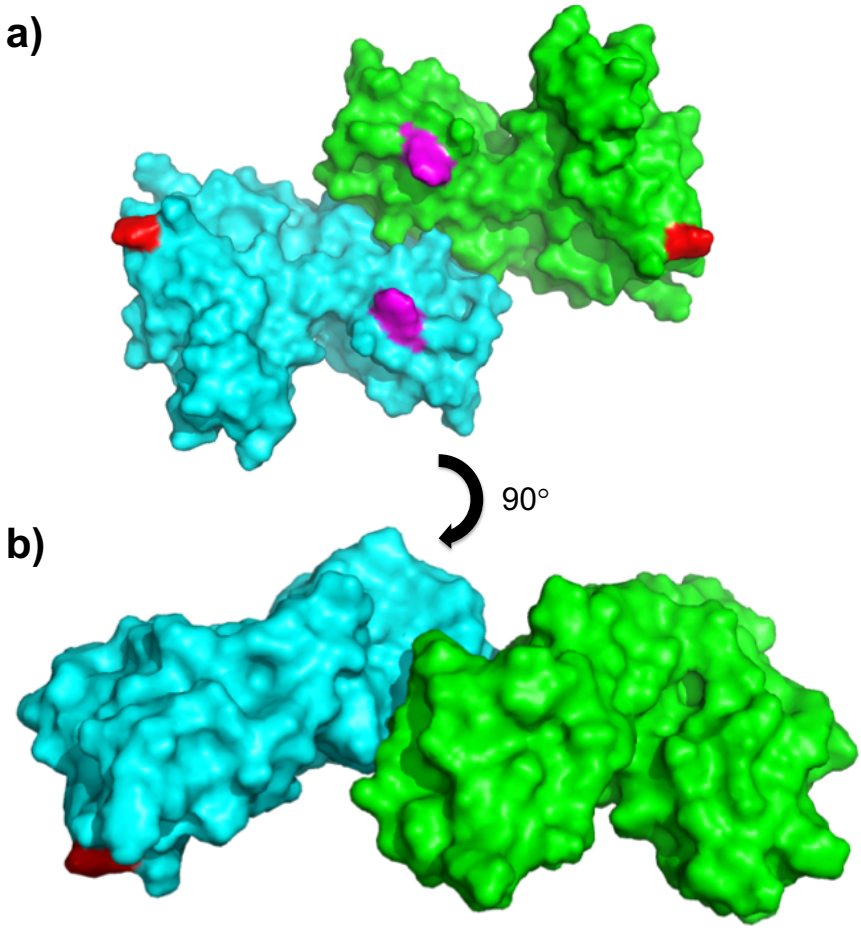

Figure 4.17 Crystallographic dimer of the 27W-131H ectodomain.

Monomer 1 in cyan, monomer 2 in green. Residue 27 is shown in magenta and residue 131H in red. **a)** View from the bottom of the dimer. **b)** View from the side of the dimer.

4.2.4.3.5 Carbohydrates

Carbohydrates were present in the structure, attached to N145 of FcγRIIa. The density for these sugars was strong allowing them to be modelled accurately (Figure 4.18).

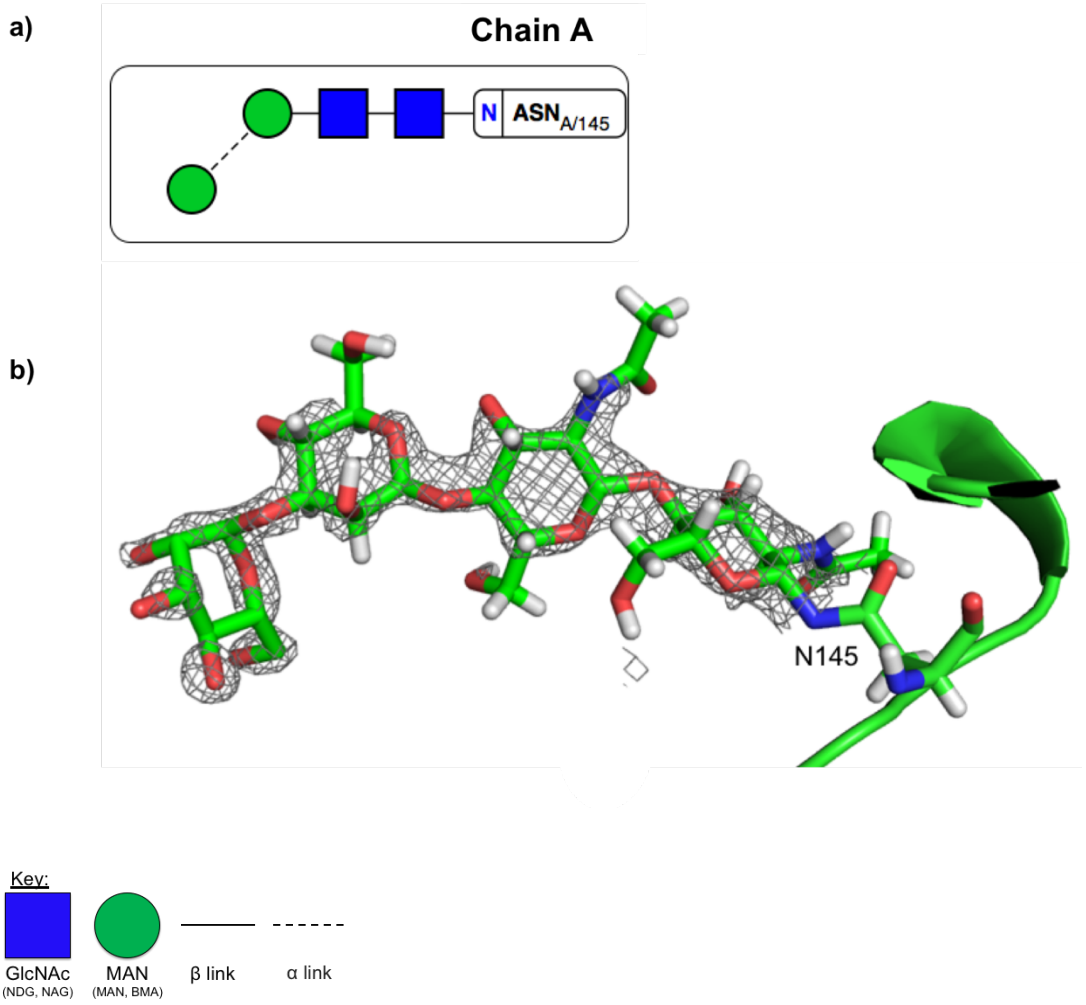

Figure 4.18 Sugars attached to N145 of FcγRIIa, in the crystal structure of the 27W-131H allotype at 1.8 Å resolution.

a) Glycoblocks representation of the sugars which were present. **b)** The sugars modelled into the 2*Fo-Fc* map contoured to 1.5σ.

Although the validation report from the PDB (Appendix C.1) showed 'major validation errors' these can be explained. First of all, a symmetry-related clash was seen between the O2 atom of MAN178 and the OD_2 atom of D115

in another ASU (Figure 4.19). However, clear density was present for this residue, suggesting that it has been modelled correctly. These atoms had an interatomic distance of 2.16 Å and the clash overlap for these atoms was 0.04 Å. Additionally, there is a phosphate ion present in the structure which sits on the crystallographic two-fold axis (Figure 4.20). Again this showed strong electron density in the 2*Fo-Fc* map suggesting that this ion is modelled correctly; however, this clashes with the phosphate ion present in the crystallographic symmetry mate which also showed strong electron density. Only one of these phosphate ions can be present at any one time; to account for this, the phosphate ion was assigned an occupancy of 0.5.

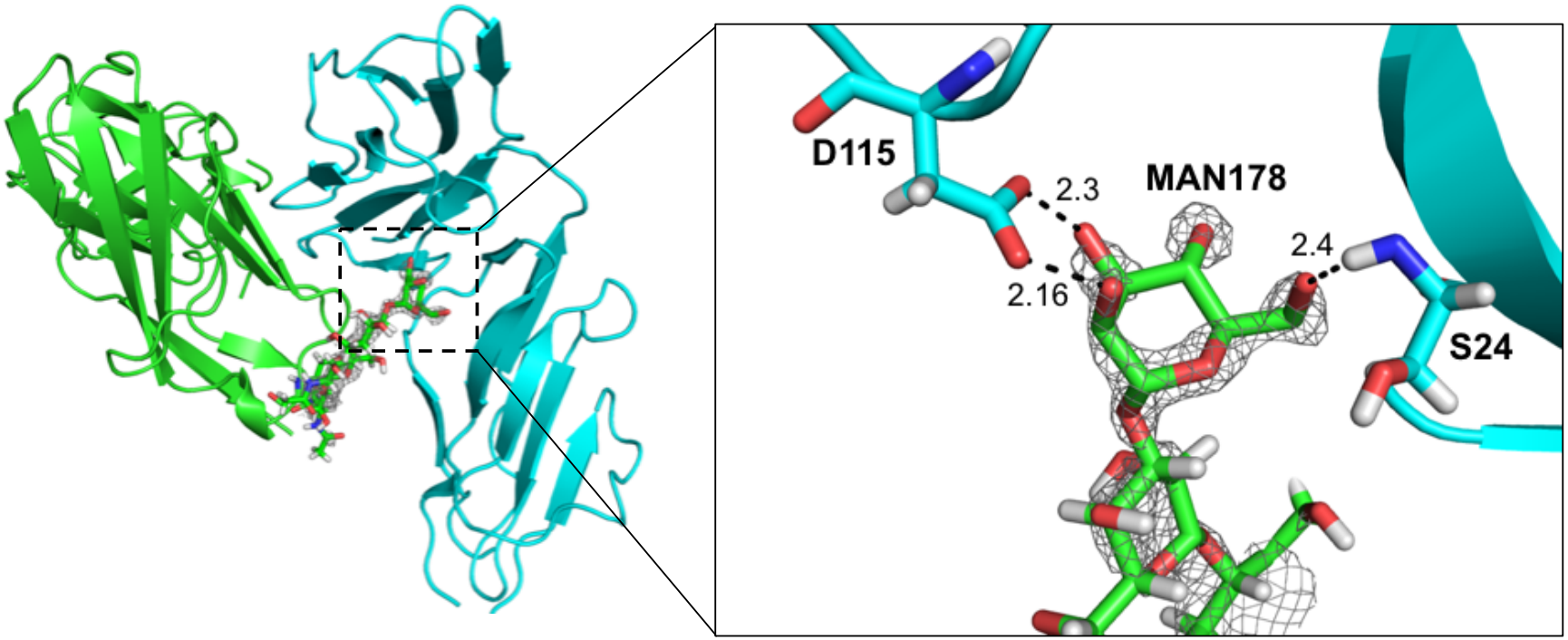

Figure 4.19 Carbohydrate clashes between the 27W-131H allotype of FcγRIIa ectodomain at 1.8 Å resolution (green) and a crystallographic symmetry mate (cyan).

MAN178 at the end of the carbohydrate chain attached to N145 of FcγRIIa clashes with D115 of the symmetry mate. The clash occurs between D115 OD_2 and MAN178 O_2, with an interatomic distance of 2.16 Å. Clear density was present for this residue suggesting that it has been modelled correctly. 2*Fo-Fc* map contoured to 1.5σ.

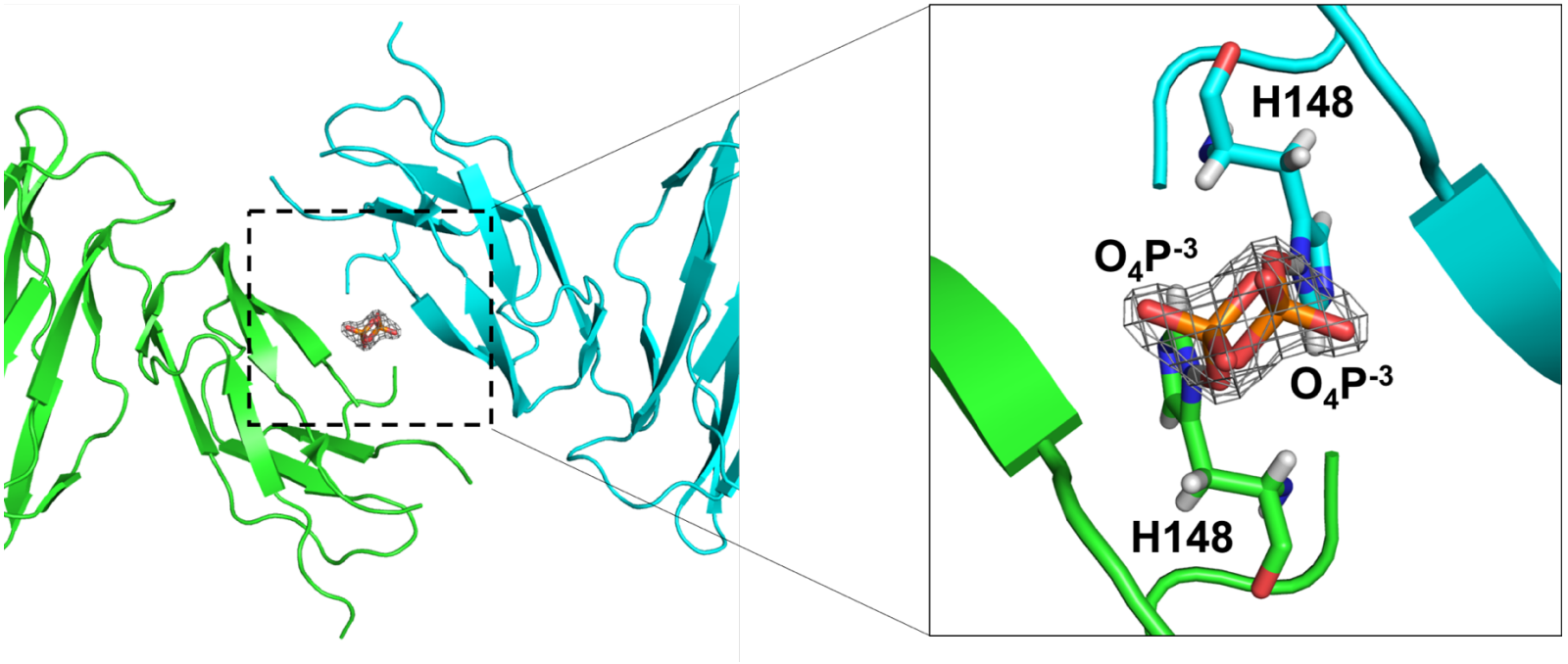

Figure 4.20 The O_4P^{-3} ion sits between the 27W-131H allotype of FcγRIIa ectodomain at 1.8 Å resolution (green) and a crystallographic symmetry mate (cyan).

The O4P-3 ion sits in the 2-fold crystallographic axis, where a O4P-3 ion from a crystallographic symmetry mate also sits, causing a clash. 2Fo-Fc map contoured at 1.5σ.

4.2.5 Comparison of the structures of the allotypic variants

The ectodomain structures were compared to assess if the polymorphisms affect the overall structure of the receptor. The backbone traces largely overlay with each other (Figure 4.21). However, a small region of the receptors differed, from residues 29-36. In the new crystal structure of the 27W-131H allotype, no density was present for this region, so no model was built (red), and for the 27Q-131H and 27Q-131R structures, the protein backbones in this region were different. This is likely to be a flexible region of the protein rather than a direct effect of the polymorphisms. It can therefore be concluded that the polymorphisms do not affect the overall structure of FcγRIIa.

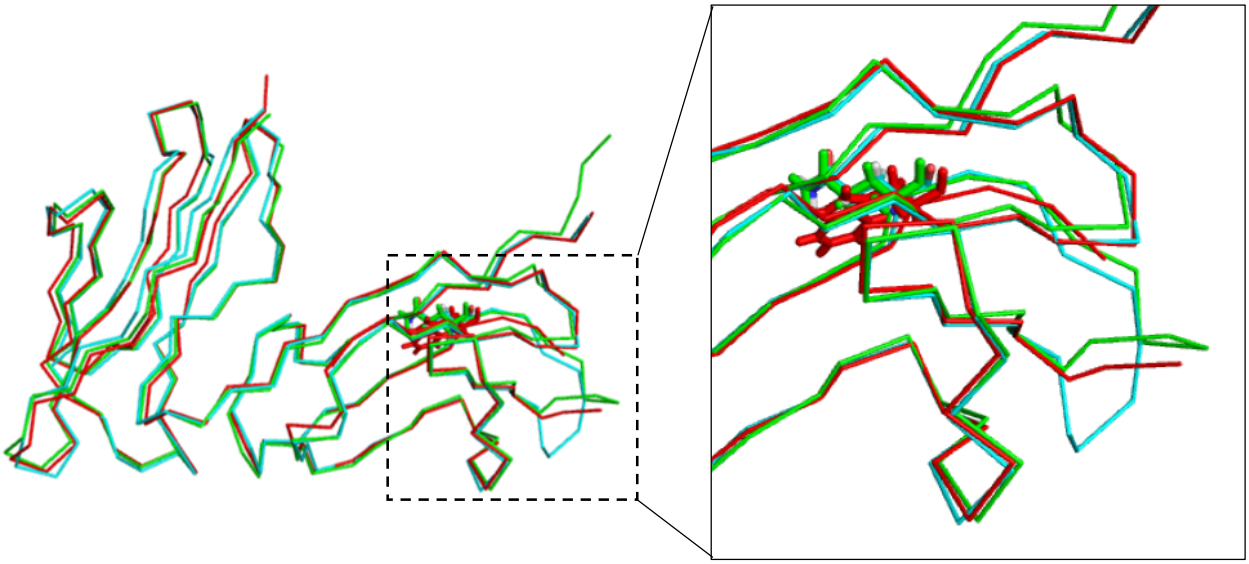

Figure 4.21 Overlay of the backbone traces of 27W-131H (red, all-atom rmsd = 0.78 Å), 27Q-131H (cyan) and 27Q-131R (green, all-atom rmsd = 1.01 Å) produced in PyMol.

The backbone traces are largely the same but differ in the region between residues 29-36. The polymorphic residue 27 is shown as sticks.

4.3 Discussion and conclusions

4.3.1 Analysis of the unbound homodimers

Initial studies of the dimer structures proposed by Ramsland *et al*. [97] raised doubts, as the models were not sufficiently refined and the buried surface area of the dimers was small. The 27Q-131H allotype showed that the buried surface area of each monomer was 237 Å^2. Given that the solvent accessible surface area of the monomer is 9326 Å^2, the buried surface area represents only 2.5% of this. The buried surface area of each monomer of the 27Q-131R allotype was found to be 649 Å^2. Although this was higher than the buried surface area of the FcγRIIa-131H dimer, it was still only 7% of the solvent accessible total surface area. Again this is smaller than expected for a protein with accessible surface area of 9463 Å^2. It would be expected that the buried surface of a biological dimer would be significantly greater than this, as it is known that on average, homodimer interfaces have a buried surface of around 16% of the total surface area [156]. Additionally, the orientations of the dimers were not optimal for C-terminal insertion into the cell membrane. The ClusPro-DC server predicted that the dimers were likely to be artefacts of crystallisation. Furthermore, SAXS on the ectodomain of the 27Q-131H allotype showed the same *ab initio* envelope as the S126P monomeric control, indicating that they were both the same size. As this is a structural technique which is carried out in solution, it eliminated the problem of crystallographic contacts. However, as radiation damage occurred, conclusions on the molar mass of the ectodomains and hence the oligomeric state could not be made. Thus, SEC-MALLS was also carried out. This technique allows absolute determination of protein

molecular weights and oligomerisation states [124]. SEC-MALLS showed that all allotypes of FcγRIIa are monomeric in solution at the concentration tested, with a molecular weight of ~30 kDa. Based on the work carried out in this chapter, it can therefore be concluded that the dimer structures of the ectodomains proposed by Ramsland *et al.* are likely to be incorrect.

4.3.1.1 Effect of glycosylation on dimerisation

As FcγRIIa glycosylation is important for ligand binding, it may also be important for dimerisation. The crystal structures by Ramsland *et al.* are from protein produced in *Sf9* cells, therefore core mammalian-like N-glycosylation was present [149]. After re-refinement the sugars attached to N145 of FcγRIIa-131H were close to the dimer interface, so it was important that sugars were present when carrying out all following experiments. SEC-MALLS was performed with protein produced in HEK293T cells, hence mammalian N-linked glycosylation was present. The RA-associated 27W-131H ectodomain structure was obtained from protein produced in HEK293S GnTI$^-$ cells. HEK293S GnTI$^-$ cells have been engineered to lack N-acetyl-glucosaminyltransferase I (GnTI) activity, so any proteins produced by these cells lack complex N-glycans but still possess core mammalian glycans (Figure 4.22) [157, 158]. This is advantageous for crystallography, as complex glycans are often heterogenous and flexible which can prevent crystallisation or produce crystals which diffract at low-resolution. Crystallisation was attempted in this project using FcγRIIa ectodomains produced in HEK293T cells, and although crystals did grow, they only diffracted to 8 Å. Protein produced in HEK293S GnTI$^-$ cells was also used for HPLC-SAXS.

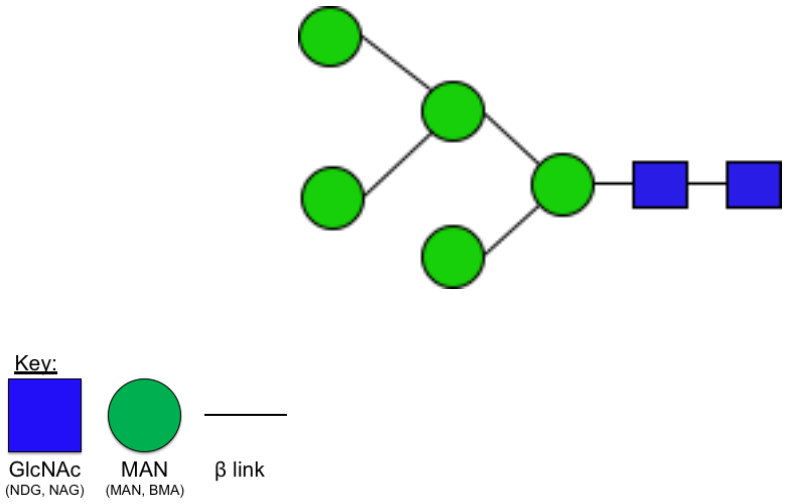

Figure 4.22 A schematic of the core N-glycans present on proteins produced in GnTI$^-$ cells [158].

Since the proteins have been shown to be monomeric when produced in both HEK293T cells and HEK293S GnTI$^-$ cells, this suggests that FcγRIIa ectodomains are monomeric regardless of the glycosylation state.

Results from SEC-MALLS showed that sugar modifications contributed around 20% of the total MW. Interestingly, the 27W allotypes displayed larger sugar modifications than the 27Q allotypes, with an extra ~1kDa of glycosylation. This may help to explain how the 27W-131H allotype is associated with an increased risk of RA: It is widely accepted that glycosylation is important in the FcγR-IgG interaction, so changes in glycosylation may enhance IC binding, leading to enhanced activation of FcγRs and inflammation which is seen in RA. It is not known how this polymorphism causes increased glycosylation, but intriguingly there is a known to be a rare type of glycosylation, named C-glycosylation, in which a mannose is linked to the indole ring of a tryptophan residue [159]. To test whether this modification is occurring, mass spectrometry could be carried out to compare the carbohydrate composition between the allotypes.

Alternatively, these changes in glycosylation may be due to hindrance of the glycosylation machinery. It is known that sugar modifications are added to proteins, then trimmed by enzymes such as glucosidases and mannosidases [160]. Tryptophan has a large indole ring in its side chain, and is larger than glutamine, therefore in combination with the large sugar modifications, the Q27W polymorphism may hinder the ability of these enzymes from binding, thus preventing the sugar modifications from being trimmed.

4.3.2 Analysis of the IgG1-Fc-bound dimer

Before re-refinement, the proposed dimer interface of FcγRIIa in the structure bound to IgG1-Fc had weak electron density, with the model poorly fitting the electron density that was present. Although this was improved upon re-refinement, several residues in this area had no electron density and were thus not modelled. This again raised questions about this proposed dimer structure, as poor electron density suggested that the protein was flexible in this area; if the dimer was real, the contacts in the dimer interface would have stabilised this area of the protein consequently producing a strong electron density map. Further doubts arose due to the buried surface area and the orientation of the dimer. Results from PISA showed a buried surface area of only 336 $Å^2$. With a total surface area of 9254 $Å^2$, this represents only 3.6% of the total surface area. As previously mentioned, a typical homodimer interface buries 16% of the surface area of each monomer on average [156]. Moreover, the C-terminals were not optimally oriented for insertion into the membrane, and the distance between the C-terminal residues was found to be 56.7 Å. As Ramsland *et al.* proposed that this dimer represents the active signalling complex, it is

essential that trans-phosphorylation would be possible. However, it is widely accepted in the field that ITAMs have to be within a distance of 40 Å or less to allow trans-phosphorylation to occur [161]. Thus, a distance of 56.7 Å would not allow trans-phosphorylation. However, the dimer structure may represent the inactive ITAMi form of FcγRIIa, in which transphosphorylation is not required; the absence of immune complexes leads to transient receptor dimers which recruit SHP-1, maintaining low levels of inflammation [48, 162]. Furthermore, there are limitations in the interpretation of the dimer structure, as it represents the extracellular domains of FcγRIIa only. It is not known how conformational changes in these extracellular domains may affect the cytoplasmic domains, which are likely to be disordered and flexible.

To further assess whether this dimer has any biological relevance, it was submitted to the ClusPro-DC server. Again, ClusPro-DC predicted that this dimeric arrangement is likely a result of crystal packing, rather than a genuine biological dimer.

4.3.3 Implications

Showing that the dimer structures proposed by Ramsland *et al*. are incorrect has huge implications for the field. Firstly, the dimer structure of FcγRIIa-131H was used by Powell *et al.* [99] to design an FcγRIIa mutant that was unable to dimerise. They predicted that the S126P mutation would block the dimer interface stopping FcγRIIa-mediated signalling [99]. Interestingly, this mutation does affect receptor signalling, but the authors made no attempts to show that this was through disruption of the dimer interface. As the mutation was based on the incorrect dimer structures, it is likely the mutation probably exerts its effects by a different mechanism. The S126P mutation

does not affect ligand binding [99], therefore further work is needed to decipher how this mutation causes its effects on downstream signalling. Moreover, the S126P may not serve as a relevant monomeric control.

The dimer structure of the 27Q-131H allotype was used by Pietersz *et al.* [96] to design a series of small chemical entities, intended to bind in the groove of the FcγRIIa dimer interface to disrupt IC binding and inflammatory signalling. Although this study shows evidence that some of these SCEs could ameliorate collagen-induced arthritis, there is a fundamental flaw in this study: the SCEs used were designed based on the 27Q-131H dimer structure proposed by Ramsland *et al.* [97], yet the experiments in the paper tested the SCEs only on the 27Q-131R allotype of FcγRIIa. Additionally, the study provides no evidence that the SCEs actually bind to FcγRIIa. Even more importantly, it has now been shown through the SEC-MALLS experiments that none of the FcγRIIa ectodomain allotypes dimerise in solution. This has important implications in this field; the dimer on which the SCEs were based does not exist, making it an invalid target for drug design.

4.3.4 Full-length FcγRIIa oligomerisation

Although all the evidence in this chapter suggests that the ectodomains of FcγRIIa do not dimerise, full-length receptors do cluster upon IC binding [163]. It is not known whether this clustering is heterogeneous and random, or whether the receptors form defined oligomers. It is also not known what the oligomeric state of the full-length receptors are in the inactive ITAMi. One consideration is that for FcγRIIa to form true dimers in a cell membrane, it may require contacts between the transmembrane domains. This has previously been reported for other single-pass membrane proteins, including glycophorin A [164]. To investigate this further, SEC-MALLS on the full-

length protein could be carried out. To extract the receptors from the cell membrane without disturbing any potential oligomers, styrene maleic acid lipid particles (SMALPs) could be used. These are amphipathic polymers that can extract sections of a lipid bilayer and the resulting membrane proteins, enabling them to be purified in a detergent-free system in their native states [165].

As the SEC-MALLS glyco-analysis revealed, the 27W allotypes displayed a higher level of glycosylation, with an additional ~1kDa of carbohydrates compared with the 27Q allotypes. It is possible that this could contribute to the differences in FcγRIIa signalling. One possible theory is that these additional carbohydrates may promote full-length FcγRIIa oligomerisation of the RA-associated 27W-131H allotype, which could stabilise the activatory signalling complex and so amplify the activatory signalling cascade and hence lead to the persistent inflammation that is observed in RA.

To further assess the oligomeric state of the full-length receptors, single-molecule tracking could be carried out to monitor the receptors movement in the cell membrane [166].

5. Implications of re-refined structure on therapeutic antibody design

5.1 Introduction

FcγRs are a family of highly homologous proteins, displaying high sequence identity in their extracellular domains (Table 5.1). Consequently, a highly conserved pattern for ligand binding might be expected. However, this was not thought to be the case for FcγRs based on the publicly available protein structures; the binding interface of FcγRIIa-IgG1-Fc was always believed to differ from other FcγRs. Therefore, in an attempt to explain this phenomenon, the structure was analysed in detail after re-refinement of 3RY6, and compared with other structures of FcγR-IgG complexes. This showed that the reason FcγRIIa-IgG1 interaction was thought to be different was because the structure solved by Ramsland *et al.* [97] was incorrect. Consequently, new conclusions may be drawn about the FcγRIIa-IgG interaction following re-refinement. This demonstrates the importance of accuracy in refining and interpreting protein structures, as an inaccurate model could lead to invalid interpretations and hence cause months or even years of wasted time and money. In 2007 it was found that there were over 10 million anomalies present in all of the structures on the PDB [167], and as previously mentioned this is a huge problem in the IgG/FcR field

	FcγRI	FcγRIIa	FcγRIIb	FcγRIIc	FcγRIIIa	FcγRIIIb
FcγRI	100%	44%	45%	44%	43%	44%
FcγRIIa	-	100%	94%	100%	50%	51%
FcγRIIb	-	-	100%	94%	49%	50%
FcγRIIc	-	-	-	100%	50%	51%
FcγRIIIa	-	-	-	-	100%	97%
FcγRIIIb	-	-	-	-	-	100%

Table 5.1 Sequence identity of the extracellular domains of FcγRs.

5.1.1 Objectives

Following re-refinement of the structure of IgG1-Fc in complex with the 27Q-131R allotype of FcγRIIa, it was clear that the structure had changed considerably. Therefore, the objective of this chapter was to analyse the re-refined structure, and compare it with other available IgG-FcγR structures to see if any novel conclusions could be drawn. This provides an enhanced insight into the IgG-FcγR interaction, which can aid the design of therapeutic antibodies and guide antibody engineering, with the ultimate aim of improving the efficacy of therapeutic antibodies.

5.3 Results

5.3.1 FcγRIIa makes 2 distinct contacts with IgG

Following re-refinement, the IgG-binding sites on FcγRIIa were analysed. In common with other FcγRs, FcγRIIa makes two main contacts with IgG Fc, subsite 1 and subsite 2 (Figure 5.1).

5.3.1.1 Subsite 1

Subsite 1 consists mainly of hydrophobic residues making contacts between the IgG-C_H2 domain and domain 1 of the receptor. Two tryptophan residues of FcγRIIa form a hydrophobic hollow for P329 of IgG. This so-called 'tryptophan sandwich' is formed by the strictly conserved residues W87, W110 of FcγRIIa and IgG-G237, IgG-L328 and IgG-P329. No significant changes were observed for subsite 1 between the old and new model.

5.3.1.2 Subsite 2

The binding site of subsite 2 on FcγRIIa represents a highly variable region in the Fc receptor family. Following re-refinement, the new model shows a significant difference in the C-α trace for the IgG-Fc C_H2 domain of chain B, where subsite 2 is located. The C_H1-C_H2 interdomain angle closes by 10° relative to the unrefined model (Figure 5.2a) and hence the positions of the C_H2(B) loops are shifted by around 7.3 Å (Figure 5.2b). This results in dramatic changes of the previously assumed protein-protein-interaction interface of FcγRIIa to the C_H2(B) domain of IgG. Due to this, the new re-refined model shows a different hydrogen bonding network. The polymorphic residue 131 resides in subsite 2.

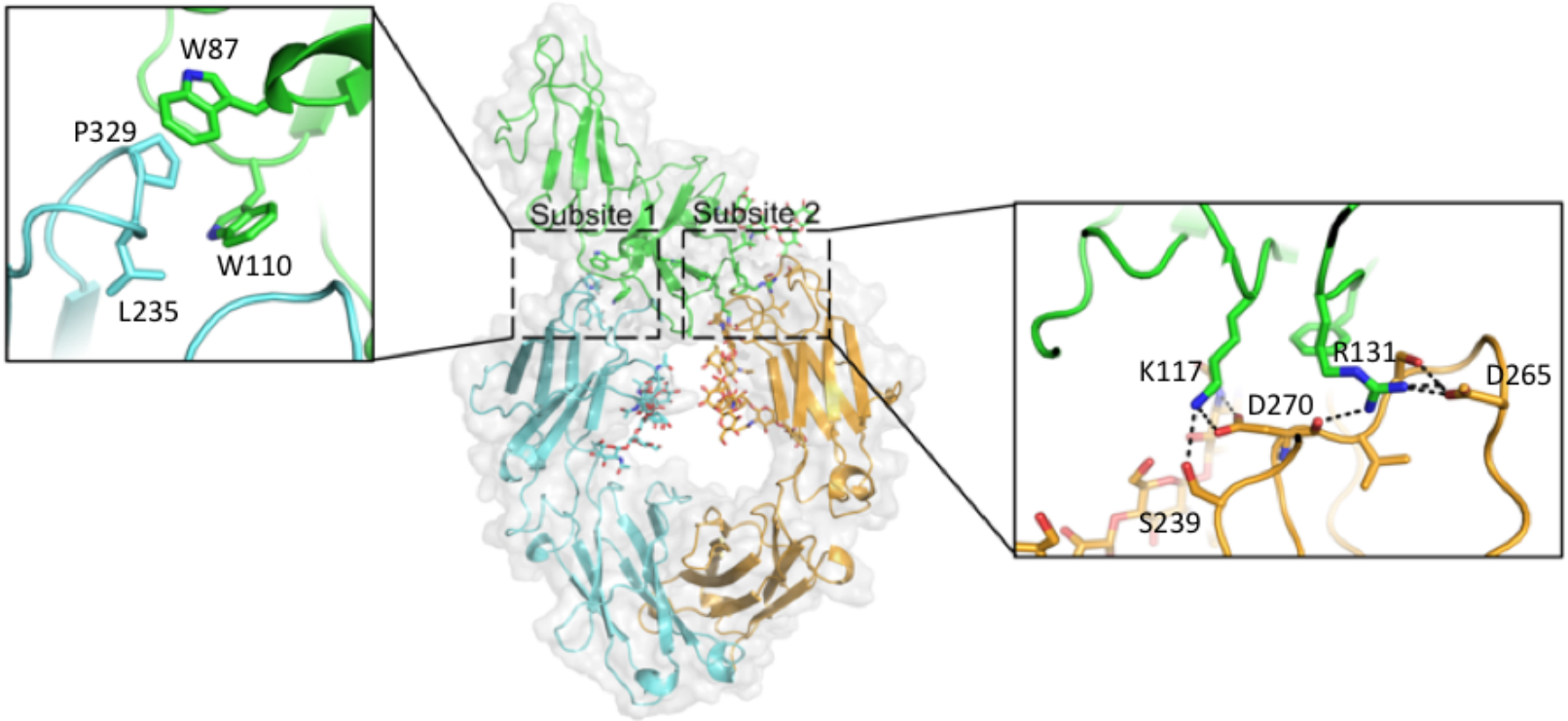

Figure 5.1 FcγRIIa makes two distinct binding contacts with IgG1 – subsite 1 and subsite 2.

Subsite 1 is dominated by hydrophobic residues, which are highly conserved amongst Fc-receptors. W87 and W110 of FcγRIIa form a 'sandwich' in which P329 of IgG binds. Subsite 2 is where FcγRIIa's polymorphic residue 131 resides. 131R of FcγRIIa binds in a deep groove of IgG loop D265-D270. K117 of FcγRIIa also makes contacts with IgG, forming hydrogen bonds with S239 and D270. Green, FcγRIIa; Blue, IgG-Fc chain A; Orange, IgG-Fc chain B.

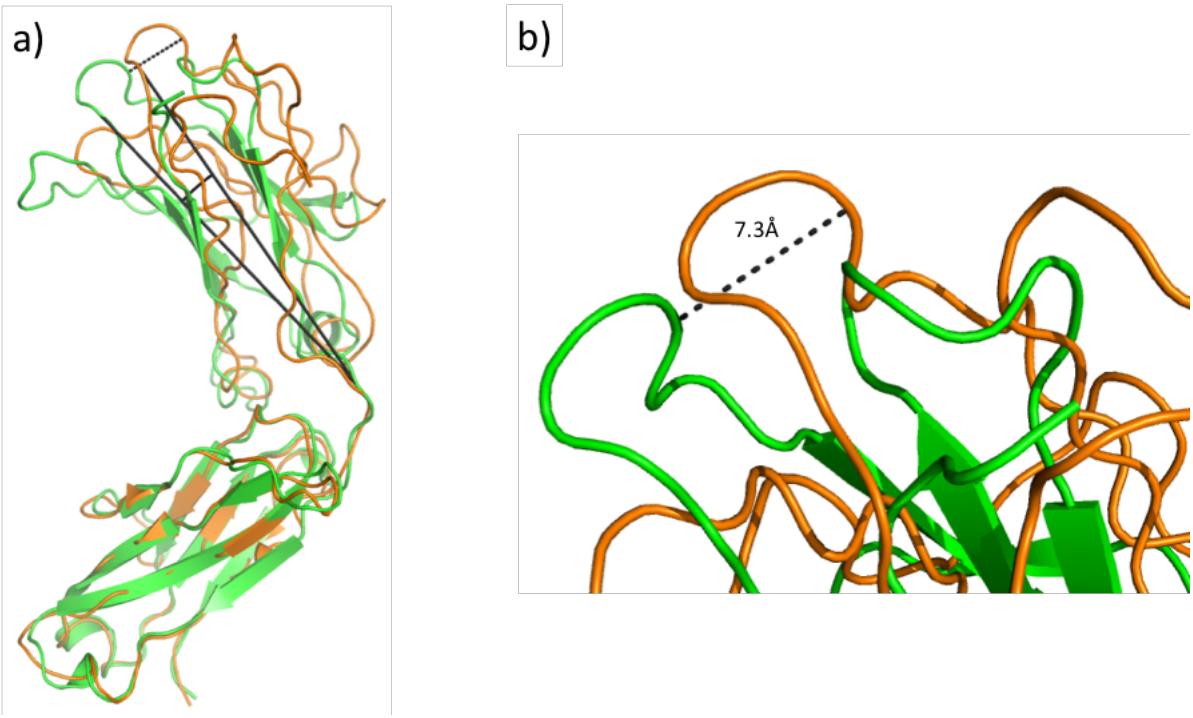

Figure 5.2 The movement of the C_{H2}(B) domain of IgG following re-refinement.

Orange: before re-refinement. Green: after re-refinement. A) The C_{H2}(B) domain is rotated around 10° altering the position of the C_{H2}(B) loops. B) The IgG loops are shifted approximately 7.3 Å.

5.3.2 Polymorphic residue H131R

Before re-refinement, the side chain of 131R had little electron density, and was poorly fitted. In the old the structure (3RY6), 131R was shown to be bound in a hollow cleft on top of the IgG loop D265-D270. However, after re-refinement, there was clear density present around this residue, allowing it to be modelled accurately. The new model shows that 131R binds in a deep cleft between the hinge region of IgG and IgG loop D265-D270, forming a

salt bridge with D270 and a hydrogen bond with the carbonyl oxygen atom of D265 (Figure 5.3).

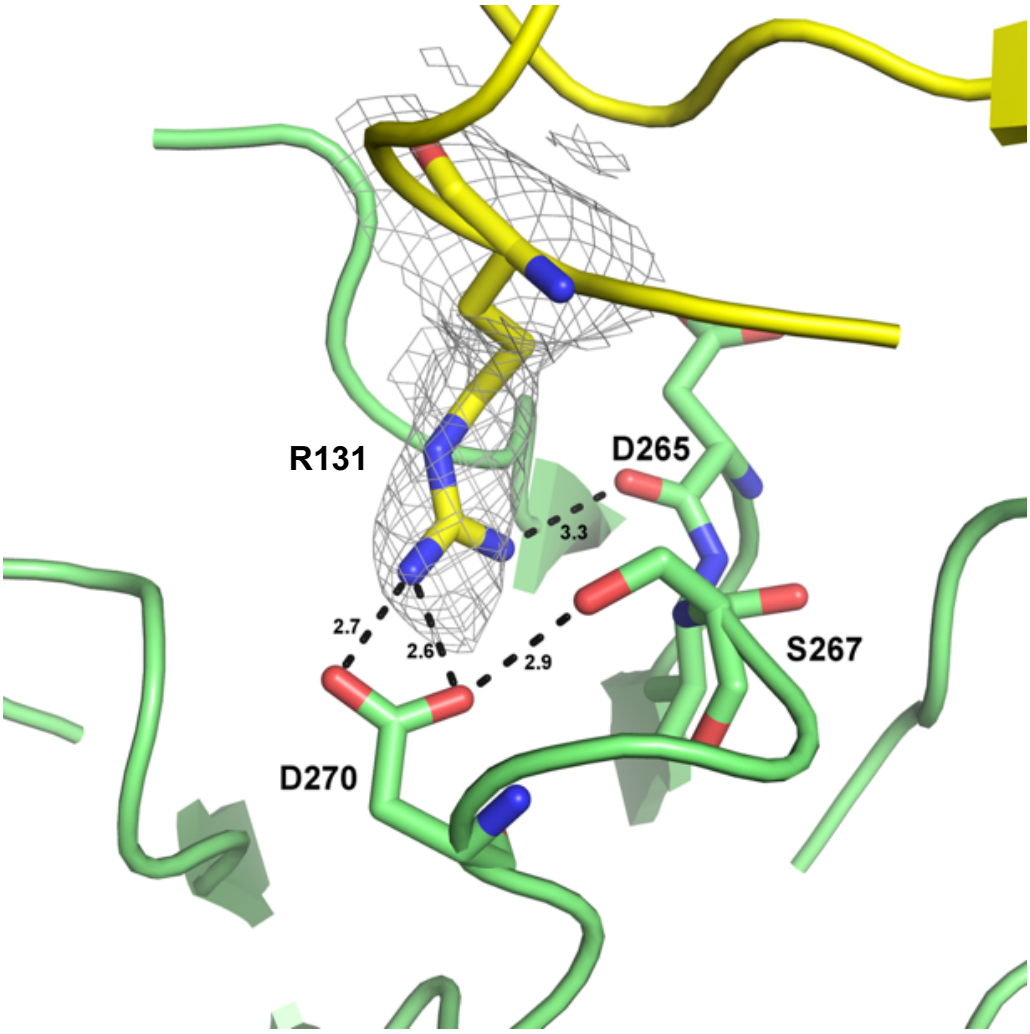

Figure 5.3 The involvement of residue 131R in IgG binding in more detail. Following re-refinement, the density for this residue was clear, allowing it to be modelled accurately. 131R forms a salt bridge with IgG D270 and hydrogen bond with the carbonyl oxygen atom of D265. Green, IgG1-Fc; Yellow, FcγRIIa.

5.3.2.1 Mechanism of allotype preference

As described above, 131R forms a salt bridge with IgG-D270 and a hydrogen bond with the carbonyl oxygen atom of IgG-D265. Thus, the H131R polymorphism results in a newly formed salt bridge creating a significant free energy gain, leading to the assumption that 131R would have a higher binding affinity than 131H to IgG1. However, it is known that 131H binds IgG1 with slightly higher affinity than 131R. Previously, there was no structural explanation as to why this was the case, and the old model provided little insight into this. As a structure of FcγRIIa-131H bound to IgG1-Fc was not available, the re-refined model was compared to different FcγR complexes of FcγRIa (PDB 4W4O) [106] and FcγRIIIb (PDB 1T83) [104], which display a histidine at position 131 (Figure 5.4). For all of the FcγRs, IgG1 showed structural rearrangement in loops D265-D270 and N325-P331 upon binding. However, for FcγRIIa, due to the longer arginine sidechain, the N325-P331 loop had to move a significant amount more in order to broaden the binding pocket and to prevent a steric clash with IgG-A327. Hence, due to the longer arginine sidechain 131R cannot be accommodated as well in the deep binding pocket compared to 131H. This could not previously be explained due to the incorrect structure and subsequently incorrect binding interface of FcγRIIa-131R to Fc. The new improved structure reveals for the first time the structural basis for the H131R allotypic differences in IgG1 affinity.

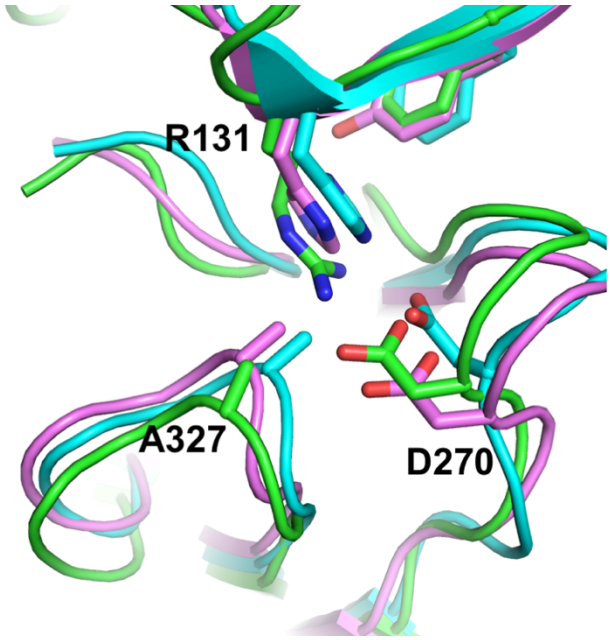

Figure 5.4 Structural rearrangements of IgG1 when bound to different FcγRs. Although IgG loop 325-331 does undergo rearrangement upon binding FcγRI (cyan) and FcγRIIIb (pink), the structural rearrangement when binding to FcγRIIa-131R (green) is much more pronounced, due to the long arginine side chain. FcγRIa – 4W4O (cyan, all-atom rmsd = 1.05 Å), FcγRIIa – 6fF8I (green), FcγRIIIb – 1T83 (pink, all-atom rmsd = 0.74 Å).

5.3.2.2 Preference for IgG2

It is widely known that the H131R polymorphism modulates IgG2 binding significantly [94]. This has also been confirmed using SPR and LigandTracer, however there was no structural basis identified as to why. In IgG2 there is an alanine present at position 236, compared to a glycine in the other IgG subclasses. This residue is located in subsite 2 where 131R contacts IgG. Glycine, since it has no sidechain, is a very flexible residue [168], so, substituting glycine with an alanine causes an increase in

Ramachandran restraints. This reduces the flexibility of the hinge region significantly and obstructs the long 131R sidechain.

5.3.3 Contribution of carbohydrates in the FcγRIIa-IgG interaction

Figure 5.5 shows the difference in sugars before and after re-refinement; sugars are truncated, and the more complex modifications such sialyation can no longer be seen. Interestingly, before re-refinement, the link between N297 and N-Acetyl-D-glucosamine (NAG) in Chain A, and N145 and NAG in Chain C were α ASN–NAG linkages. It is known that all eukaryotic N-glycans share a common core sugar sequence, with the β ASN-NAG linkage, hence the α ASN–NAG linkages which were present in the published structure were incorrect. Furthermore, the fucose molecules attached to the first NAG were attached with a β link, where this should be α [169].

In the re-refined structure, correct β ASN-NAG linkages and α NAG-FUC linkages were added, improving the stereochemistry of the carbohydrate residues and thus improving the structure. One of the conclusions from Ramsland *et al.* was that the sugars attached to N297 of the IgG-Fc domain made interactions with FcγRIIa-S126. It is clear after refinement that this statement cannot be supported; since the C_{H2} domain of chain B rotated, the positions of the carbohydrate modifications attached to N297 were also altered. Thus, the supposedly carbohydrate interacting residues, S126 and K125, point away from the carbohydrates, and the closest contact is now 9.8 Å. The sugars are not in close enough proximity for any hydrogen bonds or other interactions to form with S126 (Figure 5.6). Residue S126 does still

appear to participate in IgG binding, forming a hydrogen bond with Y296 and S298 of IgG (Figure 5.7).

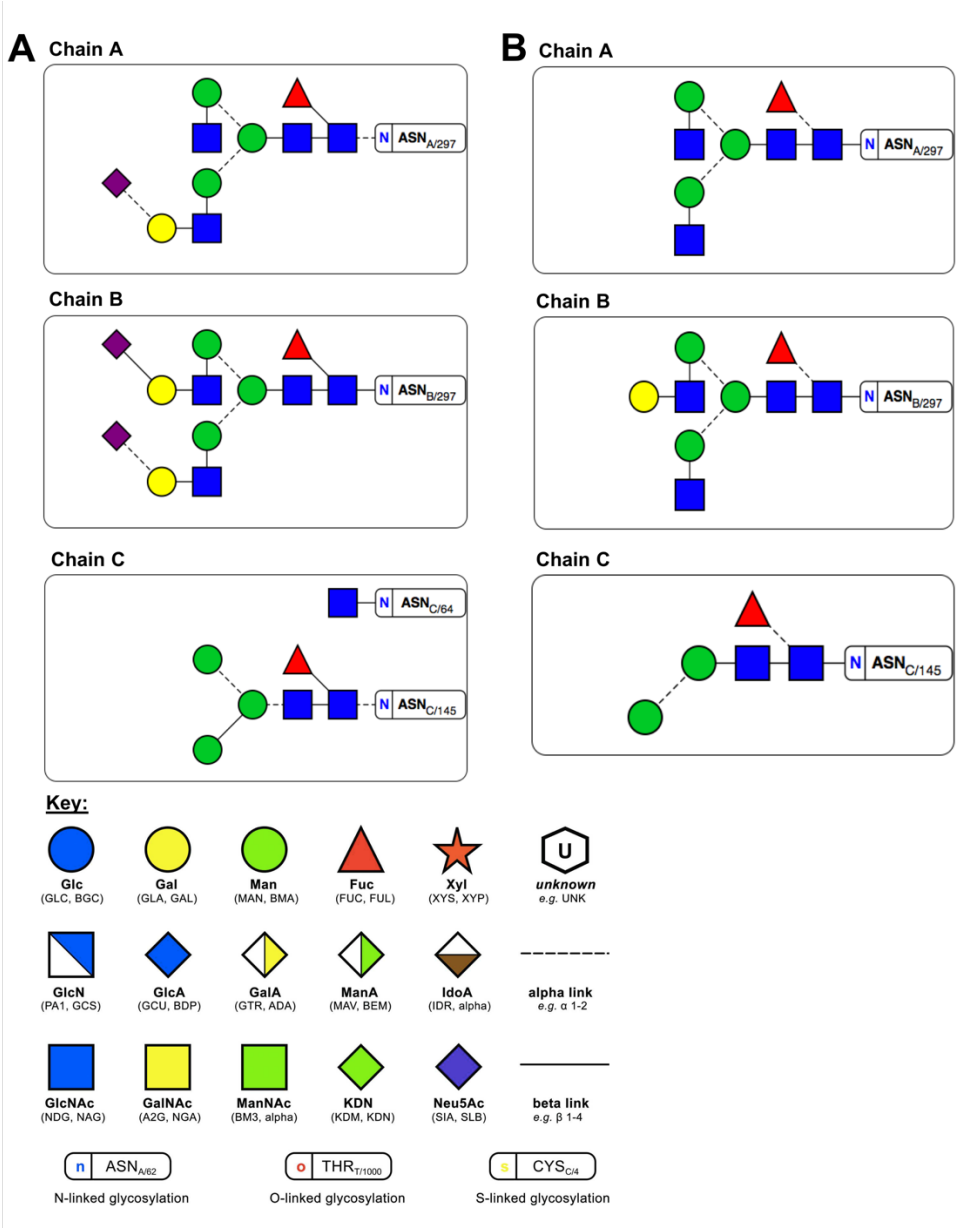

Figure 5.5 Comparison of sugar modifications in the old (a) and new (b) model, created in CCP4 Molecular Graphics (CCP4mg) [140].

A) In the old model, complex modifications such as sialyation can be seen in chain A and B. In Chain C there are 2 residues which have sugar modifications attached: N64 and N145. Both Chain A and Chain C contain ASN-NAG alpha-linkages. **B)** In the new model, sugars are comparatively truncated. Chain C shows only 1 residue with sugar modifications: N145. All ASN-NAG linkages are beta-links and all NAG-FUC linkages are alpha-links.

ASN, asparagine; FUC, D-Fucose; FUL, L-Fucose; NAG, N-acetylglucosamine.

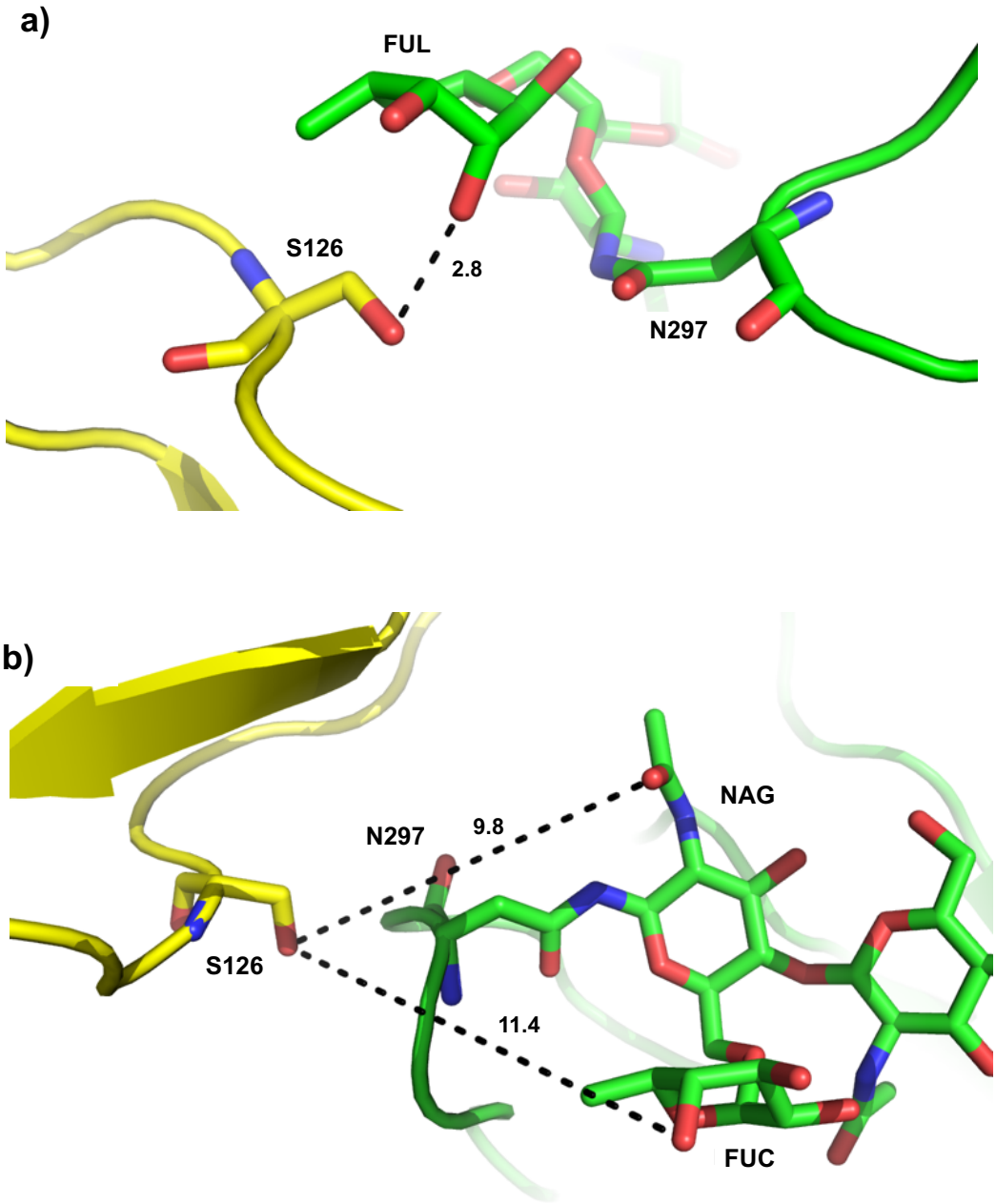

Figure 5.6 Comparison of FcγRIIa-S126 contacts with the N297 sugars of IgG in the old model (A) and new model (B).

Yellow: FcγRIIa, Green: IgG1-Fc. **A)** Before refinement, S126 was thought to make contacts with FUL attached to N297 of IgG. **B)** After re-refinement, positions of N297 sugar modifications have changed dramatically. Sugars are no longer in close enough proximity for any interaction to occur.

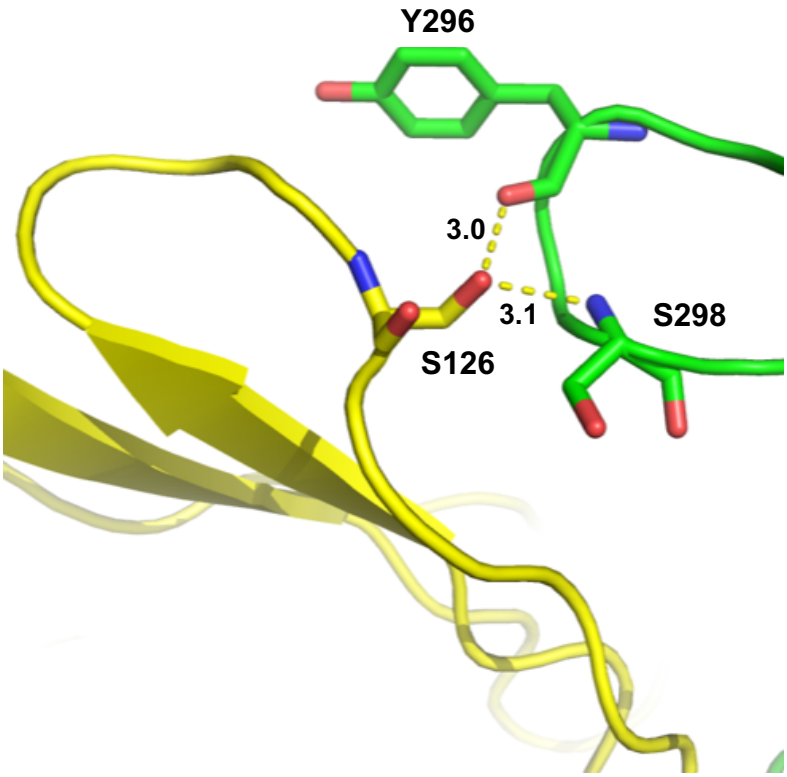

Figure 5.7 S126 of FcγRIIa forms 2 hydrogen bonds with IgG: Y296 and S298.

Yellow: FcγRIIa, Green: IgG1-Fc.

5.3.4 Asymmetric binding pattern of FcγRIIa

Due to the significant movement of the C_H2 domain of chain B, the cavity between the C_H2(A) and C_H2(B) increased by 3.2 Å (distance between Cα's of P238). This therefore destroyed the previous two-fold symmetry of the Fc-fragment and created an asymmetric binding pattern of FcγRIIa. This phenomenon is known as the 'opening' of the Fc fragment, and has previously been described for FcγRIIIa [105], FcγRI [106] and FcεRIα [107].

Consequently, this can be considered as a conserved binding mechanism for the whole FcR family.

5.3.5 Conserved mechanism of FcγR binding

The re-refined model of FcγRIIa in complex with IgG1-Fc enabled structural comparisons across the FcγR family. As various other structures and publications had shown, it is very likely that the different binding specificities of FcRs towards different IgG subclasses were largely determined by the hinge region of IgG. However, this region was very flexible in this structure and poor electron density led to shortening of the hinge region significantly, with C_H2(A) starting at L234 and C_H2(B) starting at L235. Therefore, this limited the ability to analyse the contribution of the hinge region to IgG binding for FcγRIIa.

After overlaying the different FcRs in complex with IgG1-Fc I found that unlike subsite 1, not all residues in subsite 2 were conserved; each receptor was shown to have a unique IgG recognition sequence (Table 5.2). In addition, there were two defined areas of the FcγRs, area A and area B, which were close to the binding interface of the hinge region of IgG (Figure 5.8). Hence these residues may allow IgG to distinguish between different FcγRs. Area A is defined by FcγR residues 114, 116 and 132 and area B by FcγR 157-160.

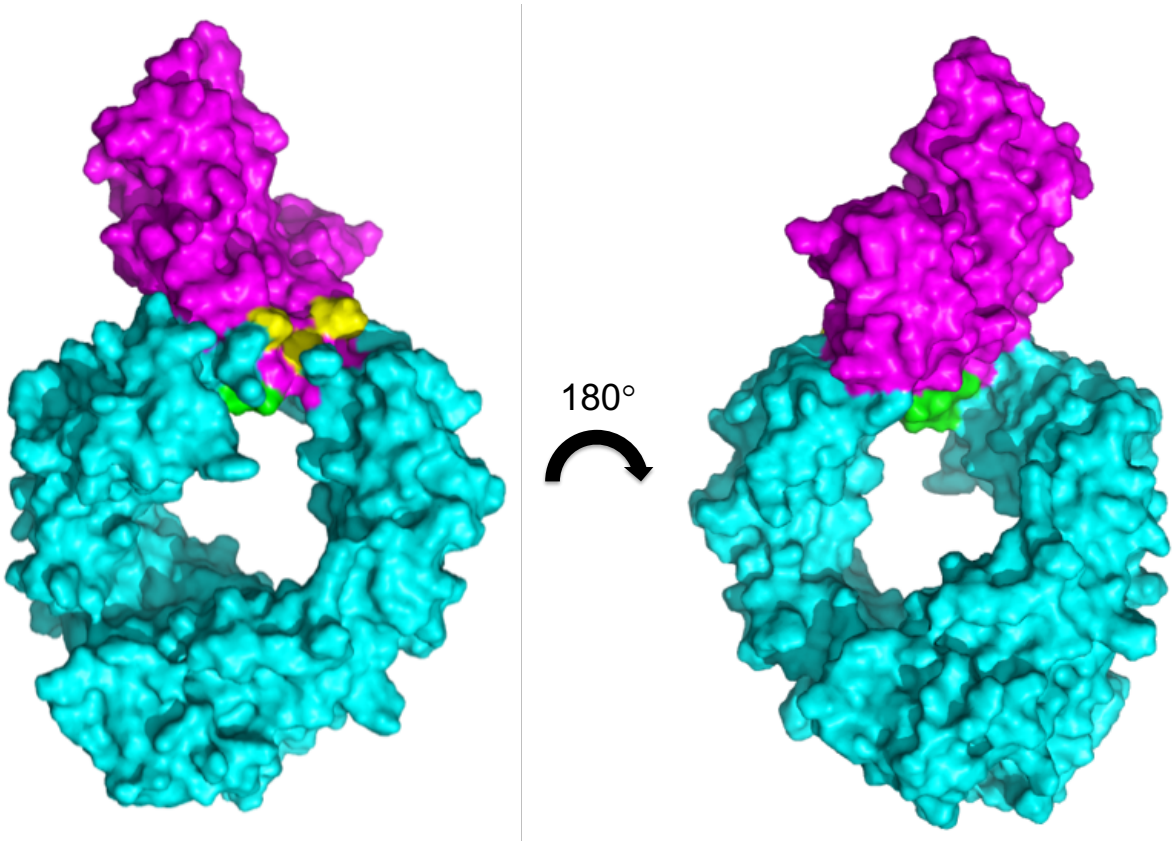

Figure 5.8 Surface representation of IgG1-Fc (magenta) bound to FcγRIIa (cyan).

Area A of FcγRIIa is highlighted in yellow and area B in green.

5.3.6 Differences between FcγRIIa and FcγRIIb

Only two residues differ between FcγRIIa and FcγRIIb in the receptor ectodomains, excluding the polymorphic residue 131. These are residues L/S132 in area A, and F/Y160 in area B (Figure 5.9).

Residue	87	110	111	113	114	116	117	126	129	131	132	156	157	158	160
FcγRI	W	W	K	K	L	Y	N	A	F	H	W	G	K	H	Y
FcγRIIa^{131H}	W	W	K	K	P	V	K	S	F	H	L	G	Y	T	F
FcγRIIa^{131R}	W	W	K	K	P	V	K	S	F	R	L	G	Y	T	F
FcγRIIb	W	W	K	K	P	V	K	S	F	R	S	G	Y	T	Y
FcγRIIIa	W	W	K	T	A	H	K	G	Y	H	H	G	S	K	V
FcγRIIIb	W	W	K	T	A	H	K	D	Y	H	H	G	S	K	V

Table 5.2 Sequence alignment of all Fc-interacting amino acid residues within the FcγR family.

Highly conserved residues in subsite 1 are highlighted in red, residues in subsite 2 are shown in blue, residues in area A in purple and area B in orange.

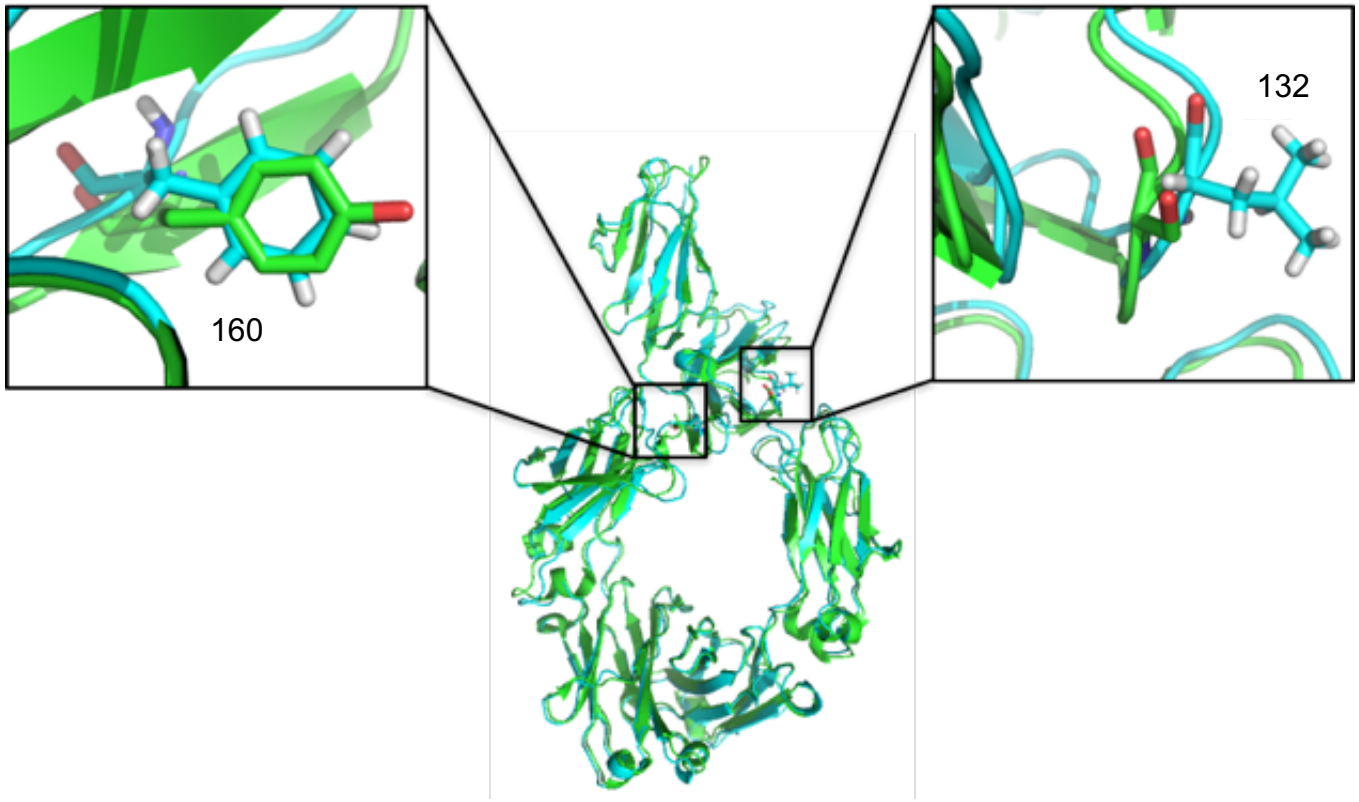

Figure 5.9 Two residues discriminate between FcγRIIa and FcγRIIb ectodomains.

Residue 132 is a leucine in FcγRIIa and a serine in FcγRIIb. Residue 160 is a phenylalanine in FcγRIIa and a tyrosine in FcγRIIb. These residues are close to the binding interface of the hinge region and are likely to modulate their affinity for different IgG subclasses. Blue, FcγRIIa; Green, FcγRIIb.

5.3.7 Why does FcγRI have high affinity for IgG?

Despite the different FcγRs having a conserved mechanism of binding, FcγRI binds monomeric IgG with a higher affinity and is hence known as the high affinity receptor for IgG [94]. By comparing the structures of all FcγRs bound to IgG-Fc, including the re-refined 3RY6 structure, a novel structural analysis could be attempted. An asparagine at position 117 of FcγRI stabilises residue 131H and forms a hydrogen bond with the backbone oxygen of G237 in the hinge region of IgG. This diverse branching hydrogen network stabilises and links IgG loop D265-D270 with the hinge region via subsite 2. However, FcγRII and FcγRIII, have a Lysine at position 117, which cannot form this interaction; instead it binds to IgG D265 and S239. Due to the interaction with IgG-S239, FcγRII and FcγRIII also creates a connection between subsite 2 and the hinge region. However, K117 interacts with IgG-S239 at a much lower point in the hinge compared to the interaction of N117 of FcγRI, and the hydrogen network does not connect the IgG-D265-D270 loop (Figure 5.10). Therefore, this IgG loop is unbound and therefore not stabilised. This could help to explain why FcγRI has a higher affinity for IgG1 than the other FcγRs. Additionally, residue L235 in chain A of IgG has previously been shown to contribute to the high affinity binding of FcγRI [106, 170]. This residue sits in the hydrophobic pocket of subsite 1, and accounts for a total of 25% of IgG chain A's interaction surface. In comparison with the other FcγRs, several residues differ in this hydrophobic pocket, including a crucial residue 155 (Figure 5.11). In FcγRI, there is a deletion at this position, whereas the other FcγRs have large hydrophobic residues such as isoleucine, valine or phenylalanine present [171]. These

sidechains therefore fill this hydrophobic pocket, preventing IgG L235 from binding (Figure 5.12).

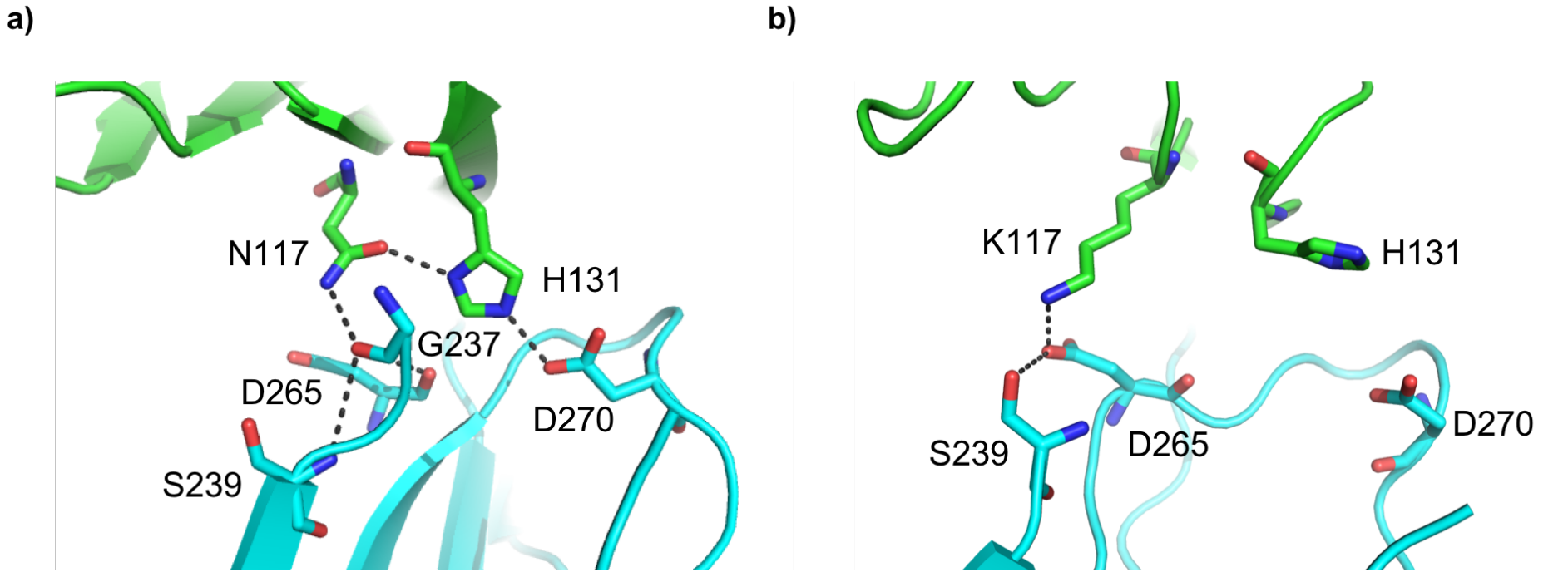

Figure 5.10 The molecular basis for FcγRI's high affinity for IgG1; N117K substitution.

a) In FcγRI, an asparagine exists at position 117. This can make an intramolecular hydrogen bond with H131, and stabilises and links IgG loop D265-D270 with the hinge region via subsite 2. **b)** In FcγRII and FcγRIII, a lysine is at position 117. This reaches out past H131, and hence cannot form a bond with this residue. Furthermore, H131 is unable to make any contacts with D270. Therefore, the hydrogen network does stabilise the IgG-D265-D270 loop

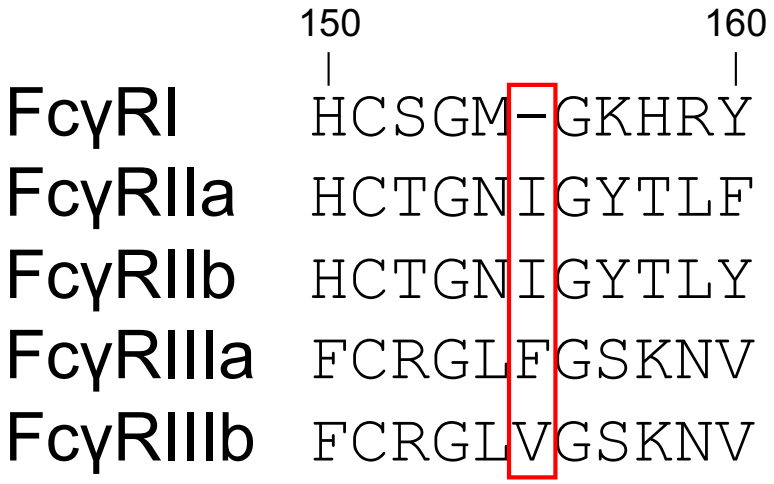

Figure 5.11 Sequence alignment of FcγR residues 150-160.

Residue 155 is highlighted in red. In FcγRI there is a deletion, allowing IgG L235 to bind into this hydrophobic pocket. In the other FcγRs, large hydrophobic amino acids are present, which fills the hydrophobic pocket and blocks the accommodation of IgG L235.

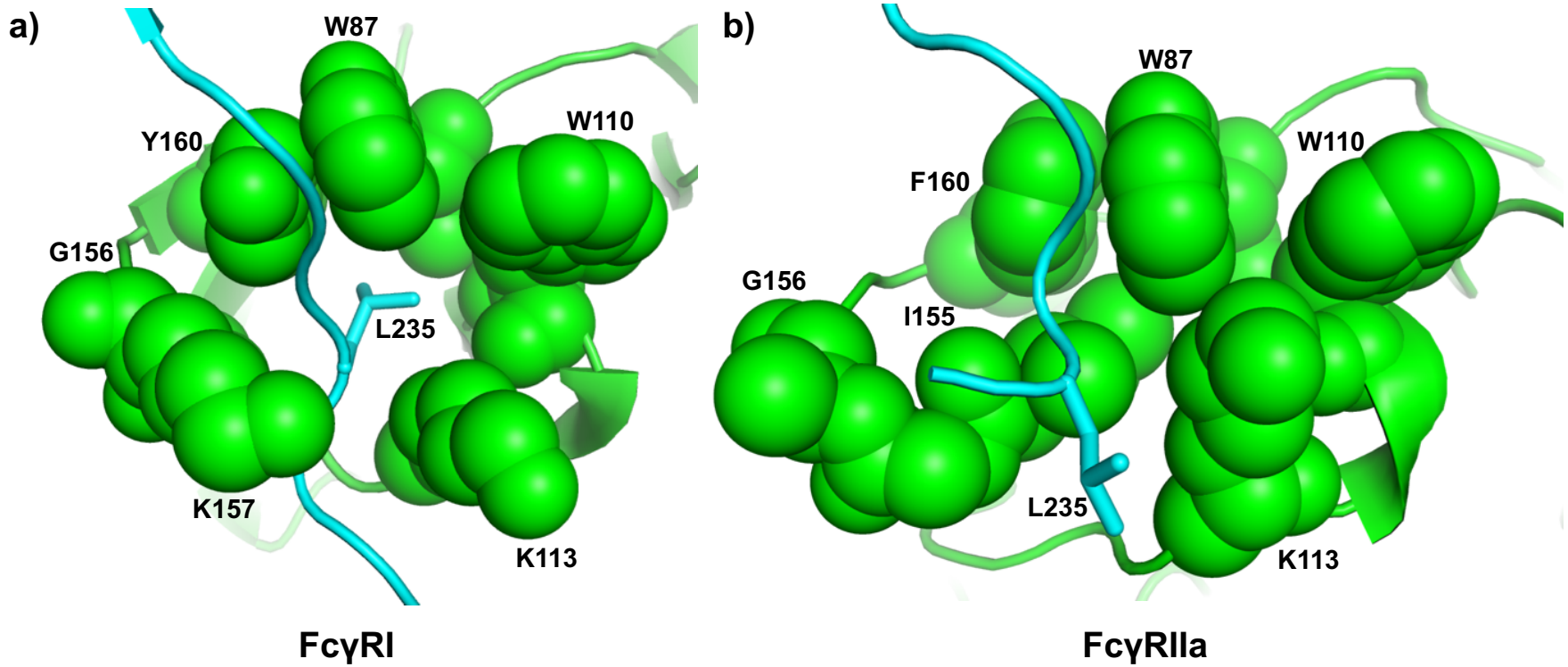

Figure 5.12 Mechanism of FcγRI's high affinity; 155 deletion**.**

a) L235 of IgG chain A sits in the hydrophobic pocket created by residues W87, W110, K113, V115, G156 K157 and Y160 of FcγRI, contributing to the high affinity interaction. Green: FcγRI, Cyan: IgG1-Fc. **b)** L235 of IgG chain A does not bind into the hydrophobic pocket of FcγRIIa, but instead orientates away from the ligand . Residue 155, which is a deletion in FcγRI, is replaced with an isoleucine in FcγRIIa. This has a long hydrophobic sidechain which hinders the accommodation of L235 in the hydrophobic pocket. Green: FcγRIIa, Cyan: IgG1-Fc. Created in PyMol (FcγRI PDB 4W4O). Numbering based on FcγRIIa.

5.4 Discussion

5.4.1 Fc-engineering

Historically, antibody engineering has focussed on mutations of the variable region in order to enhance antigen binding [172]. However, an emerging trend in the field of monoclonal antibodies is Fc-engineering; this is useful producing antibodies which can bind certain FcγRs, resulting in enhanced effector functions for the effective elimination of malignant cells such as tumour cells. Fc-engineering has been carried out on many therapeutic mAbs to enhance FcγR binding and consequently enhance effector functions [173]. However, the incorrect IgG1-Fc-FcγRIIa structure has misled researchers for several years into thinking that the FcγRIIa-IgG binding interface was different to other FcγRs, so rational approaches of antibody engineering were not fully appreciated. This led to researchers screening several random mutations on the Fc, which was both expensive and time consuming; in one study, carried out by Monnet *et al.* [174], a random mutagenesis technology known as MutaGen^{TM} was used in order to generate mutations evenly distributed over the whole Fc sequence of human IgG1. This led to the creation of a library of 1.1×10^{7} Fc-mutants which required screening and characterisation. Re-analysis of the Fc-FcR interface concluded that only 15 amino acid residues of the FcR interact with the Fc-fragment. Of these 15 residues, three are highly conserved and essential for the tryptophan-sandwich, three are in subsite 2 which is too conserved to be targeted specifically, and another residue is, due to protein folding requirements, a highly conserved glycine (G156). Therefore 8 IgG residues remain as potential discriminating residues in the Fc-FcγR interface

(sequence alignment in Table 5.2). Nevertheless, even though these residues are not highly conserved, they are chemically very similar, making it difficult to target specific FcγRs.

5.4.2 'Effector Silent' antibodies

As well as antibodies with enhanced effector functions, Fc-engineering is also useful for creating 'effector silent' antibodies. These are monoclonal antibodies that bind to their antigen, but do not bind activatory FcγRs and hence do not trigger activatory signalling and effector functions such as ADCC. For immunomodulatory functions such as induction of immunological tolerance, or the use of check-point inhibitors in cancer, it may be preferable to have a silent Fc domain to avoid toxicity [175]. Additionally, silencing the IgG-Fc effector functions could be advantageous for producing Fc-fusion proteins which can still bind FcRn, in order to extend the serum half-life of a biologic [176]. Previously, silent IgG molecules have been produced [177, 178], but these had large numbers of mutations, making it likely that the body would recognise these as foreign, and hence mount an immune response against them. An example of this is a study by Vafa *et al*. [178] in which IgG2-Fc was engineered to contain 5 mutations: V234A/G237A/P238S/H268A/V309L/A330S/P331S. Now that the binding interface is known, a reduced number of more specific mutations could be made, reducing the likelihood of an immune response being mounted.

5.4.3 Implications for aglycosylated antibodies

Due to the poorly refined structure, it was previously thought that the carbohydrates attached to N297 of IgG were important for the FcγRIIa-IgG interaction. However, my work shows that this is not true. This has huge

implications in terms of producing silent antibodies, as extensive work has been carried out to produce aglycosylated antibodies that can bind to their targets without binding to FcγRs [179, 180]. However, if the carbohydrates are not involved in this interaction, the aglycosylated antibodies may still bind to FcγRIIa. It has in fact previously been shown that an aglycosylated version of IgG1 is able to actively engage FcγRIIa [181, 182]. However, other studies have found that aglycosylated versions of IgG1 are not able to bind FcγRIIa [178]. It may be that this is due to changes in the structure of IgG rather than disruption of the IgG-FcγRIIa interface, as it is known that the glycosylation state of N297 on IgG plays a crucial role in maintaining IgG-Fc structure [10]. Studies by Borrok *et al*. [183] have shown that aglycosylated IgG-Fc has a larger hydrodynamic radius (Rh) than glycosylated IgG-Fc, suggesting that the C_H2 domains adopt a more open confirmation which could prevent binding to FcγRIIa. Furthermore, it has been shown that N-linked glycans present on IgG can affect the Fc quaternary structure, stabilising the C'E loop which is found in subsite 2. Removal of these glycans causes destabilisation of this loop, which reduces binding to FcγRIIIa, yet the effect on FcγRIIa binding is not known [11]. It is important to note that although IgG binding to FcγRIIa may be affected by the glycosylation state of IgG, FcγRIIa is less affected by this than the other FcγR subclasses [182]. Interestingly, in inflammatory disease states such as RA, IgG glycans become truncated and display lower levels of complexity [61]. Whilst this may affect their ability to bind to FcγRIIIa [182], these G0 forms of IgG may still bind to FcγRIIa, allowing this receptor to drive inflammation.

5.4.4. Discriminating between FcγRIIa and FcγRIIb

As FcγRIIa is primarily activatory and FcγRIIb inhibitory, it would be beneficial to have antibodies that can discriminate between the two receptors. However, these receptors are highly homologous, with only two amino acid residues (excluding the polymorphic residue 131) differing between them: L/S132 and F/Y160. These residues reside in two separate areas but are both close to the binding interface of the hinge region of IgG (Figure 5.9). Therefore, these may be areas which can be targeted to create antibodies that can distinguish between the FcγRIIa and FcγRIIb.

5.4.5 A published structure does not mean an accurate structure

It is clear from this work that although an x-ray structure is published, it does not necessarily mean that it is accurate. Inaccurate protein structures are a huge problem amongst the scientific community; As these structures are publicly available in the PDB, often non-structural biologists will download a structure with the assumption that it is correct. Of course, if an inaccurate structure is then being used to design a drug that binds to this protein, the chances are that the drug will not work. This can cause months of wasted time and money. Nonetheless, measures are being taken to address this problem. An initiative called ‘PDB_REDO’ has been set up, where poor quality structures can be submitted to the server, and the structure is then re-refined and validated to improve it [184]. Additionally, validation reports are now available on the PDB alongside protein structures, making it easier for non-structural biologists to assess the overall quality of the structure and to spot any major errors. The work presented in this chapter highlights the importance of accurate refinement, and the importance of checking PDB

structures. It is clear that further work in re-refining structures in the FcγR/antibody field is required.

6. Final discussion and future work

6.1 FcγRIIa oligomerisation

Although previous work suggested that FcγRIIa forms dimers, which act as active signalling complexes [96], the work carried out in this thesis shows that the ectodomain dimer structures presented by Ramsland *et al.* [97] were in fact artefacts of crystallisation, and that the FcγRIIa are monomeric in solution (Chapter 4). It is thought that full-length FcγRIIa does cluster upon ligand binding; however, it is unknown whether this clustering is random and heterogenous, or whether they form distinct oligomeric states which could be targeted. In order to investigate this further, SEC-MALLS on the full-length protein could be carried out, as the transmembrane domain and cytoplasmic domains may mediate oligomeric contacts. This could be done using protein extracted using SMALPs; amphipathic polymers which can extract sections of a lipid bilayer and the resulting membrane proteins, enabling them to be purified in a detergent free system in their native states. In order to further probe whether full-length FcγRIIa is capable of forming dimers when expressed on the cell surface, fluorescence resonance energy transfer (FRET) experiments could be carried out. A double transfection with full length *FCGR2A* tagged with a donor and acceptor FRET pair could be used, and the fluorescent signal measured using flow cytometry [185]. If the donor and acceptor fluorophore come into close enough proximity due to FcγRIIa dimerisation, FRET will occur and the acceptor emission will increase.

It may also be important to consider whether IgG-containing ligands are required in order to promote the formation of these oligomeric structures. It is

possible ligand binding brings the receptors into close proximity allowing them to oligomerise: future work in this area could involve carrying out SEC-MALLS in the presence of IgG. If regular IgG-based conformations that induce ITAM and ITAMi signalling exist, techniques such as SEC-MALLS, Cryo-EM and crystallography could be used to determine the structures of the opposing signalling mechanisms, with the aim of defining the structural basis of activatory and inhibitory signalling through FcγRIIa for therapeutic modulation. It should be noted that reductionist methods which consider single domains will provide limited information. Only by considering the full length receptor, can the understanding of the signalling structure be furthered.

6.2 FcγRIIa as a target for drug design

One way to target FcγRIIa in RA is by using blocking antibodies or SCEs which prevent IgG binding. Re-refinement of FcγRIIa-131R in complex with IgG1-Fc revealed a completely different binding interface than what was originally thought. The re-refined model allowed comparisons with other FcγRs to be made, and a conserved pattern of binding was deduced. It is now known, that in common with other FcγRs, FcγRIIa displays an asymmetric binding pattern. This work therefore has huge implications in therapeutic antibody design. Using the structural information obtained from the re-refinement, further work can be carried out to design and create antibodies with engineered Fc regions. These could be used to target specific FcγRs, or to create effector silent antibodies which do not bind FcγRs.

6.2 Measuring ligand binding

Measuring the same interaction using two different systems resulted in different kinetics, with the LigandTracer results demonstrating a higher affinity interaction than SPR. LigandTracer is a more biologically relevant system, as receptors are free to move around in the cell membrane and associate with lipid rafts, resulting in more complex interactions than a simple ‘one-to-one’ interaction, as demonstrated by the ‘one-to-two’ model seen for IgG3 and IgG4. Therefore, LigandTracer technology has implications in therapeutic drug characterisation, where there is a need to measure kinetics; LigandTracer may reveal a more complex interaction.

Monomeric IgG subclasses were used in these experiments, which are known to bind to FcγRIIa with lower affinity than immune complexes. Furthermore, autoantibody-positive RA is driven by the presence of ICs, therefore it would be advantageous to measure IC binding to FcγRIIa to further asses how this receptor contributes to RA. Additional work could involve generating standardised ICs which are the same molecular weight and shape, to allow binding kinetics to be derived using these. Previous work by Pepponi *et al* [186] describes a reproducible method to produce ‘Immune Complex Mimics’, consisting of an oligomeric antigen in complex with multiple copies of a single monoclonal antibody. However, these are still over-simplified compared to the ICs seen in disease states.

As the receptor ectodomain proteins used for both SPR and SEC-MALLS were produced in a human cell line (HEK293T), all necessary human post-translational modifications are present on the proteins, particularly

glycosylation. This will produce results similar to those that would occur *in vivo* [187]. This is important as it is evident that glycosylation can greatly affect IgG binding to Fc receptors [17]. However, it is known that glycosylation does differ between cell lines, particularly between protein expressed endogenously in primary cells and recombinant protein produced in HEK293 cells [19]. It would be possible to use primary cells expressing FcγRIIa on the Ligand Tracer to overcome this, but it is known that glycosylation can differ in disease states also. Furthermore, the only cells which express FcγRIIa exclusively are platelets which are hard to work with. Therefore, designing the perfect Ligand Tracer experiment is difficult. It is clear that there are limitations, but this assay represents a much more biologically relevant system than SPR.

6.3 Structural biology of the full-length receptor

A major gap in our understanding lies in the intracellular portions of FcγRIIa. By solving the full-length structure of this receptor, it will provide information about the transmembrane helix and the cytoplasmic ITAM, which could give an insight into how FcγRIIa interacts with other proteins and signalling molecules. In turn, this could help to design new therapeutics to target this receptor. An integrated structural biology approach could be used, combining a number of structural techniques with different advantages to attempt to solve the full-length structure of FcγRIIa.

One technique that could be used to obtain structural information on the full-length receptor would be electron microscopy (cryo-EM), however, this requires large sizes of 150kDa or above, making the monomeric form of

FcγRIIa too small; to overcome this, the receptor could be complexed with other molecules such as regularised ligands. This could include IgG cross-linked to the receptor, or kinases, which can be covalently linked to the receptor using Adenosine Triphosphate (ATP) analogues such as 5′-fluorosulfonylbenzoyl adenosine [188]. This would help to create a stable receptor complex, which would facilitate cryo-EM.

Ultimately, the biology underlying the role of FcγRIIa in autoimmune disease such as RA is complex and not fully understood. Although technology is improving, it still limits our ability to define the structure and function of the different FcγRIIa signalling processes. My work presented in this thesis provides further clarity on the structure of monomeric FcγRIIa ectodomains and IgG1-bound FcγRIIa, as well as the effect of polymorphic variants on IgG binding. LigandTracer technology provides a new biophysical technique to analyse these interactions in a biologically relevant way, providing firm foundations for further work in this field.

Bibliography

1. Gessner, J.E., et al., *The IgG Fc receptor family.* Ann Hematol, 1998. **76**(6): p. 231-48.
2. Shields, R.L., et al., *High resolution mapping of the binding site on human IgG1 for FcγRI, FcγRII, FcγRIII, and FcRn and design of IgG1 variants with improved binding to the FcγR.* J Biol Chem, 2001. **276**(9): p. 6591-604.
3. Syed, S.N., et al., *Both FcgammaRIV and FcgammaRIII are essential receptors mediating type II and type III autoimmune responses via FcRgamma-LAT-dependent generation of C5a.* Eur J Immunol, 2009. **39**(12): p. 3343-56.
4. Duncan, A.R. and G. Winter, *The binding site for C1q on IgG.* Nature, 1988. **332**(6166): p. 738-40.
5. Roopenian, D.C. and S. Akilesh, *FcRn: the neonatal Fc receptor comes of age.* Nat Rev Immunol, 2007. **7**(9): p. 715-25.
6. Lu, J., et al., *Pentraxins and Fc receptors.* Immunol Rev, 2012. **250**(1): p. 230-8.
7. Warmerdam, P.A., et al., *A single amino acid in the second Ig-like domain of the human Fcγ receptor II is critical for human IgG2 binding.* J Immunol, 1991. **147**(4): p. 1338-43.
8. Janeway, C.A., P. Travers, and M. Walport, *The structure of a typical antibody molecule*, in *Immunobiology: The Immune System in Health and Disease*. 2001, Garland Science: New York
9. Abes, R. and J.L. Teillaud, *Impact of Glycosylation on Effector Functions of Therapeutic IgG.* Pharmaceuticals (Basel), 2010. **3**(1): p. 146-157.
10. Hayes, J.M., et al., *Glycosylation and Fc receptors.* Curr Top Microbiol Immunol, 2014. **382**: p. 165-99.
11. Subedi, G.P. and A.W. Barb, *The Structural Role of Antibody N-Glycosylation in Receptor Interactions.* Structure, 2015. **23**(9): p. 1573-1583.
12. Sutton, B.J. and D.C. Phillips, *The three-dimensional structure of the carbohydrate within the Fc fragment of immunoglobulin G* Biochem Soc Trans, 1983. **11**: p. 130-132.
13. Prabakaran, P., et al., *Structure of an isolated unglycosylated antibody C(H)2 domain.* Acta Crystallogr D Biol Crystallogr, 2008. **64**(Pt 10): p. 1062-7.
14. Kiyoshi, M., et al., *Glycosylation of IgG-Fc: a molecular perspective.* Int Immunol, 2017. **29**(7): p. 311-317.
15. Walker, M.R., et al., *Aglycosylation of human IgG1 and IgG3 monoclonal antibodies can eliminate recognition by human cells expressing Fc gamma RI and/or Fc gamma RII receptors.* Biochem J, 1989. **259**(2): p. 347-53.
16. Tao, M.H. and S.L. Morrison, *Studies of aglycosylated chimeric mouse-human IgG. Role of carbohydrate in the structure and effector*

functions mediated by the human IgG constant region. J Immunol, 1989. **143**(8): p. 2595-601.
17. Hayes, J.M., et al., *Fcγ receptor glycosylation modulates the binding of IgG glycoforms: a requirement for stable antibody interactions.* J Proteome Res, 2014. **13**(12): p. 5471-85.
18. Ferrara, C., et al., *Unique carbohydrate-carbohydrate interactions are required for high affinity binding between FcγRIII and antibodies lacking core fucose.* Proc Natl Acad Sci U S A, 2011. **108**(31): p. 12669-74.
19. Patel, K.R., et al., *Restricted processing of CD16a/Fc gamma receptor IIIa N-glycans from primary human NK cells impacts structure and function.* J Biol Chem, 2018. **293**(10): p. 3477-3489.
20. Edberg, J.C., et al., *FcγRIII expressed on cultured monocytes is a N-glycosylated transmembrane protein distinct from FcγRIII expressed on natural killer cells.* Immunology, 1990. **144**(12): p. 4729-34.
21. Edberg, J.C. and R.P. Kimberly, *Cell type-specific glycoforms of FcγRIIIa (CD16): differential ligand binding.* J Immunol, 1997. **159**(8): p. 3849-57.
22. Hayes, J.M., et al., *Identification of Fc Gamma Receptor Glycoforms That Produce Differential Binding Kinetics for Rituximab.* Mol Cell Proteomics, 2017. **16**(10): p. 1770-1788.
23. Li, X. and R.P. Kimberly, *Targeting the Fc receptor in autoimmune disease.* Expert Opin Ther Targets, 2014. **18**(3): p. 335-50.
24. Mellor, J.D., et al., *A critical review of the role of Fc gamma receptor polymorphisms in the response to monoclonal antibodies in cancer.* J Hematol Oncol, 2013. **6**: p. 1.
25. Jungi, T.W. and S. Hafner, *Quantitative assessment of Fc receptor expression and function during in vitro differentiation of human monocytes to macrophages.* Immunology, 1986. **58**(1): p. 131-7.
26. Worth, R.G., et al., *Platelet FcgammaRIIA binds and internalizes IgG-containing complexes.* Exp Hematol, 2006. **34**(11): p. 1490-5.
27. Nimmerjahn, F. and J.V. Ravetch, *Fcgamma receptors: old friends and new family members.* Immunity, 2006. **24**(1): p. 19-28.
28. Vogelpoel, L.T., et al., *Control of cytokine production by human fc gamma receptors: implications for pathogen defense and autoimmunity.* Front Immunol, 2015. **6**: p. 79.
29. Takai, T., *Roles of Fc receptors in autoimmunity.* Nat Rev Immunol, 2002. **2**(8): p. 580-92.
30. de Haas, M., et al., *A triallelic Fcγ receptor type IIIA polymorphism influences the binding of human IgG by NK cell FcγRIIIa.* J Immunol, 1996. **156**(8): p. 2948-55.
31. Nimmerjahn, F. and J.V. Ravetch, *Fcgamma recpetors as regulators of immune responses.* Nature Reviews Immunology, 2008. **8**(1): p. 34-47.
32. Claustres, M., et al., *Recommendations for reporting results of diagnostic genetic testing (biochemical, cytogenetic and molecular genetic).* Eur J Hum Genet, 2014. **22**(2): p. 160-70.
33. Bournazos, S., et al., *Association of FcγRIIa (CD32a) with lipid rafts regulates ligand binding activity.* J Immunol, 2009. **182**(12): p. 8026-36.

34. Kwiatkowska, K. and A. Sobota, *The clustered Fcγ receptor II is recruited to Lyn-containing membrane domains and undergoes phosphorylation in a cholesterol-dependent manner.* Eur J Immunol, 2001. **31**(4): p. 989-98.
35. Garcia-Garcia, E. and C. Rosales, *Signal transduction during Fc receptor-mediated phagocytosis.* J Leukoc Biol, 2002. **72**(6): p. 1092-108.
36. Pawson, T., G.D. Gish, and P. Nash, *SH2 domains, interaction modules and cellular wiring.* Trends Cell Biol, 2001. **11**(12): p. 504-11.
37. Getahun, A. and J.C. Cambier, *Of ITIMs, ITAMs, and ITAMis: revisiting immunoglobulin Fc receptor signaling.* Immunol Rev, 2015. **268**(1): p. 66-73.
38. Jaumouille, V., et al., *Actin cytoskeleton reorganization by Syk regulates Fcgamma receptor responsiveness by increasing its lateral mobility and clustering.* Dev Cell, 2014. **29**(5): p. 534-546.
39. Cox, D. and S. Greenberg, *Phagocytic signaling strategies: Fcγ receptor-mediated phagocytosis as a model system.* Semin Immunol, 2001. **13**(6): p. 339-45.
40. Rollet-Labelle, E., et al., *Recruitment of the cross-linked opsonic receptor CD32A (FcγRIIA) to high-density detergent-resistant membrane domains in human neutrophils.* Biochem J, 2004. **381**(Pt 3): p. 919-28.
41. Sobota, A., et al., *Binding of IgG-opsonized particles to FcγR is an active stage of phagocytosis that involves receptor clustering and phosphorylation.* J Immunol, 2005. **175**(7): p. 4450-7.
42. Mendez Romero, A., et al., *Stereotactic body radiation therapy for liver tumors: impact of daily setup corrections and day-to-day anatomic variations on dose in target and organs at risk.* Int J Radiat Oncol Biol Phys, 2009. **75**(4): p. 1201-8.
43. Berg, J.M., J.L. Tymoczko, and L. Stryer, *The Hydrolysis of Phosphatidyl Inositol Bisphosphate by Phospholipase C Generates Two Messengers*, in *Biochemistry* 2002, W. H. Freeman and Company: New York.
44. Wang, D., et al., *Phospholipase Cγ2 is essential in the functions of B cell and several Fc receptors.* Immunity, 2000. **13**(1): p. 25-35.
45. Herik-Oudijk, I.E.V.d., et al., *Identification of Signaling Motifs Within Human FcyRIIa and FcyRIIb Isoforms.* Blood, 1995. **85**: p. 2202-2211.
46. Huang, Z.Y., et al., *The effect of phosphatases SHP-1 and SHIP-1 on signaling by the ITIM- and ITAM-containing Fcgamma receptors FcgammaRIIB and FcgammaRIIA.* J Leukoc Biol, 2003. **73**(6): p. 823-9.
47. Hunter, S., et al., *Inhibition of Fcgamma receptor-mediated phagocytosis by a nonphagocytic Fcgamma receptor.* Blood, 1998. **91**(5): p. 1762-8.
48. Ben Mkaddem, S., et al., *Shifting FcγRIIA-ITAM from activation to inhibitory configuration ameliorates arthritis.* J Clin Invest, 2014. **124**(9): p. 3945-59.

49. Bharadwaj, D., et al., *Serum amyloid P component binds to Fcγ receptors and opsonizes particles for phagocytosis.* J Immunol, 2001. **166**(11): p. 6735-41.
50. Bodman-Smith, K.B., et al., *C-reactive protein-mediated phagocytosis and phospholipase D signalling through the high-affinity receptor for immunoglobulin G (FcγRI).* Immunology, 2002. **107**(2): p. 252-60.
51. Du Clos, T.W. and C. Mold, *Pentraxins (CRP, SAP) in the process of complement activation and clearance of apoptotic bodies through Fcγ receptors.* Curr Opin Organ Transplant, 2011. **16**(1): p. 15-20.
52. Hiemstra, P.S., Daha, M. R., *Opsonization.* Encycolpedia of Immunology, 1998: p. 1885-1888.
53. Huang, Z.Y., et al., *Human platelet FcγRIIA and phagocytes in immune-complex clearance.* Mol Immunol, 2011. **48**(4): p. 691-6.
54. Alamanos, Y. and A.A. Drosos, *Epidemiology of adult rheumatoid arthritis.* Autoimmun Rev, 2005. **4**(3): p. 130-6.
55. Schett, G. and E. Gravallese, *Bone erosion in rheumatoid arthritis: mechanisms, diagnosis and treatment.* Nat Rev Rheumatol, 2012. **8**(11): p. 656-64.
56. Catrina, A.I., et al., *Mechanisms involved in triggering rheumatoid arthritis.* Immunol Rev, 2016. **269**(1): p. 162-74.
57. Ziff, M., *The agglutination reaction in rheumatoid arthritis.* J Chronic Dis, 1957. **5**(6): p. 644-67.
58. Magnusson, S.E., et al., *Dysregulated Fc receptor function in active rheumatoid arthritis.* Immunol Lett, 2014. **162**(1 Pt A): p. 200-6.
59. Sokolove, J., et al., *Rheumatoid factor as a potentiator of anti-citrullinated protein antibody-mediated inflammation in rheumatoid arthritis.* Arthritis Rheumatol, 2014. **66**(4): p. 813-21.
60. Perricone, C., et al., *Smoke and autoimmunity: The fire behind the disease.* Autoimmun Rev, 2016. **15**(4): p. 354-74.
61. Parekh, R.B., et al., *Association of rheumatoid arthritis and primary osteoarthritis with changes in the glycosylation pattern of total serum IgG.* Nature, 1985. **316**(6027): p. 452-7.
62. Gindzienska-Sieskiewicz, E., et al., *Changes of glycosylation of IgG in rheumatoid arthritis patients treated with methotrexate.* Adv Med Sci, 2016. **61**(2): p. 193-197.
63. Kobata, A., *Function and pathology of the sugar chains of human immunoglobulin G.* Glycobiology, 1990. **1**(1): p. 5-8.
64. Matsumoto, A., et al., *Autoantibody activity of IgG rheumatoid factor increases with decreasing levels of galactosylation and sialylation.* J Biochem, 2000. **128**(4): p. 621-8.
65. Ohmi, Y., et al., *Sialylation converts arthritogenic IgG into inhibitors of collagen-induced arthritis.*

. Nat Communications 2016. **5**(7).

66. Kaneko, Y., F. Nimmerjahn, and J.V. Ravetch, *Anti-inflammatory activity of immunoglobulin G resulting from Fc sialylation.* Science, 2006. **313**(5787): p. 670-3.
67. Van Beneden, K., et al., *Reversible changes in serum immunoglobulin galactosylation during the immune response and treatment of inflammatory autoimmune arthritis.* Ann Rheum Dis, 2009. **68**(8): p. 1360-5.

68. Collins, E.S., et al., *Glycosylation status of serum in inflammatory arthritis in response to anti-TNF treatment.* Rheumatology (Oxford), 2013. **52**(9): p. 1572-82.
69. Wang, J., et al., *Fc-Glycosylation of IgG1 is Modulated by B-cell Stimuli.* Mol Cell Proteomics, 2011. **10**(5).
70. Du Clos, T.W., *Pentraxins: structure, function, and role in inflammation.* ISRN Inflamm, 2013. **2013**: p. 379040.
71. Lu, J., et al., *Structural recognition and functional activation of FcgammaR by innate pentraxins.* Nature, 2008. **456**(7224): p. 989-92.
72. Gitlin, J.D., J.I. Gitlin, and D. Gitlin, *Localizing of C-reactive protein in synovium of patients with rheumatoid arthritis.* Arthritis Rheum, 1977. **20**(8): p. 1491-9.
73. Mc, E.C. and M. Ziff, *Basic sciences in relation to rheumatic diseases.* Med Clin North Am, 1955. **New York No.**: p. 765-82.
74. Ballou, S.P. and G. Lozanski, *Induction of inflammatory cytokine release from cultured human monocytes by C-reactive protein.* Cytokine, 1992. **4**(5): p. 361-8.
75. Clavel, C., et al., *Induction of macrophage secretion of tumor necrosis factor alpha through Fcγ receptor IIa engagement by rheumatoid arthritis-specific autoantibodies to citrullinated proteins complexed with fibrinogen.* Arthritis Rheum, 2008. **58**(3): p. 678-88.
76. Cox, D., S.W. Kerrigan, and S.P. Watson, *Platelets and the innate immune system: mechanisms of bacterial-induced platelet activation.* J Thromb Haemost, 2011. **9**(6): p. 1097-107.
77. Qiao, J., et al., *The platelet Fc receptor, FcgammaRIIa.* Immunol Rev, 2015. **268**(1): p. 241-52.
78. Pamuk, G.E., et al., *Increased platelet activation markers in rheumatoid arthritis: are they related with subclinical atherosclerosis?* Platelets, 2008. **19**(2): p. 146-54.
79. Knijff-Dutmer, E.A., et al., *Elevated levels of platelet microparticles are associated with disease activity in rheumatoid arthritis.* Arthritis Rheum, 2002. **46**(6): p. 1498-503.
80. Habets, K.L., T.W. Huizinga, and R.E. Toes, *Platelets and autoimmunity.* Eur J Clin Invest, 2013. **43**(7): p. 746-57.
81. Blom, A.B., et al., *Increased expression of Fcγ receptors II and III on macrophages of rheumatoid arthritis patients results in higher production of tumor necrosis factor alpha and matrix metalloproteinase.* Arthritis Rheum, 2003. **48**(4): p. 1002-14.
82. Hogarth, P.M., *Fc receptors are major mediators of antibody based inflammation in autoimmunity.* Curr Opin Immunol, 2002. **14**(6): p. 798-802.
83. Manolov, D.E., et al., *Ultrasensitive confocal fluorescence microscopy of C-reactive protein interacting with FcgammaRIIa.* Arterioscler Thromb Vasc Biol, 2004. **24**(12): p. 2372-7.
84. Bharadwaj, D., et al., *The major receptor for C-reactive protein on leukocytes is Fcγ receptor II.* J Exp Med, 1999. **190**(4): p. 585-90.
85. Chi, M., et al., *C-reactive protein induces signaling through FcγRIIa on HL-60 granulocytes.* J Immunol, 2002. **168**(3): p. 1413-8.

86. Sanders, L.A.M. and J.G. van de Winkel, *Human C-reactive protein does not bind to FcγRIIa on phagocytic cells.* J Clin Invest, 2001. **107**(5): p. 642-643.
87. Warmerdam, P.A., et al., *Molecular basis for a polymorphism of human Fc gamma receptor II (CD32).* J Exp Med, 1990. **172**(1): p. 19-25.
88. Robinson, J.I., et al., *FCGR2A ASSOCIATION WITH SUSCEPTIBILITY TO AUTOIMMUNE AND INFLAMMATORY DISEASES* Annals of the Rheumatic Diseases 2016: p. A54-A55.
89. Bruhns, P., et al., *Specificity and affinity of human Fcgamma receptors and their polymorphic variants for human IgG subclasses.* Blood, 2009. **113**(16): p. 3716-25.
90. Brun, J.G., T.M. Madland, and C.A. Vedeler, *Immunoglobulin G fc-receptor (FcγR) IIA, IIIA, and IIIB polymorphisms related to disease severity in rheumatoid arthritis.* J Rheumatol, 2002. **29**(6): p. 1135-40.
91. Roux, K.H., L. Strelets, and T.E. Michaelsen, *Flexibility of human IgG subclasses.* J Immunol, 1997. **159**(7): p. 3372-82.
92. Ramsland, P.A., et al., *Structural basis for Fc gammaRIIa recognition of human IgG and formation of inflammatory signaling complexes.* J Immunol, 2011. **187**(6): p. 3208-17.
93. Vidarsson, G., G. Dekkers, and T. Rispens, *IgG subclasses and allotypes: from structure to effector functions.* Front Immunol, 2014. **5**: p. 520.
94. Bruhns, P., et al., *Specificity and affinity of human Fcγ receptors and their polymorphic variants for human IgG subclasses.* Blood, 2009. **113**(16): p. 3716-25.
95. *State of Musculoskeletal Health 2017*, in *Arthritis & other musculoskeletal conditions in numbers*. 2017: Arthriris Research UK
96. Pietersz, G.A., et al., *Inhibition of destructive autoimmune arthritis in FcgammaRIIa transgenic mice by small chemical entities.* Immunol Cell Biol, 2009. **87**(1): p. 3-12.
97. Ramsland, P.A., et al., *Structural basis for FcγRIIa recognition of human IgG and formation of inflammatory signaling complexes.* J Immunol, 2011. **187**(6): p. 3208-17.
98. Maxwell, K.F., et al., *Crystal structure of the human leukocyte Fc receptor, FcγRIIa.* Nat Struct Biol, 1999. **6**(5): p. 437-42.
99. Powell, M.S., et al., *Alteration of the Fc gamma RIIa dimer interface affects receptor signaling but not ligand binding.* J Immunol, 2006. **176**(12): p. 7489-94.
100. Carugo, O. and P. Argos, *Protein-protein crystal-packing contacts.* Protein Sci, 1997. **6**(10): p. 2261-3.
101. Sondermann, P., *The FcγR/IgG Interaction as Target for the Treatment of Autoimmune Diseases.* J Clin Immunol, 2016. **36 Suppl 1**: p. 95-9.
102. Li, T., et al., *Modulating IgG effector function by Fc glycan engineering.* Proc Natl Acad Sci U S A, 2017. **114**(13): p. 3485-3490.
103. Lopez, D.H., et al., *Acidic pH increases the avidity of FcgammaR for immune complexes.* Immunology, 1999. **98**(3): p. 450-5.
104. Radaev, S., et al., *The structure of a human type III Fcγ receptor in complex with Fc.* J Biol Chem, 2001. **276**(19): p. 16469-77.

105. Sondermann, P., et al., *The 3.2-A crystal structure of the human IgG1 Fc fragment-FcγRIII complex.* Nature, 2000. **406**(6793): p. 267-73.
106. Kiyoshi, M., et al., *Structural basis for binding of human IgG1 to its high-affinity human receptor FcgammaRI.* Nat Commun, 2015. **6**: p. 6866.
107. Garman, S.C., et al., *Structure of the Fc fragment of human IgE bound to its high-affinity receptor Fc epsilonRI alpha.* Nature, 2000. **406**(6793): p. 259-66.
108. Joosten, R.P., et al., *Re-refinement from deposited X-ray data can deliver improved models for most PDB entries.* Acta Crystallogr D Biol Crystallogr, 2009. **65**(Pt 2): p. 176-85.
109. Khan, T. and D.M. Salunke, *Structural elucidation of the mechanistic basis of degeneracy in the primary humoral response.* J Immunol, 2012. **188**(4): p. 1819-27.
110. Khan, T. and D.M. Salunke, *Adjustable locks and flexible keys: plasticity of epitope-paratope interactions in germline antibodies.* J Immunol, 2014. **192**(11): p. 5398-405.
111. Tapryal, S., et al., *Structural evaluation of a mimicry-recognizing paratope: plasticity in antigen-antibody interactions manifests in molecular mimicry.* J Immunol, 2013. **191**(1): p. 456-63.
112. Stanfield, R., E. Pozharski, and B. Rupp, *Comment on Three X-ray Crystal Structure Papers.* J Immunol, 2016. **196**(2): p. 521-4.
113. Lu, J., et al., *Structure of FcgammaRI in complex with Fc reveals the importance of glycan recognition for high-affinity IgG binding.* Proc Natl Acad Sci U S A, 2015. **112**(3): p. 833-8.
114. Becker, D.J. and J.B. Lowe, *Fucose: biosynthesis and biological function in mammals.* Glycobiology, 2003. **13**(7): p. 41R-53R.
115. Bird, L.E., et al., *Application of In-Fusion cloning for the parallel construction of E. coli expression vectors.* Methods Mol Biol, 2014. **1116**: p. 209-34.
116. Hall, T.A., *BioEdit: a user-friendly biological sequence alignment editor and analysis program for Windows 95/98/NT.* Nucleic Acids Symposium, 1999. **41**: p. 95-98.
117. Nettleship, J.E., et al., *Transient expression in HEK 293 cells: an alternative to E. coli for the production of secreted and intracellular mammalian proteins.* Methods Mol Biol, 2015. **1258**: p. 209-22.
118. *Seeding cells for LigandTracer®*. Ridgeview Instruments AB: www.ligandtracer.com.
119. Bondza, S., et al., *Real-time Characterization of Antibody Binding to Receptors on Living Immune Cells.* Front Immunol, 2017. **8**: p. 455.
120. *SUNBRIGHT® OE Series (Biocompatible PEG Anchors)*. [cited 2019 June]; Available from: https://www.nofamerica.com/store/index.php?dispatch=categories.view&category_id=192.
121. Altschuh, D., et al., *Deciphering complex protein interaction kinetics using Interaction Map.* Biochem Biophys Res Commun, 2012. **428**(1): p. 74-9.
122. Volkov, V.V. and D.I. Svergun, *Uniqueness of ab initio shape determination in small-angle scattering.* Journal of Applied Crystallography, 2003. **36**: p. 860-864.

123. Kozin, M.B. and D.I. Svergun, *Automated matching of high- and low-resolution structural models.* Journal of Applied Crystallography, 2001. **34**: p. 33-41.
124. Folta-Stogniew, E., *Oligomeric states of proteins determined by size-exclusion chromatography coupled with light scattering, absorbance, and refractive index detectors.* Methods Mol Biol, 2006. **328**: p. 97-112.
125. *SEC-MALS-QELS*. [cited 2018 July]; Available from: https://keckbio.facilities.northwestern.edu/instruments/analytical/sec-mals-qels/.
126. Kabsch, W., *Xds.* Acta Crystallogr D Biol Crystallogr, 2010. **66**(Pt 2): p. 125-32.
127. Evans, P.R. and G.N. Murshudov, *How good are my data and what is the resolution?* Acta Crystallogr D Biol Crystallogr, 2013. **69**(7): p. 1204-1214.
128. McCoy, A.J., et al., *Phaser crystallographic software.* J Appl Crystallogr, 2007. **40**(Pt 4): p. 658-674.
129. Afonine, P.V., et al., *Towards automated crystallographic structure refinement with phenix.refine.* Acta Crystallogr D Biol Crystallogr, 2012. **68**(Pt 4): p. 352-67.
130. Emsley, P., et al., *Features and development of Coot.* Acta Crystallogr D Biol Crystallogr, 2010. **66**(Pt 4): p. 486-501.
131. Chen, V.B., et al., *MolProbity: all-atom structure validation for macromolecular crystallography.* Acta Crystallogr D Biol Crystallogr, 2010. **66**(Pt 1): p. 12-21.
132. *User guide to the wwPDB X-ray validation reports*. [cited 2019 January]; Available from: https://www.wwpdb.org/validation/legacy/XrayValidationReportHelp#_torsion_angles.
133. *Torsion Angles and the Ramachandran Plot*. [cited 2019; Available from: https://proteinstructures.com/Structure/Structure/Ramachandran-plot.html.
134. *Guide to Understanding PDB Data*. R-value and R-free [cited 2018 9th August]; Available from: https://pdb101.rcsb.org/learn/guide-to-understanding-pdb-data/r-value-and-r-free.
135. Comeau, S.R., et al., *ClusPro: an automated docking and discrimination method for the prediction of protein complexes.* Bioinformatics, 2004. **20**(1): p. 45-50.
136. Yueh, C., et al., *ClusPro-DC: Dimer Classification by the Cluspro Server for Protein-Protein Docking.* J Mol Biol, 2017. **429**(3): p. 372-381.
137. Krissinel, E. and K. Henrick, *Inference of macromolecular assemblies from crystalline state.* J Mol Biol, 2007. **372**(3): p. 774-97.
138. McNicholas, S. and J. Agirre, *Glycoblocks: a schematic three-dimensional representation for glycans and their interactions.* Acta Crystallogr D Struct Biol, 2017. **73**(Pt 2): p. 187-194.
139. Agirre, J., *Strategies for carbohydrate model building, refinement and validation.* Acta Crystallogr D Struct Biol, 2017. **73**(Pt 2): p. 171-186.

140. McNicholas, S., et al., *Presenting your structures: the CCP4mg molecular-graphics software.* Acta Crystallogr D Biol Crystallogr, 2011. **67**(Pt 4): p. 386-94.
141. Jason-Moller, L., M. Murphy, and J. Bruno, *Overview of Biacore Systems and Their Applications.* Current Protocols in Protein Science, 2006. **45**(1): p. 19.13.1-19.13.14.
142. Tudos, A.J. and R.B.M. Schasfoort, *Introduction to Surface Plasmon Resonance*, in *Handbook of Surface Plasmon Resonance* 2008, Springer.
143. *Anti-Human CD32 Antibody, Clone IV.3*, S. Technologies, Editor.: https://www.stemcell.com/anti-human-cd32-antibody-clone-iv-3.html.
144. Davies, A.M., et al., *Structural determinants of unique properties of human IgG4-Fc.* J Mol Biol, 2014. **426**(3): p. 630-44.
145. Chesla, S.E., et al., *The membrane anchor influences ligand binding two-dimensional kinetic rates and three-dimensional affinity of FcγRIII (CD16).* J Biol Chem, 2000. **275**(14): p. 10235-46.
146. Avisar, D., et al., *Cell-cycle-dependent resistance to Bacillus thuringiensis Cry1C toxin in Sf9 cells.* J Cell Sci, 2005. **118**(Pt 14): p. 3163-71.
147. Patel, K.R., J.T. Roberts, and A.W. Barb, *Multiple Variables at the Leukocyte Cell Surface Impact Fc gamma Receptor-Dependent Mechanisms.* Front Immunol, 2019. **10**: p. 223.
148. Reinke, S.O., et al., *Analysis of Cell Surface N-glycosylation of the Human Embryonic Kidney 293T Cell Line.* Journal of Carbohydrate Chemistry, 2011. **30**: p. 218-232.
149. Shi, X. and D.L. Jarvis, *Protein N-Glycosylation in the Baculovirus-Insect Cell System.* Current Drug Targets, 2007. **8**(10): p. 1116-1125.
150. Karassa, F.B., et al., *Role of the Fcgamma receptor IIa polymorphism in susceptibility to systemic lupus erythematosus and lupus nephritis: a meta-analysis.* Arthritis Rheum, 2002. **46**(6): p. 1563-71.
151. Wlodawer, A., et al., *Protein crystallography for non-crystallographers, or how to get the best (but not more) from published macromolecular structures.* FEBS J, 2008. **275**(1): p. 1-21.
152. Brunger, A.T., *Free R value: a novel statistical quantity for assessing the accuracy of crystal structures.* Nature, 1992. **355**(6359): p. 472-5.
153. *'Protein interfaces, surfaces and assemblies' service PISA at the European Bioinformatics Institute*. [cited 2017; Available from: http://www.ebi.ac.uk/pdbe/prot_int/pistart.html.
154. *Dimer Classification Tutorial*. [cited 2018 11/11/2018]; Available from: https://cluspro.org/tut_dimer_class.php.
155. Svergun, D.I., *Restoring low resolution structure of biological macromolecules from solution scattering using simulated annealing.* Biophys J, 1999. **76**(6): p. 2879-2886.
156. Bahadur, R.P., et al., *Dissecting subunit interfaces in homodimeric proteins.* Proteins, 2003. **53**(3): p. 708-19.
157. Reeves, P.J., et al., *Structure and function in rhodopsin: high-level expression of rhodopsin with restricted and homogeneous N-glycosylation by a tetracycline-inducible N-acetylglucosaminyltransferase I-negative HEK293S stable*

mammalian cell line. Proc Natl Acad Sci U S A, 2002. **99**(21): p. 13419-24.
158. Chang, V.T., et al., *Glycoprotein structural genomics: solving the glycosylation problem.* Structure, 2007. **15**(3): p. 267-73.
159. Vliegenthart, J.F. and F. Casset, *Novel forms of protein glycosylation.* Curr Opin Struct Biol, 1998. **8**(5): p. 565-71.
160. Martinez-Duncker, I., D.F. Diaz-Jimenez, and H.M. Mora-Montes, *Comparative Analysis of Protein Glycosylation Pathways in Humans and the Fungal Pathogen Candida albicans.* Int J Microbiol, 2014. **2014**: p. 267497.
161. Sigalov, A.B., *Multichain immune recognition receptor signaling from spatiotemporal organization to human disease. Preface.* Adv Exp Med Biol, 2008. **640**: p. ix-xi.
162. Blank, U., et al., *Inhibitory ITAMs as novel regulators of immunity.* Immunol Rev, 2009. **232**(1): p. 59-71.
163. Swanson, J.A. and A.D. Hoppe, *The coordination of signaling during Fc receptor-mediated phagocytosis.* J Leukoc Biol, 2004. **76**(6): p. 1093-103.
164. Lemmon, M.A., et al., *Sequence specificity in the dimerization of transmembrane alpha-helices.* Biochemistry, 1992. **31**(51): p. 12719-25.
165. Dorr, J.M., et al., *The styrene-maleic acid copolymer: a versatile tool in membrane research.* Eur Biophys J, 2016. **45**(1): p. 3-21.
166. Clayton, A.H., *Fluorescence-based approaches for monitoring membrane receptor oligomerization.* J Biosci, 2018. **43**(3): p. 463-469.
167. Joosten, R.P. and G. Vriend, *PDB improvement starts with Data Deposition.* Science 2007. **317**: p. 195-196.
168. Yan, B.X. and Y.Q. Sun, *Glycine residues provide flexibility for enzyme active sites.* J Biol Chem, 1997. **272**(6): p. 3190-4.
169. Stanley, P., H. Schachter, and N. Taniguchi, *N-Glycans* in *Essentials of Glycobiology*. 2009, Cold Spring Harbor Laboratory Press: Cold Spring Harbor NY.
170. Oganesyan, V., et al., *Structural insights into the interaction of human IgG1 with FcγRI: no direct role of glycans in binding.* Acta Crystallogr D Biol Crystallogr, 2015. **71**: p. 2354-2361.
171. Lu, J. and P.D. Sun, *Structural mechanism of high affinity FcgammaRI recognition of immunoglobulin G.* Immunol Rev, 2015. **268**(1): p. 192-200.
172. Igawa, T., et al., *Engineering the variable region of therapeutic IgG antibodies.* MAbs, 2011. **3**(3): p. 243-52.
173. Kellner, C., et al., *Modulating Cytotoxic Effector Functions by Fc Engineering to Improve Cancer Therapy.* Transfusion Medicine and Hemotherapy, 2017. **44**: p. 327-336.
174. Monnet, C., et al., *Combined glyco- and protein-Fc engineering simultaneously enhance cytotoxicity and half-life of a therapeutic antibody.* MAbs, 2014. **6**(2): p. 422-36.
175. Chen, X., et al., *FcγR-Binding Is an Important Functional Attribute for Immune Checkpoint Antibodies in Cancer Immunotherapy.* Front Immunol, 2019. **10**: p. 292.

176. Jazayeri, J.A. and G.J. Carroll, *Half-Life Extension by Fusion to the Fc Region*, in *Therapeutic Proteins: Strategies to Modulate Their Plasma Half-Lives*, R. Kontermann, Editor. 2012, Wiley.
177. Schlothauer, T., et al., *Novel human IgG1 and IgG4 Fc-engineered antibodies with completely abolished immune effector functions.* Protein Eng Des Sel, 2016. **29**(10): p. 457-466.
178. Vafa, O., et al., *An engineered Fc variant of an IgG eliminates all immune effector functions via structural perturbations.* Methods, 2014. **65**(1): p. 114-26.
179. Labrijn, A.F., R.C. Aalberse, and J. Schuurman, *When binding is enough: nonactivating antibody formats.* Current Opinions in Immunology, 2008. **20**(4): p. 479-485.
180. Cordoba, F., et al., *A novel, blocking, Fc-silent anti-CD40 monoclonal antibody prolongs nonhuman primate renal allograft survival in the absence of B cell depletion.* Am J Transplant, 2015. **15**(11): p. 2825-36.
181. Sazinsky, S.L., et al., *Aglycosylated immunoglobulin G1 variants productively engage activating Fc receptors.* Proc Natl Acad Sci U S A, 2008. **105**(51): p. 20167-72.
182. Subedi, G.P. and A.W. Barb, *The immunoglobulin G1 N-glycan composition affects binding to each low affinity Fc gamma receptor.* MAbs, 2016. **8**(8): p. 1512-1524.
183. Borrok, M.J., et al., *Revisiting the role of glycosylation in the structure of human IgG Fc.* ACS Chem Biol, 2012. **7**(9): p. 1596-602.
184. Joosten, R.P., et al., *PDB_REDO: automated re-refinement of X-ray structure models in the PDB.* J Appl Crystallogr, 2009. **42**(Pt 3): p. 376-384.
185. Banning, C., et al., *A flow cytometry-based FRET assay to identify and analyse protein-protein interactions in living cells.* PLoS One, 2010. **5**(2): p. e9344.
186. Pepponi, I., et al., *Immune-complex mimics as a molecular platform for adjuvant-free vaccine delivery.* PLoS One, 2013. **8**(4): p. e60855.
187. Dalton, A.C. and W.A. Barton, *Over-expression of secreted proteins from mammalian cell lines.* Protein Sci, 2014. **23**(5): p. 517-25.
188. Maly, D.J., J.A. Allen, and K.M. Shokat, *A mechanism-based cross-linker for the identification of kinase-substrate pairs.* J Am Chem Soc, 2004. **126**(30): p. 9160-1.

List of Abbreviations

ACPAs	Anti-citrullinated protein antibodies
ADCC	Antibody-dependent cell cytotoxicity
BAM	Biocompatible anchor for membrane
BSA	Bovine Serum Albumin
CRP	C-reactive protein
DAG	Diacyl-glycerol
DMEM	Dulbecco's Modified Eagle Medium
ER	Endoplasmic Reticulum
FcγR	Fc-gamma Receptor
FCS	Fetal calf serum
FcγR	Fc-gamma Receptor
FITC	Fluorescein isothiocyanate
FPLC	Fast Protein Liquid Chromatography
HAGG	Heat aggregated gamma-globulin
HEK293	Human Embryonic Kidney 293 cells
HRP	Horseradish peroxidase
IC	Immune complex
IF	Immunofluorescence
IgG	Immunoglobulin G
IL	Interlukin
IP3	Inositol triphosphate
ITAM	Immunotyrosine based activation motif
ITIM	Immunotyrosine based inhibitory motif
PADs	Peptodyl arginine deaminases
PBS	Phosphate buffered saline
PEI	Polyethylenimine
PIP2	Phosphatidylinositol 4,5-bisphosphate
PKC	Protein Kinase C
PLCγ	Phospholipase-C gamma
RA	Rheumatoid Arthritis
RF	Rheumatoid Factor
ROS	Reactive oxygen species
SAP	Serum amyloid P
SCE	Small chemical entity
SEC-MALLS	Size-exclusion chromatogprhy and laser-light scattering
SH2	Src-homology 2
TNF-α	Tumour Necrosis Factor α

Appendix A
Buffer recipes

The recipes for all buffers used in this thesis can be found in Appendix A.

Buffer	Use	Recipe
6X SDS sample buffer (Reducing)	Running reducing protein SDS-PAGE gels	375 mM Tris-HCl 9% SDS 50% glycerol 9% betamercatoethanol 0.03% bromophenol blue
Borate buffer	Labelling IgG with DyLight 650	50mM Borate buffer pH 9
Coomassie de-stain solution	Remove excess coomassie stain from gel	10% acetic acid
Coomassie fixing buffer	Fixing proteins on gels before staining with coomassie	25% isopropanol 10% acetic acid
Coomassie stain solution	Staining proteins on a gel	10% acetic acid 0.006% coomassie blue R-250
Denaturing PAGE running buffer	Running denaturing SDS-PAGE gels	25mM Tris 200mM Glycine 0.1% SDS
His-trap elution buffer	Eluting ectodomain proteins from His-trap column	10mM sodium phosphate 500mM NaCl 500mM imidazole pH 7.4
His-trap wash buffer	Washing His-trap column during	10mM sodium phosphate 500mM NaCl

	ectodomain purification	pH 7.4
IgG column elution buffer	Eluting ectodomain proteins from IgG column	0.5M Acetic acid pH 3.4
IgG column wash buffer	Washing IgG column during ectodomain purification (Wash 2)	5mM ammonium acetate pH 5
Native PAGE running buffer	Running native PAGE gels	25mM Tris 200mM Glycine
Neutralisation buffer	Neutralising ectodomains after elution from IgG column	1M Tris-HCl pH 8.0
Transfer buffer	Transferring protein from gel to PDVF membrane	25mM Tris 200mM Glycine 20% Methanol
Tris-acetate-EDTA (TAE)	Making and running agarose gels	40mM Tris 20mM Acetic acid 1mM EDTA
Tris-saline-tween (TST)	Washing western blot membranes Washing IgG column during ectodomain purification (Wash 1)	50 mM Tris 150 mM NaCl 0.1% Tween 20 pH 7.6
Western blot blocking buffer	Blocking western blot membranes	5% BSA

Appendix B
Published protocols

Common published protocols that were used in this thesis can be found in Appendix B.

B.1 Gel extraction – QIAquick Gel Extraction Kit

1. Excise the DNA fragment from the agarose gel with a clean, sharp scalpel. Minimize the size of the gel slice by removing extra agarose.

2. Weigh the gel slice in a colourless tube. Add 3 volumes of Buffer QG to 1 volume of gel (100 mg ~ 100 µl), e.g. add 300 µl of Buffer QG to each 100 mg of gel. For >2% agarose gels, add 6 volumes of Buffer QG. The maximum amount of gel slice per QIAquick column is 400 mg; for gel slices >400 mg use more than one QIAquick column.

3. Incubate at 50˚C for 10 minutes (or until gel is completely dissolved). Mix by vortexing the tube ever 2-3 min during incubation.

4. After gel slice has completely dissolved, check that the colour of the mixture is yellow (similar to colour of Buffer QG). If colour is orange or violet, add 10uL of 3M sodium acetate, pH 5.0 and mix. The colour of the mixture will turn yellow.

5. Add 1 gel volume of isopropanol to the sample and mix, e.g. if gel is 100mg add 100uL of isopropanol. Do not centrifuge sample at this stage.

6. Place a QIAquick spin column in a provided 2ml collection tube.

7. To bind DNA, apply sample to QIAquick column and centrifuge for 1 minute. Max volume of column reservoir is 800uL – for samples with larger volumes simply load and spin again.

8. Discard flow-through and place QIAquick column back in the same collection tube.

9. Optional – add 0.5ml of Buffer QG to QIAquick column and centrifuge for 1 minute. This step will remove all traces of agarose.

10. To wash, add 0.75ml of Buffer PE to QIAquick column and centrifuge for 1 minute. Note: If the DNA will be used for salt sensitive applications, such as blunt-end ligation and direct sequencing, let the column stand 2–5 min after addition of Buffer PE, before centrifuging. Discard the flow-through and centrifuge QIAquick column for an additional 1 minute at ≥10,000 x g (~13,000 rpm).

11. Place QIAquick column into a clean 1.5ml microcentrifuge tube.

12. To elute DNA, add 50uL buffer EB (10mM Tris-Cl, pH 8.5) or H20 to the centre of the QUIquick membrane and centrifuge the column for 1 minute at maximum speed. For increased DNA concentration, add 30uL elution buffer to the centre of the QIAquick membrane, let the column stand for 1 minute and then centrifuge for 1 minute.

B.2 QIAGEN QIAprep® Spin Miniprep Kit

1. Pick a single colony from LB-amp agar plates, and inoculate appropriate volume of LB medium containing ampicillin. Leave to grow in 37˚C shaking incubators overnight.

2. Pellet 1-5ml bacterial overnight culture by centrifugation at >8000 rpm (6800 x g) for 3 min at room temperature.

3. Suspend pelleted bacterial cells in 250uL Buffer P1 and transfer to a micro centrifuge tube.

4. Add 250uL Buffer P2 and mix thoroughly by inverting the tube 4-6 times until the solution becomes clear. Do not allow the lysis reaction to proceed for more than 5 min. if using LyseBlue reagent, the solution will turn blue.

5. Add 350uL Buffer N3 and mix immediately and thoroughly by inverting the tube 4-6 times. If using LyseBlue reagent the solution will turn colourless.

6. Centrifuge for 10 min at 13,000 rpm (~17,900 x g) in a table-top micro centrifuge.

7. Apply the supernatant from step 6 to the QIAprep spin column by decanting or pipetting. Centrifuge for 30-60 sec and discard the flow-through.

8. Recommended: wash the QIAprep spin column by adding 0.5ml buffer PB. Centrifuge for 30-60sec and discard flow-through.

9. Note: this step is only required when using endA+ strains or other bacteria strains with high nuclease activity or carbohydrate content.

10. Wash the QIAprep spin column by adding 0.75mL Buffer PE. Centrifuge for 30-60 sec and discard flow-through.

11. Centrifuge for a further 1 min to remove residual wash buffer.

12. Place the QIAprep column in a clean 1.5ml micro centrifuge tube. To elute DNA, add 50uL Buffer EB (10mM Tris-HCl, pH 8.5) or water to the centre of the QIAprep spin column, let stand for 1 min, and centrifuge for 1 min.

B.3 QIAGEN EndoFree® Plasmid Purification

Maximum recommended culture volumes:

- High-copy plasmids – 2.5L
- Low-copy plasmids – not recommended

1. Pick a single colony from a freshly streaked selective plate and inoculate a starter culture of 5–10 ml LB medium containing the appropriate selective antibiotic. Incubate for approx. 8 h at 37°C with vigorous shaking (approx. 300 rpm).
   Use a flask with a volume of at least 4 times the volume of the culture.
   Dilute the starter culture 1/500 to 1/1000 into selective LB medium.
   Inoculate 2.5L medium with 2.5–5 ml of starter culture.
   Grow at 37°C for 12–16 h with vigorous shaking (approx. 300 rpm).
   Use a flask or vessel with a volume of at least 4 times the volume of the culture. The culture should reach a cell density of approximately 3–4 x 10^9 cells per milliliter, which typically corresponds to a pellet wet weight of approximately 3 g/L medium.

2. Harvest the bacterial cells by centrifugation at 6000 x g for 15 min at 4°C. If you wish to stop the protocol and continue later, freeze the cell pellets at –20 °C.

3. Screw the QIAfilter Mega-Giga Cartridge onto a 45 mm-neck glass bottle and connect it to a vacuum source.
   Do not overtighten the QIAfilter Cartridge on the bottle neck, because the QIAfilter Cartridge plastic may crack.

4. Resuspend the bacterial pellet in 125 ml of Buffer P1.
   For efficient lysis it is important to use a vessel that is large enough to allow complete mixing of the lysis buffers. We recommend a 500 ml bottle for Mega preparations and a 1000 ml bottle for Giga preparations. Ensure that the RNase A has been added to Buffer P1. If LyseBlue reagent has been added to Buffer P1, vigorously shake the buffer bottle before use to ensure LyseBlue particles are completely resuspended.
   The bacteria should be resuspended completely by vortexing or pipetting up and down until no cell clumps remain.

5. Add 125 ml of Buffer P2, mix thoroughly by vigorously inverting 4–6 times, and incubate at room temperature (15–25°C) for 5 min.
   Do not vortex, as this will result in shearing of genomic DNA. The lysate should appear viscous. Do not allow the lysis reaction to proceed for more than 5 min.
   After use, the bottle containing Buffer P2 should be closed immediately to avoid acidification of Buffer P2 from CO2 in the air.
   If LyseBlue has been added to Buffer P1 the cell suspension will turn blue after addition of Buffer P2. Mixing should result in a homogeneously coloured suspension. If the suspension contains localized colourless regions or if brownish cell clumps are still visible, continue mixing the solution until a homogeneously coloured suspension is achieved.

6. Add 125 ml chilled Buffer P3 and mix thoroughly by vigorously inverting 4–6 times. Mix well until white, fluffy material has formed and the lysate is no longer viscous. Proceed directly to step 8. Do not incubate on ice.
   Precipitation is enhanced by using chilled Buffer P3. After addition of Buffer P3, a fluffy, white precipitate containing genomic DNA, proteins, cell debris, and KDS becomes visible. The lysate should be mixed well to reduce the viscosity and prevent clogging of the QIAfilter Cartridge.
   If LyseBlue reagent has been used, the suspension should be mixed until all trace of blue has gone and the suspension is colourless. A homogeneous colourless suspension indicates that the SDS has been effectively precipitated.

7. Pour the lysate into the QIAfilter Mega-Giga Cartridge and incubate at room temperature for 10 min.
   Important: This 10 min incubation at room temperature is essential for optimal performance of the QIAfilter Mega-Giga Cartridge. Do not agitate the QIAfilter Cartridge during this time. A precipitate containing

proteins, genomic DNA, and detergent will float and form a layer on top of the solution. This ensures convenient filtration without clogging. Switch on the vacuum source. After all liquid has been pulled through, switch off the vacuum source. Leave the QIAfilter Cartridge attached.

8. Add 50 ml Buffer FWB2 to the QIAfilter Cartridge and gently stir the precipitate using a sterile spatula. Switch on the vacuum source until the liquid has been pulled through completely.
   Gentle stirring of the precipitate enhances the flow of liquid through the filter unit.
   Take care not to disperse the precipitate, as this may result in carryover of cell debris and KDS, which will affect flow and binding characteristics of the QIAGEN column. The filtered lysate in the bottle contains the plasmid DNA.
   Optional: Remove a 75 µl sample from the cleared lysate and save for an analytical gel (sample 1) to determine whether growth and lysis conditions were optimal.

9. Add 30 ml Buffer ER to the filtered lysate, mix by inverting the bottle approximately 10 times, and incubate on ice for 30 min.
   After addition of Buffer ER the lysate appears turbid, but will become clear again during the incubation on ice.

10. Equilibrate a QIAGEN-tip 10000 by applying 75 ml Buffer QBT, and allow the column to empty by gravity flow.
    Flow of buffer will begin automatically by reduction in surface tension due to the presence of detergent in the equilibration buffer. Allow the QIAGEN-tip to drain completely. QIAGEN-tips can be left unattended, since the flow of buffer will stop when the meniscus reaches the upper frit in the column.

11. Apply the filtered lysate from step 11 onto the QIAGEN-tip and allow it to enter the resin by gravity flow.
    Due to the presence of Buffer ER the lysate may become turbid again, however this does not affect the performance of the procedure.
    Optional: Remove a 75 µl sample from the flow-through and save for an analytical gel (sample 2) to determine efficiency of DNA binding to the QIAGEN resin.

12. Wash the QIAGEN-tip with a total of 600 ml Buffer QC.
    Allow Buffer QC to move through the QIAGEN-tip by gravity flow. The first half of the volume of wash buffer is sufficient to remove contaminants in the majority of plasmid DNA preparations. The second half is particularly necessary when large culture volumes or bacterial strains producing large amounts of carbohydrates are used.
    Optional: Remove a 120 µl sample from the combined wash fractions and save for an analytical gel (sample 3).
    Important: For all subsequent steps use endotoxin-free or pyrogen-free plasticware (e.g., new polypropylene centrifuge tubes) or pretreated glassware.

13. Elute DNA with 100 ml Buffer QN.
    Use of polycarbonate centrifuge tubes for collection is not recommended as polycarbonate is not resistant to the alcohol used in subsequent steps.
    Optional: Remove a 20 µl sample of the eluate and save for an analytical gel (sample 4).
    Note: For constructs larger than 45–50 kb, prewarming the elution buffer to 65°C may help to increase yield.
    If you wish to stop the protocol and continue later, store the eluate at 4°C. Storage periods longer than overnight are not recommended.

14. Precipitate DNA by adding 70 ml (0.7 volumes) room-temperature isopropanol to the eluted DNA. Mix and centrifuge immediately at ≥15,000 x g for 30 min at 4°C. Carefully decant the supernatant.
    All solutions should be at room temperature to minimize salt precipitation, although centrifugation is carried out at 4°C to prevent overheating of the sample.
    Alternatively, disposable conical bottom centrifuge tubes can be used for centrifugation at 5000 x g for 60 min at 4°C. Isopropanol pellets have a glassy appearance and may be more difficult to see than the fluffy, salt-containing pellets that result from ethanol precipitation. Marking the outside of the tube before centrifugation allows the pellet to be more easily located. Isopropanol pellets are also more loosely attached to the side of the tube, and care should be taken when removing the supernatant.

15. Wash DNA pellet with 10 ml of endotoxin-free room-temperature 70% ethanol (add 40 ml of 96–100% ethanol to the endotoxin-free water supplied with the kit) and centrifuge at ≥15,000 x g for 10 min. Carefully decant the supernatant without disturbing the pellet.
    Alternatively, disposable conical-bottom centrifuge tubes can be used for centrifugation at 5000 x g for 60 min at 4°C. The 70% ethanol removes precipitated salt and replaces isopropanol with the more volatile ethanol, making the DNA easier to redissolve.

16. Air-dry the pellet for 10–20 min, and redissolve the DNA in a suitable volume of endotoxin-free Buffer TE.
    Redissolve the DNA pellet by rinsing the walls to recover the DNA, especially if glass tubes have been used. Pipetting the DNA up and down to promote resuspension may cause shearing and should be avoided. Overdrying the pellet will make the DNA difficult to redissolve. DNA dissolves best under slightly alkaline conditions; it does not easily dissolve in acidic buffers.

B.4 QIAGEN DNeasy® Purification of Total DNA from Cells (Spin-Column Protocol)

1. Cultured cells: Centrifuge the appropriate number of cells (maximum 5 x 10^6) for 5 min at 300 x g. Resuspend the pellet in 200 µl PBS. Add 20 µl proteinase K.
   Optional: If RNA-free genomic DNA is required, add 4 µl RNase A (100 mg/ml), mix by vortexing, and incubate for 2 min at room temperature before continuing with step 2.

2. Add 200 µl Buffer AL (without added ethanol). Mix thoroughly by vortexing, and incubate at 56°C for 10 min. Ensure that ethanol has not been added to Buffer AL. It is essential that the sample and Buffer AL are mixed immediately and thoroughly by vortexing or pipetting to yield a homogeneous solution.
3. Add 200 µl ethanol (96–100%) to the sample, and mix thoroughly by vortexing. It is important that the sample and the ethanol are mixed thoroughly to yield a homogeneous solution.

4. Pipet the mixture from step 3 into the DNeasy Mini spin column placed in a 2 ml collection tube (provided). Centrifuge at 6000 x g (8000 rpm) for 1 min. Discard flow-through and collection tube.
5. Place the DNeasy Mini spin column in a new 2 ml collection tube (provided), add 500 µl Buffer AW1, and centrifuge for 1 min at 6000 x g (8000 rpm). Discard flow-through and collection tube.

6. Place the DNeasy Mini spin column in a new 2 ml collection tube (provided), add 500 µl Buffer AW2, and centrifuge for 3 min at 20,000 x g (14,000 rpm) to dry the DNeasy membrane. Discard flow-through and collection tube. It is important to dry the membrane of the DNeasy Mini spin column, since residual ethanol may interfere with subsequent reactions. This centrifugation step ensures that no residual ethanol will be carried over during the following elution. Following the centrifugation step, remove the DNeasy Mini spin column carefully so that the column does not come into contact with the flow-through, since this will result in carryover of ethanol. If carryover of ethanol occurs, empty the collection tube, then reuse it in another centrifugation for 1 min at 20,000 x g (14,000 rpm).

7. Place the DNeasy Mini spin column in a clean 1.5 ml or 2 ml microcentrifuge tube (not provided), and pipet 200 µl Buffer AE directly onto the DNeasy membrane. Incubate at room temperature for 1 min, and then centrifuge for 1 min at 6000 x g (8000 rpm) to

elute. Elution with 100 µl (instead of 200 µl) increases the final DNA concentration in the eluate, but also decreases the overall DNA yield.

8. Recommended: For maximum DNA yield, repeat elution once as described in step 7. This step leads to increased overall DNA yield. A new microcentrifuge tube can be used for the second elution step to prevent dilution of the first eluate. Alternatively, to combine the eluates, the microcentrifuge tube from step 7 can be reused for the second elution step. Note: Do not elute more than 200 µl into a 1.5 ml microcentrifuge tube because the DNeasy Mini spin column will come into contact with the eluate.

Appendix C

C.1 PDB Validation Report for the re-refined model of FcγRIIa bound to IgG-Fc

Preliminary Full wwPDB X-ray Structure Validation Report (i)

Dec 13, 2017 – 09:49 AM GMT

Deposition ID : D_1200007939
PDB ID : *(not yet assigned)*

This is a Preliminary Full wwPDB X-ray Structure Validation Report.

This report is produced by the wwPDB Deposition System during initial deposition but before annotation of the structure.

We welcome your comments at *validation@mail.wwpdb.org*
A user guide is available at
http://wwpdb.org/validation/2016/XrayValidationReportHelp
with specific help available everywhere you see the (i) symbol.

The following versions of software and data (see references (1)) were used in the production of this report:

MolProbity	:	4.02b-467
Mogul	:	1.7.2 (RC1), CSD as538be (2017)
Xtriage (Phenix)	:	1.9-1692
EDS	:	rb-20030345
Percentile statistics	:	20161228.v01 (using entries in the PDB archive December 28th 2016)
Refmac	:	5.8.0135
CCP4	:	6.5.0
Ideal geometry (proteins)	:	Engh & Huber (2001)
Ideal geometry (DNA, RNA)	:	Parkinson et al. (1996)
Validation Pipeline (wwPDB-VP)	:	rb-20030345

1 Overall quality at a glance

The following experimental techniques were used to determine the structure:
X-RAY DIFFRACTION

The reported resolution of this entry is 3.78 Å.

Percentile scores (ranging between 0-100) for global validation metrics of the entry are shown in the following graphic. The table shows the number of entries on which the scores are based.

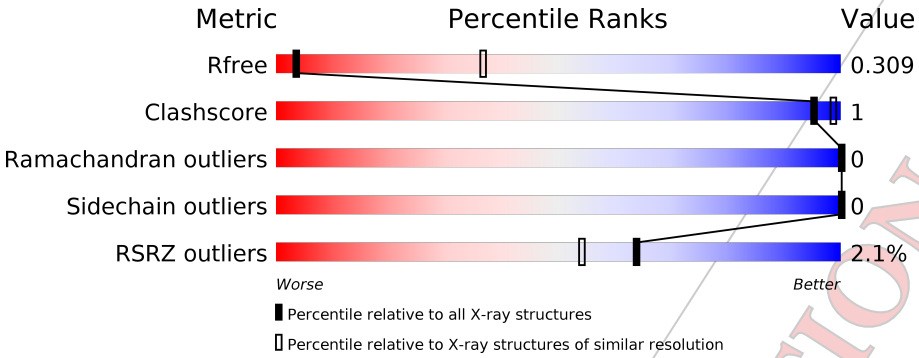

Metric	Whole archive (#Entries)	Similar resolution (#Entries, resolution range(Å))
R_{free}	100719	1011 (4.04-3.52)
Clashscore	112137	1017 (4.00-3.56)
Ramachandran outliers	110173	1006 (4.02-3.54)
Sidechain outliers	110143	1000 (4.02-3.54)
RSRZ outliers	101464	1024 (4.04-3.52)

The table below summarises the geometric issues observed across the polymeric chains and their fit to the electron density. The red, orange, yellow and green segments on the lower bar indicate the fraction of residues that contain outliers for >=3, 2, 1 and 0 types of geometric quality criteria. A grey segment represents the fraction of residues that are not modelled. The numeric value for each fraction is indicated below the corresponding segment, with a dot representing fractions <=5% The upper red bar (where present) indicates the fraction of residues that have poor fit to the electron density. The numeric value is given above the bar.

Mol	Chain	Length	Quality of chain
1	A	211	2% 99%
2	B	210	% 98%
3	C	163	3% 98%

2 Entry composition

There are 8 unique types of molecules in this entry. The entry contains 9450 atoms, of which 4533 are hydrogens and 0 are deuteriums.

In the tables below, the ZeroOcc column contains the number of atoms modelled with zero occupancy, the AltConf column contains the number of residues with at least one atom in alternate conformation and the Trace column contains the number of residues modelled with at most 2 atoms.

- Molecule 1 is a protein.

Mol	Chain	Residues	Atoms						ZeroOcc	AltConf	Trace
			Total	C	H	N	O	S			
1	A	211	3327	1072	1644	286	319	6	0	0	0

- Molecule 2 is a protein.

Mol	Chain	Residues	Atoms						ZeroOcc	AltConf	Trace
			Total	C	H	N	O	S			
2	B	210	3320	1067	1643	285	318	7	0	0	0

- Molecule 3 is a protein.

Mol	Chain	Residues	Atoms						ZeroOcc	AltConf	Trace
			Total	C	H	N	O	S			
3	C	163	2468	817	1180	222	244	5	0	0	0

- Molecule 4 is N-ACETYL-D-GLUCOSAMINE (three-letter code: NAG) (formula: $C_8H_{15}NO_6$).

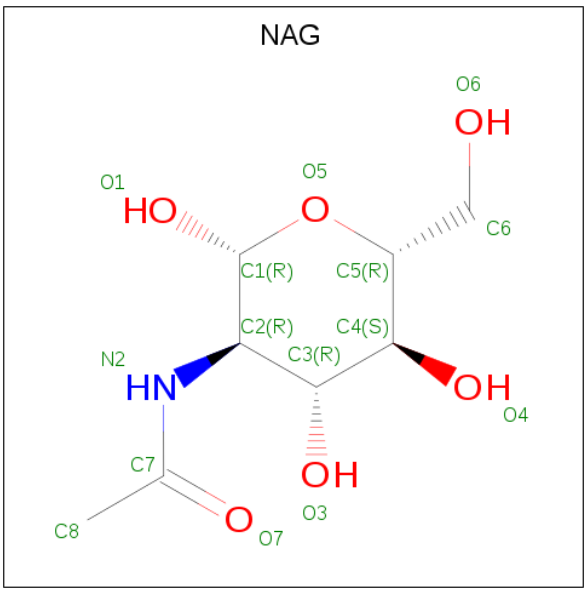

Mol	Chain	Residues	Atoms	ZeroOcc	AltConf
4	A	1	Total C N O 14 8 1 5	0	0
4	A	1	Total C N O 14 8 1 5	0	0
4	A	1	Total C H N O 28 8 14 1 5	0	0
4	A	1	Total C H N O 28 8 14 1 5	0	0
4	B	1	Total C N O 14 8 1 5	0	0
4	B	1	Total C N O 14 8 1 5	0	0
4	B	1	Total C H N O 27 8 13 1 5	0	0
4	B	1	Total C H N O 28 8 14 1 5	0	0
4	C	1	Total C N O 14 8 1 5	0	0
4	C	1	Total C N O 14 8 1 5	0	0

- Molecule 5 is BETA-D-MANNOSE (three-letter code: BMA) (formula: $C_6H_{12}O_6$).

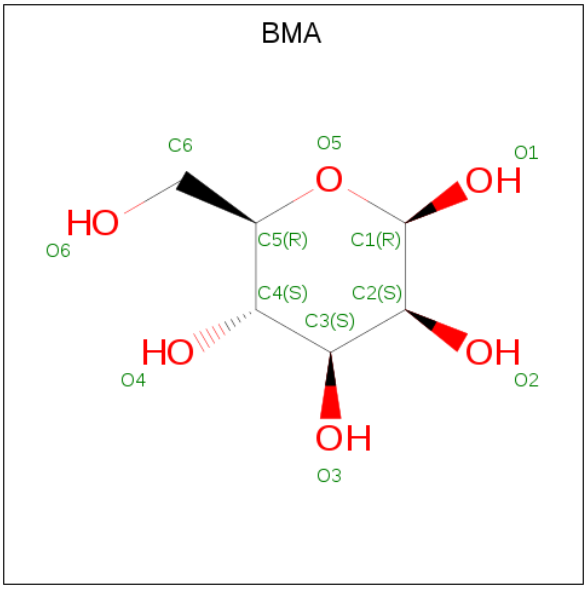

Mol	Chain	Residues	Atoms	ZeroOcc	AltConf
5	A	1	Total C O 11 6 5	0	0
5	B	1	Total C O 11 6 5	0	0

Continued on next page...

Continued from previous page...

Mol	Chain	Residues	Atoms	ZeroOcc	AltConf
5	C	1	Total C O 11 6 5	0	0

- Molecule 6 is ALPHA-D-MANNOSE (three-letter code: MAN) (formula: $C_6H_{12}O_6$).

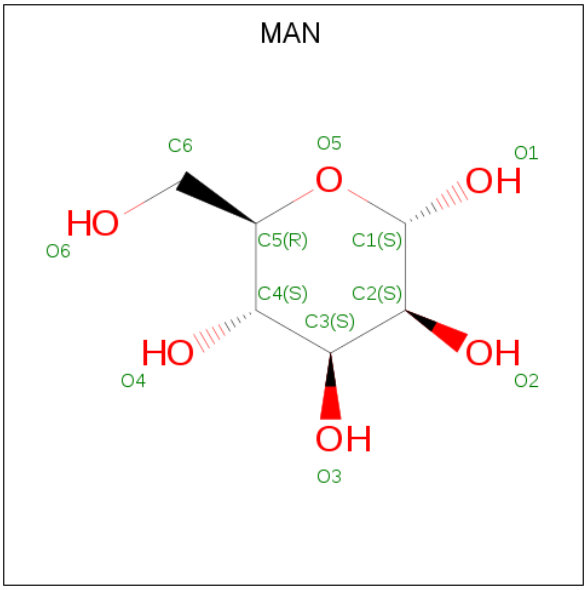

Mol	Chain	Residues	Atoms	ZeroOcc	AltConf
6	A	1	Total C O 11 6 5	0	0
6	A	1	Total C O 11 6 5	0	0
6	B	1	Total C O 11 6 5	0	0
6	B	1	Total C O 11 6 5	0	0
6	C	1	Total C O 11 6 5	0	0

- Molecule 7 is ALPHA-L-FUCOSE (three-letter code: FUC) (formula: $C_6H_{12}O_5$).

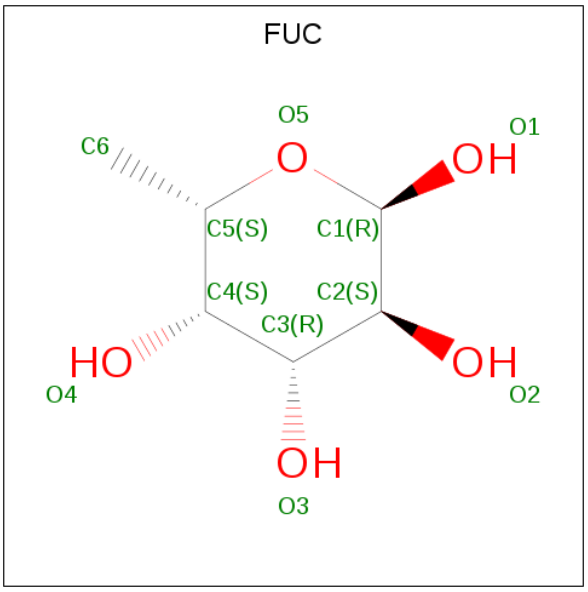

Mol	Chain	Residues	Atoms	ZeroOcc	AltConf
7	A	1	Total C O 10 6 4	0	0
7	B	1	Total C O 10 6 4	0	0
7	C	1	Total C O 10 6 4	0	0

- Molecule 8 is BETA-D-GALACTOSE (three-letter code: GAL) (formula: $C_6H_{12}O_6$).

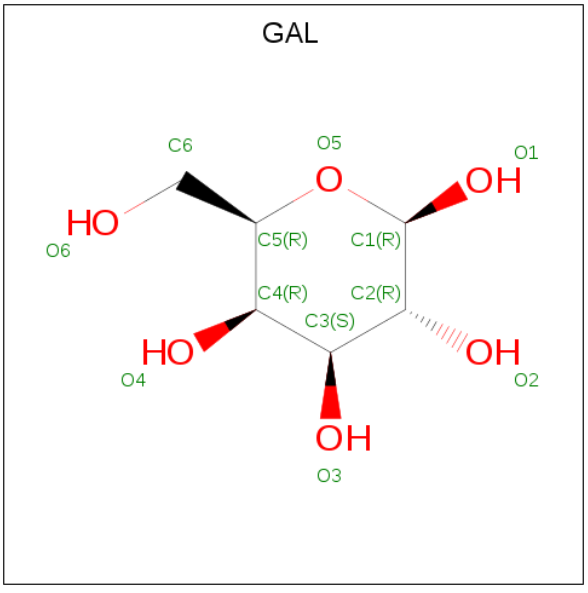

Mol	Chain	Residues	Atoms	ZeroOcc	AltConf
8	B	1	Total C H O 22 6 11 5	0	0

3 Residue-property plots

These plots are drawn for all protein, RNA and DNA chains in the entry. The first graphic for a chain summarises the proportions of the various outlier classes displayed in the second graphic. The second graphic shows the sequence view annotated by issues in geometry and electron density. Residues are color-coded according to the number of geometric quality criteria for which they contain at least one outlier: green = 0, yellow = 1, orange = 2 and red = 3 or more. A red dot above a residue indicates a poor fit to the electron density (RSRZ > 2). Stretches of 2 or more consecutive residues without any outlier are shown as a green connector. Residues present in the sample, but not in the model, are shown in grey.

- Molecule 1:

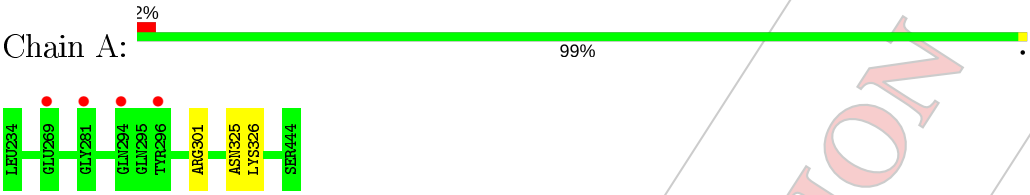

- Molecule 2:

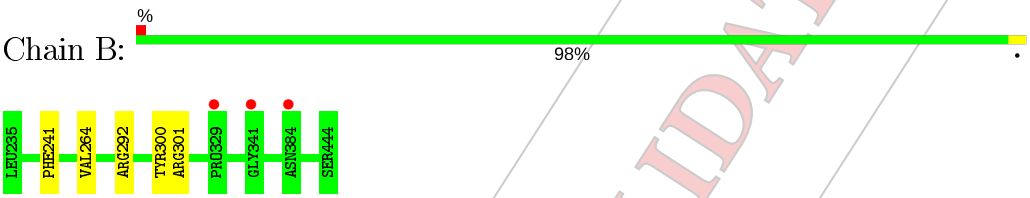

- Molecule 3:

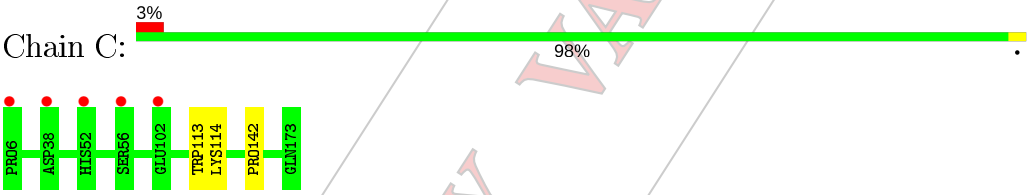

4 Data and refinement statistics (i)

Property	Value	Source
Space group	C 2 2 21	Depositor
Cell constants a, b, c, α, β, γ	153.38Å 255.55Å 58.44Å 90.00° 90.00° 90.00°	Depositor
Resolution (Å)	29.71 – 3.78 29.71 – 3.78	Depositor EDS
% Data completeness (in resolution range)	98.3 (29.71-3.78) 98.3 (29.71-3.78)	Depositor EDS
R_{merge}	(Not available)	Depositor
R_{sym}	(Not available)	Depositor
$< I/\sigma(I) >$ [1]	4.48 (at 3.75Å)	Xtriage
Refinement program	PHENIX (1.11.1_2575: ???)	Depositor
R, R_{free}	0.244 , 0.313 0.237 , 0.309	Depositor DCC
R_{free} test set	593 reflections (5.04%)	DCC
Wilson B-factor (Å^2)	73.7	Xtriage
Anisotropy	0.512	Xtriage
Bulk solvent k_{sol}(e/Å^3), B_{sol}(Å^2)	0.37 , 40.5	EDS
L-test for twinning[2]	$< \|L\| > = 0.48$, $< L^2 > = 0.31$	Xtriage
Estimated twinning fraction	0.015 for 1/2*h-1/2*k,-3/2*h-1/2*k,-l 0.019 for 1/2*h+1/2*k,3/2*h-1/2*k,-l	Xtriage
F_o,F_c correlation	0.85	EDS
Total number of atoms	9450	wwPDB-VP
Average B, all atoms (Å^2)	86.0	wwPDB-VP

Xtriage's analysis on translational NCS is as follows: *The largest off-origin peak in the Patterson function is 5.05% of the height of the origin peak. No significant pseudotranslation is detected.*

[1] Intensities estimated from amplitudes.

[2] Theoretical values of $< |L| >$, $< L^2 >$ for acentric reflections are 0.5, 0.333 respectively for untwinned datasets, and 0.375, 0.2 for perfectly twinned datasets.

5 Model quality

5.1 Standard geometry

Bond lengths and bond angles in the following residue types are not validated in this section: FUC, GAL, NAG, BMA, MAN

The Z score for a bond length (or angle) is the number of standard deviations the observed value is removed from the expected value. A bond length (or angle) with $|Z| > 5$ is considered an outlier worth inspection. RMSZ is the root-mean-square of all Z scores of the bond lengths (or angles).

Mol	Chain	Bond lengths		Bond angles	
		RMSZ	$\#\|Z\| > 5$	RMSZ	$\#\|Z\| > 5$
1	A	0.24	0/1729	0.40	0/2355
2	B	0.24	0/1723	0.41	0/2346
3	C	0.23	0/1324	0.43	0/1804
All	All	0.24	0/4776	0.41	0/6505

There are no bond length outliers.

There are no bond angle outliers.

There are no chirality outliers.

There are no planarity outliers.

5.2 Too-close contacts

In the following table, the Non-H and H(model) columns list the number of non-hydrogen atoms and hydrogen atoms in the chain respectively. The H(added) column lists the number of hydrogen atoms added and optimized by MolProbity. The Clashes column lists the number of clashes within the asymmetric unit, whereas Symm-Clashes lists symmetry related clashes.

Mol	Chain	Non-H	H(model)	H(added)	Clashes	Symm-Clashes
1	A	1683	1644	1656	2	0
2	B	1677	1643	1650	5	0
3	C	1288	1180	1237	3	0
4	A	56	28	49	2	0
4	B	56	27	48	4	0
4	C	28	0	23	1	0
5	A	11	0	8	0	0
5	B	11	0	8	0	0
5	C	11	0	9	2	0
6	A	22	0	18	0	0

Continued on next page...

Continued from previous page...

Mol	Chain	Non-H	H(model)	H(added)	Clashes	Symm-Clashes
6	B	22	0	18	0	0
6	C	11	0	10	2	0
7	A	10	0	10	0	0
7	B	10	0	10	0	0
7	C	10	0	10	1	0
8	B	11	11	10	0	0
All	All	4917	4533	4774	14	0

The all-atom clashscore is defined as the number of clashes found per 1000 atoms (including hydrogen atoms). The all-atom clashscore for this structure is 1.

All (14) close contacts within the same asymmetric unit are listed below, sorted by their clash magnitude.

Atom-1	Atom-2	Interatomic distance (Å)	Clash overlap (Å)
2:B:264:VAL:HG11	4:B:454:NAG:H83	1.72	0.70
2:B:301:ARG:HE	4:B:454:NAG:H81	1.63	0.60
1:A:325:ASN:OD1	1:A:326:LYS:N	2.35	0.59
5:C:202:BMA:H2	6:C:203:MAN:C5	2.36	0.56
3:C:113:TRP:CH2	3:C:114:LYS:HE3	2.43	0.54
2:B:241:PHE:CE2	4:B:454:NAG:H4	2.48	0.49
2:B:241:PHE:CZ	4:B:454:NAG:H61	2.48	0.49
1:A:301:ARG:HE	4:A:450:NAG:H81	1.80	0.45
4:A:449:NAG:H61	4:A:450:NAG:HN2	1.84	0.43
4:C:200:NAG:H61	4:C:201:NAG:C1	2.49	0.43
5:C:202:BMA:H2	6:C:203:MAN:O5	2.18	0.43
3:C:113:TRP:O	3:C:114:LYS:HB2	2.19	0.41
3:C:142:PRO:O	7:C:204:FUC:H4	2.20	0.41
2:B:292:ARG:HD2	2:B:300:TYR:CD2	2.56	0.40

There are no symmetry-related clashes.

5.3 Torsion angles

5.3.1 Protein backbone

In the following table, the Percentiles column shows the percent Ramachandran outliers of the chain as a percentile score with respect to all X-ray entries followed by that with respect to entries of similar resolution.

The Analysed column shows the number of residues for which the backbone conformation was analysed, and the total number of residues.

Mol	Chain	Analysed	Favoured	Allowed	Outliers	Percentiles	
1	A	209/211 (99%)	201 (96%)	8 (4%)	0	100	100
2	B	208/210 (99%)	203 (98%)	5 (2%)	0	100	100
3	C	159/163 (98%)	153 (96%)	6 (4%)	0	100	100
All	All	576/584 (99%)	557 (97%)	19 (3%)	0	100	100

There are no Ramachandran outliers to report.

5.3.2 Protein sidechains (i)

In the following table, the Percentiles column shows the percent sidechain outliers of the chain as a percentile score with respect to all X-ray entries followed by that with respect to entries of similar resolution.

The Analysed column shows the number of residues for which the sidechain conformation was analysed, and the total number of residues.

Mol	Chain	Analysed	Rotameric	Outliers	Percentiles	
1	A	195/196 (100%)	195 (100%)	0	100	100
2	B	195/195 (100%)	195 (100%)	0	100	100
3	C	148/150 (99%)	148 (100%)	0	100	100
All	All	538/541 (99%)	538 (100%)	0	100	100

There are no protein residues with a non-rotameric sidechain to report.

Some sidechains can be flipped to improve hydrogen bonding and reduce clashes. All (2) such sidechains are listed below:

Mol	Chain	Res	Type
1	A	294	GLN
3	C	75	GLN

5.3.3 RNA (i)

There are no RNA molecules in this entry.

5.4 Non-standard residues in protein, DNA, RNA chains (i)

There are no non-standard protein/DNA/RNA residues in this entry.

5.5 Carbohydrates

There are no carbohydrates in this entry.

5.6 Ligand geometry

22 ligands are modelled in this entry.

In the following table, the Counts columns list the number of bonds (or angles) for which Mogul statistics could be retrieved, the number of bonds (or angles) that are observed in the model and the number of bonds (or angles) that are defined in the Chemical Component Dictionary. The Link column lists molecule types, if any, to which the group is linked. The Z score for a bond length (or angle) is the number of standard deviations the observed value is removed from the expected value. A bond length (or angle) with $|Z| > 2$ is considered an outlier worth inspection. RMSZ is the root-mean-square of all Z scores of the bond lengths (or angles).

Mol	Type	Chain	Res	Link	Bond lengths			Bond angles		
					Counts	RMSZ	$\#\|Z\| > 2$	Counts	RMSZ	$\#\|Z\| > 2$
4	NAG	A	449	1,4,7	14,14,15	0.20	0	15,19,21	0.45	0
4	NAG	A	450	5,4	14,14,15	0.21	0	15,19,21	0.44	0
5	BMA	A	451	4,6	11,11,12	0.65	0	13,15,17	0.94	0
6	MAN	A	453	5,4	11,11,12	0.68	0	13,15,17	0.99	1 (7%)
6	MAN	A	454	5,4	11,11,12	0.60	0	13,15,17	0.99	2 (15%)
4	NAG	A	455	6	14,14,15	0.22	0	15,19,21	0.46	0
4	NAG	A	456	6	14,14,15	0.19	0	15,19,21	0.46	0
7	FUC	A	457	4	9,10,11	0.65	0	13,14,16	0.85	0
4	NAG	B	453	2,4,7	14,14,15	0.19	0	15,19,21	0.51	0
4	NAG	B	454	5,4	14,14,15	0.20	0	15,19,21	0.45	0
5	BMA	B	455	4,6	11,11,12	0.62	0	13,15,17	0.96	0
6	MAN	B	457	5,4	11,11,12	0.59	0	13,15,17	1.35	2 (15%)
6	MAN	B	458	5,4	11,11,12	0.71	1 (9%)	13,15,17	1.11	2 (15%)
4	NAG	B	459	8,6	14,14,15	0.36	0	15,19,21	0.45	0
4	NAG	B	460	6	14,14,15	0.20	0	15,19,21	0.57	0
7	FUC	B	461	4	9,10,11	0.64	0	13,14,16	0.89	0
8	GAL	B	462	4	11,11,12	0.54	0	13,15,17	0.88	0
4	NAG	C	200	3,4,7	14,14,15	0.24	0	15,19,21	0.46	0
4	NAG	C	201	5,4	14,14,15	0.18	0	15,19,21	0.47	0
5	BMA	C	202	4,6	11,11,12	0.41	0	13,15,17	0.81	0
6	MAN	C	203	5	11,11,12	0.81	1 (9%)	13,15,17	1.32	2 (15%)
7	FUC	C	204	4	9,10,11	0.66	0	13,14,16	0.85	0

In the following table, the Chirals column lists the number of chiral outliers, the number of chiral centers analysed, the number of these observed in the model and the number defined in the Chemical Component Dictionary. Similar counts are reported in the Torsion and Rings columns.

'-' means no outliers of that kind were identified.

Mol	Type	Chain	Res	Link	Chirals	Torsions	Rings
4	NAG	A	449	1,4,7	-	0/6/23/26	0/1/1/1
4	NAG	A	450	5,4	-	0/6/23/26	0/1/1/1
5	BMA	A	451	4,6	-	0/2/19/22	0/1/1/1
6	MAN	A	453	5,4	-	0/2/19/22	0/1/1/1
6	MAN	A	454	5,4	-	0/2/19/22	0/1/1/1
4	NAG	A	455	6	-	0/6/23/26	0/1/1/1
4	NAG	A	456	6	-	0/6/23/26	0/1/1/1
7	FUC	A	457	4	-	0/0/17/20	0/1/1/1
4	NAG	B	453	2,4,7	-	0/6/23/26	0/1/1/1
4	NAG	B	454	5,4	-	0/6/23/26	0/1/1/1
5	BMA	B	455	4,6	-	0/2/19/22	0/1/1/1
6	MAN	B	457	5,4	-	0/2/19/22	0/1/1/1
6	MAN	B	458	5,4	-	0/2/19/22	0/1/1/1
4	NAG	B	459	8,6	-	0/6/23/26	0/1/1/1
4	NAG	B	460	6	-	0/6/23/26	0/1/1/1
7	FUC	B	461	4	-	0/0/17/20	0/1/1/1
8	GAL	B	462	4	-	0/2/19/22	0/1/1/1
4	NAG	C	200	3,4,7	-	0/6/23/26	0/1/1/1
4	NAG	C	201	5,4	-	0/6/23/26	0/1/1/1
5	BMA	C	202	4,6	-	0/2/19/22	0/1/1/1
6	MAN	C	203	5	-	0/2/19/22	0/1/1/1
7	FUC	C	204	4	-	0/0/17/20	0/1/1/1

All (2) bond length outliers are listed below:

Mol	Chain	Res	Type	Atoms	Z	Observed(Å)	Ideal(Å)
6	B	458	MAN	C1-C2	2.02	1.57	1.52
6	C	203	MAN	C1-C2	2.31	1.57	1.52

All (9) bond angle outliers are listed below:

Mol	Chain	Res	Type	Atoms	Z	Observed(^{o})	Ideal(^{o})
6	B	457	MAN	O2-C2-C3	-3.12	104.04	110.17
6	B	458	MAN	O2-C2-C3	-2.32	105.62	110.17
6	C	203	MAN	O2-C2-C3	-2.25	105.75	110.17
6	A	453	MAN	O2-C2-C3	-2.09	106.07	110.17
6	A	454	MAN	O2-C2-C3	-2.05	106.15	110.17
6	A	454	MAN	C1-O5-C5	2.18	115.17	112.17
6	B	458	MAN	C1-O5-C5	2.42	115.50	112.17
6	C	203	MAN	C1-O5-C5	2.89	116.15	112.17
6	B	457	MAN	C1-O5-C5	2.92	116.20	112.17

There are no chirality outliers.

There are no torsion outliers.

There are no ring outliers.

8 monomers are involved in 10 short contacts:

Mol	Chain	Res	Type	Clashes	Symm-Clashes
4	A	449	NAG	1	0
4	A	450	NAG	2	0
4	B	454	NAG	4	0
4	C	200	NAG	1	0
4	C	201	NAG	1	0
5	C	202	BMA	2	0
6	C	203	MAN	2	0
7	C	204	FUC	1	0

5.7 Other polymers (i)

There are no such residues in this entry.

5.8 Polymer linkage issues (i)

The following chains have linkage breaks:

Mol	Chain	Number of breaks
3	C	1

All chain breaks are listed below:

Model	Chain	Residue-1	Atom-1	Residue-2	Atom-2	Distance (Å)
1	C	32:ALA	C	38:ASP	N	7.42

6 Fit of model and data

6.1 Protein, DNA and RNA chains

In the following table, the column labelled '#RSRZ> 2' contains the number (and percentage) of RSRZ outliers, followed by percent RSRZ outliers for the chain as percentile scores relative to all X-ray entries and entries of similar resolution. The OWAB column contains the minimum, median, 95^{th} percentile and maximum values of the occupancy-weighted average B-factor per residue. The column labelled 'Q< 0.9' lists the number of (and percentage) of residues with an average occupancy less than 0.9.

Mol	Chain	Analysed	<RSRZ>	#RSRZ>2	OWAB(Å^2)	Q<0.9
1	A	211/211 (100%)	0.14	4 (1%) 67 58	42, 72, 122, 148	0
2	B	210/210 (100%)	0.12	3 (1%) 75 67	43, 74, 97, 113	0
3	C	163/163 (100%)	0.31	5 (3%) 49 39	57, 84, 120, 148	0
All	All	584/584 (100%)	0.18	12 (2%) 64 54	42, 76, 114, 148	0

All (12) RSRZ outliers are listed below:

Mol	Chain	Res	Type	RSRZ
1	A	281	GLY	4.7
1	A	296	TYR	4.3
3	C	56	SER	2.9
3	C	38	ASP	2.6
1	A	294	GLN	2.4
2	B	329	PRO	2.4
3	C	52	HIS	2.4
1	A	269	GLU	2.3
2	B	384	ASN	2.3
3	C	102	GLU	2.1
3	C	6	PRO	2.0
2	B	341	GLY	2.0

6.2 Non-standard residues in protein, DNA, RNA chains

There are no non-standard protein/DNA/RNA residues in this entry.

6.3 Carbohydrates

There are no carbohydrates in this entry.

6.4 Ligands

In the following table, the Atoms column lists the number of modelled atoms in the group and the number defined in the chemical component dictionary. LLDF column lists the quality of electron density of the group with respect to its neighbouring residues in protein, DNA or RNA chains. The B-factors column lists the minimum, median, 95^{th} percentile and maximum values of B factors of atoms in the group. The column labelled 'Q< 0.9' lists the number of atoms with occupancy less than 0.9.

Mol	Type	Chain	Res	Atoms	RSCC	RSR	LLDF	B-factors(Å^2)	Q<0.9
6	MAN	C	203	11/?	0.81	0.33	2.00	80,88,100,109	0
7	FUC	C	204	10/?	0.86	0.39	1.38	81,88,95,105	0
4	NAG	A	455	14/?	0.86	0.40	1.34	85,102,119,120	0
8	GAL	B	462	11/?	0.81	0.40	0.67	61,101,121,130	0
4	NAG	C	201	14/?	0.86	0.30	0.49	80,95,98,102	0
5	BMA	C	202	11/?	0.77	0.28	0.30	80,98,103,104	0
4	NAG	C	200	14/?	0.83	0.30	0.27	78,99,103,104	0
4	NAG	A	449	14/?	0.79	0.36	0.26	90,111,127,133	0
4	NAG	B	454	14/?	0.90	0.24	-0.54	50,64,72,78	0
4	NAG	B	453	14/?	0.92	0.20	-1.59	62,71,74,77	0
6	MAN	A	454	11/?	0.78	0.44	-	74,84,93,95	0
7	FUC	A	457	10/?	0.66	0.77	-	92,117,128,131	0
6	MAN	A	453	11/?	0.83	0.31	-	99,104,113,114	0
4	NAG	B	459	14/?	0.79	0.35	-	74,102,128,129	0
6	MAN	B	457	11/?	0.90	0.28	-	74,88,104,108	0
7	FUC	B	461	10/?	0.92	0.25	-	48,69,75,75	0
5	BMA	B	455	11/?	0.91	0.19	-	65,69,78,85	0
4	NAG	A	456	14/?	0.85	0.41	-	87,121,149,152	0
5	BMA	A	451	11/?	0.85	0.25	-	78,87,102,108	0
4	NAG	B	460	14/?	0.77	0.41	-	82,105,129,138	0
4	NAG	A	450	14/?	0.91	0.31	-	75,94,109,114	0
6	MAN	B	458	11/?	0.89	0.33	-	72,87,93,114	0

6.5 Other polymers

There are no such residues in this entry.

C.2 6R6C PDB Validation Report

Full wwPDB X-ray Structure Validation Report (i)

Mar 27, 2019 – 07:08 am GMT

PDB ID	:	6R6C
Title	:	Fc gamma RIIa ectodomain 27W, 131H allotype
Deposited on	:	2019-03-26
Resolution	:	1.81 Å(reported)

This is a Full wwPDB X-ray Structure Validation Report.

This report is produced by the wwPDB biocuration pipeline after annotation of the structure.

We welcome your comments at *validation@mail.wwpdb.org*
A user guide is available at
https://www.wwpdb.org/validation/2017/XrayValidationReportHelp
with specific help available everywhere you see the (i) symbol.

The following versions of software and data (see references (i)) were used in the production of this report:

MolProbity	:	4.02b-467
Mogul	:	1.8.0 (224370), CSD as540be (2019)
Xtriage (Phenix)	:	1.13
EDS	:	2.1
Percentile statistics	:	20171227.v01 (using entries in the PDB archive December 27th 2017)
Refmac	:	5.8.0158
CCP4	:	7.0 (Gargrove)
Ideal geometry (proteins)	:	Engh & Huber (2001)
Ideal geometry (DNA, RNA)	:	Parkinson et al. (1996)
Validation Pipeline (wwPDB-VP)	:	2.1

1 Overall quality at a glance

The following experimental techniques were used to determine the structure:
X-RAY DIFFRACTION

The reported resolution of this entry is 1.81 Å.

Percentile scores (ranging between 0-100) for global validation metrics of the entry are shown in the following graphic. The table shows the number of entries on which the scores are based.

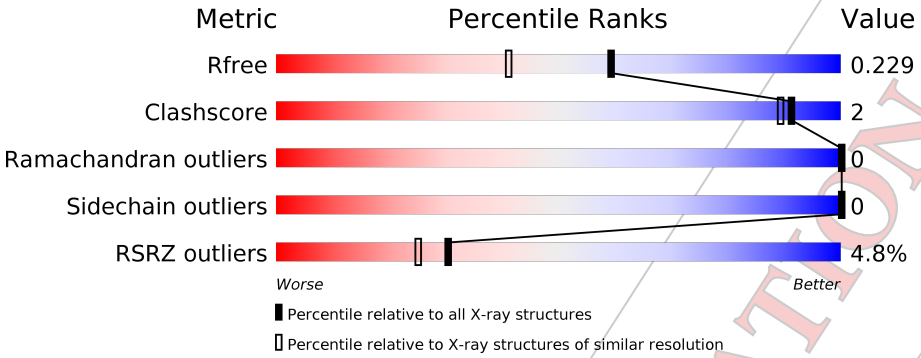

Metric	Whole archive (#Entries)	Similar resolution (#Entries, resolution range(Å))
R_{free}	111664	6455 (1.84-1.80)
Clashscore	122126	7349 (1.84-1.80)
Ramachandran outliers	120053	7272 (1.84-1.80)
Sidechain outliers	120020	7272 (1.84-1.80)
RSRZ outliers	108989	6347 (1.84-1.80)

The table below summarises the geometric issues observed across the polymeric chains and their fit to the electron density. The red, orange, yellow and green segments on the lower bar indicate the fraction of residues that contain outliers for >=3, 2, 1 and 0 types of geometric quality criteria. A grey segment represents the fraction of residues that are not modelled. The numeric value for each fraction is indicated below the corresponding segment, with a dot representing fractions <=5% The upper red bar (where present) indicates the fraction of residues that have poor fit to the electron density. The numeric value is given above the bar.

Mol	Chain	Length	Quality of chain
1	A	171	5% 95%

2 Entry composition

There are 11 unique types of molecules in this entry. The entry contains 1587 atoms, of which 0 are hydrogens and 0 are deuteriums.

In the tables below, the ZeroOcc column contains the number of atoms modelled with zero occupancy, the AltConf column contains the number of residues with at least one atom in alternate conformation and the Trace column contains the number of residues modelled with at most 2 atoms.

- Molecule 1 is a protein called Low affinity immunoglobulin gamma Fc region receptor II-a.

Mol	Chain	Residues	Atoms					ZeroOcc	AltConf	Trace
1	A	168	Total	C	N	O	S	0	8	0
			1349	863	229	252	5			

There is a discrepancy between the modelled and reference sequences:

Chain	Residue	Modelled	Actual	Comment	Reference
A	30	TRP	GLN	conflict	UNP V9GY83

- Molecule 2 is N-ACETYL-D-GLUCOSAMINE (three-letter code: NAG) (formula: $C_8H_{15}NO_6$).

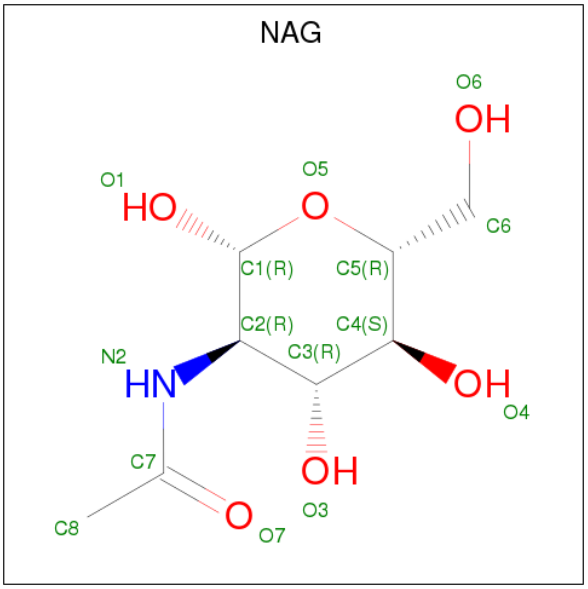

Mol	Chain	Residues	Atoms				ZeroOcc	AltConf
2	A	1	Total	C	N	O	0	0
			14	8	1	5		
2	A	1	Total	C	N	O	0	0
			14	8	1	5		

- Molecule 3 is BETA-D-MANNOSE (three-letter code: BMA) (formula: $C_6H_{12}O_6$).

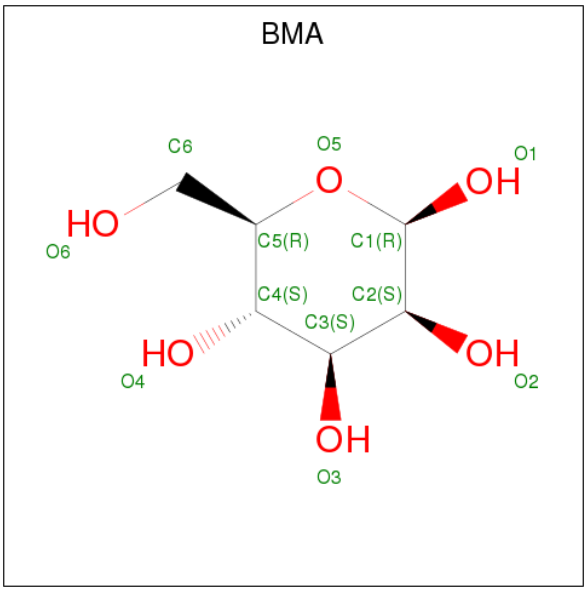

Mol	Chain	Residues	Atoms			ZeroOcc	AltConf
			Total	C	O		
3	A	1	11	6	5	0	0

- Molecule 4 is ALPHA-D-MANNOSE (three-letter code: MAN) (formula: $C_6H_{12}O_6$).

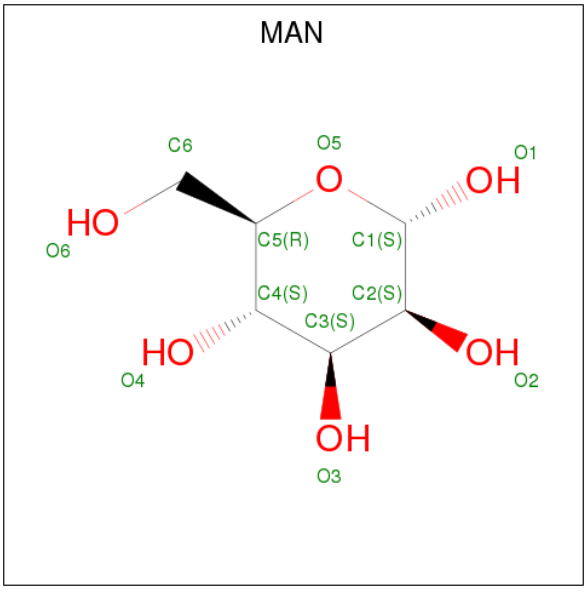

Mol	Chain	Residues	Atoms			ZeroOcc	AltConf
			Total	C	O		
4	A	1	11	6	5	0	0

- Molecule 5 is CITRATE ANION (three-letter code: FLC) (formula: $C_6H_5O_7$).

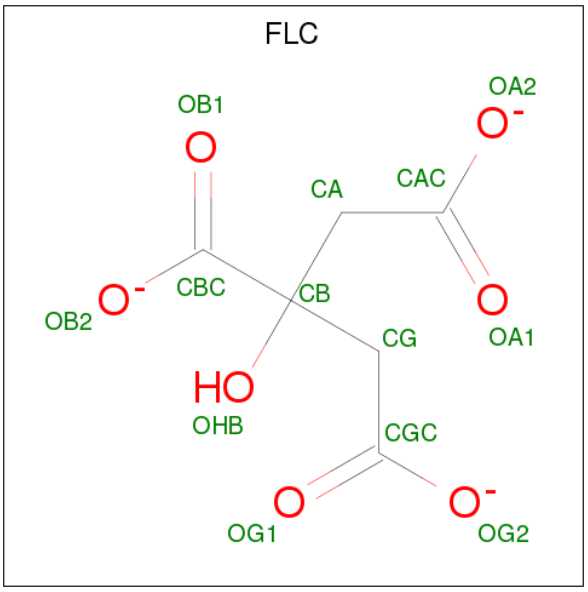

Mol	Chain	Residues	Atoms	ZeroOcc	AltConf
5	A	1	Total C O 13 6 7	0	0

- Molecule 6 is PHOSPHATE ION (three-letter code: PO4) (formula: O_4P).

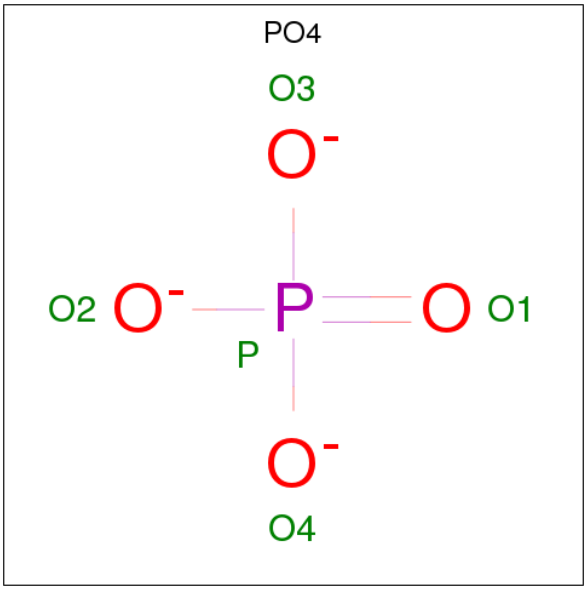

Mol	Chain	Residues	Atoms	ZeroOcc	AltConf
6	A	1	Total O P 5 4 1	0	0
6	A	1	Total O P 5 4 1	0	0
6	A	1	Total O P 5 4 1	0	0

- Molecule 7 is NONAETHYLENE GLYCOL (three-letter code: 2PE) (formula: $C_{18}H_{38}O_{10}$).

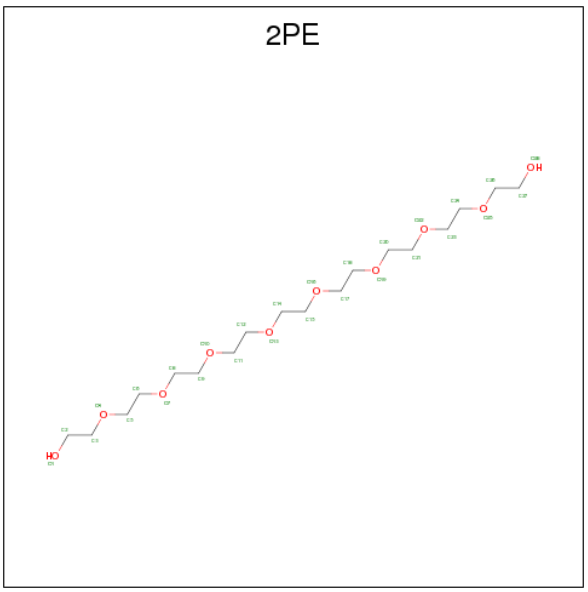

Mol	Chain	Residues	Atoms	ZeroOcc	AltConf
7	A	1	Total C O 20 14 6	0	0

- Molecule 8 is TRIETHYLENE GLYCOL (three-letter code: PGE) (formula: $C_6H_{14}O_4$).

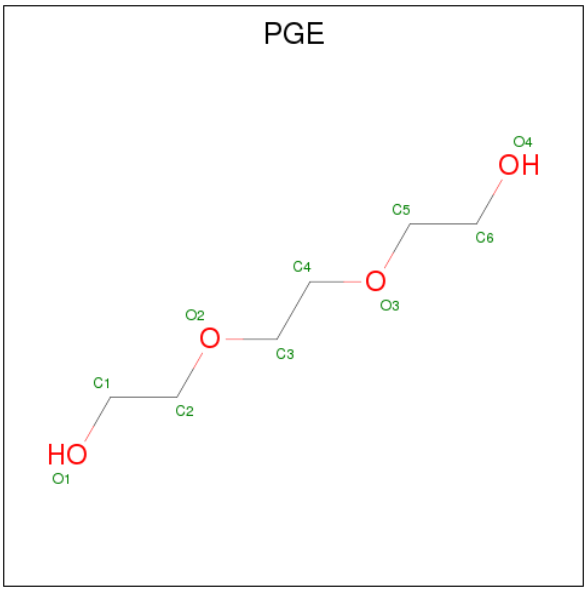

Mol	Chain	Residues	Atoms	ZeroOcc	AltConf
8	A	1	Total C O 10 6 4	0	0
8	A	1	Total C O 6 4 2	0	0

- Molecule 9 is TETRAETHYLENE GLYCOL (three-letter code: PG4) (formula: $C_8H_{18}O_5$).

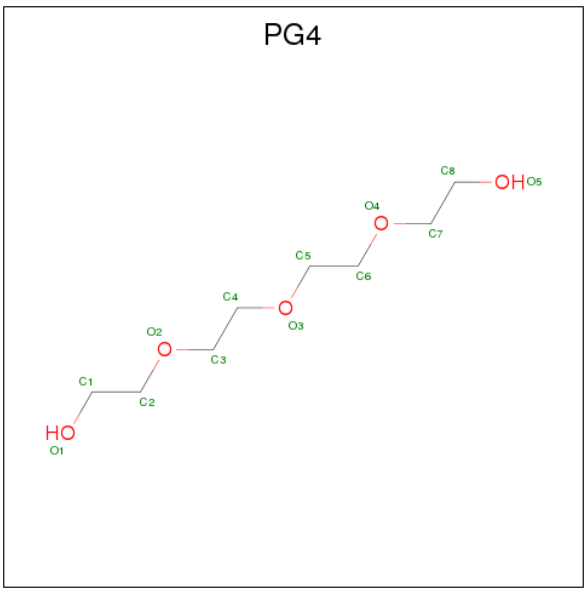

Mol	Chain	Residues	Atoms	ZeroOcc	AltConf
9	A	1	Total C O 12 8 4	0	0

- Molecule 10 is SODIUM ION (three-letter code: NA) (formula: Na).

Mol	Chain	Residues	Atoms	ZeroOcc	AltConf
10	A	1	Total Na 1 1	0	0

- Molecule 11 is water.

Mol	Chain	Residues	Atoms	ZeroOcc	AltConf
11	A	111	Total O 111 111	0	0

3 Residue-property plots

These plots are drawn for all protein, RNA and DNA chains in the entry. The first graphic for a chain summarises the proportions of the various outlier classes displayed in the second graphic. The second graphic shows the sequence view annotated by issues in geometryand electron density. Residues are color-coded according to the number of geometric quality criteria for which they contain at least one outlier: green = 0, yellow = 1, orange = 2 and red = 3 or more. A red dot above a residue indicates a poor fit to the electron density (RSRZ > 2). Stretches of 2 or more consecutive residues without any outlier are shown as a green connector. Residues present in the sample, but not in the model, are shown in grey.

- Molecule 1: Low affinity immunoglobulin gamma Fc region receptor II-a

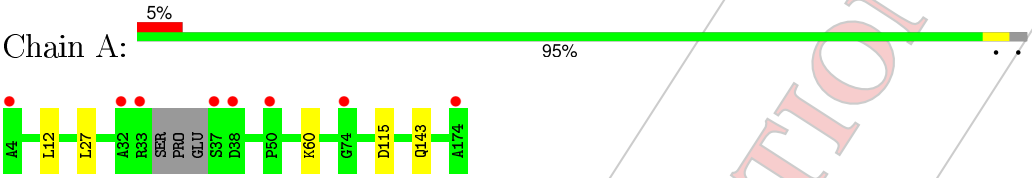

4 Data and refinement statistics (i)

Property	Value	Source
Space group	C 2 2 21	Depositor
Cell constants a, b, c, α, β, γ	49.93Å 76.53Å 108.28Å 90.00° 90.00° 90.00°	Depositor
Resolution (Å)	41.82 – 1.81 41.82 – 1.81	Depositor EDS
% Data completeness (in resolution range)	99.0 (41.82-1.81) 99.0 (41.82-1.81)	Depositor EDS
R_{merge}	0.15	Depositor
R_{sym}	(Not available)	Depositor
$< I/\sigma(I) >$ [1]	1.36 (at 1.81Å)	Xtriage
Refinement program	PHENIX (1.12_2829: ???)	Depositor
R, R_{free}	0.193 , 0.225 0.199 , 0.229	Depositor DCC
R_{free} test set	907 reflections (4.74%)	wwPDB-VP
Wilson B-factor (Å^2)	21.7	Xtriage
Anisotropy	0.597	Xtriage
Bulk solvent k_{sol}(e/Å^3), B_{sol}(Å^2)	0.39 , 61.2	EDS
L-test for twinning[2]	$< \|L\| > = 0.50$, $< L^2 > = 0.33$	Xtriage
Estimated twinning fraction	No twinning to report.	Xtriage
F_o,F_c correlation	0.96	EDS
Total number of atoms	1587	wwPDB-VP
Average B, all atoms (Å^2)	32.0	wwPDB-VP

Xtriage's analysis on translational NCS is as follows: *The largest off-origin peak in the Patterson function is 8.59% of the height of the origin peak. No significant pseudotranslation is detected.*

[1] Intensities estimated from amplitudes.

[2] Theoretical values of $< |L| >$, $< L^2 >$ for acentric reflections are 0.5, 0.333 respectively for untwinned datasets, and 0.375, 0.2 for perfectly twinned datasets.

5 Model quality

5.1 Standard geometry

Bond lengths and bond angles in the following residue types are not validated in this section: PGE, NAG, NA, PO4, PG4, BMA, 2PE, FLC, MAN

The Z score for a bond length (or angle) is the number of standard deviations the observed value is removed from the expected value. A bond length (or angle) with $|Z| > 5$ is considered an outlier worth inspection. RMSZ is the root-mean-square of all Z scores of the bond lengths (or angles).

Mol	Chain	Bond lengths		Bond angles	
		RMSZ	$\#\|Z\| > 5$	RMSZ	$\#\|Z\| > 5$
1	A	0.27	0/1401	0.52	0/1918

There are no bond length outliers.

There are no bond angle outliers.

There are no chirality outliers.

There are no planarity outliers.

5.2 Too-close contacts

In the following table, the Non-H and H(model) columns list the number of non-hydrogen atoms and hydrogen atoms in the chain respectively. The H(added) column lists the number of hydrogen atoms added and optimized by MolProbity. The Clashes column lists the number of clashes within the asymmetric unit, whereas Symm-Clashes lists symmetry related clashes.

Mol	Chain	Non-H	H(model)	H(added)	Clashes	Symm-Clashes
1	A	1349	0	1268	3	1
2	A	28	0	24	2	0
3	A	11	0	9	0	0
4	A	11	0	10	0	1
5	A	13	0	5	0	0
6	A	15	0	0	0	0
7	A	20	0	24	0	0
8	A	16	0	18	0	0
9	A	12	0	15	0	0
10	A	1	0	0	0	0
11	A	111	0	0	1	0
All	All	1587	0	1373	5	1

The all-atom clashscore is defined as the number of clashes found per 1000 atoms (including

hydrogen atoms). The all-atom clashscore for this structure is 2.

All (5) close contacts within the same asymmetric unit are listed below, sorted by their clash magnitude.

Atom-1	Atom-2	Interatomic distance (Å)	Clash overlap (Å)
2:A:201:NAG:H61	2:A:202:NAG:C1	2.37	0.54
1:A:143:GLN:HG3	1:A:143:GLN:O	2.12	0.49
1:A:60:LYS:NZ	11:A:303:HOH:O	2.43	0.49
1:A:12:LEU:HD12	1:A:27:LEU:HD23	1.95	0.48
2:A:201:NAG:C6	2:A:202:NAG:C1	2.93	0.45

All (1) symmetry-related close contacts are listed below. The label for Atom-2 includes the symmetry operator and encoded unit-cell translations to be applied.

Atom-1	Atom-2	Interatomic distance (Å)	Clash overlap (Å)
1:A:115:ASP:OD2	4:A:204:MAN:O2[4_555]	2.16	0.04

5.3 Torsion angles (i)

5.3.1 Protein backbone (i)

In the following table, the Percentiles column shows the percent Ramachandran outliers of the chain as a percentile score with respect to all X-ray entries followed by that with respect to entries of similar resolution.

The Analysed column shows the number of residues for which the backbone conformation was analysed, and the total number of residues.

Mol	Chain	Analysed	Favoured	Allowed	Outliers	Percentiles	
1	A	172/171 (101%)	170 (99%)	2 (1%)	0	100	100

There are no Ramachandran outliers to report.

5.3.2 Protein sidechains (i)

In the following table, the Percentiles column shows the percent sidechain outliers of the chain as a percentile score with respect to all X-ray entries followed by that with respect to entries of similar resolution.

The Analysed column shows the number of residues for which the sidechain conformation was analysed, and the total number of residues.

Mol	Chain	Analysed	Rotameric	Outliers	Percentiles
1	A	151/156 (97%)	151 (100%)	0	100 100

There are no protein residues with a non-rotameric sidechain to report.

Some sidechains can be flipped to improve hydrogen bonding and reduce clashes. All (2) such sidechains are listed below:

Mol	Chain	Res	Type
1	A	21	GLN
1	A	63	ASN

5.3.3 RNA

There are no RNA molecules in this entry.

5.4 Non-standard residues in protein, DNA, RNA chains

There are no non-standard protein/DNA/RNA residues in this entry.

5.5 Carbohydrates

There are no carbohydrates in this entry.

5.6 Ligand geometry

Of 13 ligands modelled in this entry, 1 is monoatomic - leaving 12 for Mogul analysis.

In the following table, the Counts columns list the number of bonds (or angles) for which Mogul statistics could be retrieved, the number of bonds (or angles) that are observed in the model and the number of bonds (or angles) that are defined in the Chemical Component Dictionary. The Link column lists molecule types, if any, to which the group is linked. The Z score for a bond length (or angle) is the number of standard deviations the observed value is removed from the expected value. A bond length (or angle) with $|Z| > 2$ is considered an outlier worth inspection. RMSZ is the root-mean-square of all Z scores of the bond lengths (or angles).

Mol	Type	Chain	Res	Link	Bond lengths			Bond angles		
					Counts	RMSZ	$\#\|Z\| > 2$	Counts	RMSZ	$\#\|Z\| > 2$
2	NAG	A	201	1,2	14,14,15	0.18	0	17,19,21	0.92	1 (5%)
2	NAG	A	202	3,2	14,14,15	0.18	0	17,19,21	0.62	0
3	BMA	A	203	2,4	11,11,12	0.55	0	15,15,17	0.86	0
4	MAN	A	204	3	11,11,12	0.51	0	15,15,17	1.12	2 (13%)

Mol	Type	Chain	Res	Link	Bond lengths			Bond angles		
					Counts	RMSZ	$\#\|Z\|>2$	Counts	RMSZ	$\#\|Z\|>2$
5	FLC	A	205	-	3,12,12	1.15	0	3,17,17	1.50	1 (33%)
6	PO4	A	206	-	4,4,4	0.88	0	6,6,6	0.42	0
6	PO4	A	207	-	4,4,4	0.88	0	6,6,6	0.42	0
6	PO4	A	208	-	4,4,4	0.87	0	6,6,6	0.42	0
7	2PE	A	209	-	19,19,27	0.50	0	18,18,26	0.37	0
8	PGE	A	210	-	9,9,9	0.47	0	8,8,8	0.22	0
8	PGE	A	211	-	5,5,9	0.42	0	4,4,8	0.21	0
9	PG4	A	212	-	11,11,12	0.45	0	10,10,11	0.26	0

In the following table, the Chirals column lists the number of chiral outliers, the number of chiral centers analysed, the number of these observed in the model and the number defined in the Chemical Component Dictionary. Similar counts are reported in the Torsion and Rings columns. '-' means no outliers of that kind were identified.

Mol	Type	Chain	Res	Link	Chirals	Torsions	Rings
2	NAG	A	201	1,2	-	0/6/23/26	0/1/1/1
2	NAG	A	202	3,2	-	0/6/23/26	0/1/1/1
3	BMA	A	203	2,4	-	0/2/19/22	0/1/1/1
4	MAN	A	204	3	-	0/2/19/22	0/1/1/1
5	FLC	A	205	-	-	0/6/16/16	0/0/0/0
6	PO4	A	206	-	-	0/0/0/0	0/0/0/0
6	PO4	A	207	-	-	0/0/0/0	0/0/0/0
6	PO4	A	208	-	-	0/0/0/0	0/0/0/0
7	2PE	A	209	-	-	0/17/17/25	0/0/0/0
8	PGE	A	210	-	-	0/7/7/7	0/0/0/0
8	PGE	A	211	-	-	0/3/3/7	0/0/0/0
9	PG4	A	212	-	-	0/9/9/10	0/0/0/0

There are no bond length outliers.

All (4) bond angle outliers are listed below:

Mol	Chain	Res	Type	Atoms	Z	Observed(^{o})	Ideal(^{o})
5	A	205	FLC	CB-CA-CAC	-2.40	111.15	114.98
4	A	204	MAN	O2-C2-C3	-2.26	105.74	110.16
4	A	204	MAN	C1-O5-C5	2.16	115.14	112.20
2	A	201	NAG	C1-O5-C5	2.18	115.16	112.20

There are no chirality outliers.

There are no torsion outliers.

There are no ring outliers.

3 monomers are involved in 3 short contacts:

Mol	Chain	Res	Type	Clashes	Symm-Clashes
2	A	201	NAG	2	0
2	A	202	NAG	2	0
4	A	204	MAN	0	1

5.7 Other polymers

There are no such residues in this entry.

5.8 Polymer linkage issues

There are no chain breaks in this entry.

6 Fit of model and data

6.1 Protein, DNA and RNA chains

In the following table, the column labelled '#RSRZ> 2' contains the number (and percentage) of RSRZ outliers, followed by percent RSRZ outliers for the chain as percentile scores relative to all X-ray entries and entries of similar resolution. The OWAB column contains the minimum, median, 95^{th} percentile and maximum values of the occupancy-weighted average B-factor per residue. The column labelled 'Q< 0.9' lists the number of (and percentage) of residues with an average occupancy less than 0.9.

Mol	Chain	Analysed	<RSRZ>	#RSRZ>2	OWAB(Å^2)	Q<0.9
1	A	168/171 (98%)	0.00	8 (4%) 30 25	16, 27, 54, 79	0

All (8) RSRZ outliers are listed below:

Mol	Chain	Res	Type	RSRZ
1	A	32	ALA	4.6
1	A	37	SER	3.3
1	A	174	ALA	2.7
1	A	74	GLY	2.6
1	A	33	ARG	2.4
1	A	38	ASP	2.2
1	A	4	ALA	2.1
1	A	50[A]	PRO	2.0

6.2 Non-standard residues in protein, DNA, RNA chains

There are no non-standard protein/DNA/RNA residues in this entry.

6.3 Carbohydrates

There are no carbohydrates in this entry.

6.4 Ligands

In the following table, the Atoms column lists the number of modelled atoms in the group and the number defined in the chemical component dictionary. The B-factors column lists the minimum, median, 95^{th} percentile and maximum values of B factors of atoms in the group. The column labelled 'Q< 0.9' lists the number of atoms with occupancy less than 0.9.

Mol	Type	Chain	Res	Atoms	RSCC	RSR	B-factors(Å^2)	Q<0.9
10	NA	A	213	1/1	0.72	0.15	47,47,47,47	0
2	NAG	A	201	14/15	0.74	0.27	69,76,86,87	0
8	PGE	A	210	10/10	0.77	0.15	59,64,67,68	0
7	2PE	A	209	20/28	0.78	0.19	46,57,64,64	0
3	BMA	A	203	11/12	0.79	0.21	67,68,74,77	0
2	NAG	A	202	14/15	0.79	0.25	66,68,72,73	0
4	MAN	A	204	11/12	0.81	0.25	23,26,31,31	11
6	PO4	A	208	5/5	0.82	0.23	36,47,58,60	5
5	FLC	A	205	13/13	0.87	0.11	38,45,51,54	0
8	PGE	A	211	6/10	0.88	0.14	39,44,51,51	0
9	PG4	A	212	12/13	0.90	0.16	32,43,51,51	0
6	PO4	A	207	5/5	0.94	0.13	55,58,58,68	0
6	PO4	A	206	5/5	0.96	0.11	25,31,32,34	5

6.5 Other polymers

There are no such residues in this entry.